

MAX-PLANCK-INSTITUT FÜR POLYMERFORSCHUNG IN MAINZ

**From Polyarylated
Cycloparaphenylenes to Carbon
Nanotube Segments
and
Metallo N₄-Macrocycles as Fuel Cell
Catalysts**

Dissertation zur Erlangung des Grades

“Doktor der Naturwissenschaften”

am Fachbereich Chemie, Pharmazie und Geowissenschaften

der Johannes Gutenberg-Universität Mainz

Dipl. Chem. Martin Quernheim

Geboren in Tuttlingen

Mainz im Jahr 2015

Tag der mündlichen Prüfung: 18. Mai 2015

Dekan:




1. Berichterstatter:



2. Berichterstatter:



Die vorliegende Arbeit wurde in der Zeit von Februar 2011 bis Februar 2015 im Max-Planck-Institut für Polymerforschung in Mainz unter Anleitung von  durchgeführt.

Meiner Familie

“Wir brauchen nicht so fortzuleben,
wie wir gestern gelebt haben.
Macht euch nur von dieser Anschauung los,
und tausend Möglichkeiten
laden uns zu neuem Leben ein.“

Christian Morgenstern



danke ich im Besonderen für die Stellung
dieser spannenden Aufgabe, der kontinu-
ierlichen wissenschaftlichen wie auch per-
sönlichen Förderung und für das große
Vertrauen, das mir entgegengebracht
wurde.

Table of Contents

1. Introduction	1
1.1. Carbon Materials	1
1.1.1. Graphene and Nanographene	1
1.1.2. The <i>Scholl</i> Reaction	4
1.1.3. Graphene Nanoribbons.....	4
1.1.4. Carbon Nanotubes	5
1.2. Cycloparaphenylenes.....	8
1.3. From Cycloparaphenylenes to Carbon Nanotubes	12
1.4. Macrocyclic N ₄ -Metal Complexes	14
1.4.1. The Fuel Cell – Types and Fundamental Principles	14
1.4.2. Metallo Macrocycles for ORR	17
1.4.3. Rotating Disk- and Rotating Ring Disk Electrode	21
2. Motivation and Objectives	25
3. <i>Cyclo-hexa-peri-hexabenzocoronenes</i>	31
3.1. Introduction	31
3.2. Results and Discussion	33
3.2.1. Synthesis of π -extended <i>Cyclo-p</i> -hexaphenylbenzenes	33
3.2.2. Characterization of [3]CHPBs	36
3.2.3. Cyclodehydrogenation towards [3]CHBCs.....	41
3.3. Summary.....	60
4. Blocked <i>Cyclo-hexa-peri-hexabenzocoronenes</i>	63

4.1.	Introduction	63
4.2.	Results and Discussion	64
4.2.1.	Synthesis of Alkyl Substituted [3]CHPBs	64
4.2.2.	Characterization of Alkyl Substituted [3]CHPBs	69
4.2.3.	Cyclodehydrogenation towards Alkyl Substituted [3]CHBCs.....	77
4.3.	Summary.....	86
5.	Phenanthroline-Indole N ₄ -Macrocycles	89
5.1.	Introduction	89
5.2.	Results and Discussion	91
5.2.1.	Synthesis and Characterization	91
5.2.2.	Crystal Structure.....	98
5.2.3.	Metal Complexation.....	99
5.2.4.	RDE measurements	103
5.2.5.	RRDE measurements	107
5.3.	Summary.....	110
6.	Conclusion and Outlook.....	113
7.	Experimental Part.....	121
7.1.	General Methods.....	121
7.2.	Analytical Methods.....	122
7.3.	Synthesis.....	126
7.3.1.	<i>Cyclo-hexa-peri-hexabenzocoronenes</i>	126
7.3.2.	Blocked <i>Cyclo-hexa-peri-hexabenzocorones</i>	140
7.3.3.	Phenanthroline-Indole N ₄ -Macrocycles	158
7.4.	Crystal Data	174

8. Bibliography.....	179
9. Acknowledgement.....	191
10. List of Publications.....	193
11. Curriculum Vitae.....	195

Index of Abbreviations

AcOH	acetic acid
AFC	alkaline fuel cell
¹³ C-APT	attached proton test – (NMR)
B3LYP	BECKE, three-parameter, LEE-YANG-PARR (DFT hybrid functional)
BuLi	butyl lithium
br	broad signal (NMR)
[3]CHPB	<i>cyclo-para</i> -hexaphenylbenzene-trimer
[3]CHBC	<i>cyclo-para-hexa-peri</i> -hexabenzocoronene-trimer
CID	collision induced dissociation
CNT	carbon nanotube
COSY	correlation spectroscopy
CPP	cycloparaphenylene
CT	charge- transfer
CV	cyclic voltammetry
CVD	chemical vapor deposition
d	doublet (NMR)
d	days
DCM	dichloromethane
dd	doublet of doublets (NMR)
DDQ	2,3-dichlor-5,6-dicyano-1,4-benzoquinone
DFT	density functional theory
DMF	<i>N,N</i> -dimethylformamide
ε	extinction coefficient
EA	elemental Analysis
ESI MS	electrospray ionization mass spectrometry

EtOAc	ethyl acetate
Et ₂ O	diethylether
EtOH	ethanol
FD MS	field desorption mass spectrometry
FET	field effect transistor
GNR	graphene nanoribbon
GPC	gel permeation chromatography
h	hours
HBC	hexa- <i>peri</i> -hexabenzocoronene
HMBC	hetero single quantum coherence
HOMO	highest occupied molecular orbital
HPB	hexaphenylbenzene
HR-MS	high resolution mass spectrometry
HSQC	hetero single quantum coherence
IR	infrared spectroscopy
LUMO	lowest unoccupied molecular orbital
m	multiplet (NMR)
MALDI-TOF	matrix-assisted laser desorption/ionization time-of-flight
MCFC	molten carbonate fuel cell
Me	methyl
MEA	membrane electrode assembly
MeOH	methanol
min	minutes
MS	mass spectrometry
MWCNT	multi-walled carbon nanotube
NG	nanographene
NMR	nuclear magnetic resonance
NOE	nuclear Overhauser effect
NOESY	nuclear Overhauser enhancement spectroscopy

NPMC	non precious metal catalyst
OFET	organic field-effect transistor
OLED	organic light emitting diode
OMe	methoxy
ORR	oxygen reduction reaction
PAFC	phosphoric acid fuel cell
PAH	polycyclic aromatic hydrocarbon
PEMFC	polymer electrolyte membrane fuel cell
Ph	phenyl
PIM	phenanthroline-indole macrocycle
PL	photoluminescence
ppm	parts per million
q	quartet (NMR)
RDE	rotating disk electrode
RRDE	rotating ring disk electrode
rGO	reduced graphene oxide
RT	room temperature
s	singlet (NMR)
sec	seconds
SOFC	solid oxide fuel cell
S-Phos	2-dicyclohexylphosphino-2',6'-dimethoxybiphenyl
SWCNT	single-walled carbon nanotube
t	triplet (NMR)
TBAF	tetra-iso-butyl ammonium fluoride
^t Bu	<i>tert</i> -butyl
THF	tetrahydrofuran
TMS	trimethylsilyl
UHV	ultra-high vacuum
UV-Vis	ultraviolet-visible absorption spectroscopy

1. Introduction

1.1. Carbon Materials

1.1.1. Graphene and Nanographene

Graphene is a monolayer of pure carbon, sp^2 -hybridized and in a honeycomb arrangement (Figure 1-1). In 1962 Boehm first described carbon monolayers and carbon foils.^[1] It was not until 2004 that this carbon monolayer, named graphene,^[2] was isolated by *Novoselov* and *Geim*.^[3] For the elucidation of the superior electronic properties of graphene, they received the Nobel Prize and furthermore, spurred the extensive research in this field.

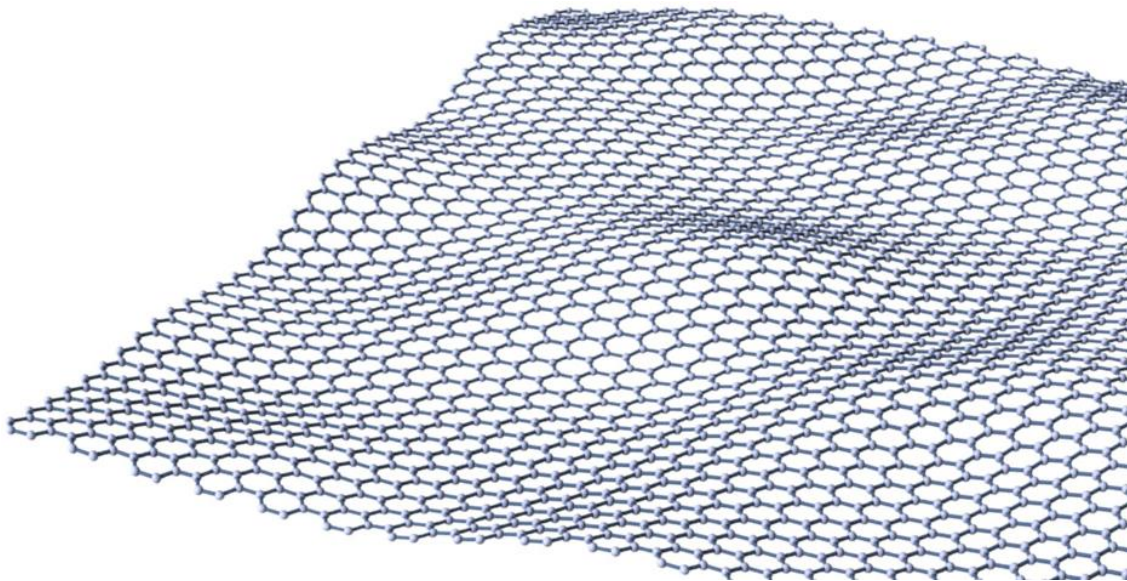


Figure 1-1: Graphical illustration of a graphene sheet.

Graphene is a half metal, also called a zero bandgap semiconductor.^[4] With its high thermal conductivities (3000-5000 W/m·K), a Young's modulus of 1 TPa and the intrinsic tensile strength of 140 GPa, graphene trumps every metal and metal alloy.^[5] Moreover, graphene

absorbs only 2.3 % of the light in the visible range qualifying it for transparent window electrodes.^[6,7]

The standard techniques for the preparation of graphene are, amongst others, the mechanical exfoliation, the reduction of graphene oxide or chemical vapor deposition (CVD). The mechanical exfoliation, also used by *Geim* and *Novoselov*, affords high quality graphene.^[8–10] However, the producible amount is rather small. The oxidation of graphite to graphene oxide (GO) followed by ultrasonic exfoliation and the subsequent reduction to reduced graphene oxide (rGO) is another common method to produce graphene. The *Hummer's* method is the most used nowadays.^[11] First, graphite is treated with concentrated sulfuric acid, sodium nitrate and potassium chlorate. After the ultrasonification and extraction with organic solvents, the resulting insulating GO needs to be thermally or chemically treated to obtain the conducting rGO.^[12,13] The production of graphene by CVD on copper foils can afford large area graphene. In the CVD process methane or acetylene gas reacts on a metal surface (iridium, platinum or ruthenium)^[14–17] at high temperatures and under ultra-high vacuum (UHV) to give graphene monolayers. The CVD process and the reduction of GO are methods applicable in an industrial production of graphene. However, the properties of graphene sensitively depend on the edge structure and all these methods produce graphene with defects, why a controlled bottom-up synthesis of graphene or rather nanographene is essential to perform fundamental research on the intrinsic properties of graphene.

Polycyclic aromatic hydrocarbons (PAHs) represent an important class of molecules in this field, containing at least two fused benzene rings. The smallest representatives in this field are naphthalene and anthracene. Since the PAHs consist only of sp^2 hybridized carbon atoms, they represent small cutouts of graphene, regarding them as nanographene. The development of larger PAHs, not naturally occurring, was pioneered by *Clar*, *Zander* and *Scholl*.^[18–21] The *Müllen* group has further driven the PAH chemistry to perfection, synthesizing super large PAHs in various shapes, like the C_{222} (Figure 1-2).^[22] The stability and reactivity of the PAHs depend on their structure. The PAHs with an all-benzenoide structure are very stable.^[23] That is why tetracene and triphenylene, both having four fused benzene rings, show a completely different reactivity. Coal, tar and oil are the natural sources of small PAHs. Also in pyrolysis processes PAHs can be formed wherefore they can be found in the atmosphere.^[24]

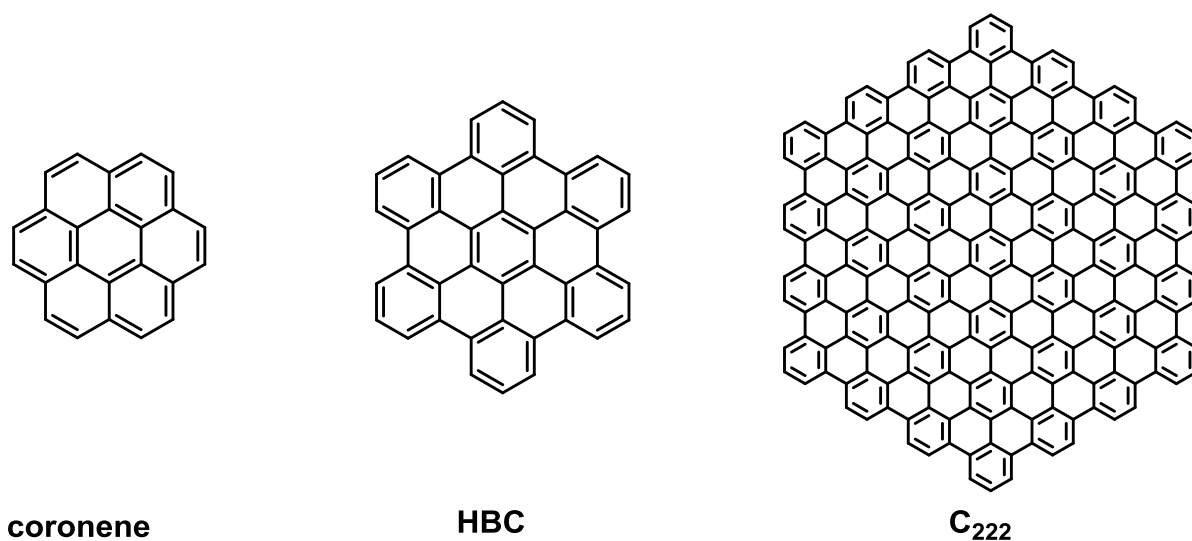
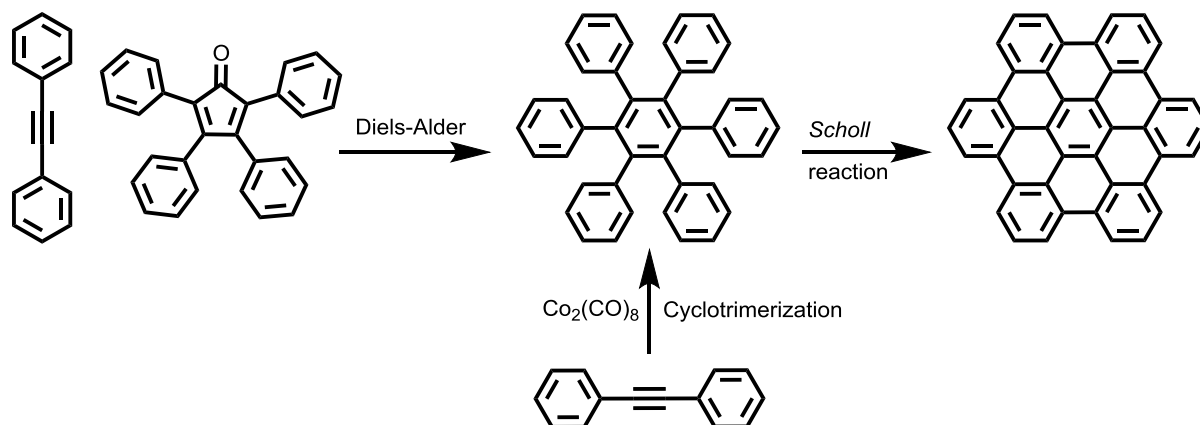


Figure 1-2: Large representatives of the class of PAHs.

Synthetically, large PAHs or nanographenes, were obtained by the oxidative cyclodehydrogenation of soluble polyphenylene precursors. The established synthetic routes are illustrated for hexa-*peri*-hexabenzocoronene (HBC) in Scheme 1-1.



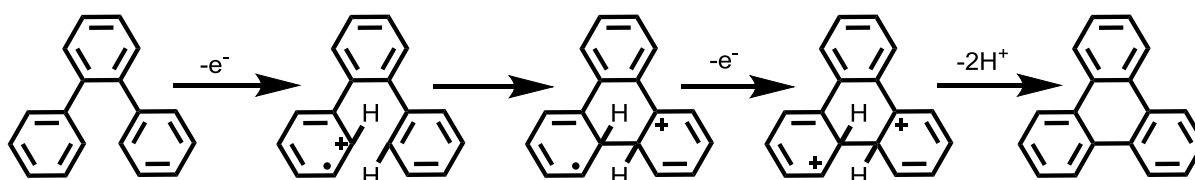
Scheme 1-1: Synthetic routes towards HBC.

There are two major synthetic routes towards the hexaphenylbenzene precursor. First, the Diels-Alder reaction, a [4+2] cycloaddition of a biphenyl tolane with a cyclopentadienone and second, the [2+2+2] cyclotrimerization of the biphenyl tolane catalyzed by a dicobalt carbonyl complex (Scheme 1-1).^[25] In the last step, the twisted and therefore soluble hexaphenylbenzene is oxidatively flattened by the intramolecular cyclodehydrogenation, the

Scholl reaction. The mechanism of the *Scholl* reaction will be discussed in the following chapter.

1.1.2. The *Scholl* Reaction

The planarization of polyphenylene precursors towards PAHs can be accomplished by chemical or photochemical oxidation, reduction or transition-metal catalysis. The oxidative aryl-aryl coupling, developed by *Scholl* in 1912, is the most established in the PAH synthesis.^[21] Two mechanisms were discussed, the radical cation and the arenium cation mechanism.^[26] The radical cation mechanism was proven and is depicted in Scheme 1-2.



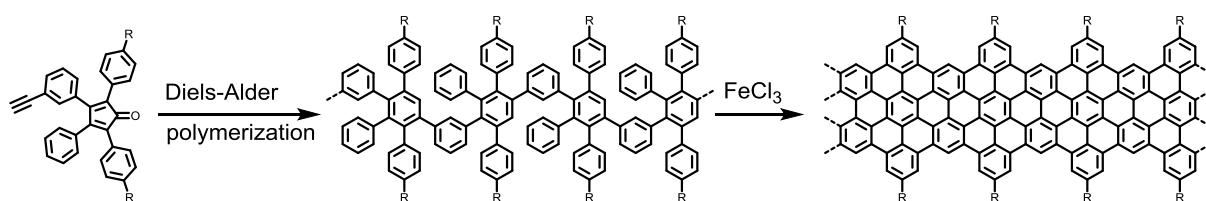
Scheme 1-2: Radical cation mechanism for the *Scholl* reaction towards triphenylene.

First, an electron transfer to the oxidant takes place, and then the aryl-aryl bond is formed, followed by a further electron transfer and the elimination of two protons. Iron chloride, acting as oxidant and *Lewis* acid, was proven to work quite well for the cyclodehydrogenation of polyphenylenes towards PAHs.^[22]

1.1.3. Graphene Nanoribbons

The major drawback of graphene is its vanishing bandgap, since the fabrication of electronic devices, like field-effect transistors, inevitably depends on semiconducting materials.^[10,27,28] However, heteroatom doping or the incorporation of structural defects can open up the bandgap of graphene. Also the limitation of the width of graphene induces a bandgap. In order to do so, the research on graphene nanoribbons (GNRs) has garnered increasing interest. GNRs are graphene stripes possessing a defined edge structure and a high aspect ratio. Both, top-down as well as bottom-up syntheses were reported. The top-down approaches include the etching of graphene and the unzipping of CNTs.^[29] However, the edge structure, which

influences the electronic properties, cannot be controlled. Therefore, several bottom-up approaches for the synthesis of GNRs were developed in our group. First, GNRs were produced by the polymerization of small molecules on surfaces in cooperation with the *Fasel* group.^[30,31] However, the transfer from a metal surface in order to process the GNRs in FETs is not easy. Therefore, the solution based synthesis of well-defined GNRs is highly desirable and was achieved by *Aki Narita*, who introduced the concept of the Diels-Alder polymerization of AB-type monomers, bearing an alkyne and cyclopentadienone unit (Scheme 1-3).^[32]



Scheme 1-3: Schematic illustration of the bottom-up synthesis of GNRs by Diels-Alder polymerization.

The polyphenylene polymer could be obtained with a high molecular weight and the subsequent cyclodehydrogenation yielded GNRs with a uniform edge structure up to 600 nm long. Due to the long alkyl chains, the GNRs were still solution processable.

1.1.4. Carbon Nanotubes

The research interest in CNTs has increased over the last decade and its success is also reflected in the increasing production capacity of several thousand tons per year.^[33] CNTs are carbon allotropes, consisting of rolled-up graphene sheets. They can be categorized as either single-walled (SWCNTs) or multi-walled CNTs (MWCNTs). *Iijima* described the synthesis of MWCNTs in 1991^[34], but unrecognized by science, the Russian scientists *Radushkevich* and *Lukyanovich* published their results on CNTs in 1952,^[35] followed by several other publications during the 1970s and 1980s.^[36-39] However, *Iijima's* work spurred the research in this field, since he also predicted the unique properties of SWCNTs. According to the chiral vector, which specifies the direction the graphene sheet was rolled-up and is indicated by the indices n and m , the structure of the CNTs can be determined. CNTs with an armchair ($n = m$), a zigzag ($n, m = 0$) or chiral (n, m) structure could be distinguished, having different lengths

and diameters (Figure 1-3). Depending on the chirality the CNTs are metallic or semiconducting, whereas all armchair CNTs are metallic.^[40]

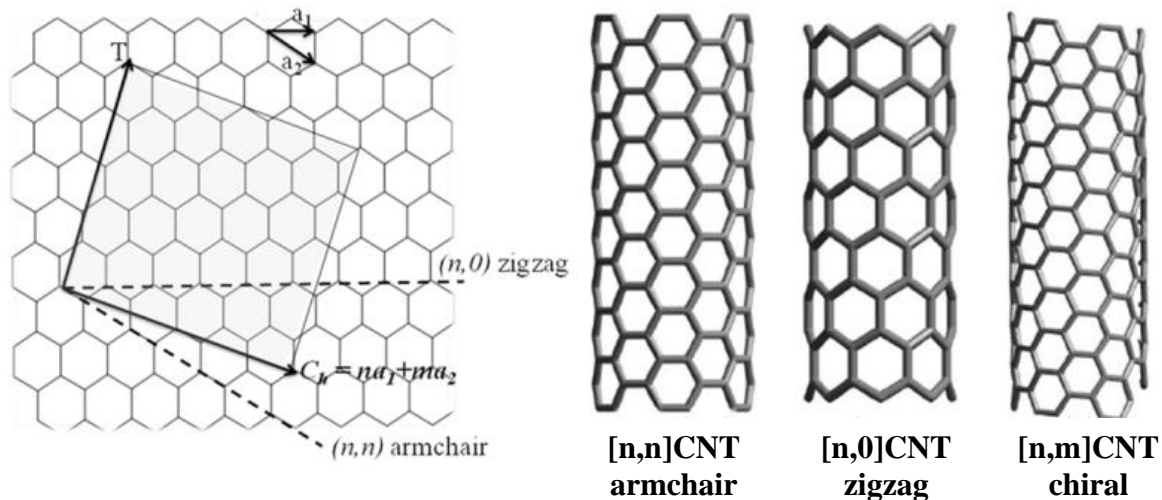


Figure 1-3: Structures of the different types of CNTs.

In small quantities, CNTs are formed in combustion processes and distributed in the environment. For large scale production, CNTs are synthesized by arc-discharge, laser ablation, plasma torch or chemical vapor deposition. The arc-discharge method produces a mixture of SWCNTs and MWCNTs by applying direct current (DC) between two graphite rods in an inert atmosphere.^[41] Smalley et. al. reported the fabrication of SWCNTs in 1995 using the laser ablation method.^[42] They found that evaporating graphite and transition metals, nickel or cobalt, by laser radiation forms high quality CNTs. However, arc-discharge and laser ablation only yield small amounts of CNTs and are very expensive methods. Producing CNTs more efficiently, the plasma torch method was developed by Smiljanic in 2000.^[43] The conditions are comparable with the arc-discharge method, but argon, ethylene gas and ferrocene are used in a microwave plasma torch. The standard method in CNT synthesis is the CVD technique, yielding high purity SWCNTs grown on metal nanoparticles.^[44] The commercially available CNTs, produced by CVD, contain up to 35% metal impurities. A further purification often causes structural defects. Therefore, a bottom-up synthesis of uniform CNTs with a defined structure and diameter is highly desirable to tune and control the properties of the respective CNTs. However, CNTs are already used in polymeric composites to dissipate elec-

trostatic charge, for electromagnetic interference shielding and as additive to increase their strength.^[33] Also, in batteries and water treatment systems, CNTs can improve the performance. The use in FETs is limited, however, because these devices require semiconducting CNTs. Despite different physical or chemical purification methods^[45], uniform CNTs with a defined diameter and chirality are needed for such sensitive applications. So far, bottom-up strategies were only considered to give armchair CNT segments. In 2008, the first successful bottom-up synthesis of cycloparaphenylenes (CPPs) was reported. The CPPs are the smallest representatives of armchair CNTs and are promising templates for the growth of structurally defined CNTs what will be discussed in the following chapters.

1.2. Cycloparaphenylenes

The smallest segments of armchair CNTs are cycloparaphenylenes CPPs (Figure 1-4). The synthesis of these macrocycles has fascinated chemists over decades. CPPs are not only the smallest segments of CNTs, but they are also envisioned to be seeds for the defined growth of monodisperse CNTs.^[46]

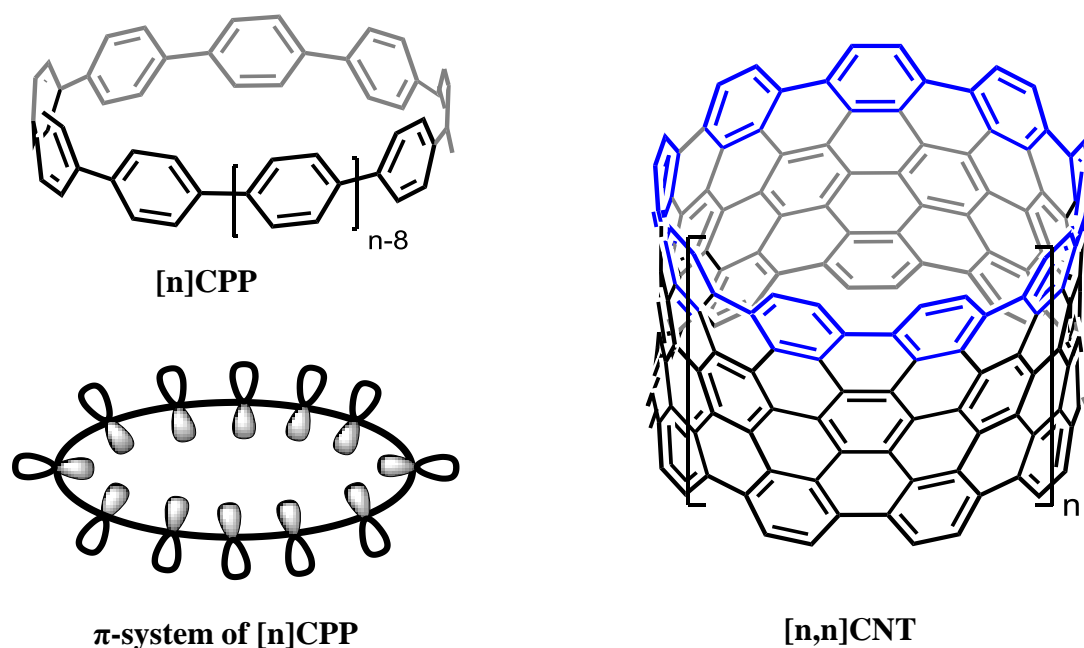


Figure 1-4: Illustration of the [n]CPPs, [n,n]CNTs and the π -system of [n]CPPs.

Besides this, CPPs have some unique properties, which are not observed in other macrocyclic systems. Different to planar macrocycles, the π -system of CPPs is bent and directed to the central axis (Figure 1-4),^[5] qualifying them for host-guest chemistry.

The synthetic challenge started in 1934 with the suggested synthetic route by the Pioneers *Parekh* and *Guha*, which believed to have accomplished [2]CPP.^[47] However, in the early 90s, the interest in the CPP synthesis was renewed by the work of *Vögtle*.^[48] Unfortunately, their supposed synthetic routes and precursors did not result in CPPs. A few years later, *Herges* et. al. dimerized the strained tetrahydrodianthracene to successfully obtain a “picotube”, which contains a central [4]CPP ring.^[49] The oxidative dehydrogenation to obtain the [4,4]CNT segment failed and simultaneously spurred research to develop routes to access

larger, less strained CPPs. The breakthrough started in 2008 with the first bottom-up synthesis of CPPs by *Jasti* and *Bertozzi*,^[50] followed by *Itami*^[51] and *Yamago*.^[52] The key point for these successful synthetic pathways was the design of precursors inducing curvature and therefore, facilitating a macrocyclic fusion. The different approaches are visualized in Figure 1-5. *Jasti* et. al. developed a kinked precursor, based on *cis*-1,4-substituted cyclohexa-2,5-dienes, which was cyclized under *Suzuki* conditions to yield cycles with up to six kinked units. After the aromatization with sodium naphthalenide, CPPs with circumferences of 9-, 12- and 18-phenylene rings were obtained (Figure 1-5). The group of *Itami* refined the protocol suggested by *Vögtle* using 1,4-substituted cyclohexane. Finally, a completely different approach was presented in 2010 by *Yamago*, who adapted the organometallic approach developed by *Bäuerle* et. al. for the synthesis of cyclo[n]thiophenes.^[53] With this approach, linear and rigid precursors could be assembled in a macrocycle *via* platinum(II) complexes, which provide the perfect biting angle. Additional to these groundbreaking strategies, a recently published work by *Wang* et. al. presented the synthesis of the kinked precursor by a Diels-Alder reaction of a butadiene derivative and benzoquinone, which also resulted in a strained CPP after cyclization and oxidative dehydrogenation.^[54]

With the recently published [5]CPP by *Yamago* and *Jasti*, synthetic protocols for a multitude of CPPs with different sizes, up to [18]CPP, are readily available.^[55,56]

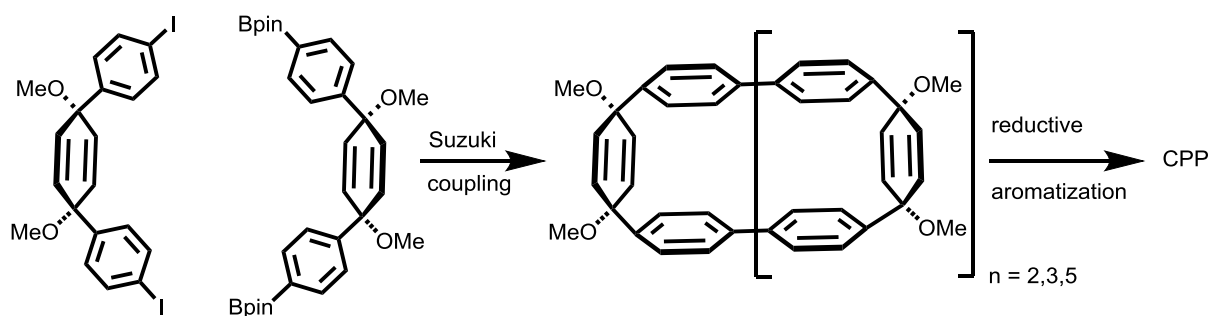
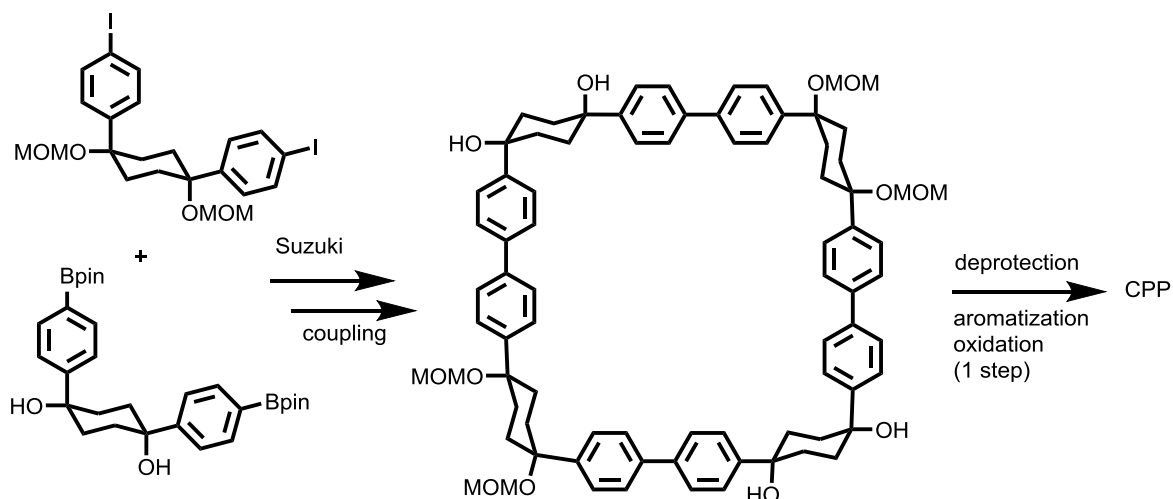
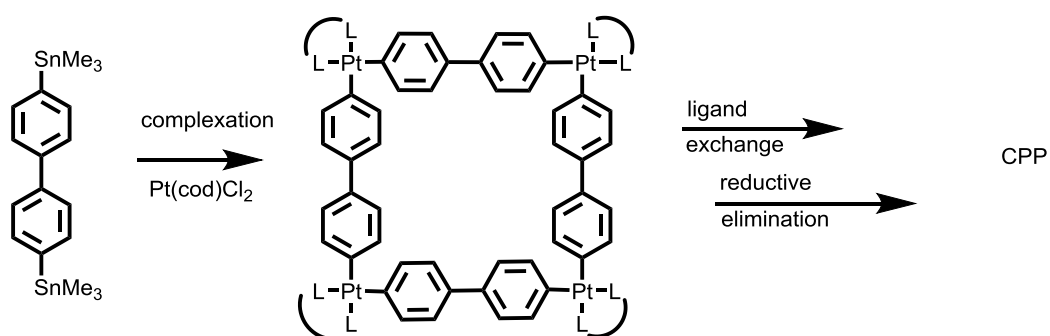
Jasti, Bertozzi et. al. (2008)**Itami et. al. (2009)****Yamago et. al. (2010)**

Figure 1-5: Synthetic pathways for the synthesis of CPPs.

Furthermore, Isobe et. al. introduced chiral segments of CNTs, based on chrysene ([4]CC_{2,8}, [4]CC_{3,9}) and anthanthrene ([4]CA_{2,8}) moieties (Figure 1-6), the latter combining armchair and helical structures.^[57-60] The synthetic strategy was based on the route of *Yamago*. The incorporation of naphthalene by *Itami* yielded a chiral segment of an [15,14]CNT.^[58]

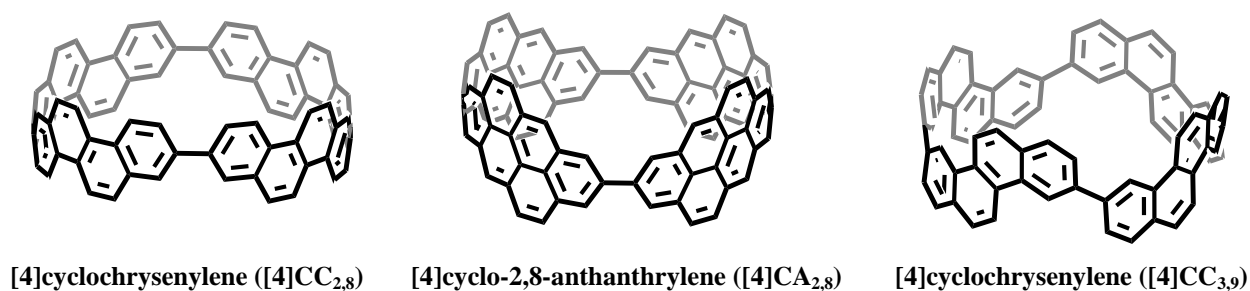


Figure 1-6: Illustration of [4]CC_{2,8}, [4]CA_{2,8} and [4]CC_{3,9}, representing chiral CNT segments.

Besides the classical CPPs and CNT segments, the incorporation of hetero atoms as well as heteroaromatic units is envisioned to be a promising way to tune the unique properties of CPPs and to create new functionalized organic materials.

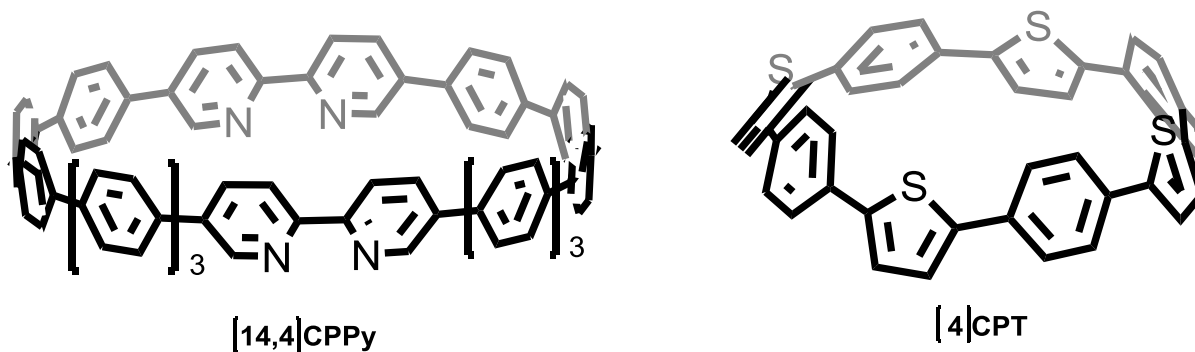


Figure 1-7: Illustration of [14,4]CPPy and [4]CPT.

In 2012, *Itami* reported the synthesis of cyclo[14]paraphenylene[4]2,5-pyridylidene ([14,4]CPPy), which contains two 2,2'-bipyridine units (Figure 1-7).^[61] Recently, the synthesis of cyclo-1,4-phenylene-2',5'-thienylenes (CPTs), a CPP with alternating phenylene and thiophene units, bearing unique structural and optical properties, was published by the same

group.^[62] However, the longitudinal extension of CPPs towards CNTs remains the hidden goal in this field.

1.3. From Cycloparaphenylenes to Carbon Nanotubes

In the last years the research in the field of CPPs was rapidly growing. CPPs of various sizes as well as with different functionalities were reported. Their unique photophysical and host guest properties were investigated in numerous studies.^[63–71] One of the original ideas, the solution based bottom-up synthesis of CNTs from CPPs, still remains challenging. So far, CPPs were deposited on sapphire surfaces to grow nanotubes with a narrow diameter distribution.^[46] However, the precise structure control resulting in monodisperse CNTs is highly desirable for the use in electronic applications.

An essential requirement to realize this goal is the longitudinal extension of CPPs towards ultrashort CNTs. The group of *Scott* showed that for a defined growth of CNTs by repetitive Diels-Alder reactions, larger π -sidewalls are needed to decrease the energy barrier.^[72] Although not achieved yet, a variety of approaches towards ultrashort CNTs were reported in literature.

The groups of *Jasti* and *Itami* showed that functionalized CPPs could be fused to dimers (Figure 1-8).^[73,74] Further, *Yamago* synthesized [4]cyclo-2,7-pyrenylene, increasing the π -system in the CPP.^[75] The *Müllen* group published a polyarylated CPP ([3]CHPB) in order to form large graphitic sidewalls by oxidative cyclodehydrogenation.^[76] The [9]cyclo-1,4-naphthylene resisted to undergo a cyclodehydrogenation, since the naphthalene units are twisted. Therefore, new strategies are needed to form fully conjugated phenylene cylinders. The goal of this work is to develop new ways to overcome these limitations and to approach the bottom-up synthesis of CNT segments.

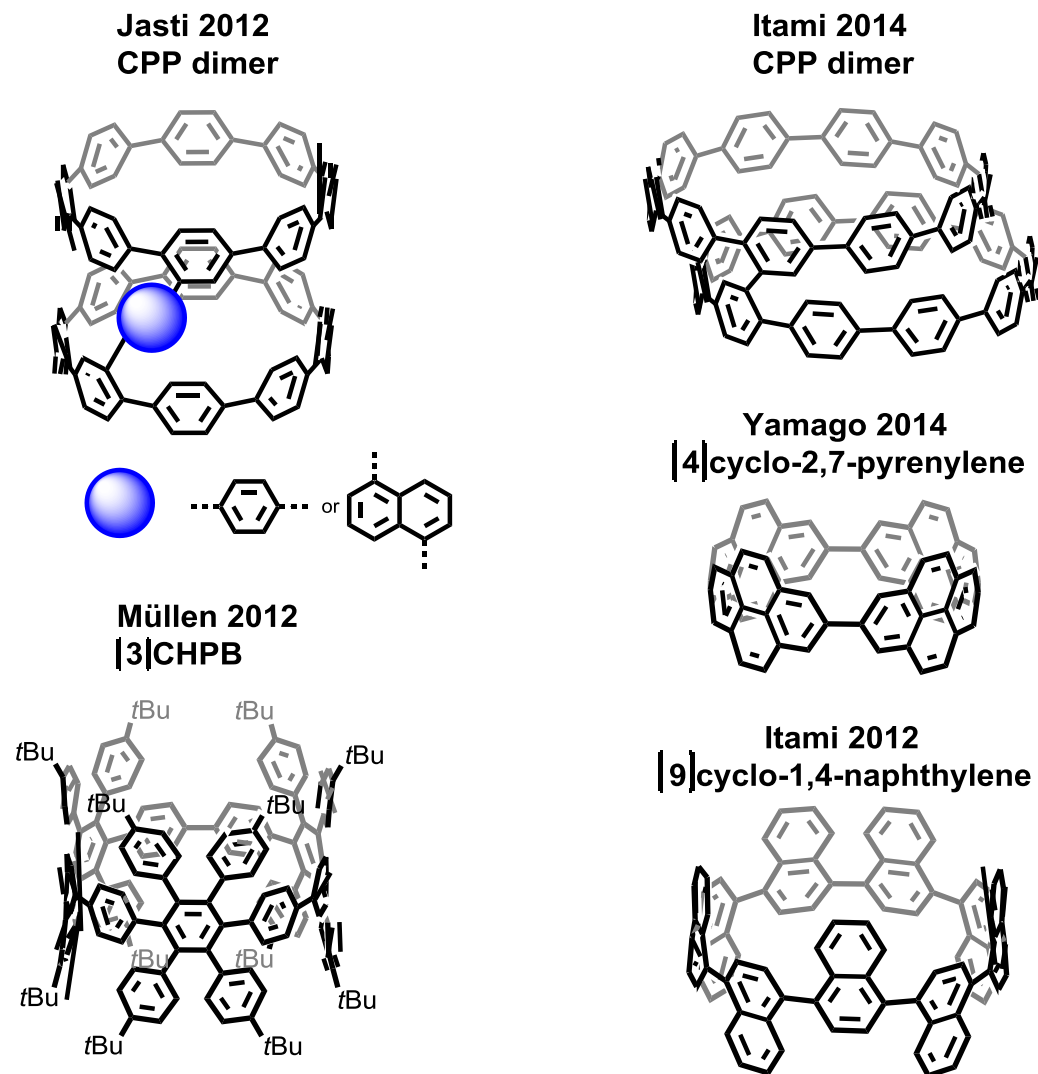


Figure 1-8: Different CNT segment derivatives.

1.4. Macrocyclic N₄-Metal Complexes

1.4.1. The Fuel Cell – Types and Fundamental Principles

The world's energy consumption and needs are rapidly growing, supposable being one third higher in the year 2035 (Figure 1-9). Concurrently, the supply with fossil fuels becomes more and more instable, as fossil fuels have anyway a finite nature. Therefore, intensive research has been done to find alternatives in energy conversion.^[77] The transition of the energy system towards a hydrogen economy is appealing, since automotive and stationary applications can be operated with hydrogen as fuel, only producing heat and water as emissions.^[78] The key device in this system is the fuel cell that converts chemical energy into electricity without combustion, using an oxidizing agent, usually oxygen from the air.^[79] There are several different types of fuel cells, having all the same working principle, which is schematically, depicted in Figure 1-10, for the most considered one, the polymeric-electrolyte-membrane fuel cell (PEMFC) operated with hydrogen and oxygen.

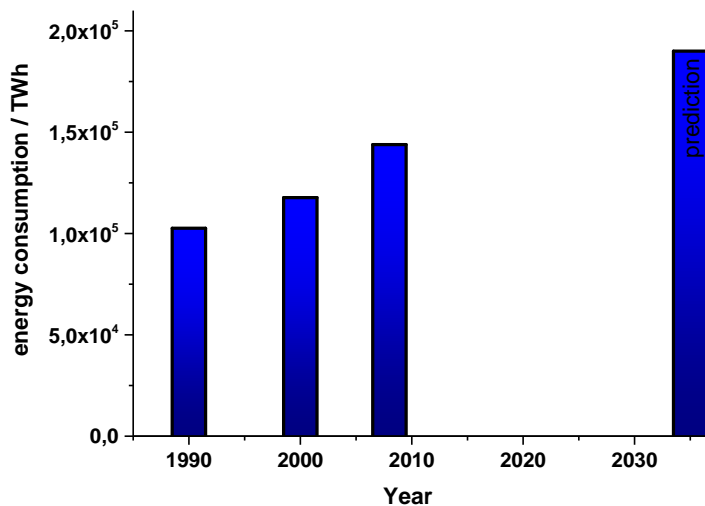


Figure 1-9: World energy consumption in terra Watt hours (TWh) (Data from the IEA, World Energy Outlook).

The PEM fuel cell contains two electrodes, the anode and cathode, each coated with a catalyst, usually platinum. The two electrodes are separated by the electrolyte membrane, which is

commonly Nafion (by Dupont). The technical entity, comprising catalyst, membrane and electrodes is called membrane electrode assembly (MEA).

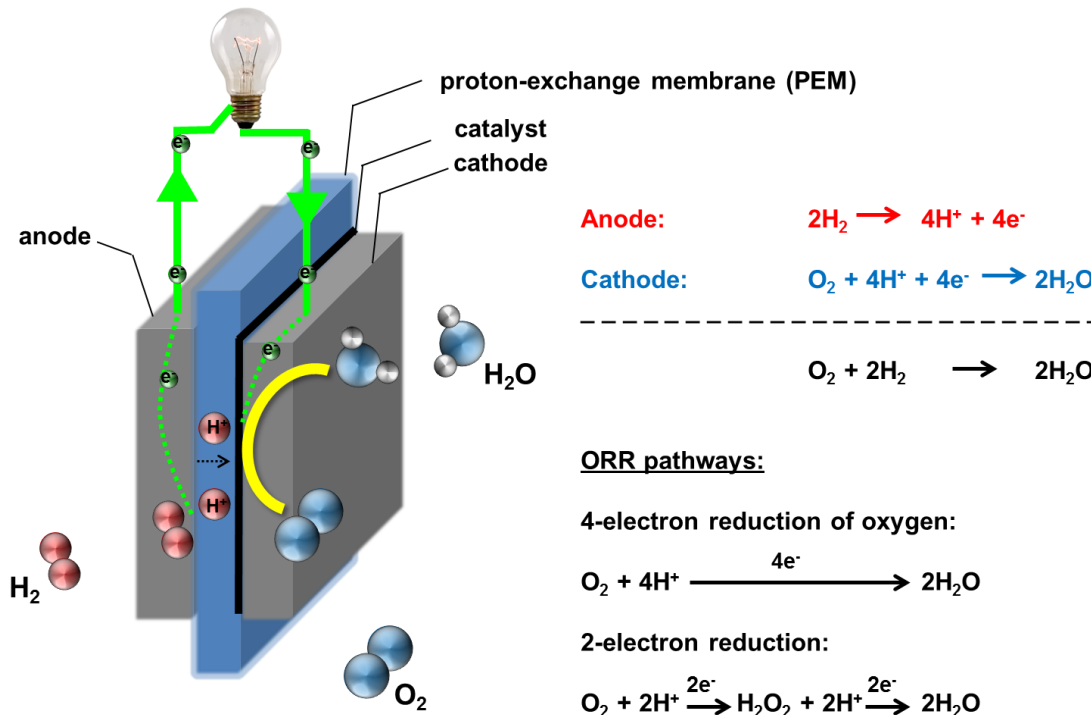


Figure 1-10: Schematic illustration of a fuel cell and the ORR pathways.

At the anode, hydrogen molecules are oxidized, resulting in two protons and two electrons. The electrons cannot pass the membrane, hence, creating a current in an external circuit. The protons pass the electrolyte membrane, forming water with the reduced oxygen at the cathode, as well as heat. There are two major pathways for the cathodic oxygen reduction reaction (ORR). The direct four-electron reduction transforms oxygen into two equivalents of water, while the two-electron pathway produces hydrogen peroxide (Figure 1-10). Hydrogen peroxide can cause serious damages of the internal components, resulting in a shorter cell lifetime. Thus, electrocatalysts are designed to minimize the amount of hydrogen peroxide.

The advantages of the PEMFCs are the low working temperature of $\sim 80\text{ }^\circ\text{C}$ and a fast start-up, which qualifies the PEMFC for future automotive applications.^[78,80] Besides the PEMFC, alkaline (AFC) and phosphoric-acid fuel cells (PAFC) are interesting for certain applications. The operating temperature of those is $135 - 200\text{ }^\circ\text{C}$, slightly higher than in PEMFCs. In the

Apollo space missions and in submarines, AFCs were applied. However, the corrosive electrolytes potassium hydroxide and phosphoric acid, as well as the low tolerance against carbon monoxide limit the lifetime and applicability of these cells. For stationary applications in power plants, high temperature fuel cells, like molten-carbonate fuel cells (MCFC) or solid-oxide fuel cells (SOFC) can be used. Due to the high temperatures of 500 to 1000 °C non-precious metals can be used as catalysts and carbon monoxide can be directly electrochemically oxidized at the anode together with hydrogen.^[81]

Despite the need of new energy conversion techniques to limit the global warming, due to the increase of greenhouse gas emissions, the introduction of a hydrogen economy faces several problems.^[77] Hydrogen is an energy carrier, but must be produced, using primary energy.^[82] The fossil-fuel based steam-reforming process is the cheapest method to produce hydrogen on a big scale.^[77,83] However, the growing renewable energy sources, such as water-, wind- and solar-energy, change the situation nowadays. Hydrogen from renewable energy is supposed to play an important role in the change of the energy system, since the fluctuating renewable energy can be stored by water electrolysis and several other methods.^[84] Therefore, the existing fuel cells have to be improved in terms of new ion conduction membranes, bipolar plates, cell frames and especially low cost and insensitive electrocatalysts.^[77] Particularly oxidation of the cathode catalyst, poisoning of the catalyst by impurities and side products, as well as the loss of active sites are major drawbacks.^[85] The scarce and expensive platinum, which is commonly used in fuel cells, has to be replaced for a commercial launch of the fuel cell technology. First improvements were done by alloying Pt with non-noble metals and the use of Pt-nanoparticles.^[86,87] Another approach is the replacement of platinum by metal-free and non-precious metal catalysts (NPMCs). The latter mainly consist of a non-precious metal centre (e.g. Fe, Co, Mn), surrounded by a N₄-environment. The N₄-motif can be formed by macrocycles, such as porphyrins and phthalocyanines^[88] or by the pyrolysis of nitrogen compounds, a carbon support and non-precious metal salts.^[89] Supported on a conductive material, like carbon black, these NPMCs have attracted considerable attention in the replacement of platinum as cathodic electrocatalyst in the ORR.^[90] The recent developments in this field will be shortly summarized in the following chapter 1.4.2.

1.4.2. Metallo Macrocycles for ORR

Contemporary fuel cells utilize platinum as electrocatalyst, because of its good performance in ORR. However, platinum is scarce, expensive and its supply is instable, since it is only mined in South Africa, Russia and North America. Therefore, the search for an alternative catalyst system, especially for the cathodic reduction of oxygen is of great interest. In nature, the most sophisticated fuel cell, the *cytochrome c oxidase*, is part of every mammal. This integral membrane protein contains, amongst others, the porphyrin based iron macrocyclic complexes heme a (**1-1**) and heme a₃ (Figure 1-11). Together with the two copper centers Cu_A and Cu_B, the *cytochrome c oxidase* efficiently catalyzes the direct four-electron reduction of oxygen to water.^[90]

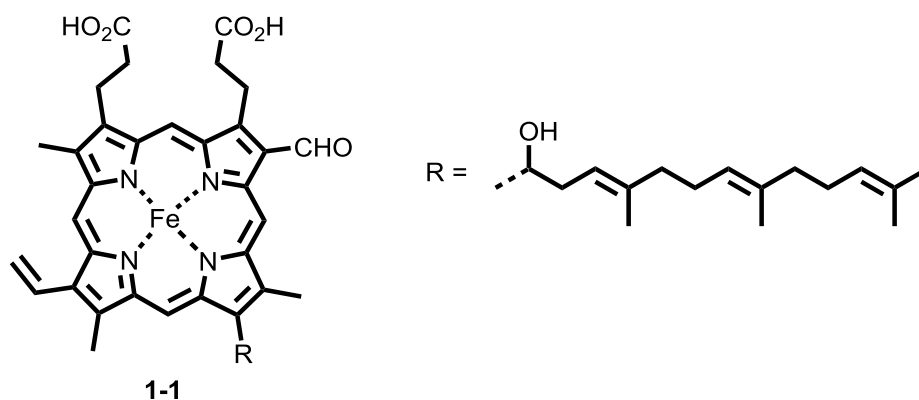


Figure 1-11: Structure of the heme a **1-1**

The structure of these naturally occurring metalloporphyrins inspired chemists to mimic these complexes for electrocatalysis. Finally, it was the discovery of the electrocatalytic activity of cobalt phthalocyanine towards ORR in 1964 by *Jasinski et. al.*, which initiated further research in ORR active N₄-metallo macrocyclic catalyst systems.^[91] Not only the low costs of NPMCs are appealing, but also the high tolerance of these catalysts against methanol. This facilitates the application in methanol fuel cells. The N₄-metal complexes are usually supported on a conductive material, like graphite or carbon black. Functional groups on the carbon surface can also enhance the stability of the complex, since they act as a fifth ligand. The activity of the complex is in close relation to the redox potential of the metals in the

M(III)/M(II) state. In contrast to a normal redox catalysis mechanism, higher activities were observed for redox pairs with a more positive redox potential. The metal ion, in its oxidation state M(II), is the active site for the O₂ binding.^[91] Besides the activity, the long-term stability is an important issue for the application of the electrocatalyst in the fuel cell. This is a critical issue for the N₄-metallo macrocyclic complexes, supported on a carbonaceous material. Hence, these materials were heat pre-treated at temperatures of 600 °C to 800 °C, resulting in a stability and activity increase.^[92] However, new structures were formed during the heat treatment and the structural information of the active site was lost. It is believed that still MN₄-motifs with different coordination spheres exist, but there is no structural uniformity present.^[93] Due to this, a precise analysis of the structure-property relationship is still challenging.

Even so, fundamental studies and newly designed complexes further closed the gap between the established catalyst platinum and the NPMCs, some already outperformed platinum.^[94] The direct four-electron reduction of oxygen to water is the key request for all new NPMCs. As already described in chapter 1.4.1, the competing two-electron reduction causes the damaging evolution of hydrogen peroxide. The dominance of either one or the other reduction pathway sensitively depends on the structure of the ligand and the nature of the metal center. Initially, the metal complexes of phthalocyanines and porphyrins were investigated. It was proven that iron and cobalt metal centers are by far the most active ones towards the ORR.^[95]

2-Electron Pathway Catalysts

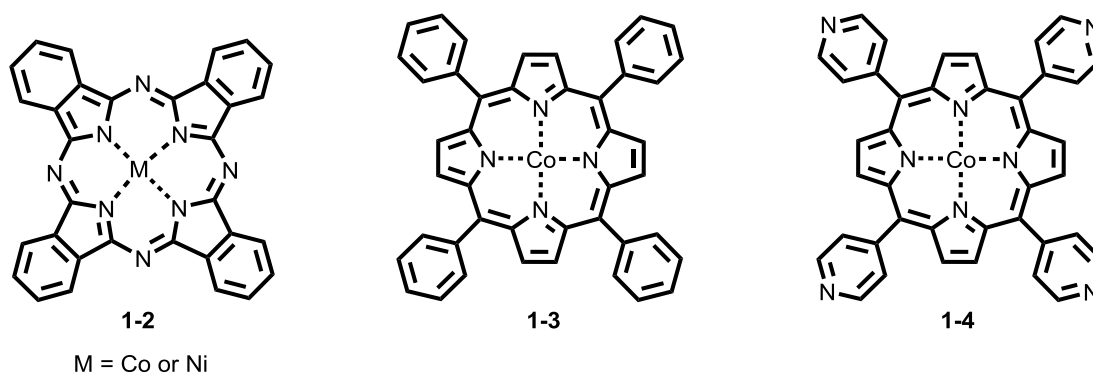


Figure 1-12: Examples of NPMCs, catalyzing the two-electron reduction of oxygen.

Cobalt or nickel phthalocyanines (**1-2**) and most of the cobalt porphyrins (**1-3**, **1-4**) only support the two-electron reduction pathway (Figure 1-12), whereas some of the respective iron analogues (**1-5**) directly reduce oxygen to water (Figure 1-13).^[96] The introduction of substituents in the periphery of the ligand, which increase an electron back-bonding, can turn a two-electron catalyst into a four-electron one.^[97] The structure of the complex **1-6** is an example for this electronic effect.

4-Electron Pathway Catalysts

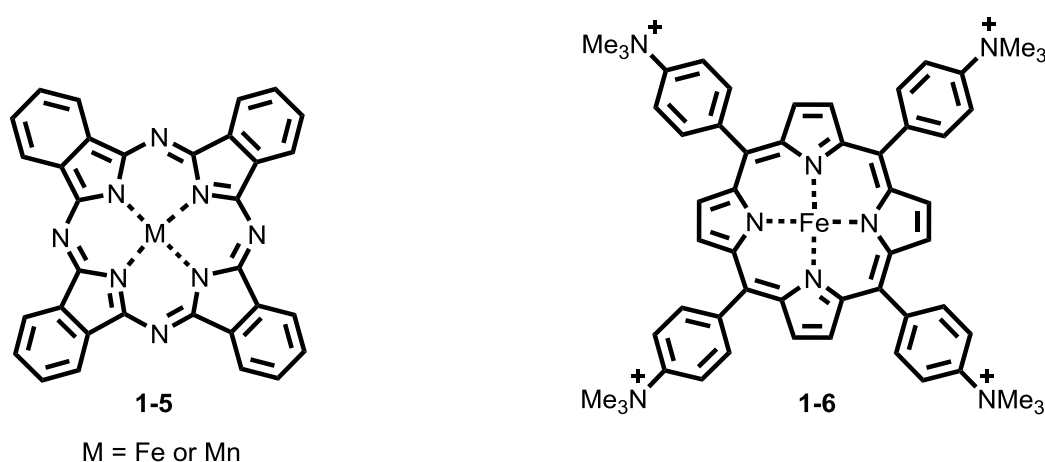


Figure 1-13: Examples of NPMCs, catalyzing the four-electron reduction of oxygen.

A further aspect in the ORR is the way oxygen interacts with the metal center, finally resulting in the oxygen bond rupture. The O_2 molecule can interact with the metal center of the metallo macrocycles in four distinguished binding modes (Figure 1-14), one-sided (end-on or side-on) or two-sided (bridge-*cis* or bridge-*trans*).

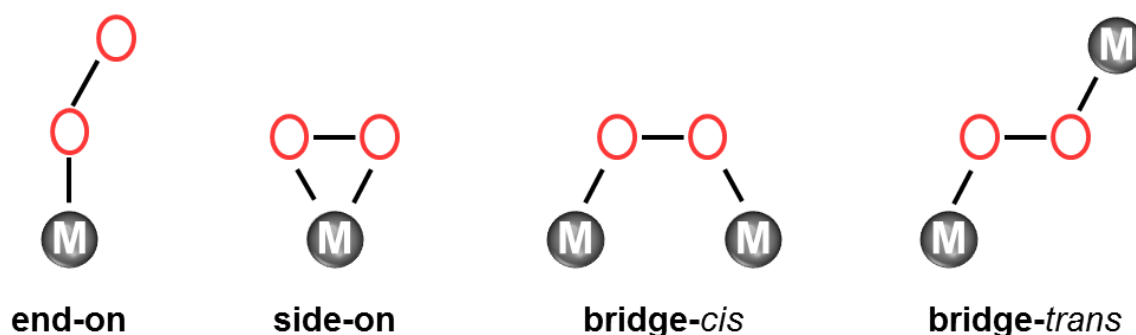


Figure 1-14: Illustration of the different oxygen binding modes.

Since the interatomic distance in platinum is optimal for a two-sided bridge-*cis* interaction, it was suggested that this is the dominant binding mode. Therefore, bi- and multinuclear metal complexes were designed to enable the two-sided binding modes and to promote the direct four-electron reduction pathway. Two different approaches were developed in the different research groups. On the one hand, cofacial metalloporphyrins (**1-7** and **1-8**) were established by *Chang* and *Collman* in the early 1980s.^[98–102] These so called Pacman porphyrins

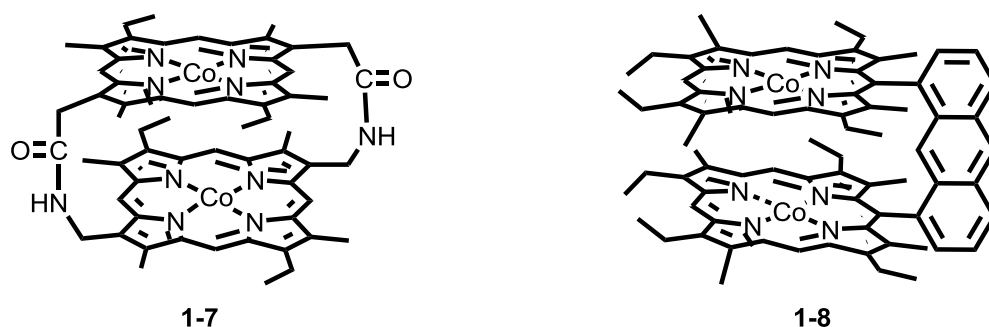


Figure 1-15: Cofacial metalloporphyrins as example for binuclear complexes.

have an Co-Co distance of 4.1 Å, providing a perfect cavity for oxygen to coordinate in a bridge-*trans* mode. In acidic media, a four-electron reduction was observed.^[100] On the other hand, planar multinuclear complexes were developed to mimic the bridge-*cis* binding of O₂ for platinum catalysts (Figure 1-16).^[94,103]

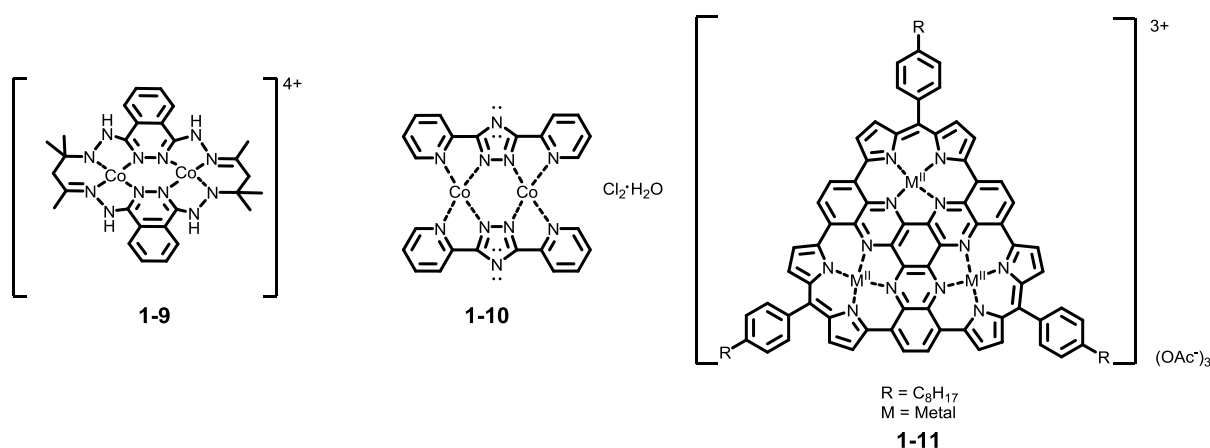


Figure 1-16: Planar, multinuclear catalysts for the cathodic ORR.

The catalysts **1-9** to **1-11** promote the direct four-electron reduction in alkaline media and a bridge-*cis* geometry for the O₂ interaction is suggested.^[94,103] It is worth mentioning that the catalysts **1-9** and **1-10** suffer from instability, whereas the trinuclear catalyst **1-11**, developed in the *Müllen* group, showed a superior long-term stability and an ORR performance, comparable to the Pt-catalyst.^[94] Moreover, **1-11** showed a high activity towards ORR, without any heat pre-treatment. With the increasing research on graphene, the field of heteroatom doped graphene materials as metal-free catalysts developed and is still growing.^[104–106]

Although, many connotatively efforts have been made in the field of NPMCs, increasing the activity and stability by heat-pretreatment,^[107] ligand functionalization and the design of novel ligands, the wide range applicability in alkaline and acidic media as well as the use as cathodic and anodic catalyst is still challenging. Furthermore, little attention has been given to the design of active and stable NPMCs, without the need of any heat-pretreatment. This work aims for NPMCs overcoming these problems what will be discussed in detail in chapter 5.

The rotating disk electrode (RDE) and the rotating ring disk electrode (RRDE) techniques are the most important instruments in the characterization of novel ORR catalysts. The fundamental principle of these tools will be introduced in the following chapter 1.4.3.

1.4.3. Rotating Disk- and Rotating Ring Disk Electrode

Electrocatalytic reactions, such as the ORR, can be studied by rotating disk voltammetry. The standard three electrode setup contains a disk as working electrode, made of glassy carbon (GC) or a noble metal, a counter electrode and a reference electrode (e.g. Ag/AgCl). This is the same assembly as for the rotating ring disk electrode (RRDE) depicted in Figure 1-17, applying no potential to the Pt-ring. The water insoluble catalyst is deposited on the disk before the electrode is doused into the electrolyte solution. Due to the rotation of the disk electrode a constant flow of reactants is brought to the catalyst. However, the detection of the products is not possible. The RDE voltammograms give information about the reactivity of the catalyst, since the on-set and the half-wave potential can be detected. Also the selectivity can be determined, constructing Koutecky-Levich plots. A different technique to gain further

information about the selectivity of the catalyst is the RRDE technique, which was proven to be an efficient tool to study electrochemical reactions, like the ORR. The method was first described by *Frumkin* and *Nekrasov* in the late 1950s.^[108]

The RRDE setup consists of two electrodes, an inner disk electrode and an outer ring electrode. The electrodes are separated by an insulating layer (Figure 1-17). The rotation axis is perpendicular to the ring's surface. Due to the rotation, the products formed at the disk electrode are swept away towards the ring electrode, where those can be detected. Therefore, a bipotentiostat is commonly used to measure the disk and the ring current. The current at the ring electrode is measured at a given potential, giving information about the production rate of specific products of the disk electrode.

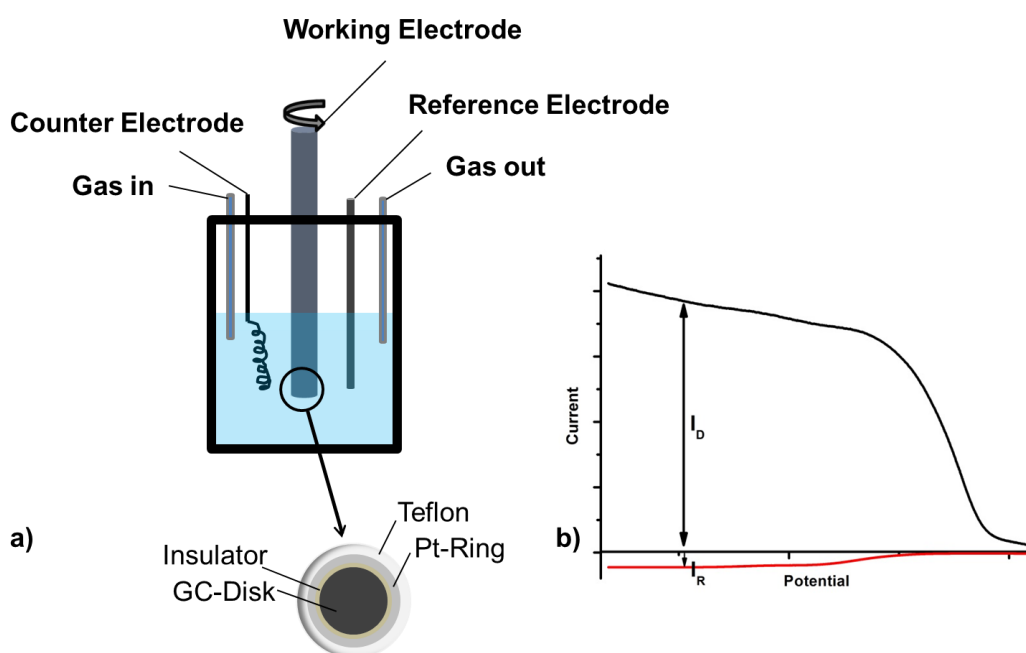


Figure 1-17: a) Schematic illustration of the RRDE setup; b) Ring-Disk Voltammogram

In terms of the ORR, the RRDE technique allows the determination of the average electron transfer number n . Hence, the ORR pathways, i.e. the ratio of the 4-electron to 2-electron reduction, can be determined by detecting the developed hydrogen peroxide at the ring electrode. The ratio of the ring- (I_R) and disk-current (I_D) gives the average number of transferred

electrons n , since the collection efficiency N is known for the ring electrode. This is illustrated in Figure 1-17 and equation ((1-1).

$$n = \frac{4I_D}{\left(I_D + \frac{I_R}{N}\right)} \quad (1-1)$$

The percentage of the developed hydrogen peroxide can be estimated from equation (1-2).

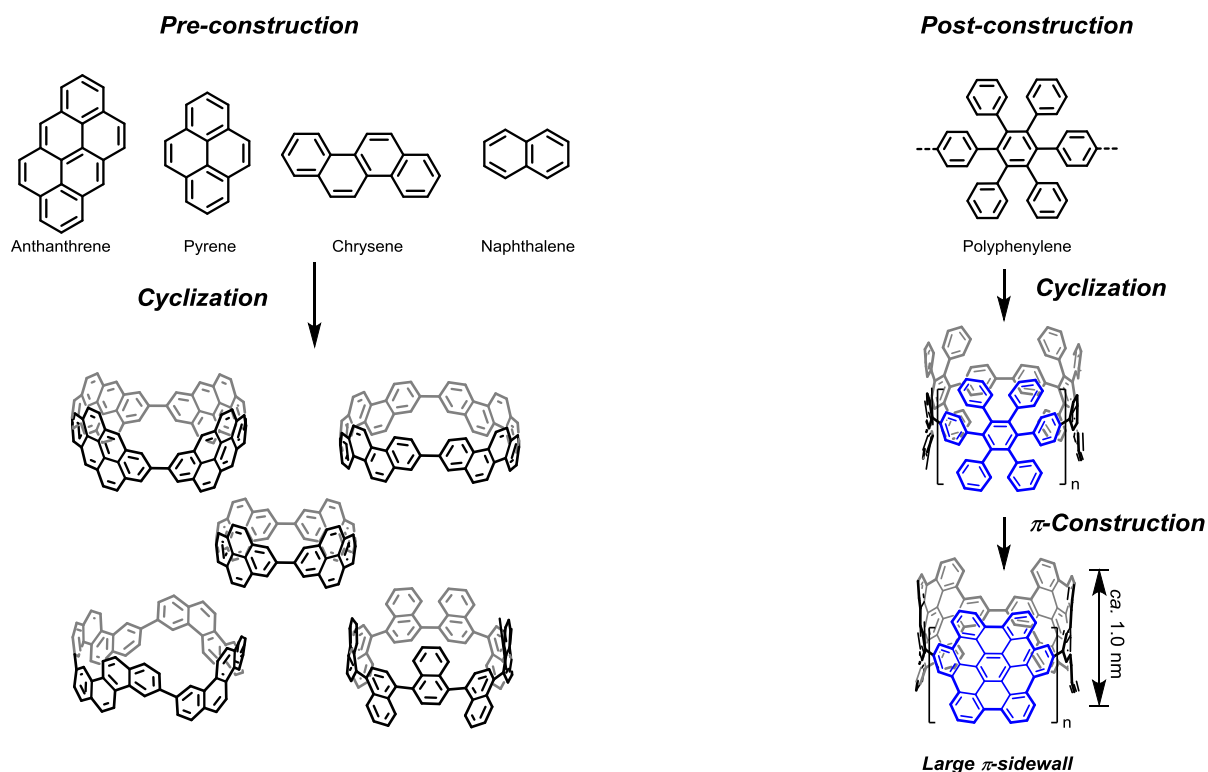
$$\%H_2O_2 = \frac{100(4 - n)}{2} \quad (1-2)$$

2. Motivation and Objectives

The variety of organic building blocks and the almost infinite toolbox of coupling- and transformation reactions^[109,110] enable organic chemists to develop new, lighter or cheaper materials for construction and energy applications. In this regard, graphenic materials have garnered increasing interest. Besides graphene, carbon nanotubes (CNTs) are supposed to positively affect material properties and play an important role as semiconductors. Furthermore, for an effective and low-cost energy conversion new catalysts are required. Therefore this work covers two topics separately, the bottom-up approach towards length- and diameter-defined carbon nanotube segments and the synthesis of non-precious metal catalysts (NPMCs) for the oxygen reduction in fuel cells, based on N₄-macrocyclic ligands.

In the chapters 3 and 4 new synthetic approaches towards the bottom-up synthesis of CNTs will be covered. Carbon nanotubes have received increasing interest in science and engineering, due to their unique properties. Not only their outstanding strength,^[111] but also their electronic properties are promising for future nanotechnology applications.^[33,112] Different ways have been exploited to synthesize CNTs, the first reported in 1991 by Iijima.^[34] The big scale production by, amongst others, arc discharge, chemical vapor deposition, laser ablation and ball milling yield polydisperse tubes, which need further separation and purification.^[113] Besides the costs and complexity for the purification, the polydispersity has dramatic influences on the electronic properties, since they sensitively depend on the chirality of the CNTs. Therefore, bottom-up approaches are highly desirable to synthesize CNTs with precise diameter- and structure-control to gain further insights into the structure-property relationship. First attempts and successful syntheses have been performed, using PAH precursors, opened C₆₀ or other suitable bowl-shaped precursors, growing uniform CNTs from metal surfaces.^[114,115] Recently, the *Fasel* group reported the successful synthesis of [6,6]-CNTs on a platinum surface.^[116] However, the further processability and the metal impurities remain a problem. Therefore, solution based methods are more favored in this context. A promising route was suggested by the group of *Scott*, in which a bowl shaped CNT endcap was formed in order to

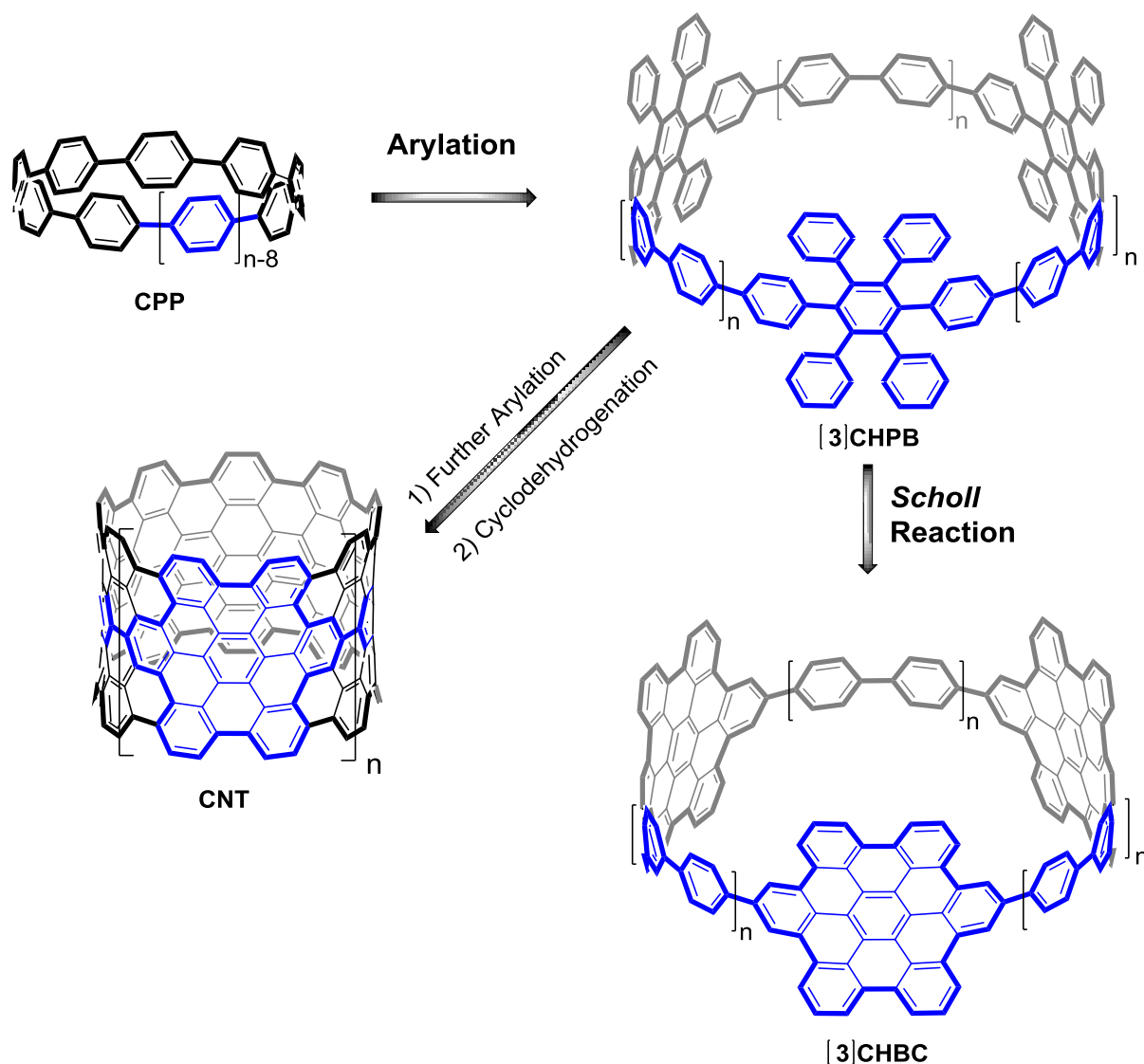
grow CNTs from it by repetitive Diels-Alder reactions.^[72,117] So far, the energy barrier for this route is too high to selectively grow CNTs. Besides this, the solution based bottom-up synthesis of ultrashort CNTs has gained a renewed interest since the successful synthesis of CPPs in 2008, which are the smallest segments of armchair CNTs.^[50–52,55–57,59,60,75,118–127] However, the central issue of a longitudinal extension or selective growth towards tubes remains unsolved, even if first attempts showed that a growth from CPPs on metal surfaces yields tubes with a narrow diameter distribution.^[46] Therefore, the prior longitudinal extension of the CPPs towards ultrashort CNTs is the challenge in this field. One approach, the pre-construction method, is to arrange naphthalene, chrysene, anthanthrene or pyrene building blocks, comprising a larger π -system, in a macrocycle (Scheme 2-1).^[57,59,60,118,121] However, this approach is limited, due to the difficulty of creating fully conjugated CNT segments and the challenging synthesis of the respective precursors. It is a well-established method in the PAH synthesis of nanographenes (NGs)^[128–132] and graphene nanoribbons (GNRs)^[32,133–136] to use soluble polyphenylene precursors and to perform the planarization in the last step by oxidative cyclodehydrogenation. The main objective in the first part of this work is the adaption of this concept, the post-construction method, for the synthesis of polyarylated CPPs, which will be converted into CNT segments by oxidative cyclodehydrogenation. This method will be introduced in detail in the chapters 3.2.3 and 4.2.3 (Scheme 2-1). In this context two major questions are raised. Initially, how to arrange the linear polyphenylene building blocks in a macrocycle and second, will it be possible to form large π -sidewalls by oxidative cyclodehydrogenation in a cyclic and strained system? The introduction of curvature can be accomplished on different synthetic routes. The formation of five-, seven-, and eight-membered rings, forming bent arenes, leads to non-planarity.^[137–141] In the CPP synthesis the preparation of kinked molecules was established by using cyclohexane, platinum complexes or 1,4-substituted cyclohexa-2,5-diene building blocks, which provide a certain angle.^[50,127,142] Since the longitudinal extension of CPPs by suitable polyphenylene precursors is the main issue, a polyarylated 1,4-substituted cyclohexa-2,5-diene was chosen as the initial building block. The cyclization was accomplished under *Yamamoto* conditions in a one-step procedure to yield phenylene-extended *cyclo-4',4'''-p*-hexaphenylbenzenes ([3]CHPBs; Scheme 2-2).



Scheme 2-1: Schematic illustration of the pre- and post-construction concept.

These macrocycles comprise three hexaphenylbenzene units, which can be transformed to hexa-*peri*-hexabenzocoronenes by the *Scholl* reaction. In the following, a systematic study of the cyclodehydrogenation of the different [3]CHPBs towards *cyclo-para-hexa-peri-hexabenzocoronene* derivatives ([3]CHBCs) will be covered (Scheme 2-2). Therefore, different ring sizes will be investigated in chapter 3 and additionally, the substitution pattern will be varied in chapter 4 to facilitate a smooth and selective cyclodehydrogenation.

The two chapters will contain all synthetic procedures and the characterization of this new class of molecules, as well as their electronic properties. The results presented herein will be important on the way to the precise bottom-up synthesis of CNTs, because this work covers the influence of strained systems on the cyclodehydrogenation. This in turn helps to design polyphenylene cylinders, sufficient in size and with the right connectivity of benzene rings, to selectively transform these cylinders into ultrashort CNTs (Scheme 2-2).



Scheme 2-2: Schematic illustration of the extension of CPPs towards CNTs via [3]CHPBs and [3]CHBCs.

In terms of the increasing energy consumption new catalysts are required for a low-cost energy conversion. In the first part, a synthetic route towards polyarylated CPPs is presented and the formation of graphenic sidewalls by oxidative cyclodehydrogenation is demonstrated. Graphene itself is catalytically inactive towards ORR, but replacing a certain amount of carbon atoms by nitrogen turns graphene into an oxygen reduction catalyst.^[106] Also nitrogen doped CNTs performed well in the ORR.^[105] However, there is still a debate about the active site in these nitrogen-doped graphene catalysts. In contrast, the active site is well-defined in

non precious metal catalysts (NPMCs). They comprise a macrocyclic N₄-environment, e.g. porphyrin or phthalocyanine and a transition-metal ion, e.g. iron or cobalt. The catalytic activity sensitively depends on the interplay of the ligand and the metal center. Therefore, the second part of this work (chapter 5) is focused on the development of new NPMCs for the cathodic oxygen reduction in fuel cell applications (Figure 2-1).

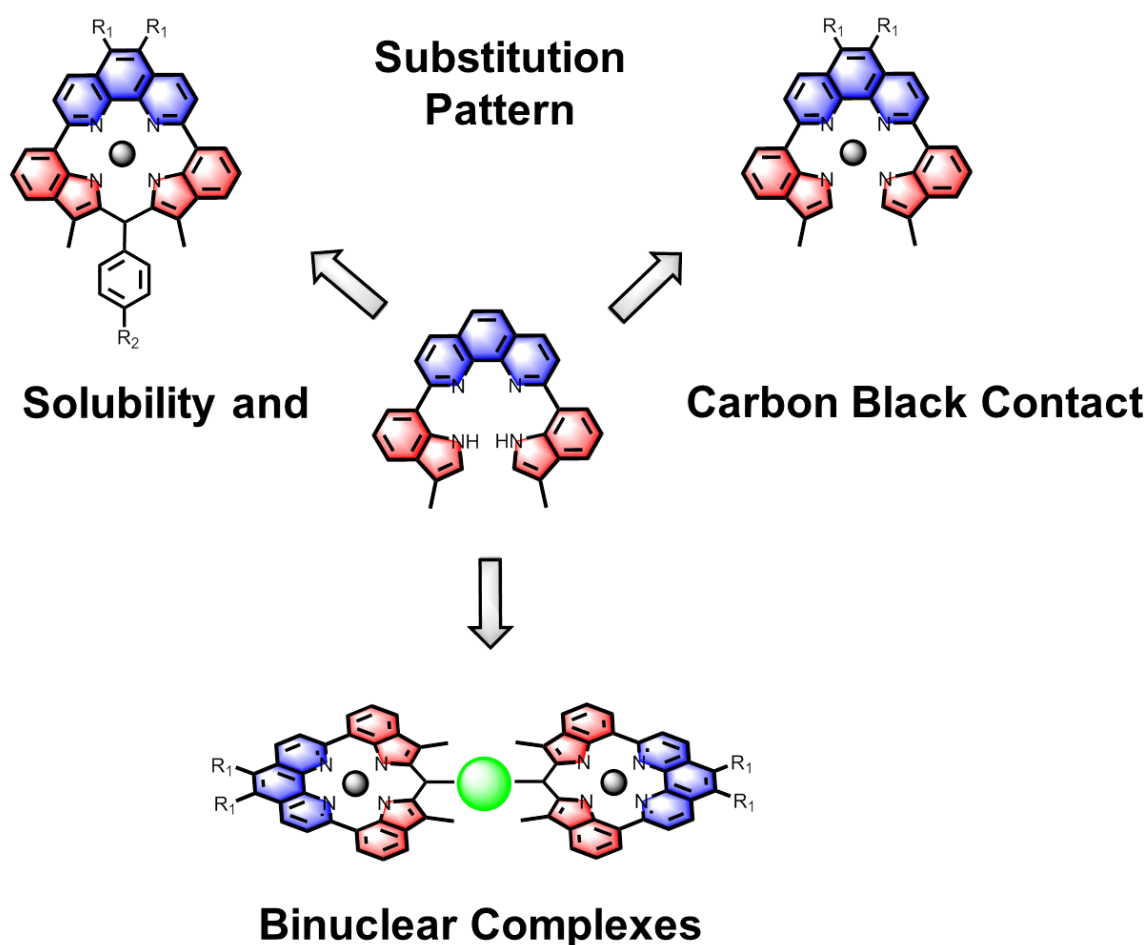


Figure 2-1: Schematic illustration of the concept for improved and novel NPMC systems.

In this context, a novel N₄-macrocyclic ligand, consisting of phenanthroline and indole moieties, was designed in the *Müllen* group.^[143] In a first approach the respective cobalt complexes, supported on carbon black needed a heat pre-treatment at 700 °C to support the 4-electron reduction pathway of oxygen. Based on these results, this work aims for an increase in the

catalytic performance of the phenanthroline-indole macrocyclic (PIM) metal complexes, tuning the properties towards the direct 4-electron reduction of oxygen to water, as well as improvements in the interaction of the complex and the support, overcoming the heat pretreatment. Therefore several structural variations were considered (Figure 2-1). The different substitution of the PIM skeleton shall influence the solubility of the resulting cobalt complexes. Since the complexes will be adsorbed on carbon black, the aggregation of individual PIM complexes in solution needs to be prevented. Aggregated complexes on the carbon black surface are catalytically inactive sites.^[90] Within the scope of this work, different substituents at the 5- and 6-position of the phenanthroline building block, as well as different aldehydes for the macrocyclization will be introduced. Furthermore, the non-macrocyclic cobalt complexes will be investigated in the oxygen reduction reaction (ORR). This promises insights into the structure-property relationship, since the sp^3 carbon in the PIM ligands influences the complex geometry and can therefore affect the performance and the interaction with the carbon black support. Moreover, the extension towards a binuclear metal complex will be in the focus of this work. The preferred reduction geometry of oxygen on platinum surfaces is supposed to be a bridge-*cis* conformation.^[90] Therefore, a variety of planar, multinuclear metal complexes and chelates were designed, as well as the binuclear cofacial porphyrins.^[94,98,103,144] They all showed an increase in the catalytic activity, affected by the high active site density or the electronic influence of the additional metal centers. The PIM skeleton is ideally suited for an extension towards a binuclear metal complex. In this work, the fusion with aromatic dialdehydes as an attempt to dimeric ligand systems will be investigated. Further, the metal centers shall interact through a conjugated ligand skeleton. Therefore, the planarization of the dimeric PIM ligand will be the aim of this work.

The chapter will cover the synthetic issues, the electronic properties as well as the catalytic performance in the ORR. The results presented herein are one more step on the way to understand the relationship between the performance and the structure of ORR catalysts.

3. *Cyclo-hexa-*peri*-hexabenzocoronenes*

3.1. Introduction

The shortest segment of an armchair CNT is represented by the CPPs, which have been successfully synthesized for the first time in 2008 (Figure 3-1).^[50–52,55–57,59,60,75,118–127] However, the longitudinal extension towards ultrashort CNTs still remains challenging.^[46]

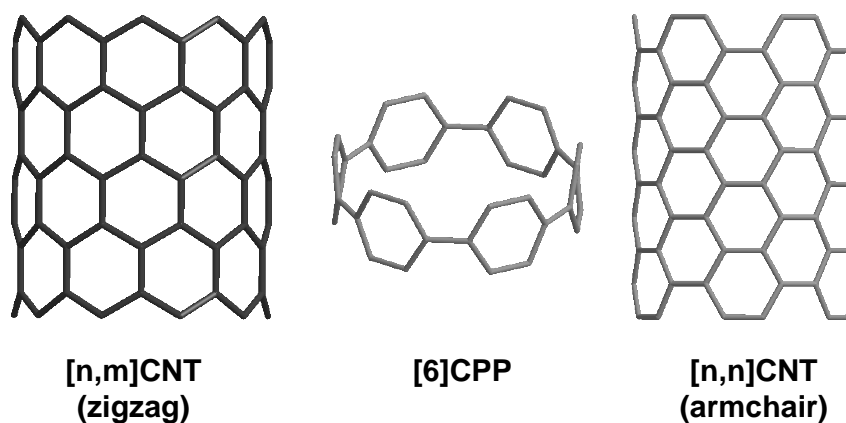


Figure 3-1: Graphical illustration of [6]CPP and the CNT structures with zigzag and armchair conformation.

A well-established synthetic procedure for the synthesis of polycyclic aromatic hydrocarbons (PAHs) is the oxidative cyclodehydrogenation, the so called *Scholl* reaction,^[21] of polyphenylene precursors to access one- (1D) and two-dimensional (2D) structures, such as graphene nanoribbons (GNR)^[32,133–136] and nanographenes (NG).^[128–132] With the variation of the polyphenylene precursors, the width and the 2D extension of the GNRs and NGs can be tuned.^[22] An ultrashort CNT segment resembles a rolled up nanoribbon (Figure 3-2) and this, in turn, contains the well-known PAH hexa-*peri*-hexabenzocoronene (HBC). From a retrosynthetic point of view, the key step for a longitudinal extension of CPPs towards ultrashort CNTs is the cyclic arrangement of HBC derivatives. Therefore, curvature needs to be induced and second, conditions for the oxidative cyclodehydrogenation of cyclic and strained systems have to be developed.

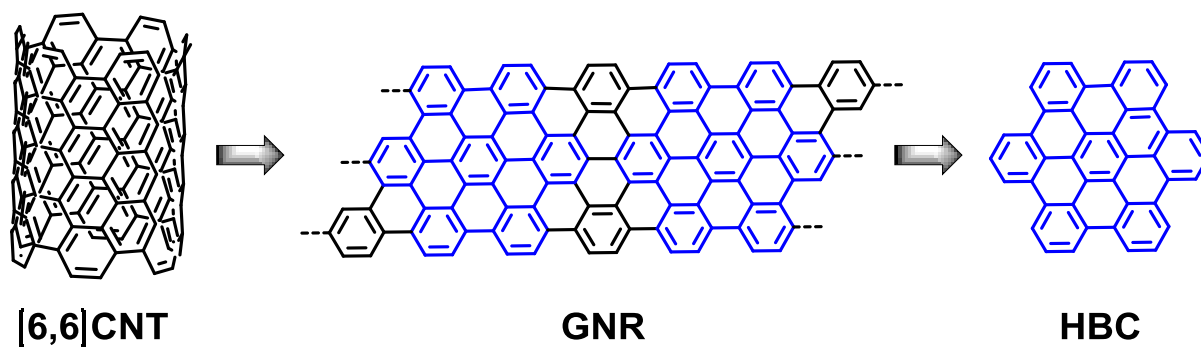


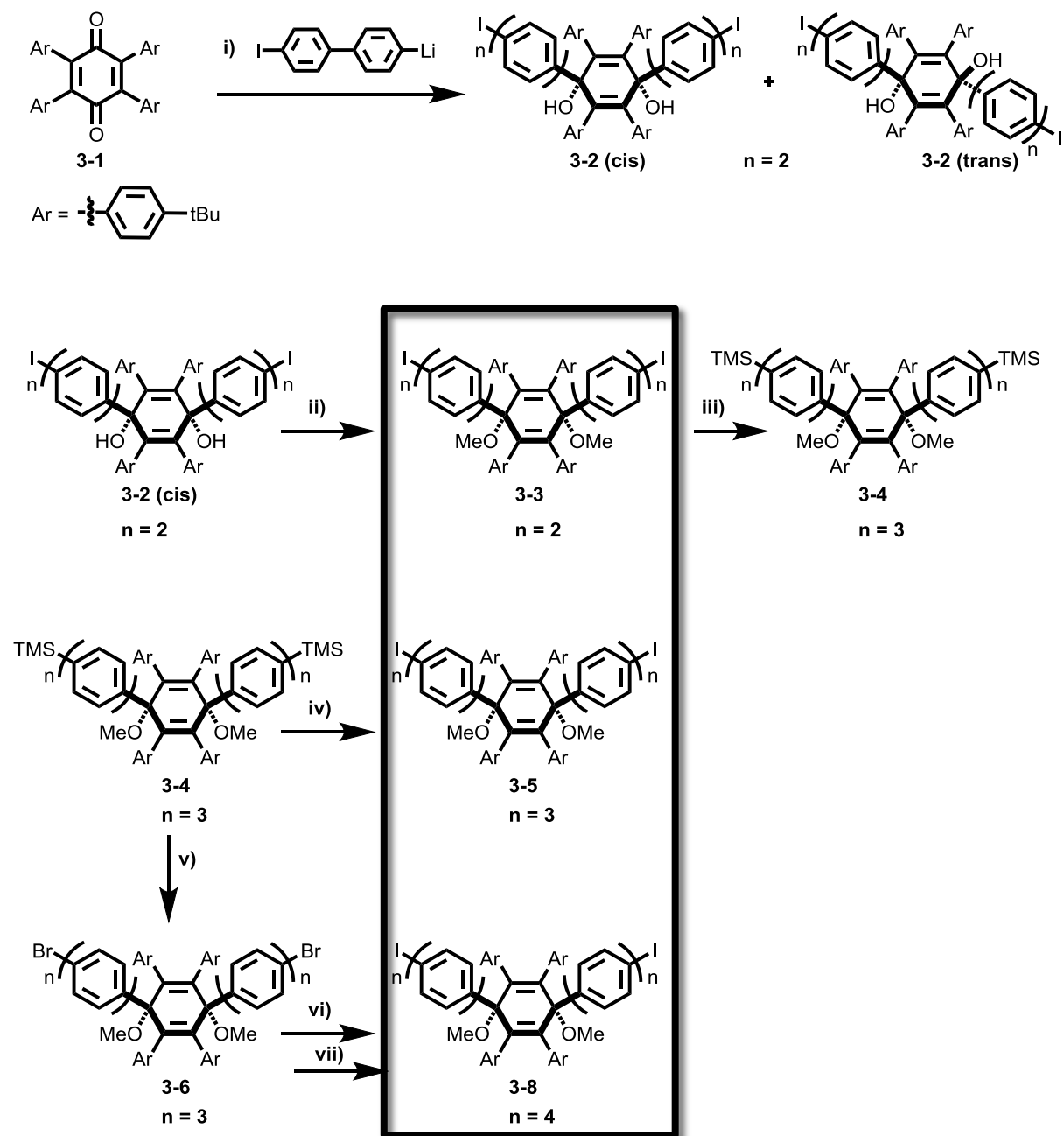
Figure 3-2: Schematic illustration of HBC as a motif in GNRs and CNTs.

In this chapter, the synthesis of phenylene-extended *cyclo-p*-hexaphenylbenzenes ([3]CHPBs) will be presented. Furthermore, the applicability of the *Scholl* reaction to form *cyclo-para-hexa-*peri**-hexabenzocoronenes ([3]CHBCs) will be described as an approach for the bottom-up synthesis of ultrashort CNTs.

3.2. Results and Discussion

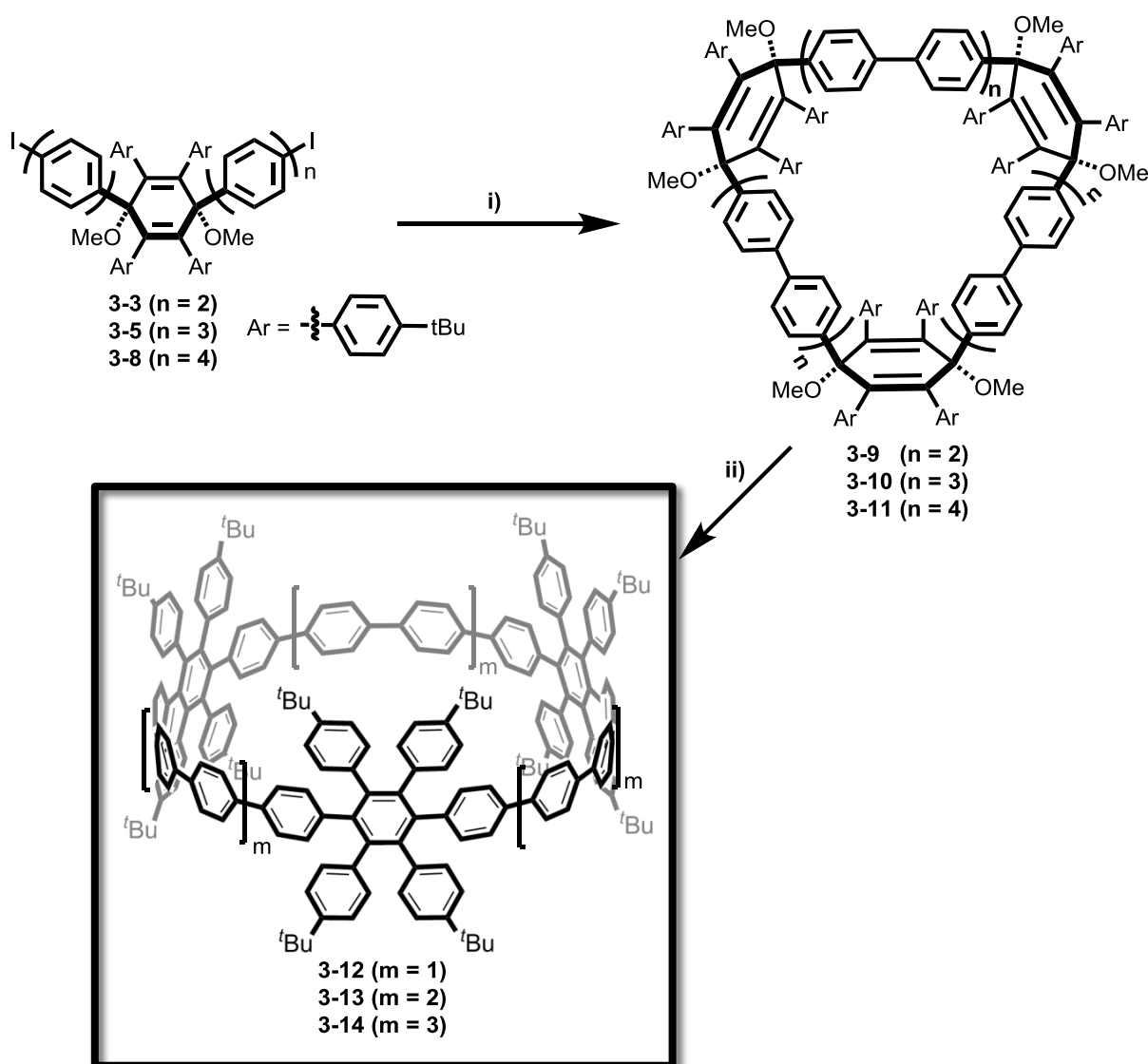
3.2.1. Synthesis of π -extended *Cyclo-p*-hexaphenylbenzenes

The phenylene-extended [3]CHPBs **3-12**, **3-13**, **3-14** were synthesized by the trimerization of the kinked key intermediates **3-3**, **3-5** and **3-8** under *Yamamoto* conditions. The synthesis of these kinked hexaphenylbenzene derivatives started with the monolithiation of 4,4'-diiodobiphenyl and the addition of tetra(4-*tert*-butylphenyl)-*p*-benzoquinone to afford mainly *cis*-diol **3-2**, which was subsequently alkylated with methyl iodide to obtain **3-3** in an overall yield of 38 %.^[50,145] The whole synthetic route is depicted in Scheme 3-1. Cyclizing precursor **3-3**, leads to the [3]CHPB **3-12** with a 15-membered CPP base. For extending the ring size, precursor **3-3** was further elongated by a *Suzuki-Miyaura* cross coupling reaction with 4-trimethylsilylphenylboronic acid pinacol ester to give **3-4**. A subsequent trimethylsilyl-iodine exchange, using iodine monochloride and silver tetrafluoroborate afforded the 21-membered [3]CHPB precursor **3-5**. Compound **3-4** served also as the basic building block for the next extension towards the 27-membered [3]CHPB **3-14**. However, the synthetic protocol had to be changed to afford **3-8** in reasonable yields. Bromo functional groups were introduced to prevent the fast dehalogenation in the *Suzuki-Miyaura* cross coupling reaction, combined with the use of the more reactive palladium catalyst system, developed by *Buchwald* et al.^[146] As the final step towards **3-8**, an iodination, using iodine monochloride was performed.



Scheme 3-1: Synthetic route towards the kinked intermediates **3-3**, **3-5** and **3-8**. Conditions: i) $-78\text{ }^{\circ}\text{C}$, THF, *n*-BuLi, 2 h; $-78\text{ }^{\circ}\text{C} \rightarrow \text{RT}$, 16 h, 40 %; ii) THF, NaH, MeI, $-78\text{ }^{\circ}\text{C}$, 1 h, $-78\text{ }^{\circ}\text{C} \rightarrow \text{RT}$, 16 h, 94 %; iii) 4-trimethylsilylphenylboronic acid pinacol ester, Pd(PPh₃)₄ (10 mol%), Aliquat 336, Cs₂CO₃, toluene/water (3/1), 16 h, 80 $^{\circ}\text{C}$, 64 %; iv) AgBF₄, THF, MeOH, ICl (1M in DCM), 0 $^{\circ}\text{C}$, 40 min., 80 %; v) bromine, THF, AgBF₄, NaOAc, 0 $^{\circ}\text{C}$, 20 min., 90 %; vi) 4-trimethylsilylphenylboronic acid pinacol ester, Pd(OAc)₂, S-Phos, K₃PO₄, toluene, water, 90 $^{\circ}\text{C}$, 16 h, 58 %; vii) AgBF₄, THF, MeOH, ICl (1M in DCM), 0 $^{\circ}\text{C}$, 40 min., 70 %.

With the precursors **3-3**, **3-5** and **3-8** in hand, the trimerization under *Yamamoto* conditions, to obtain the respective macrocycles, was performed (Scheme 3-2). The cyclic trimers **3-9** to **3-11** were the major products, but also the formation of linear dimers and higher oligomers was observed by mass spectrometry. The all-phenylene macrocycles were obtained by the aromatization of the three 1,4-cyclohexadienyl-rings with sodium naphthalenide to afford the 15-, 21- and 27-membered [3]CHPBs **3-12**, **3-13** and **3-14** in 10-37 % yield.



Scheme 3-2: Synthetic route towards the cyclo *p*-hexaphenylbenzene macrocycles **3-12**, **3-13** and **3-14**. Conditions: i) Ni(cod)₂, 1,5-cyclooctadien, 2,2'-bipyridine, toluene, THF, N,N-dimethylformamide, 80 °C, 16 h, 25-40 %; ii) sodium naphthalide, THF, -78 °C, 1 h, 10-37 %.

The macrocycles and intermediates were analyzed by mass spectrometry, NMR spectroscopy, UV-Vis spectroscopy and X-ray crystallography (chapter 3.2.2).

The [3]CHPBs are precursors for [3]CHBCs, therefore, **3-12**, **3-13** and **3-14** were subjected to oxidative cyclodehydrogenation, which will be described in detail in chapter 3.2.3.

3.2.2. Characterization of [3]CHPBs

The kinked precursors **3-3**, **3-5** and **3-8** were the key intermediates for the successful cyclization towards the [3]CHPBs, since they induce the curvature to the rigid hexaphenylene skeleton. X-ray crystallography verified the existence of the *cis*-isomer **3-3** (Figure 3-3).

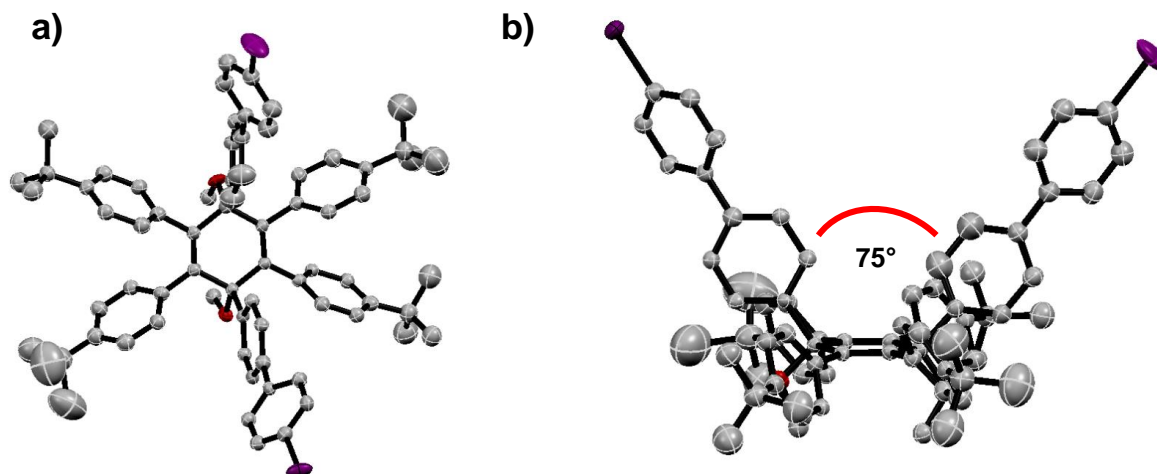


Figure 3-3: X-ray crystal structure of **3-3**; a) top view; b) side view; ellipsoids were set at 50 % probability, hydrogen atoms and solvent molecules are omitted for clarity; oxygen atoms in red, iodine atoms in violet.

The dihedral angle between the two biphenyl units was determined to be 75.5° . For Ni^0 mediated shotgun cyclizations in the CPP synthesis, precursors with dihedral angles in the range between 50° and 70° were used to afford cyclic trimers.^[76,126]

After cyclization and aromatization, the compounds **3-12** to **3-14** were analyzed by MALDI-TOF mass spectrometry. The mass isotopic patterns were clearly resolved and are in good agreement with the simulated ones (Figure 3-4).

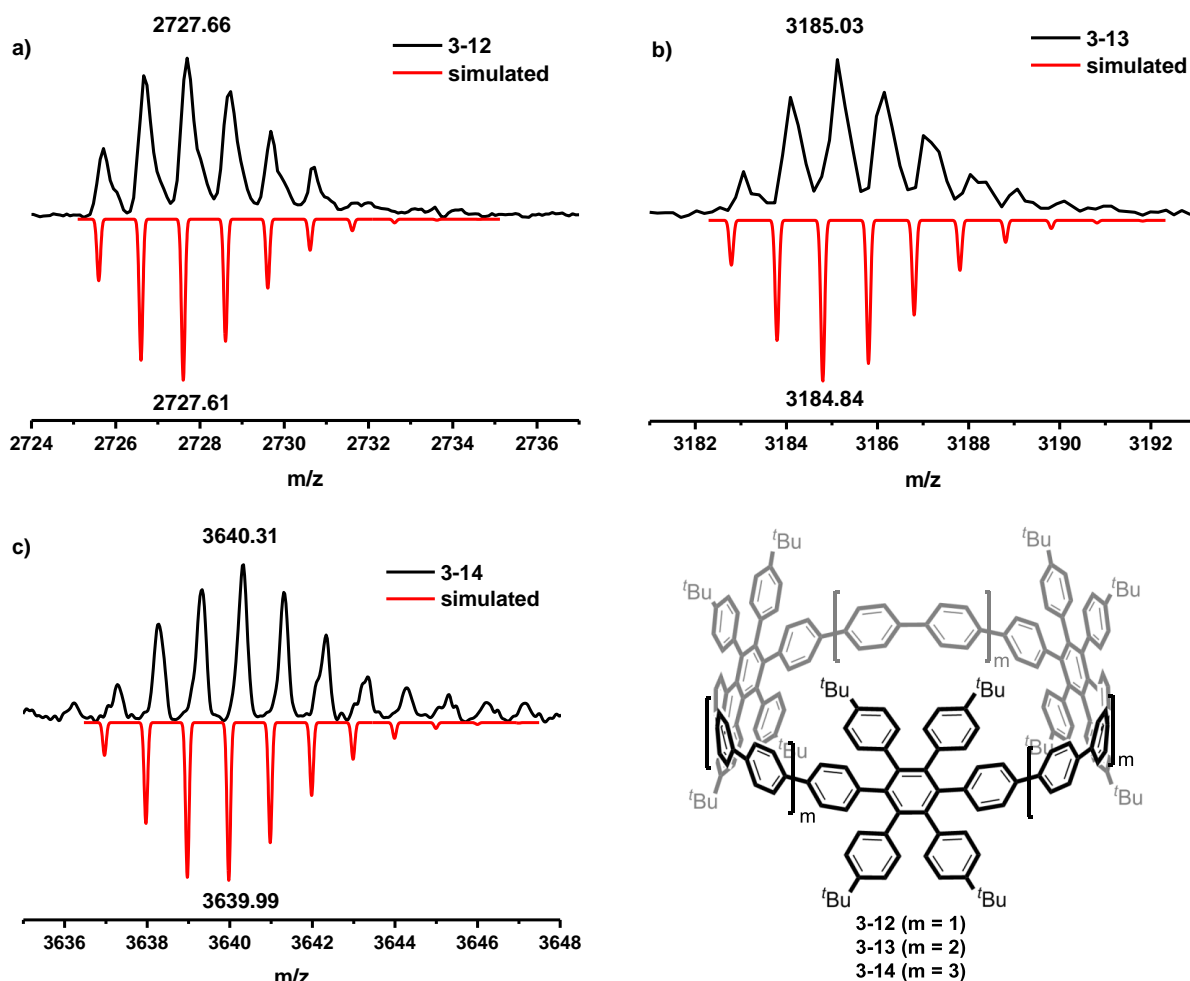


Figure 3-4: MALDI-TOF mass spectra of a) **3-12**; b) **3-13** and c) **3-14**.

Since mass spectrometry is only an indirect proof of the cyclic nature of these compounds, NMR spectroscopy provided further structure information (Figure 3-5).

Exemplarily shown for **3-12**, the high symmetry of the [3]CHPBs was also reflected in their $^1\text{H-NMR}$ spectra (Figure 3-5). In the aromatic region three different AB spin systems can be distinguished for **3-12**. Two AB spin systems originate from the phenylene rings in the CPP base, forming four distinct doublet signals at 7.53 ppm, 7.33 ppm, 7.05 ppm and 6.95 ppm. The other AB-spin system represents the proton signals from the (4-*tert*-butylphenyl)-substituents, having two doublets at 6.82 ppm and 6.74 ppm, respectively. The sharp singlet signal for the *tert*-butyl group at 1.04 ppm underlines the existence of the highly symmetric [3]CHPB **3-12**.

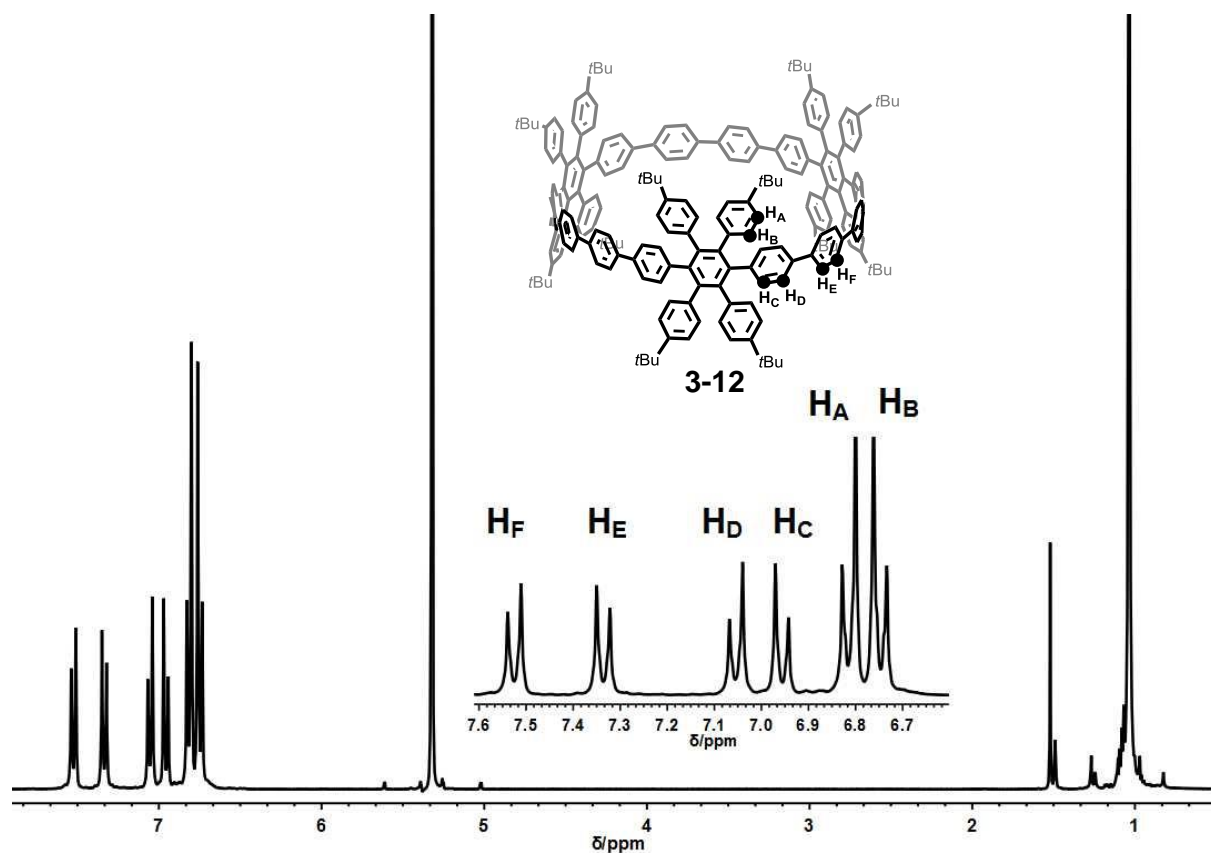


Figure 3-5: ¹H-NMR spectrum (300 MHz) of **3-12** in CD₂Cl₂ at 298 K.

Additionally, 2D-NMR techniques were applied to elucidate the whole structure. A NOESY (Nuclear Overhauser effect spectroscopy) spectrum was recorded to distinguish the different proton signals from the phenylene rings (Figure 3-6a,b). In a NOESY spectrum nuclei that are close to each other (within 4 Å) show resonances which are connected by cross peaks. Thus, cross peaks are expected for H_B, H_C and H_D, H_E. The through space coupling of H_B and H_C was not well resolved, because a weak interaction of H_A with H_C was observed. However, the through space coupling of H_D and H_E was clearly resolved (Figure 3-6a). Since a through space coupling of the protons H_A with the *tert*-butyl protons was detected, H_A and H_B could have been distinguished (Figure 3-6b). The further connectivity was resolved with the recorded ¹H, ¹H – COSY NMR spectrum (Figure 3-6c).

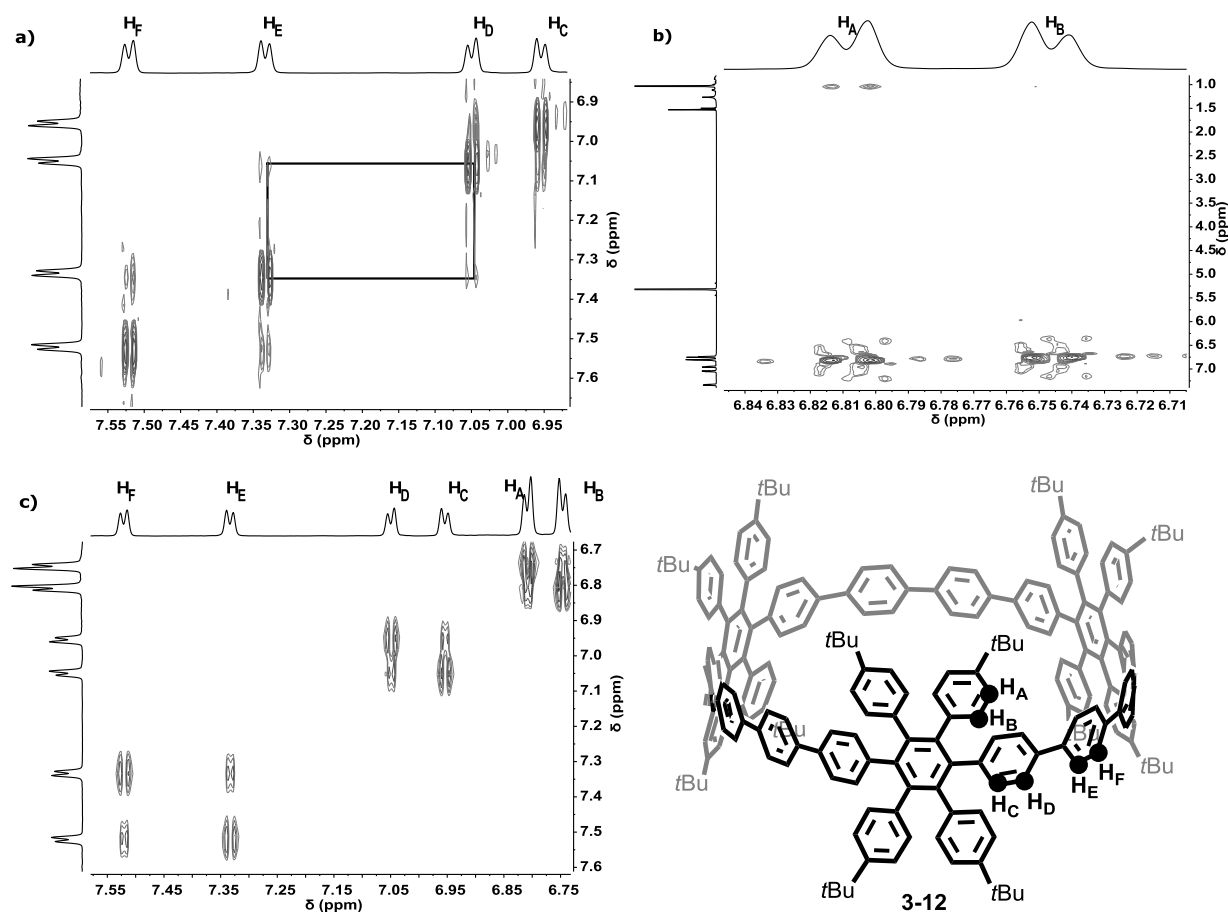


Figure 3-6: 2D-NMR spectra of **3-12**; a) $^1\text{H}, ^1\text{H}$ -NOESY NMR spectrum (aromatic region); b) $^1\text{H}, ^1\text{H}$ -NOESY NMR spectrum (aromatic-aliphatic coupling); c) $^1\text{H}, ^1\text{H}$ -COSY NMR spectrum (aromatic region); additional the structure of **3-12** is depicted; all spectra were recorded in CD_2Cl_2 , 298 K, 700 MHz.

In a $^1\text{H}, ^1\text{H}$ – COSY NMR spectrum, resonances of nuclei that are bond to each other (up to ^3J) can be detected by cross peaks. Hence, cross peaks were observed for the three different AB-spin systems $\text{H}_\text{A}\text{H}_\text{B}$, $\text{H}_\text{C}\text{H}_\text{D}$ and $\text{H}_\text{E}\text{H}_\text{F}$. The findings of the 2D-NMR spectroscopy study were consistent with the proposed structure of **3-12**.

Finally, the electronic absorption and emission spectra of the [3]CHPB macrocycles **3-12** to **3-14** were recorded (Figure 3-7). The transition from the ground state to the first excited state $\text{S}_0\text{-S}_1$ is forbidden in cyclic systems like CPPs. Therefore the absorption in CPPs mainly results from the $\text{S}_0\text{-S}_2$ transition. Since these transitions are independent of size, the absorption maximum of all CPPs larger than [8]CPP can be observed at around 340 nm.^[50] For CPPs smaller than [8]CPP the forbidden $\text{S}_0\text{-S}_1$ transition can be observed as a small shoulder

peak.^[125] The absorption spectra of the phenylene-extended [3]CHPB **3-12** to **3-14** (Figure 3-7) have similar absorption maxima like the CPPs, whereas a slight hypsochromical shift was observed. This is especially pronounced for the smallest 15-membered [3]CHPB **3-12** with an absorption maximum at 320 nm, reflecting the high degree of strain and distortion between the phenylene rings due to the aryl substitution of the CPP backbone. The absorption maxima of the less strained [3]CHPBs **3-13** and **3-14** were observed at 330 nm.

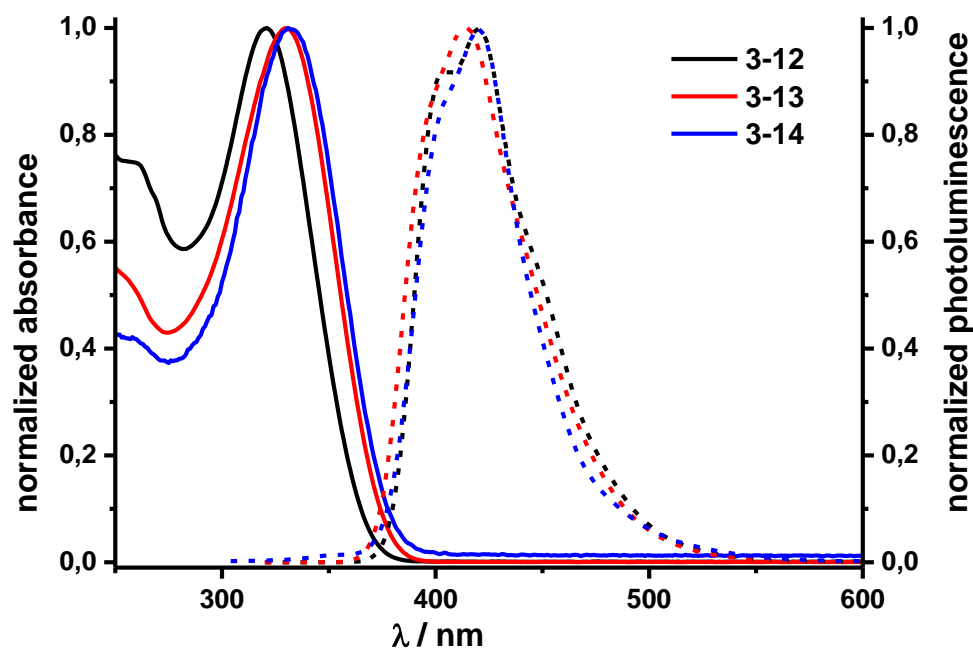


Figure 3-7: Electronic absorption (solid line) and emission (dashed line) spectra of compounds **3-12**, **3-13** and **3-14** ($c = 10^{-6}$ M in DCM).

The emission maxima of **3-12**, **3-13** and **3-14** appeared at ~ 420 nm, with the largest *Stokes* shift being observed for **3-12** (100 nm). In the excited state, a partial release of the ring strain and distortion by partial planarization of neighboring phenyl rings takes place, resulting in relatively large *Stokes* shifts.^[52,147,148] This effect is pronounced for smaller CPPs what was observed for the 15-membered [3]CHPB **3-12**. The electronic absorption and emission data for **3-12** to **3-14** are summarized in Table 3-1.

Table 3-1: The summary of the electronic absorption and emission data for **3-12**, **3-13** and **3-14** ($c = 10^{-6}$ M in DCM).

compound	λ_{abs} [nm]	λ_{em} [nm]	$\epsilon_{\lambda_{\text{max}}}$ [mol ⁻¹ m ²]
3-12	321	404, 419	15200
3-13	330	415	23370
3-14	331	420	n.d.

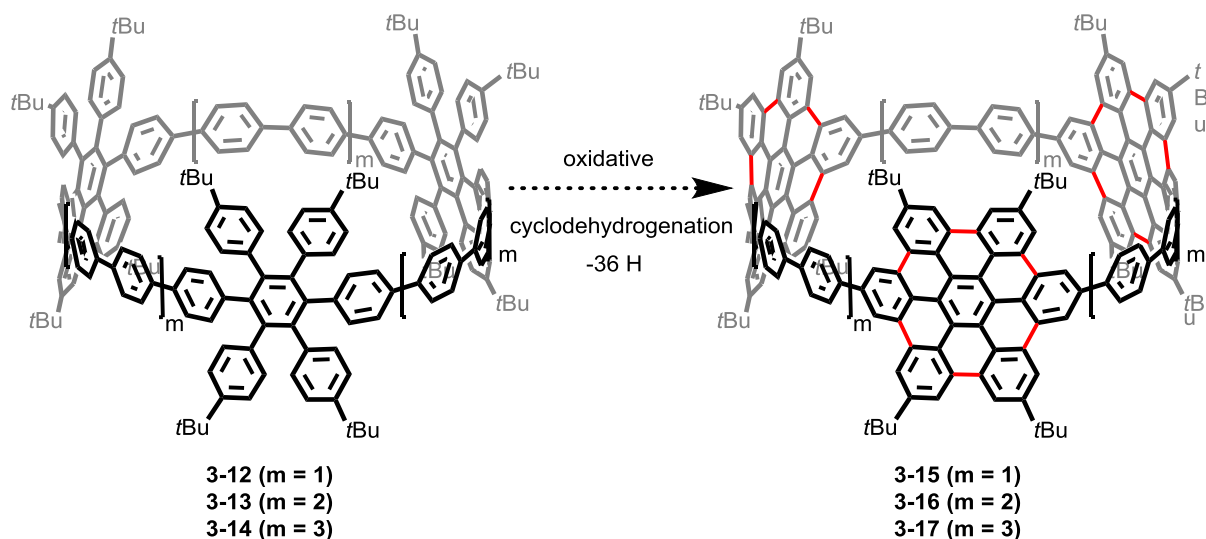
The obtained phenylene-extended [3]CHPBs **3-12** to **3-14** were subjected to oxidative cyclodehydrogenation. Since the HBC units are already predefined, the creation of graphenic sidewalls by the *Scholl* reaction represents an appropriate method. Whether the distortion or the high ring strain will influence the formation of HBC units within the macrocycle is the main focus of the following chapter 3.2.3.

3.2.3. Cyclodehydrogenation towards [3]CHBCs

The cyclodehydrogenation of polyphenylenes by the *Scholl* reaction in order to obtain planarized PAHs is a well-established method.^[21] Since planar one- (1D) and two-dimensional (2D) PAHs, like nanoribbons^[32,133–136] and nanographenes,^[128–132] were obtained on this synthetic route, and even five-, seven- and eight membered rings were formed.^[137–141] Cyclic and strained systems are rarely investigated. Therefore, the polyphenylene macrocycles **3-12**, **3-13** and **3-14** were subjected to cyclodehydrogenation (Scheme 3-3).

For all [3]CHPBs the formation of 18 new C-C bonds, i.e. a loss of 36 hydrogen atoms, was expected after the oxidative cyclodehydrogenation. Different oxidants such as CF₃SO₃H with 2,3-dichloro-5,6-dicyano-1,4-benzoquinone (DDQ) or Sc(OTf)₃/DDQ, phenyliodonium-bis(trifluoroacetate) (PIFA) with BF₃·Et₂O and FeCl₃ were applied.^[26,149–152] Completely dehydrogenated compounds, without any chlorinated side products, were obtained with FeCl₃ in a nitromethane/dichloromethane mixture at RT with a continuous flow of argon through the

solution. A reaction time of 7 h was estimated for all [3]CHPB cyclodehydrogenation reactions.

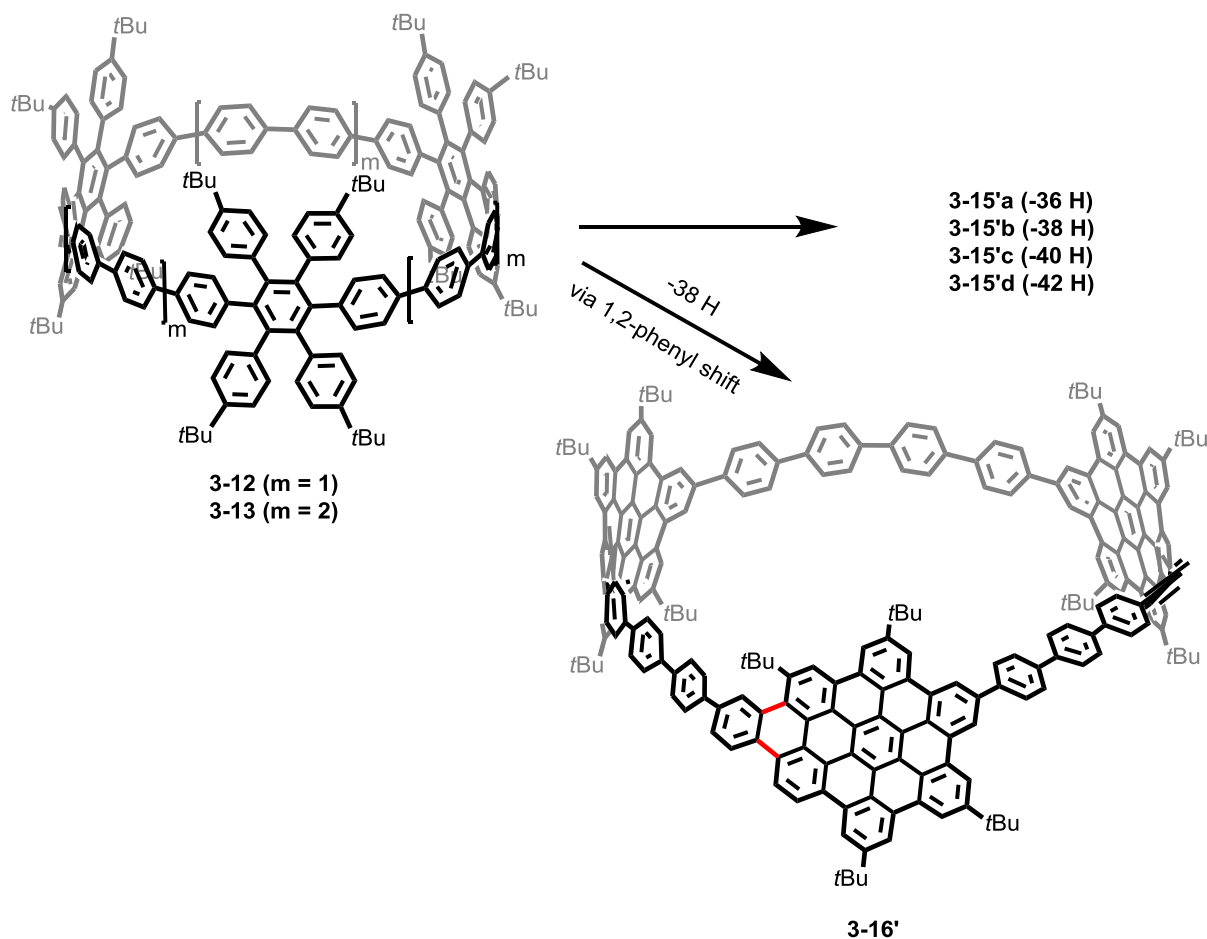


Scheme 3-3: Concept of the cyclodehydrogenation of [3]CHPBs **3-12**, **3-13** and **3-14** towards the [3]CHBCs **3-15**, **3-16** and **3-17**.

Unexpectedly, the depicted [3]CHBCs **3-15** and **3-16** were not selectively obtained. Rather, an additional loss of 2 to 6 hydrogen atoms was observed for the dehydrogenation of **3-12**, 2 more hydrogen atoms for the dehydrogenation of **3-13** (Scheme 3-4). No additional loss was observed for the dehydrogenation of **3-14**. The dehydrogenation products were initially separated by high performance liquid chromatography (HPLC), using the column Cosmosil 5PBB from Nacalai Tesque and a toluene/methanol mixture (3/1 to 9/1) as eluent. The different fractions of **3-15'** and **3-16'** were analyzed by different mass spectrometry techniques, NMR- and UV-Vis spectroscopy.

In the following paragraph, initially, the different dehydrogenation products of **3-15'** will be discussed. As above mentioned, a loss of two to six additional hydrogen atoms, i.e. the formation of one to three supplemental C-C bonds, was observed. HPLC separation afforded four fractions with different dehydrogenation products, containing **3-15'a** (-36 H), **3-15'b** (-38 H), **3-15'c** (-40 H) and **3-15'd** (-42 H), representing an additional loss of -0 H, -2 H, -4 H, -6 H (Figure 3-8). The formation of every additional bond goes along with distinct structural

changes in **3-15**. The structural analysis by NMR techniques failed for the different fractions of **3-15'**, since the loss of symmetry increased the amount of signals. Besides this, the amount of every single fraction was too small for a well-resolved NMR spectrum.



Scheme 3-4: Synthetic scheme of the cyclodehydrogenation towards **3-15'a,b,c,d** and **3-16'**; Conditions: FeCl_3 , MeNO_2 , CH_2Cl_2 , RT, 7 h.

Therefore, ion mobility-spectrometry and tandem-mass spectrometry techniques were applied, in cooperation with [REDACTED] and [REDACTED], for a further structure elucidation of the different dehydrogenation products.

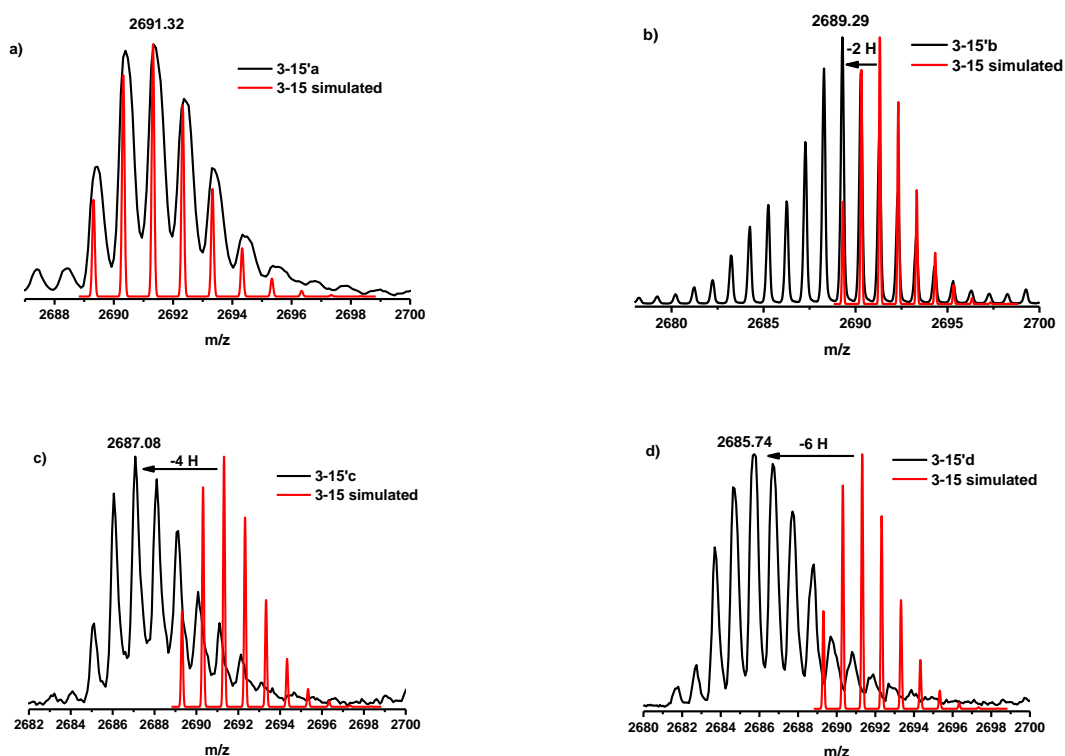


Figure 3-8: MALDI-TOF spectra of the different HPLC fractions of **3-15**; a) **3-15'a**; b) **3-15'b** c) **3-15'c**; d) **3-15'd**.

This technique combines the ion mobility mass spectrometry, which allows the separation of the different ions according to their sizes, shapes and conformations, and on the other hand the tandem-mass spectrometry, which provides additional structure information through a detailed analysis of the fragments, formed by collision induced dissociation (CID). At first, it was investigated, whether the cyclic structure of **3-15'** remained after cyclodehydrogenation. Thus, the molecules were first ionized by MALDI and only the molecular ion was selected for a further investigation by CID ion mobility-mass spectrometry. In order to achieve an efficient fragmentation, the maximum collision energy of the instrument (200 V) had to be applied, indicating the high stability of the macrocycles **3-15'** (Figure 3-9). A similar behavior for **3-15'a** to **3-15'd** was observed and in Figure 3-9 the ion mobility image of **3-15'd** is exemplarily shown.

From the mass ranges in the 2D ion mobility image, the split of the molecular ion ($m/z = 2685$) into trimeric, dimeric and monomeric fragments is clearly visible (Figure 3-9). The

coherent fragmentation patterns arise from the loss of the *tert*-butyl side chains. In the trimeric fragment region, three different fragmentation series with different drift times and thus different shapes were observed.

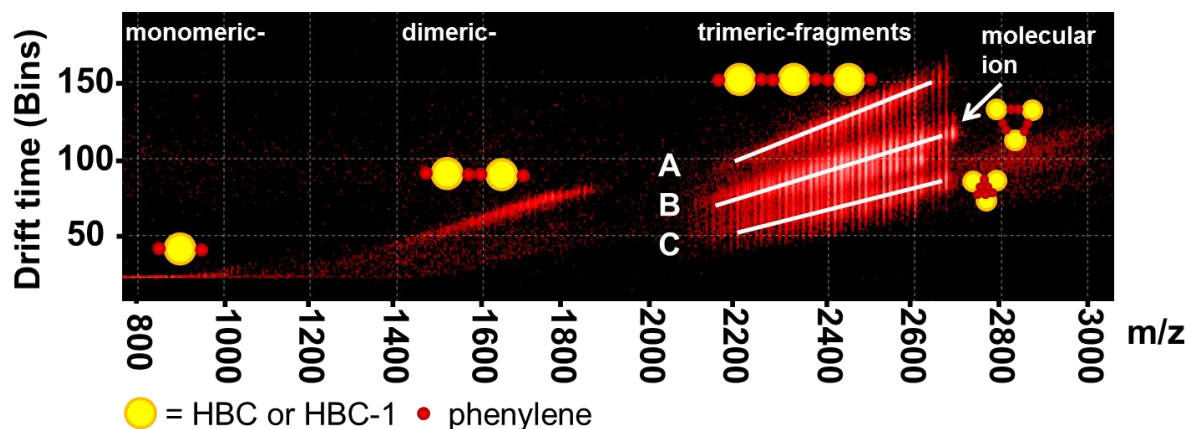
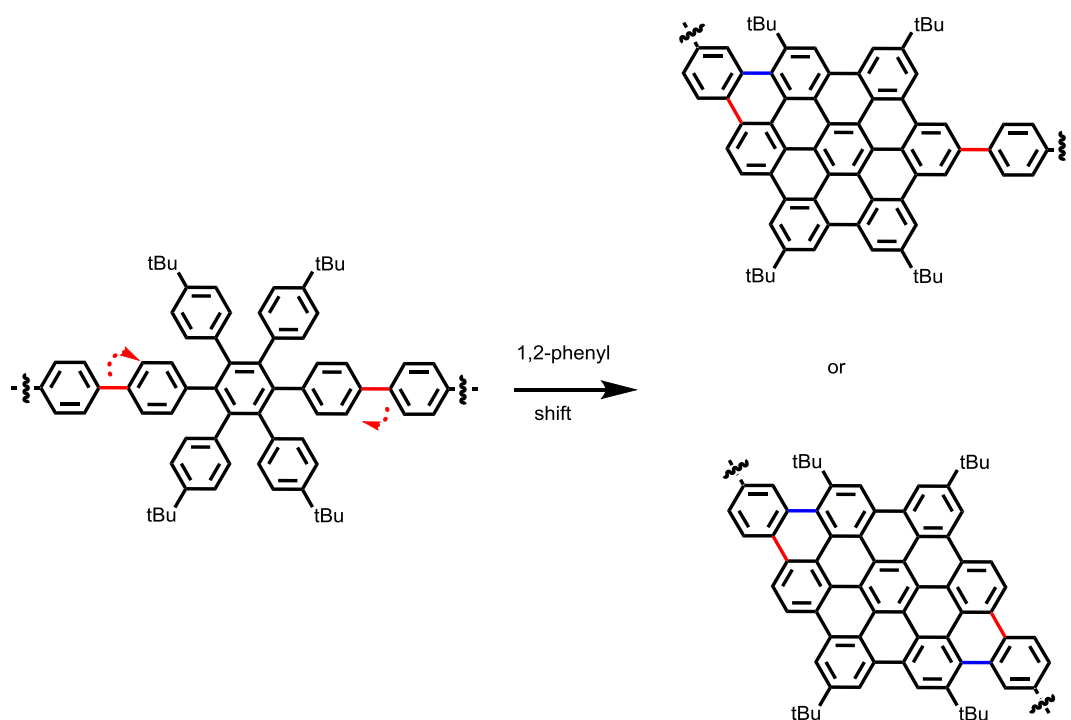


Figure 3-9: 2D drift time vs. m/z ion mobility image for **3-15'd**; collision energy: 200 V.

For clarity, three trend lines A, B and C were overlaid to mark the regions of alkyl chain fragmentation. Initially, trend line B was observed, also containing the molecular ion. By increasing the collision energy, trend line C developed and finally trend line A appeared under maximal collision energy. Simultaneously to trend line A, the dimeric and monomeric fragment series were observed. The largest drift time, i.e. the largest size or shape, was observed for fragments of trend line A, which suggests that these fragments belong to ring-opened products. This assumption is also consistent with the fact that simultaneously the dimeric and monomeric fragments appeared which have to be linear structures. A molecular ion was not observed in the fragmentation trend line A, which means that only cyclic products were present in the different fractions of **3-15'** and the ring opening was a consequence of the high collision energy. A significant smaller drift time was observed for the fragments of trend line C. These fragments are supposed to be folded or twisted macrocycles, having a smaller molecular size. These compressed structures might be intermediates on the way to the linear ring-opened structures of trend line A. With these findings, a first proof of the cyclic nature of **3-15'a** to **3-15'd** and their high stability was accomplished. The results were consistent with ion mobility studies performed on cyclic polystyrenes.^[153,154] However, the 15-membered

[3]CHPB resisted a clean and selective cyclodehydrogenation. With the analysis of the different fragments by tandem MALDI-TOF mass spectrometry, the kind of side reaction during the cyclodehydrogenation was investigated in order to design [3]CHPBs that can selectively be transformed into [3]CHBCs. In large PAHs, a 1,2-phenyl shift in the hexaphenylbenzene unit was reported in 2001 in the *Müllen* group, which resulted in an additional loss of hydrogen atoms.^[155] Supposing the same mechanism for the [3]CHPB **3-15**, a maximum of two 1,2-phenyl shifts in every HPB unit would be possible (Scheme 3-5).



Scheme 3-5: Supposed structural changes in the HBC units of **3-15'** after 1,2-phenyl shifts; the shifted bonds are marked in red, the additional bonds are marked in blue.

Since there are four different fractions with zero, one, two and three observed 1,2-phenyl shifts, three different smallest fragments should be obtained in the tandem MALDI-TOF mass spectra for the rearranged and non-rearranged units, assuming that the aromatic cores do not further fragment at 200 V (Figure 3-10).

The smallest PAH fragment that can be obtained is HBC, since the biphenyl units are too small to be detected. A 1,2-phenyl shift would transform one HPB unit into a HBC-1 unit, the second shift would produce HBC-2 (Figure 3-10).

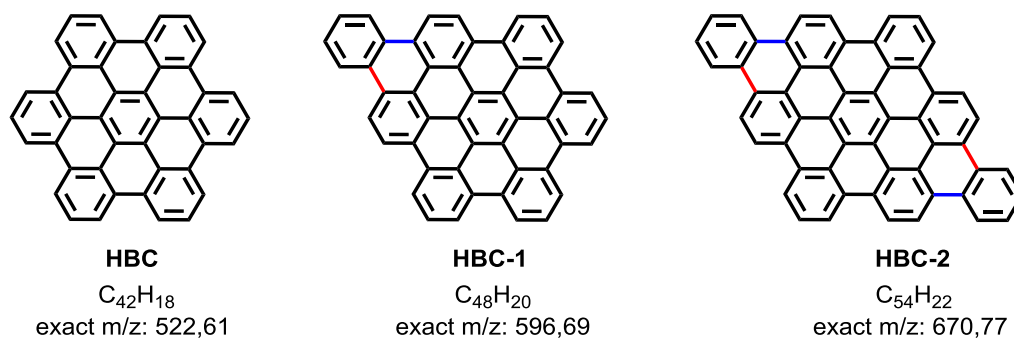


Figure 3-10: Possible fragments in tandem MALDI-TOF MS of the rearranged [3]CHBC **3-15'**; shifted bonds are marked in red, additional bonds are marked in blue.

Applying the tandem MALDI-TOF mass spectrometry, fragmentation and structure elucidation of **3-15'a** to **3-15'd** was performed. The respective spectra are depicted in Figure 3-11.

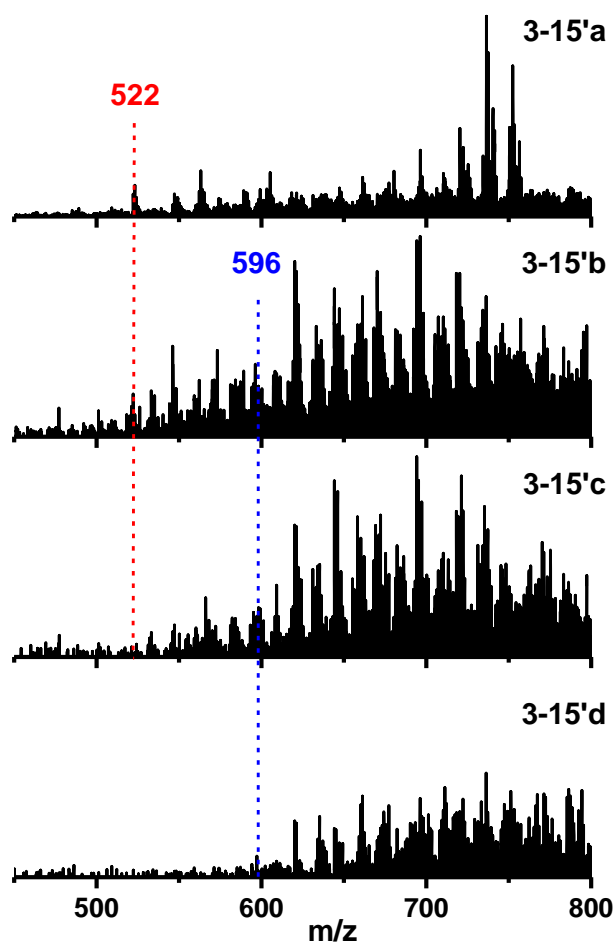


Figure 3-11: Mass spectra of the monomeric fragments of **3-15'a** to **3-15'd**.

For **3-15'd** the smallest detectable fragment had a mass to charge ratio of 596 (Figure 3-11, **3-15'd**). The formation of HBC-2 in **3-15'd** would also lead to the formation of a HBC-1- and HBC-unit. Therefore, these findings indicate that only one 1,2-phenyl shift occurred at every HPB unit. This is also consistent with the spectra of **3-15'a**, in which only HBC as the smallest fragment was detected. For **3-15'b** and **3-15'c** mass peaks at $m/z = 522$ and $m/z = 596$ were observed. According to these fragmentation patterns, theoretical structures of the compounds **3-15'a** to **3-15'd** were shown and their equilibrium covalent geometry was calculated using MM2 force field methods (Figure 3-12). An alternating occurrence of the 1,2-phenyl shifts was supposed for the structures. This might be a simplified and theoretical assumption, since other isomers could also be formed, but based on the ion mobility measurements the dominance of one isomer was assumed. As depicted in Figure 3-12 the 1,2-phenyl shifts cause a transformation from a cylindrical to a more conical structure. This is also in good agreement with the ion mobility measurements, as well as with the measured fragmentation patterns of **3-15'** (Figure 3-11).

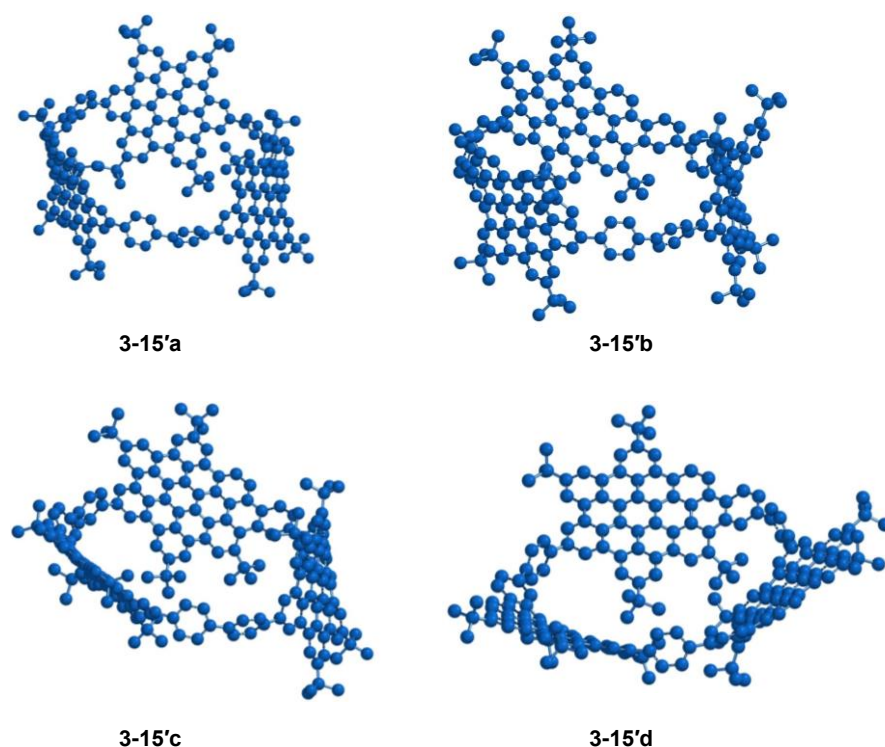


Figure 3-12: Theoretical stick and ball models of **3-15'a** to **3-15'd**, optimized MM2 geometry.

Consequently, the larger [3]CHPB **3-13** was synthesized to reduce the ring-strain and thus the 1,2-phenyl shift side reactions. After cyclodehydrogenation and purification a single compound was selectively obtained. However, cyclodehydrogenation afforded not the [3]CHBC **3-16**, but **3-16'** with an additional loss of 2 hydrogens (Figure 3-13).

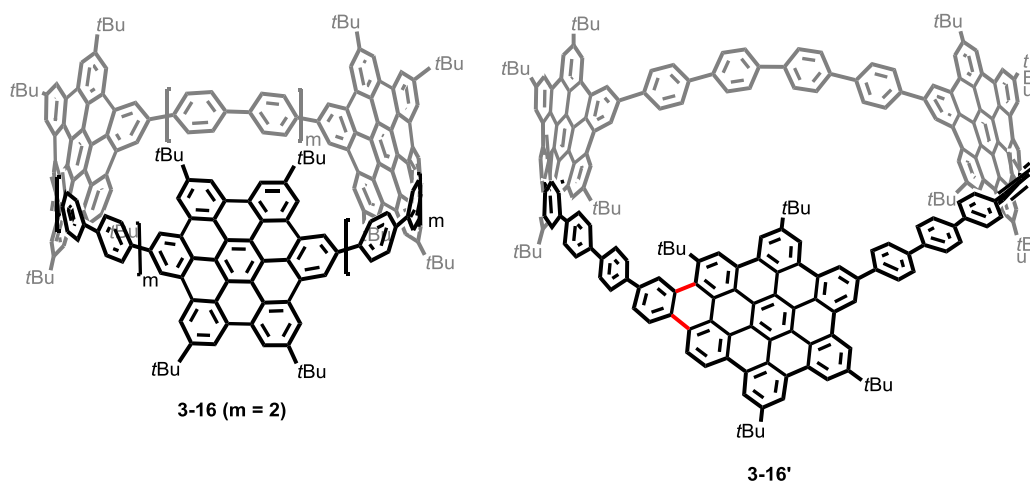


Figure 3-13: Structure of the expected [3]CHBC macrocycle **3-16** and the observed compound **3-16'**.

The purification by preparative HPLC and the subsequent analysis of the fraction by analytical HPLC verified the selective formation of **3-16'**. The HPLC chart is depicted in Figure 3-14, showing a single peak, slightly broadened what is usually observed for such big molecules.

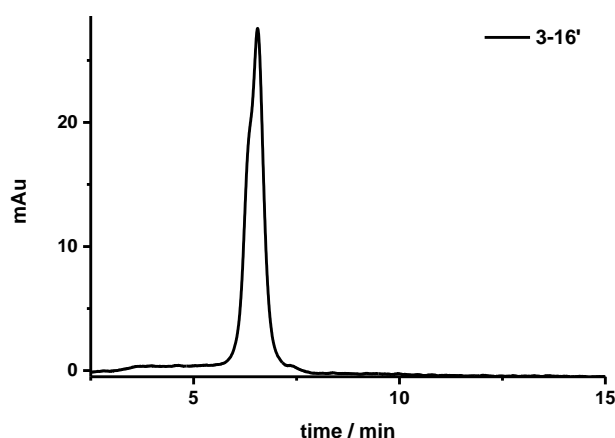


Figure 3-14: HPLC chart for **3-16'**; measured with the column MN HD18 125/4 mm (Macherey-Nagel), 5 μ m grain size; eluent: THF/MeOH (50:50 to 70:30 within 20 minutes); 298 K; 1 ml/min.

The MALDI-TOF mass spectrum clearly showed the loss of two additional hydrogen atoms (Figure 3-15).

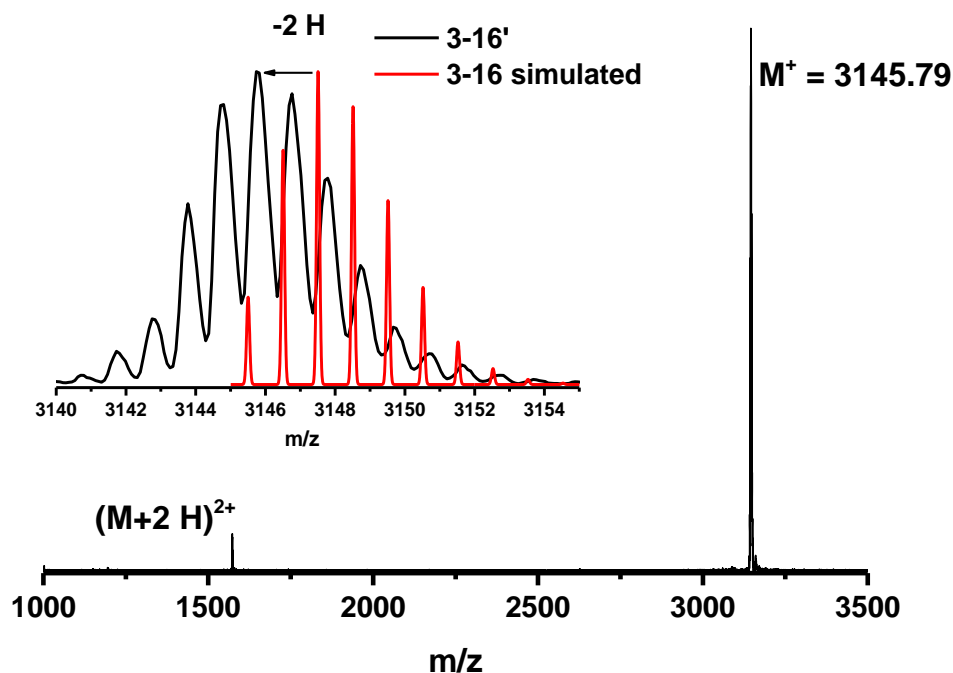


Figure 3-15: MALDI-TOF spectrum of **3-16'**; the target peak is enlarged; simulated spectrum of **3-16** in red.

Since a single product was isolated and a 1,2-phenyl shift was assumed as side reaction, a structure elucidation of **3-16'** by NMR spectroscopy was performed. For the symmetric macrocycle **3-16**, 8 different groups of signals were expected in the ^1H -NMR spectra: two AB systems for the phenylene protons, three singlets in the range between 9 ppm and 10 ppm and one singlet for the aliphatic *tert*-butyl groups, corresponding to 4 doublets and 4 singlets. However, due to a 1,2-phenyl shift, the asymmetric compound **3-16'** was obtained, having one rearranged HBC unit within the macrocycle. Therefore the assignment of the signals was performed with different 2D NMR techniques such as 2D ^1H , ^1H -COSY, 2D ^1H , ^1H -NOESY, and 2D ^1H , ^{13}C -HSQC (Heteronuclear Single Quantum Coherence Spectroscopy). In a HSQC, the ^1H signal is detected in the directly measured dimension in each experiment, while the chemical shift of ^{13}C is recorded in the indirect dimension. The single 1,2-phenyl shift caused the loss of symmetry, resulting in a highly complex 1D ^1H -NMR spectrum (Figure 3-16).

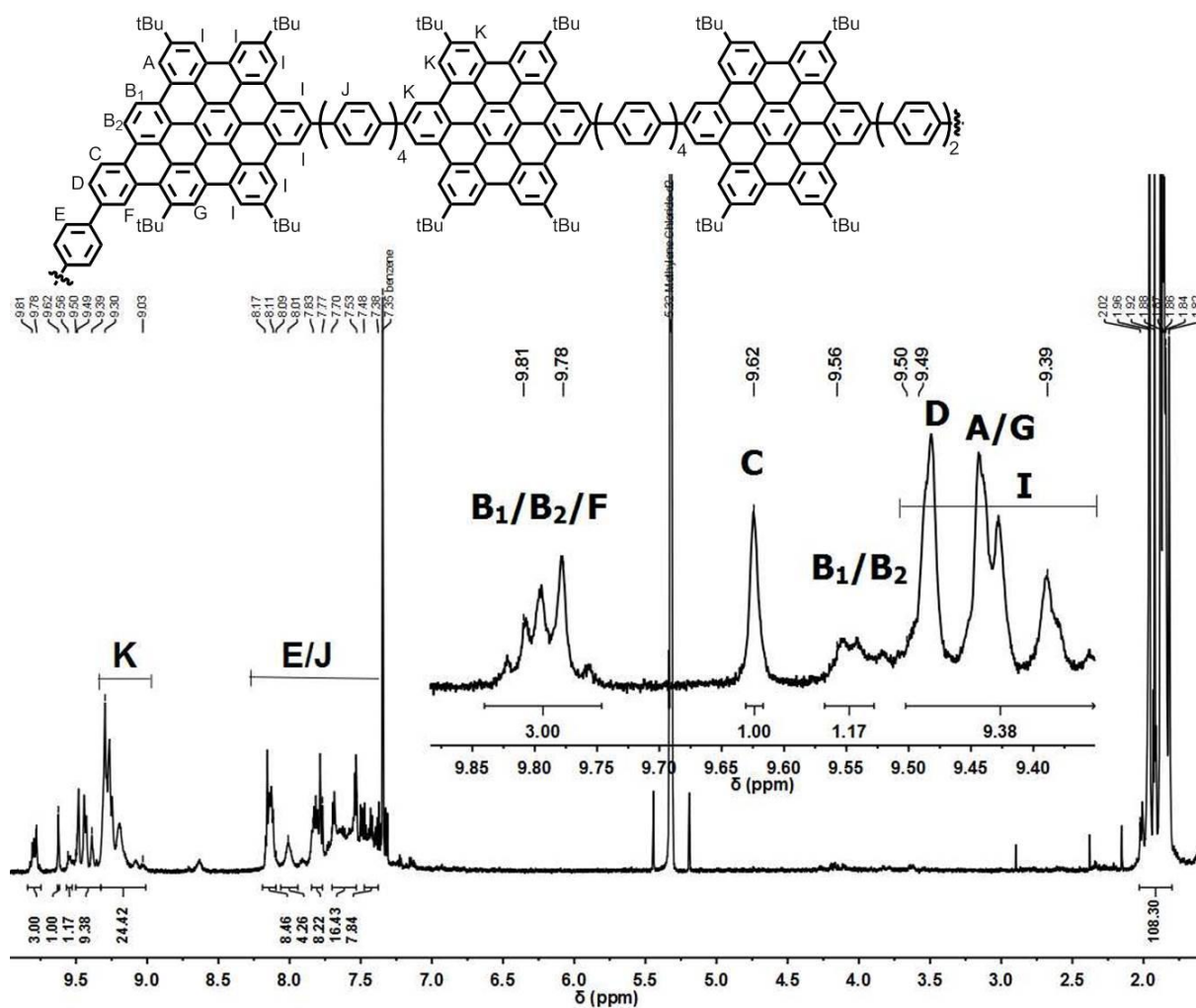


Figure 3-16: ^1H NMR (700 MHz) spectrum of **3-16'** at 298 K in $\text{CS}_2/\text{CD}_2\text{Cl}_2$ (2/1).

However, the different signal groups could have been distinguished, considering the fact that the proton signals of the HBC units were shifted downfield, in the range from 9 ppm to 10 ppm, whereas signals of the phenylene protons appeared between 7.5 ppm and 8.2 ppm. The signals of the *tert*-butyl groups were observed at around 2 ppm. For the rearranged HBC unit, two new AB-spin systems with the characteristic signals at 9.8 ppm and 9.5 ppm (B_1/B_2) and at 9.62 ppm and 9.48 ppm (C/D) appeared and in the 2D $^1\text{H}, ^1\text{H}$ -COSY NMR spectra the respective cross peaks were observed (Figure 3-17b). No through space coupling was observed in the 2D $^1\text{H}, ^1\text{H}$ -NOESY NMR spectrum (Figure 3-18) for the signals of the rearranged HBC

(9.4 ppm to 9.9 ppm) and the signals of the two remaining HBCs (8.55 ppm to 9.4 ppm) what revealed the rearrangement in only one HBC unit.

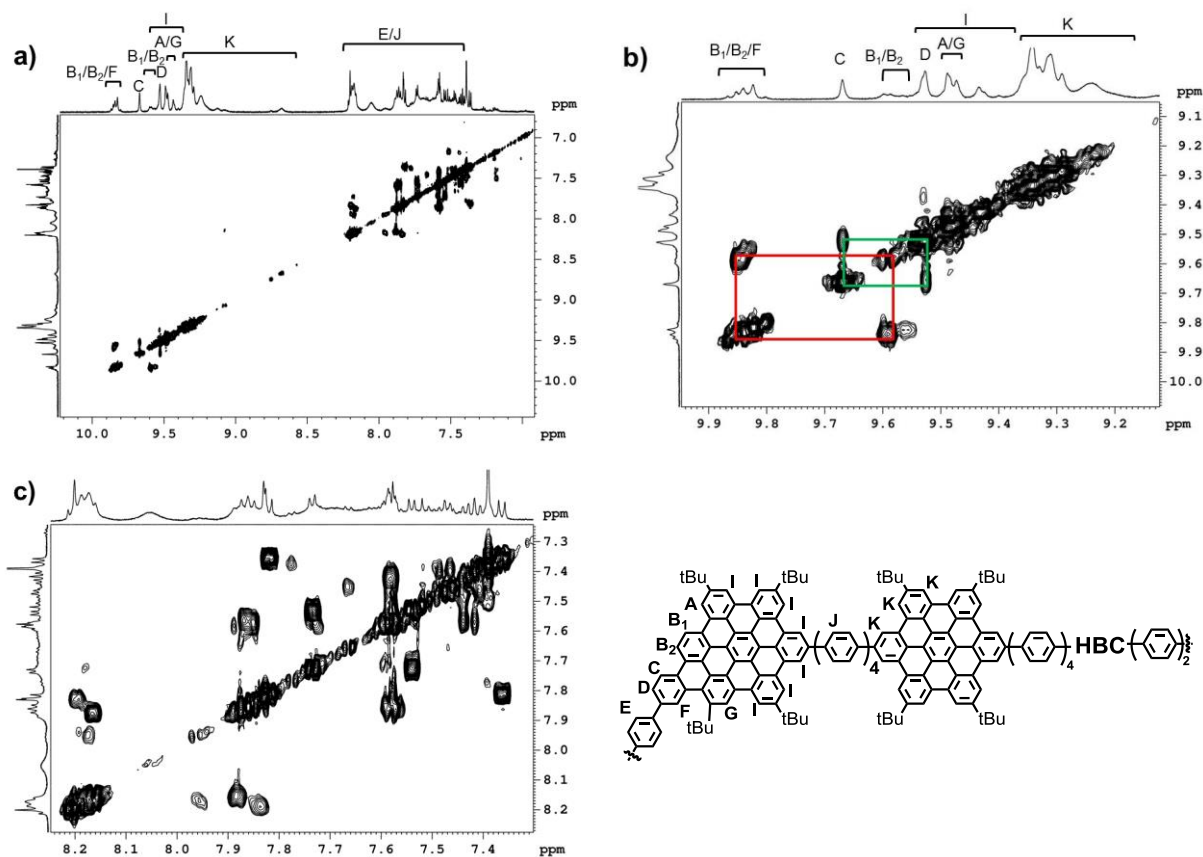


Figure 3-17: 2D $^1\text{H}, ^1\text{H}$ -COSY NMR (700 MHz) spectra of **3-16'** at 298 K in $\text{CS}_2/\text{CD}_2\text{Cl}_2/\text{THF-}d_8$ (2/1/1); a) aromatic region; b) HBC signal region, the two AB-spin systems are marked in red (B_1/B_2) and green (C/D); c) biphenylene region E/J.

Also the cross peaks of the *tert*-butyl groups with the HBC signals verify the clear separation of the rearranged part (Figure 3-18). Furthermore, the nuclear overhauser effect of proton D with the neighboring phenylene protons E was detected, while the through space coupling of the proton F with E was not resolved under these conditions. Though, the through space coupling of the proton F with the AB-spin system C/D was detected, while this showed cross peaks with B_1/B_2 . Also for the protons A and G cross peaks were observed with the neighboring protons B_1/B_2 and F.

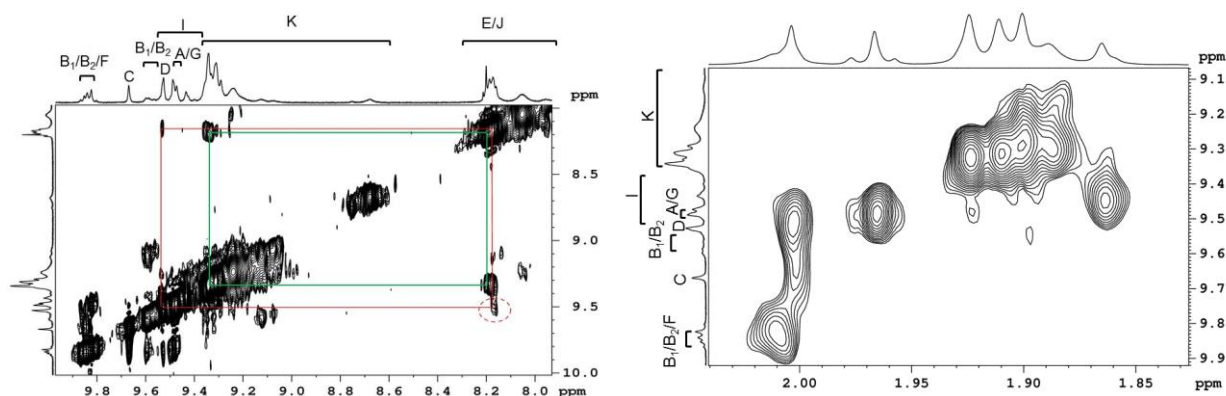


Figure 3-18: 2D ^1H , ^1H -NOESY NMR (700 MHz) spectra of **3-16'** at 298 K in $\text{CS}_2/\text{CD}_2\text{Cl}_2/\text{THF-}d_8$ (2/1/1).

Finally, the 2D ^1H , ^{13}C -HSQC NMR spectrum supports the existence of a single 1,2-phenyl shift, since two distinct signals were observed for the *tert*-butyl groups. This is consistent with the high asymmetry in **3-16'**, in contrast to the expected single signal for the symmetric structure **3-16**.

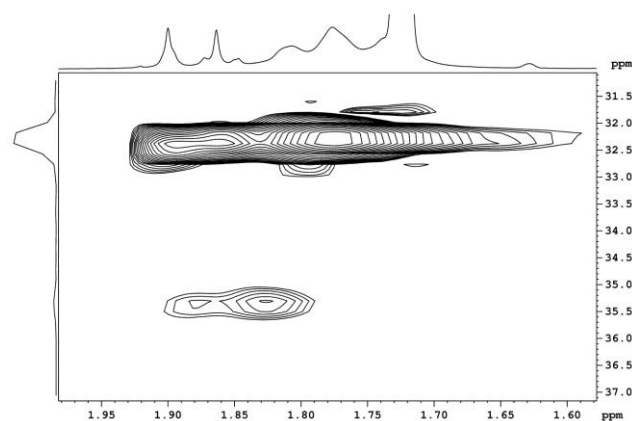
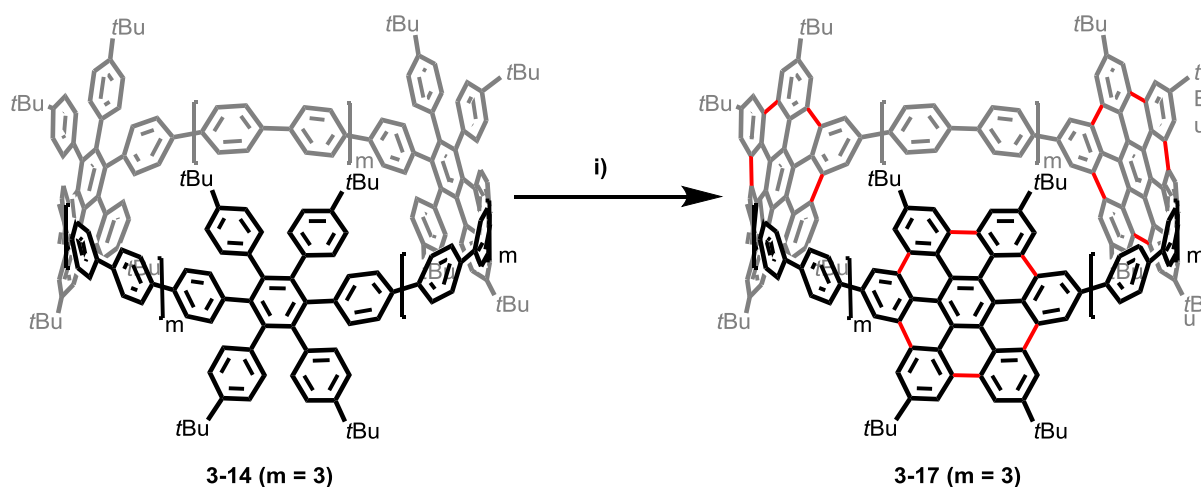


Figure 3-19: 2D ^1H , ^{13}C -HSQC NMR (700/176 MHz) spectra of **3-16'** at 298 K in $\text{CS}_2/\text{CD}_2\text{Cl}_2/\text{THF-}d_8$ (2/1/1).

Furthermore, the relative intensity of 14 protons for the rearranged part to 24 protons for the remaining HBCs support the assumed structure for **3-16'** with the occurrence of a 1,2-phenyl shift in a single HBC unit.

According to these findings, the tendency toward rearrangement reactions was significantly reduced with an increasing ring size. Therefore, further phenylenes were incorporated to afford the 27-membered [3]CHPB **3-14**, which was also subjected to cyclodehydrogenation (Scheme 3-6).



Scheme 3-6: Synthetic scheme of the cyclodehydrogenation towards **3-17**. Conditions: FeCl_3 , MeNO_2 , CH_2Cl_2 , RT, 7 h.

A circumference of 27 phenylene units marks a new dimension in the CPP synthesis, even when the initial goal of creating fully conjugated ultra-short CNTs was not the main focus anymore. However, it also was of importance to prove the concept of the post-construction method, because this method is envisioned to give access to ultrashort CNTs subject to the condition of the right connectivity of benzene rings and the right ring size. To investigate the influence of the ring size on the oxidative cyclodehydrogenation, the 27-membered [3]CHPB **3-14** is an ideally suited compound in the series of the 15- and 21-membered [3]CHPBs **3-12** and **3-13**. The conditions for the *Scholl* reaction were the same as mentioned above. The reaction control by MALDI-TOF mass spectrometry revealed a complete dehydrogenation towards **3-17** after seven hours (Figure 3-20). In the high resolution MALDI-TOF mass spectrum the molecular ion was observed at $m/z = 3601.6853$ (calc. $m/z = 3601.6902$), verifying the complete cyclodehydrogenation towards **3-17**. However, mass spectrometry only indicated the successful synthesis, but no information about the precise structure was obtained. According to the high symmetry in the molecule, NMR spectroscopy was the method of choice to gain further structural information. Theoretically, the HBC units in **3-17** would give three singlets at around 9 ppm and a singlet in the aliphatic region for the *tert*-butyl groups. Additionally, the three AB spin systems, originating from the phenylene protons, are expected to result in six doublets, located between 8.5 ppm to 7.0 ppm.

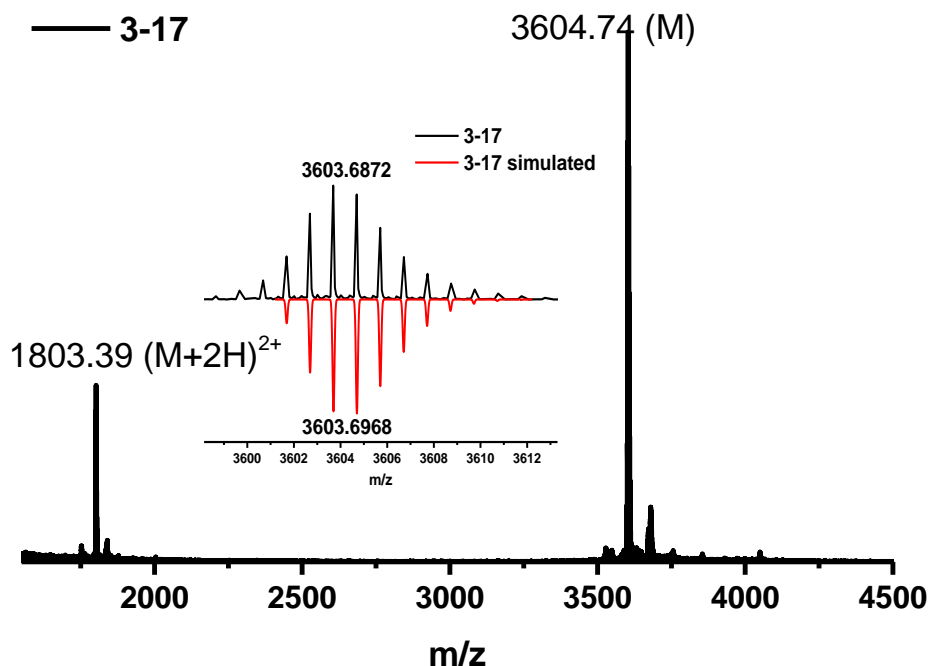


Figure 3-20: MALDI-TOF spectrum of **3-17**.

Unexpectedly, the recording of well-resolved NMR spectra was not successful. In the common deuterated solvents, CD_2Cl_2 , THF- d_8 or $C_2D_2Cl_4$, at RT or elevated temperatures, only very broad and structureless signals appeared and a differentiation from the background noise was not possible. For **3-16'** a solvent mixture of CD_2Cl_2 , THF- d_8 and carbon disulfide increased the resolution of the respective NMR spectra by preventing the aggregation of individual molecules. The best resolution for **3-17** was obtained in pure carbon disulfide without the addition of any deuterated solvents. The 1H -NMR spectrum is depicted in Figure 3-21.

The signals in the 1H -NMR spectrum of **3-17** were very broad and structureless (Figure 3-21 top). Even in carbon disulfide aggregation could not be suppressed. If only aggregation caused the broadening or other effects were responsible for the high anisotropy could not be further specified. However, three distinctive signal regions were distinguishable. At low magnetic field, centered at 9.87 ppm, a broad signal was detected and in the region between 8.95 ppm and 6.87 ppm, a multitude of broad signals appeared. At high magnetic field, around 2.56

ppm, the third signal region was detected. So far, the expectations match with the observed signal regions.

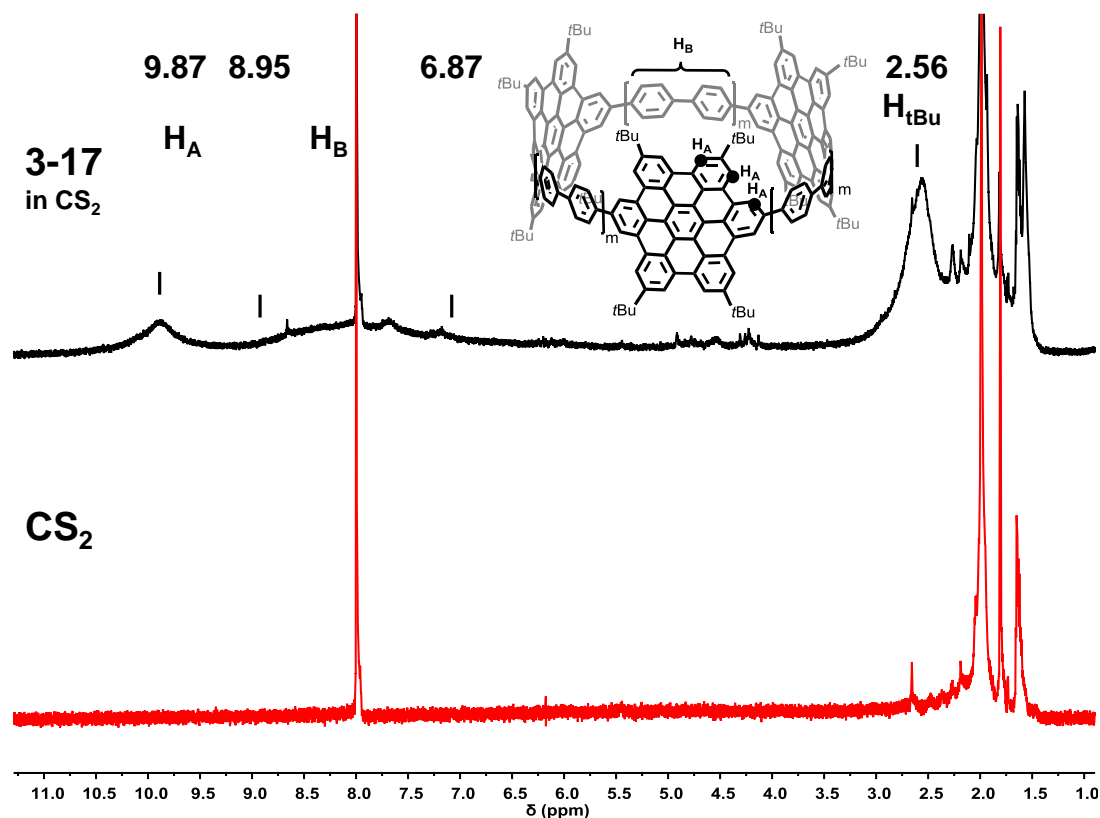


Figure 3-21: top) ¹H NMR (850 MHz) spectrum of **3-17** at 298 K in CS₂ and bottom) ¹H NMR (850 MHz) spectrum of pure CS₂ at 298 K.

Hence, 2D NMR techniques such as 2D ¹H,¹H-COSY and 2D ¹H,¹H-NOESY were applied to gain further information (Figure 3-22). In the 2D ¹H,¹H-NOESY spectrum, the protons H_A at 9.87 ppm show a cross peak with the protons in the aliphatic region at 2.56 ppm, whereas no cross peak was observable for protons H_B. This indicates that the signal at 9.87 ppm originated from the protons attached to the formed HBC units in **3-17**. Furthermore, the signal at 2.56 ppm could be assigned to the protons of the *tert*-butyl groups. In analogy to **3-16'** the remaining signal region should reflect the signals of the protons H_B. In the 2D ¹H,¹H-COSY spectrum (Figure 3-22b), a correlation between the signals of the protons H_B was found, further supporting our assumptions. The signal series is consistent with the structure of **3-17**, sup-

posed in Scheme 3-6, but the NMR analysis presented here only indicated the successful synthesis of **3-17** and was no final proof.

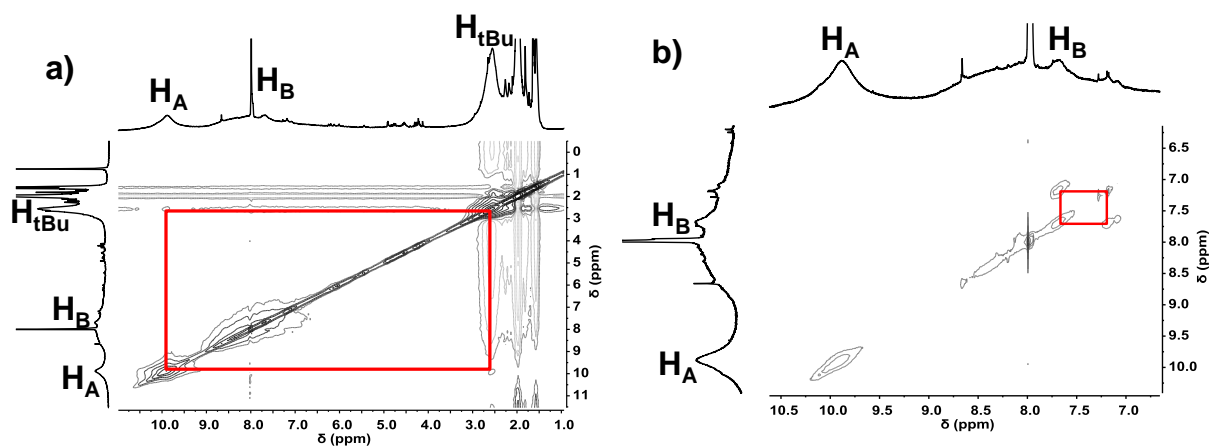


Figure 3-22: a) 2D ^1H , ^1H -NOESY NMR (850 MHz) spectra b) 2D ^1H , ^1H -COSY NMR (850 MHz) spectra of **3-17** at 298 K in CS_2 .

Encouraged by the new analytical possibilities of the mass spectrometry, more precisely the ion mobility-spectrometry and tandem mass-spectrometry, a direct proof of the cyclic nature of **3-17** could be accomplished. Like for **3-15'**, the sample was ionized by MALDI and the molecular ion was separated (Figure 3-23).

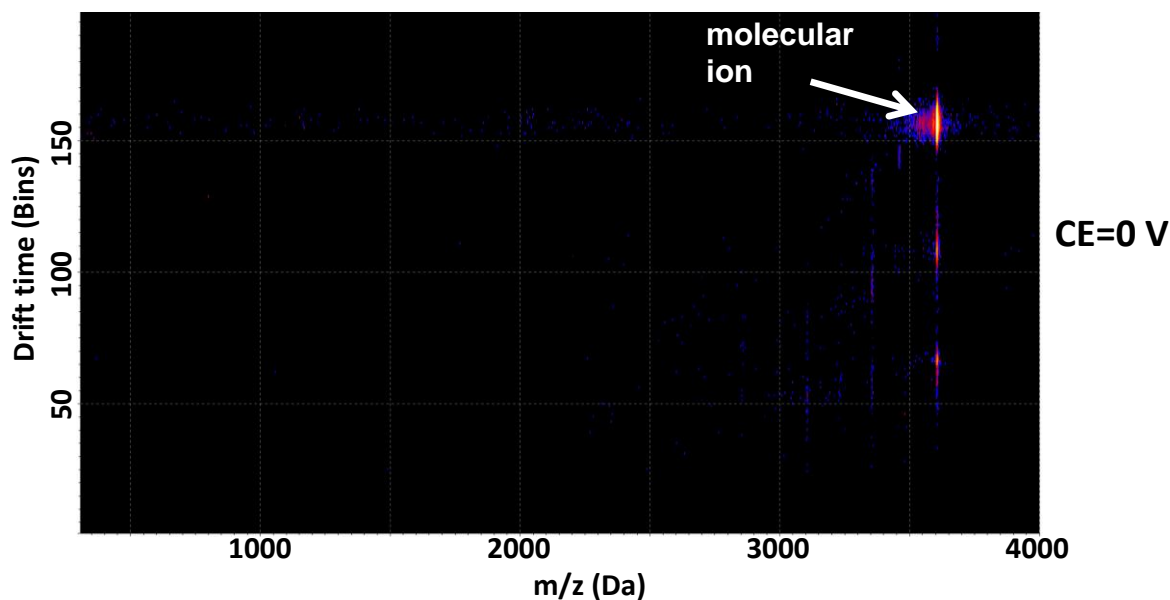


Figure 3-23: 2D drift time vs. m/z ion mobility image for **3-17**; collision energy: 0 V.

The maximum collision energy had to be applied for the detection of fragments, conformers and ring opened products (Figure 3-24). For clarity, four trend lines A to D were overlaid to mark the regions of alkyl chain fragmentation. Trend line A contained the molecular ion and the fragments, observed due to the side chain destruction during the measurement. Different from the ion mobility image of **3-15'**, two signal series (B and C) appeared which are supposed to be twisted macrocycles because of the lower drift time. Since the signals of the series B and C were quite intense, these twisted conformers have to have certain stability. Also the weak signal for the ring-opened linear structure (trend line D), was an indication for the high stability of **3-17**. Linear dimeric and monomeric fragments were not observed, because the collision energy of the system was too low to further fragment **3-17**. If the appearance of a second series of twisted conformers had to do with the higher flexibility in the larger [3]CHBC **3-17** compared to **3-15'** and how these twisted conformers looked like was beyond the scope of this work and is part of the ongoing research. Further, if these twisted conformers can also be formed in solution, the high anisotropy would cause a broadening of the NMR signals.

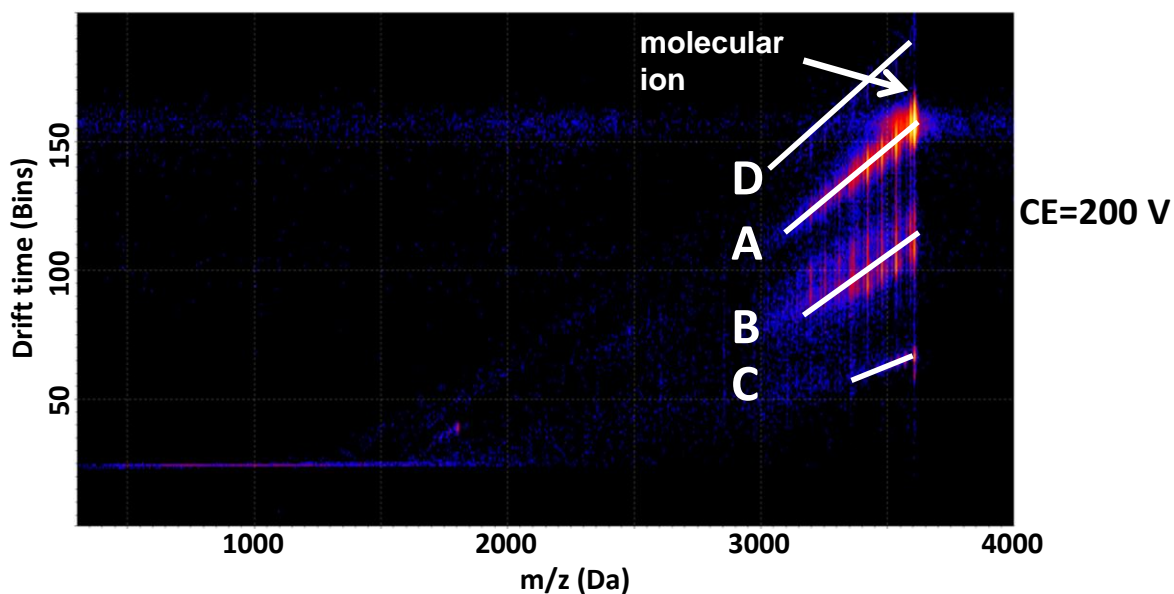


Figure 3-24: 2D drift time vs. m/z ion mobility image for **3-17**; collision energy: 200 V.

So far, these are speculations, but within the homologous series of [3]CHPBs with circumferences of 15-, 21- and 27-phenylene rings an obvious trend was observed, since the selectivity of the cyclodehydrogenation was increased with increasing ring size. Moreover, without any doubts the selective formation of **3-17** was claimed. This is a proof for a direct relation between the ring strain and the possibility to form graphenic sidewalls by oxidative cyclodehydrogenation.

Finally the electronic absorption and emission spectra of the obtained [3]CHBCs **3-15** to **3-17** were recorded (Figure 3-25). The absorption spectra of **3-15'c,d**, **3-16'** and **3-17** resemble those of substituted HBCs, with a strong absorption β -band at ~ 370 nm and local maxima at ~ 356 nm, ~ 388 nm and ~ 420 nm.^[156,157] The emission spectra of **3-15'c** and **3-16'** were identical, showing maxima at 492 nm, 525 nm and 551 nm. The emission spectrum of **3-17** was rather broad with an emission maximum at 525 nm and a small shoulder at 498 nm. In contrast, the emission maximum of **3-15'd** was bathochromically shifted to 512 nm.

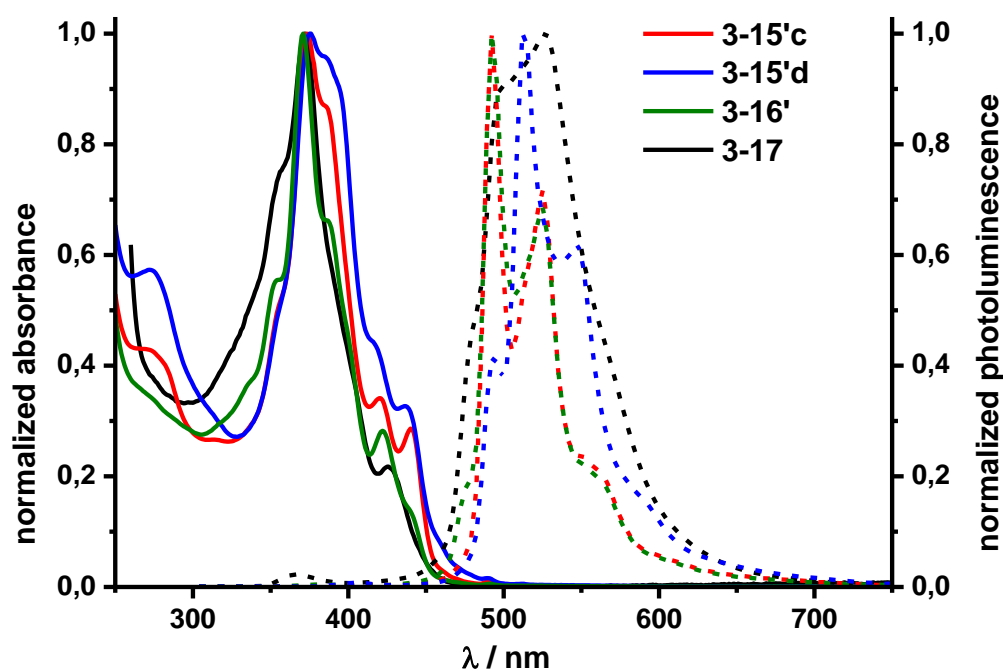


Figure 3-25: Electronic absorption (solid line) and emission (dashed line) spectra of compounds **3-15'c,d**, **3-16'** and **3-17** in dichloromethane.

Since three rearrangements were assumed for **3-15'd** the CPP base is supposed to be highly twisted and the partial relaxation in the excited state may have caused the red shift of the emission maximum, also resulting in the largest *Stokes* shift (137 nm) in this series. All electronic absorption and emission data are summarized in Table 3-2.

Table 3-2: The summary of the electronic absorption and emission data for **3-15'c,d**, **3-16'** and **3-17** in dichloromethane.

compound	λ_{abs} [nm]	λ_{em} [nm]
3-15'c	356, 373, 387, 421, 441	492, 525, 551
3-15'd	356, 375, 387, 416, 437	492, 512, 548
3-16'	353, 371, 388, 422	492, 525, 551
3-17	356, 372, 425	498, 525

3.3. Summary

In summary, the synthesis of phenylene-extended [3]CHPBs of different sizes was described and the applicability of the *Scholl* reaction to form graphenic sidewalls was demonstrated as an approach to longitudinally extend CPPs. The kinked key intermediates **3-3**, **3-5** and **3-8** were obtained by the twofold incorporation of 4,4'-iodobiphenyl into the tetraarylbenzoquinone **3-1**, the alkylation and a further arylene elongation by *Suzuki* cross coupling. In a one-pot macrocyclization of these kinked precursors under *Yamamoto* conditions, cyclic trimers were primarily obtained, which were subsequently aromatized to give the [3]CHPBs **3-12** to **3-14** with circumferences of 15-, 21- and 27-phenylene rings in the CPP base.

Finally, the [3]CHPB macrocycles **3-12** to **3-14** were subjected to oxidative cyclodehydrogenation, using iron chloride, to yield [3]CHBCs. Due to the ring strain and the distortion of the benzene rings no clean and selective cyclodehydrogenation was observed for the smallest [3]CHPB **3-12**. Products with a higher degree of dehydrogenation were obtained. It was supposed that a 1,2-phenyl shift occurred, which went along with structural changes. The separation and analysis by ion mobility mass spectrometry confirmed the 1,2-phenyl shift as the side reaction and in combination with simulations the tendency towards a conical macrocycle was

revealed. The increase of the ring size significantly reduced the side reactions, having only one 1,2-phenyl shift for the 21-membered [3]CHPB **3-16'** and a selective formation of the [3]CHBC **3-17** was observed. The structure of **3-16'**, containing one rearranged HBC unit, was elucidated by HR-MALDI-TOF mass spectrometry and NMR spectroscopy. Unexpectedly, the precise characterization of the [3]CHBC **3-17** was rather complex, since no well resolved NMR spectrum could have been recorded. The addition of CS₂ and the dilution of the sample solution also resulted in broadened signals. The reason of the high anisotropy of **3-17** in solution could not be specified. The recording of solid state NMR spectra could give more structural information, but the obtained amount was too small to use this technique so far. In the end, ion mobility mass spectrometry and further mass spectrometry techniques confirmed the successful synthesis of **3-17**.

However, the obvious trend towards the selective cyclodehydrogenation of the phenylene-extended [3]CHPBs to the respective [3]CHBCs with the increase in ring size can be claimed. Further, the applicability of the *Scholl* reaction to obtain graphenic sidewalls in the last step was successfully demonstrated. This marks an important step towards the precise synthesis of ultrashort CNTs subject to the condition aryl-extended [3]CHPB precursors are used to permit the formation of fully conjugated cylinders.

4. Blocked *Cyclo-hexa-peri-*hexabenzocoronenes

4.1. Introduction

As discussed before in chapter 3, the longitudinal extension of CPPs towards ultrashort CNTs is essential for the successful bottom-up synthesis of CNTs. Further it was already demonstrated, that polyarylated CPPs can be transformed into the respective *cyclo-para-hexa-peri-*hexabenzocoronenes. However, the high ring strain hampered a clean and selective cyclodehydrogenation towards [3]CHBCs. Detailed studies revealed that strain releasing 1,2-phenyl shifts occurred (Figure 4-1).

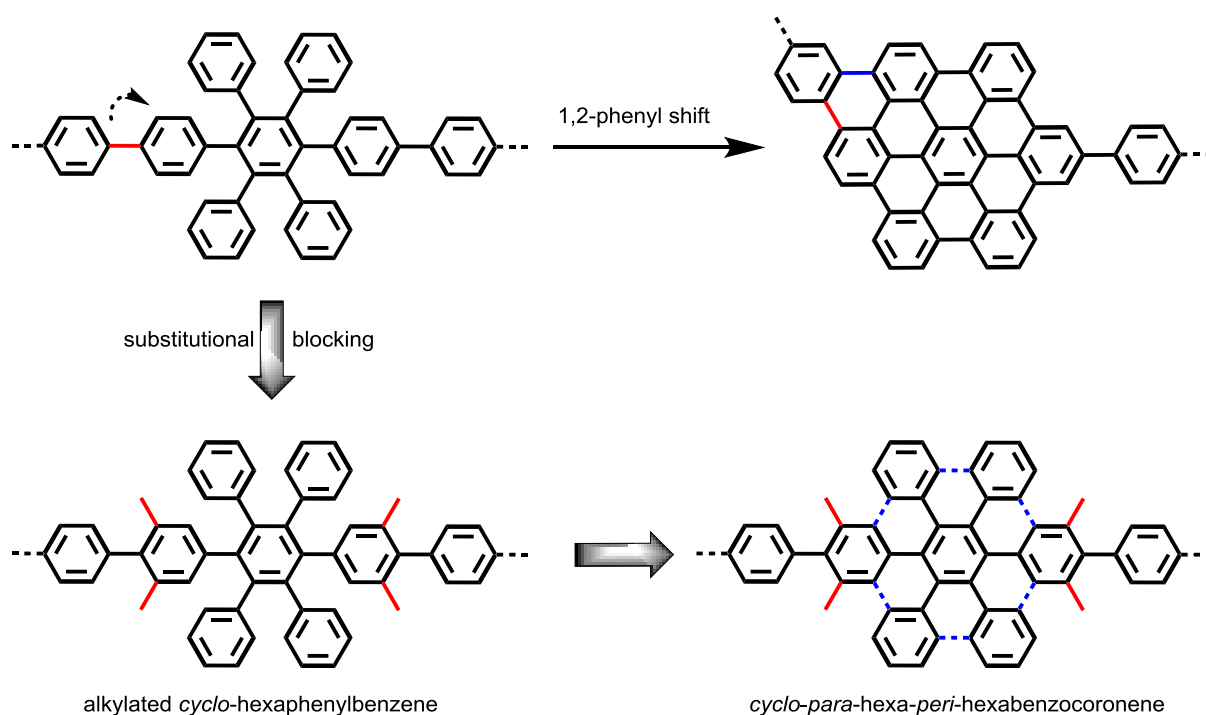


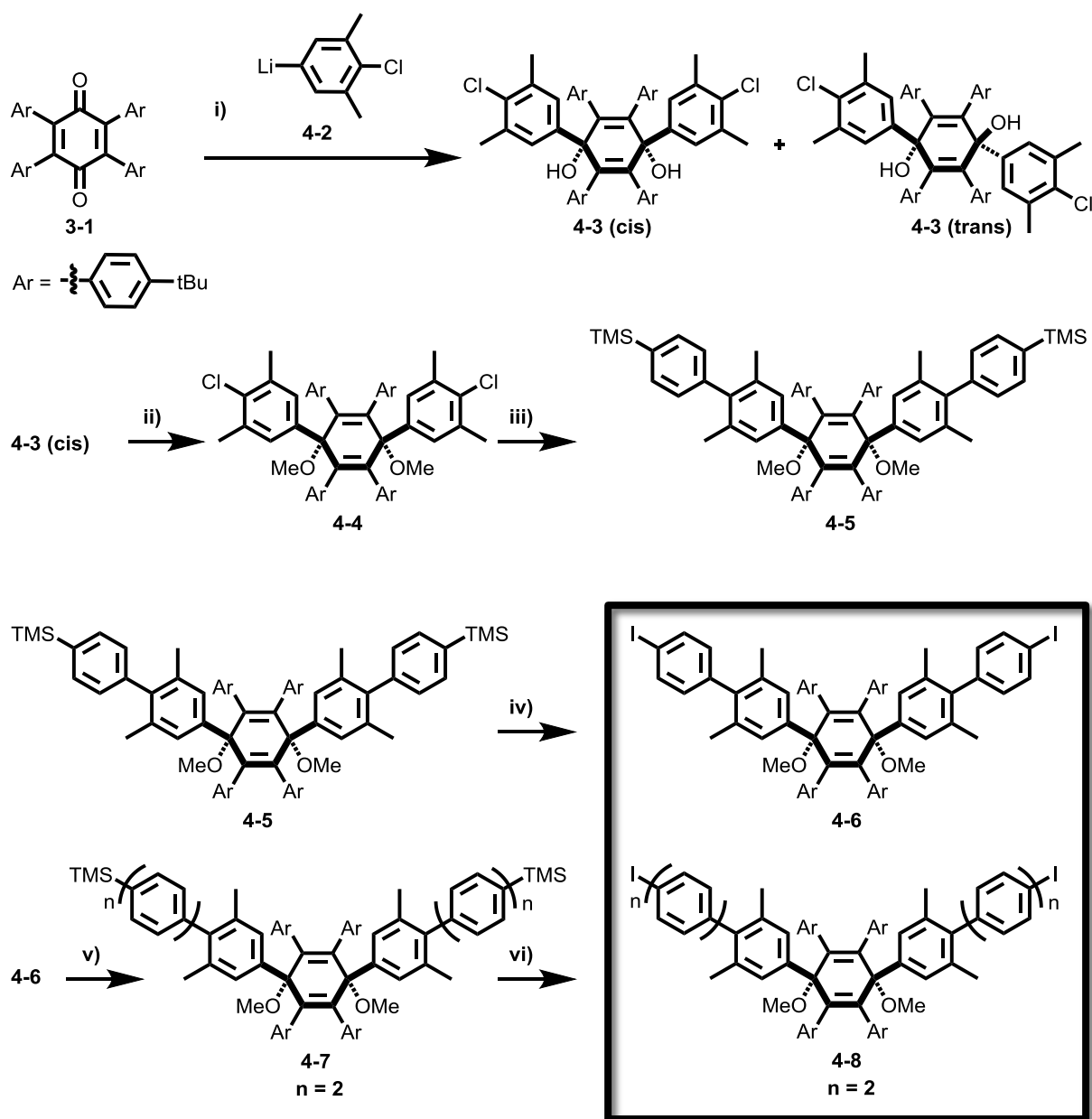
Figure 4-1: Concept of the substitutional blocking as an approach towards the selective synthesis of [3]CHBCs.

To prevent these undesired side reactions, the incorporation of blocking alkyl substituents at the critical positions of the [3]CHPB skeleton was anticipated to facilitate a smooth cyclodehydrogenation (Figure 4-1). In this chapter, the synthesis of the alkyl substituted phenylene-extended *cyclo-p*-hexaphenylbenzenes ([3]CHPBs) will be presented, as an approach to selectively obtain [3]CHBCs by oxidative cyclodehydrogenation.

4.2. Results and Discussion

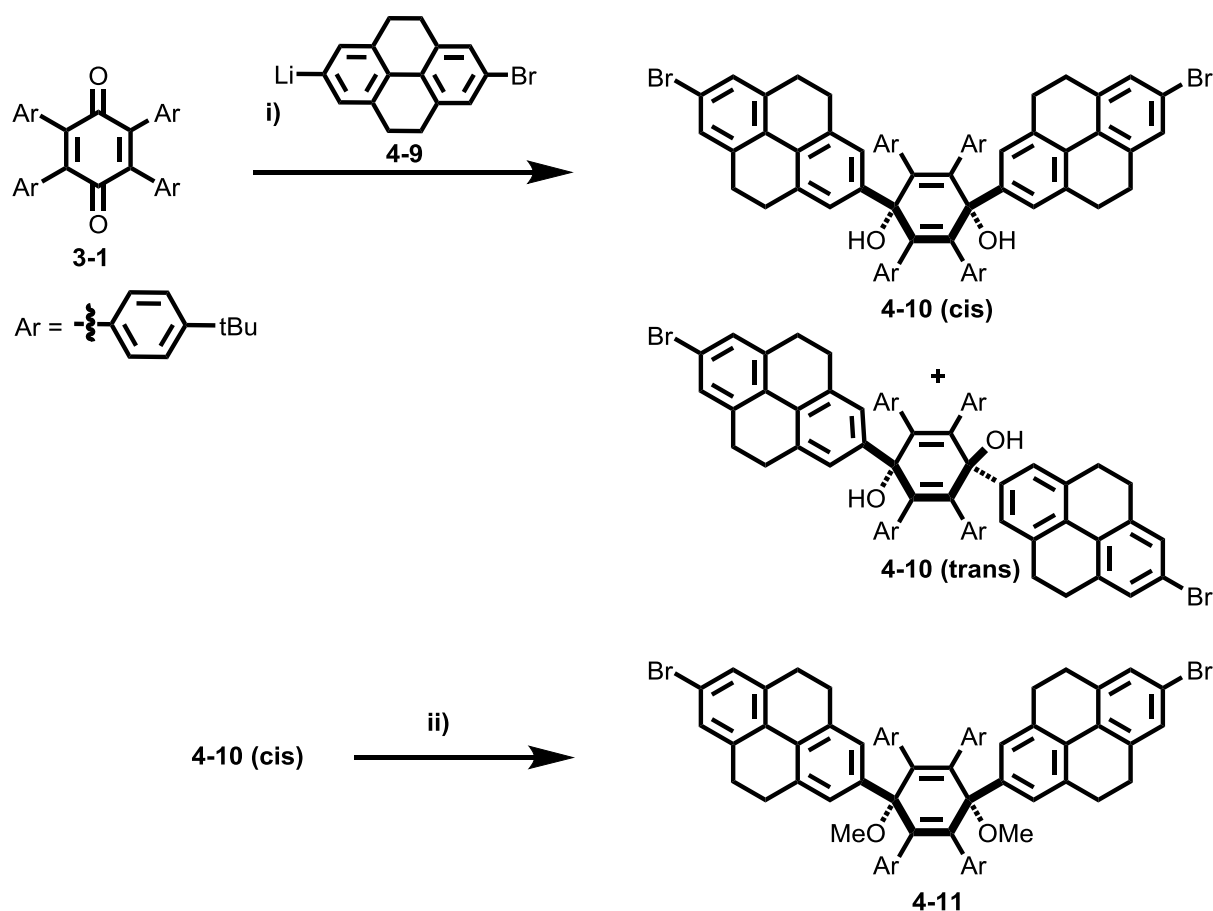
4.2.1. Synthesis of Alkyl Substituted [3]CHPBs

The alkyl substituted phenylene-extended [3]CHPBs **4-14**, **4-15**, **4-17** were synthesized under *Yamamoto* conditions, as described in chapter 3.2.1. For the introduction of the methyl substituents at the *ortho*-positions of the CPP base, 5-bromo-2-chloro-1,3-dimethylbenzene was synthesized and selectively lithiated in the 5-position (Scheme 4-1). The subsequent addition of **3-1** afforded mainly the *cis*-diol **4-3** in 60 % yield, which was alkylated with methyl iodide, leading to the key building block **4-4**.^[50,145] An elongation towards the [3]CHPB precursor **4-6** with a 15-membered CPP base was achieved by a *Suzuki-Miyaura* cross coupling reaction with 4-trimethylsilylphenylboronic acid pinacol ester, applying the catalyst system developed for the coupling of chlorine compounds by *Buchwald* et. al.^[146] In the following, a trimethylsilyl-iodine exchange reaction, using iodine monochloride and silver tetrafluoroborate was performed. For the 21-membered alkyl functionalized [3]CHPB precursor **4-8**, the elongation and iodination were repeated. For this sterically less demanding cross-coupling reaction, tetrakis(triphenylphosphine)palladium(0) was used instead of palladium(II) acetate and S-Phos.



Scheme 4-1: Synthetic route towards the kinked intermediates **4-6** and **4-8**. Conditions: i) $-78\text{ }^{\circ}\text{C}$, THF, *n*-BuLi, 0.5 h; $-78\text{ }^{\circ}\text{C} \rightarrow \text{RT}$, 16 h, 60 %; ii) THF, NaH, MeI, $-78\text{ }^{\circ}\text{C}$, 1 h, $-78\text{ }^{\circ}\text{C} \rightarrow \text{RT}$, 16 h, 89 %; iii) 4-trimethylsilylphenylboronic acid pinacol ester, Pd(OAc)₂ (10 mol %), K₃PO₄, toluene/water (10/1), 16 h, 90 $^{\circ}\text{C}$, 65 %; iv) AgBF₄, THF, MeOH, ICl (1M in DCM), 0 $^{\circ}\text{C}$, 40 min., 70 %; v) 4-trimethylsilylphenylboronic acid pinacol ester, Pd(PPh₃)₄, Ag₂CO₃, THF, 70 $^{\circ}\text{C}$, 16 h, 69 %; vi) AgBF₄, THF, MeOH, ICl (1M in DCM), 0 $^{\circ}\text{C}$, 40 min., 85 %.

For the phenylene-extended [3]CHPB **4-17**, 4,5,9,10-tetrahydropyrene units, which equal ethylene bridged biphenyls, were incorporated into the CPP backbone to stiffen and to prevent rearrangements during cyclodehydrogenation. Therefore, 2,7-dibromo-4,5,9,10-tetrahydropyrene was monolithiated and **1-1** was subsequently added to yield the *cis*-diol **4-10**, which was then alkylated to afford the macrocycle precursor **4-11** in 33 % overall yield (Scheme 4-2).



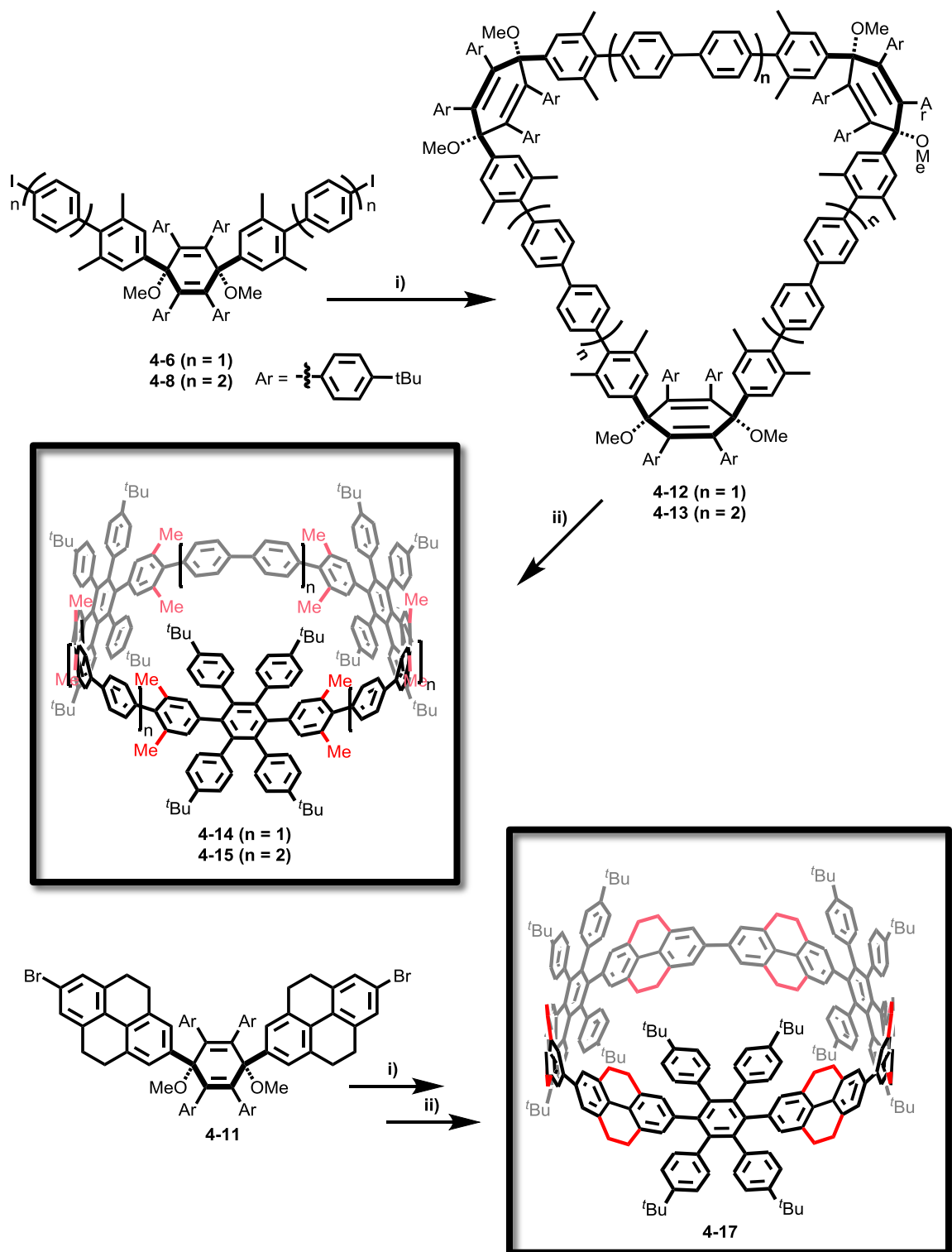
Scheme 4-2: Synthetic route towards the kinked intermediate **4-11**. Conditions: i) $-78\text{ }^{\circ}\text{C}$, THF, *n*-BuLi, 0.5 h; $-78\text{ }^{\circ}\text{C} \rightarrow \text{RT}$, 16 h, 35 %; ii) THF, NaH, MeI, $-78\text{ }^{\circ}\text{C}$, 1 h, $-78\text{ }^{\circ}\text{C} \rightarrow \text{RT}$, 16 h, 94 %;

The macrocyclization of the precursors **4-6**, **4-8** and **4-11** was performed under *Yamamoto* conditions, using nickel(0) (Scheme 4-3).^[158–160] Under these conditions, the major products were the [3]CHPB trimers **4-12**, **4-13**, **4-16**, whereas linear oligomers were separated by gel

permeation chromatography. The aromatization of the 1,4-cyclohexadienyl rings was achieved with sodium naphthalenide or low valent titanium, resulting in the all-phenylene macrocycles **4-14**, **4-15** and **4-17** (Scheme 4-3). The aromatization method was chosen according to the solubility of the cyclic trimer, since the temperature difference was around 160 K.

The macrocycles were analyzed by high resolution mass spectrometry, NMR and UV-Vis spectroscopy. The detailed analyses are described in the following chapter 4.2.2.

The alkyl functionalized macrocycles **4-14**, **4-15** and **4-17** are supposed to undergo a clean and selective cyclodehydrogenation towards the respective [3]CHBCs. The cyclodehydrogenation, as the final step, will be described in detail in chapter 4.2.3.



Scheme 4-3: Synthetic route towards the cyclic *p*-hexaphenylbenzene macrocycles **4-14**, **4-15** and **4-17**. Conditions: i) Ni(cod)₂, 1,5-cyclooctadien, 2,2'-bipyridine, toluene, THF, *N,N*-dimethylformamide, 80 °C, 16 h, 19 to 23 %; ii) sodium naphthalenide or TiCl₄/LiAlH₄, THF, -78 °C/ 80 °C, 1 h/2 d, 17 to 26 %.

4.2.2. Characterization of Alkyl Substituted [3]CHPBs

As described in chapter 3.2.2, the dihedral angle of the kinked precursors are supposed to be in the range of 50° to 75° to yield the cyclic trimer. Single crystals of the kinked precursor **4-8** and **4-11** were grown by slow evaporation from dichloromethane.

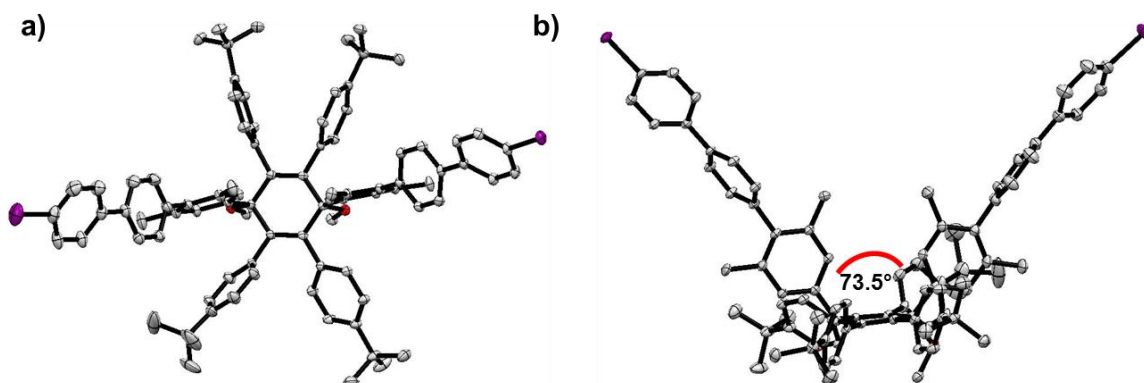


Figure 4-2: X-ray crystal structure of **4-8**; a) top view; b) side view; ellipsoids were set at 50 % probability, hydrogen atoms and solvent molecules are omitted for clarity; oxygen atoms in red, iodine atoms in violet.

The X-ray single crystal structure analysis verified the formation of the *cis*-isomer, with a dihedral angle of 73.5° and 60.6° for **4-8** and **4-11**, respectively (Figure 4-2 and Figure 4-3). The dihedral angle between the methyl-substituted terphenyls in **4-8** is comparable with the angle in the non-substituted precursor (**3-3**, chapter 3.2.2).

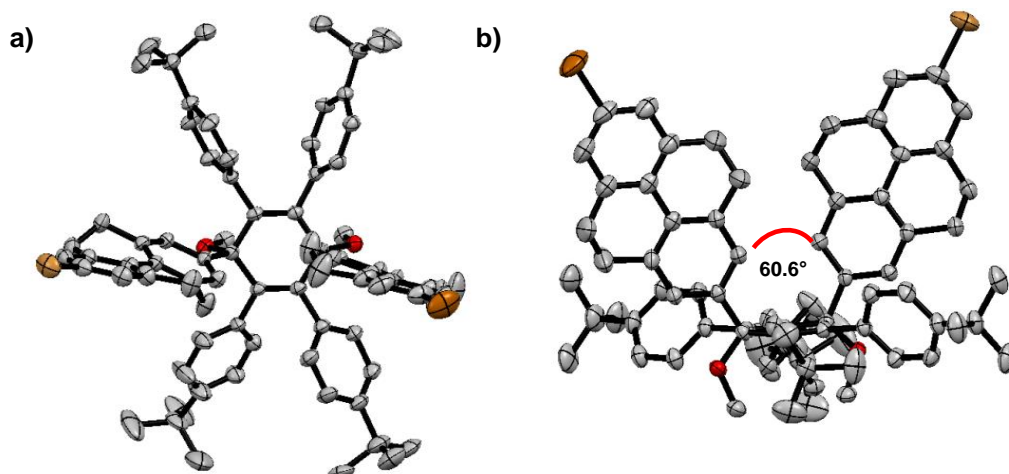


Figure 4-3: X-ray crystal structure of **4-11**; a) top view; b) side view; ellipsoids were set at 50 % probability, hydrogen atoms and solvent molecules are omitted for clarity; oxygen atoms in red, bromine atoms in brown.

For the precursor **4-11**, with the 4,5,9,10-tetrahydropyrene units, the dihedral angle was about 10 degrees smaller than for **4-8**. In the sideview of the X-ray crystal structure (Figure 4-3b), the twist of the two 4,5,9,10-tetrahydropyrenediyls and a partial overlap of these units could be observed what can explain the smaller dihedral angle.

The aromatized macrocycles **4-14**, **4-15** and **4-17** were initially analyzed by HR-MALDI-TOF MS. For **4-14** the molecular ion peak was observed at $m/z = 2895.7897$ (calcd. $m/z = 2895.7903$), for **4-15** it was observed at $m/z = 3352.9782$ (calcd. $m/z = 3352.9814$) and for **4-17** the molecular ion peak appeared at $m/z = 3039.7945$ (calcd. $m/z = 3039.7903$). The isotopic patterns of the respective mass spectra were also in good agreement with the simulated ones (Figure 4-4).

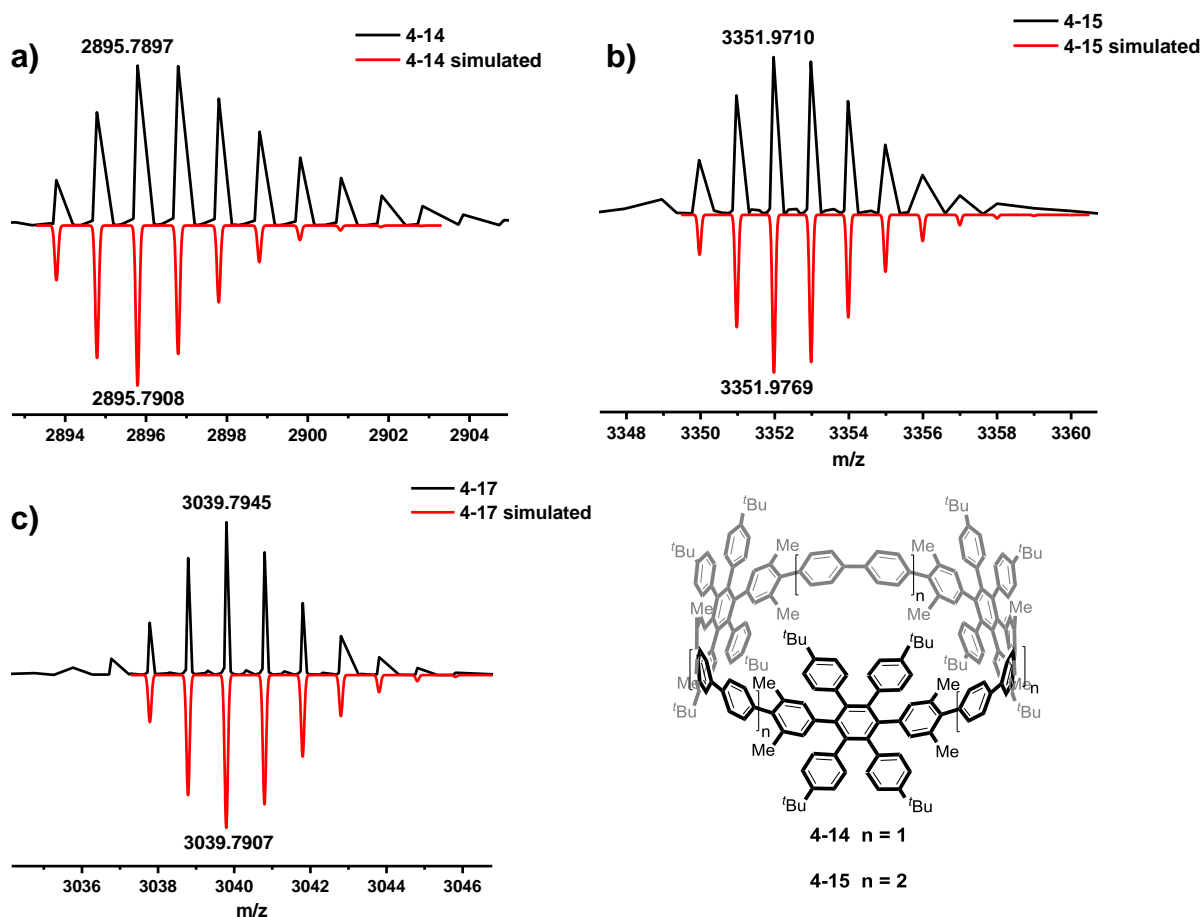


Figure 4-4: HR-MALDI-TOF mass spectra of a) **4-14**; b) **4-15** and c) **4-17** and the structure of the compounds **4-14** and **4-15**.

Additional to mass spectrometry, NMR techniques were applied to elucidate the structure of the phenylene-extended [3]CHPBs. The $^1\text{H-NMR}$ spectra of **4-14** and **4-15** are depicted in Figure 4-5. At high magnetic field, singlets at 1.17 ppm and 1.14 ppm and at 1.73 ppm and 1.67 ppm with a ratio of 3 to 1 were observed. These signals could be assigned to the *tert*-butyl and methyl substituents, indicating the highly symmetric character of the phenylene-extended [3]CHPBs **4-14** and **4-15**, respectively. Details of the aromatic region are shown in Figure 4-6.

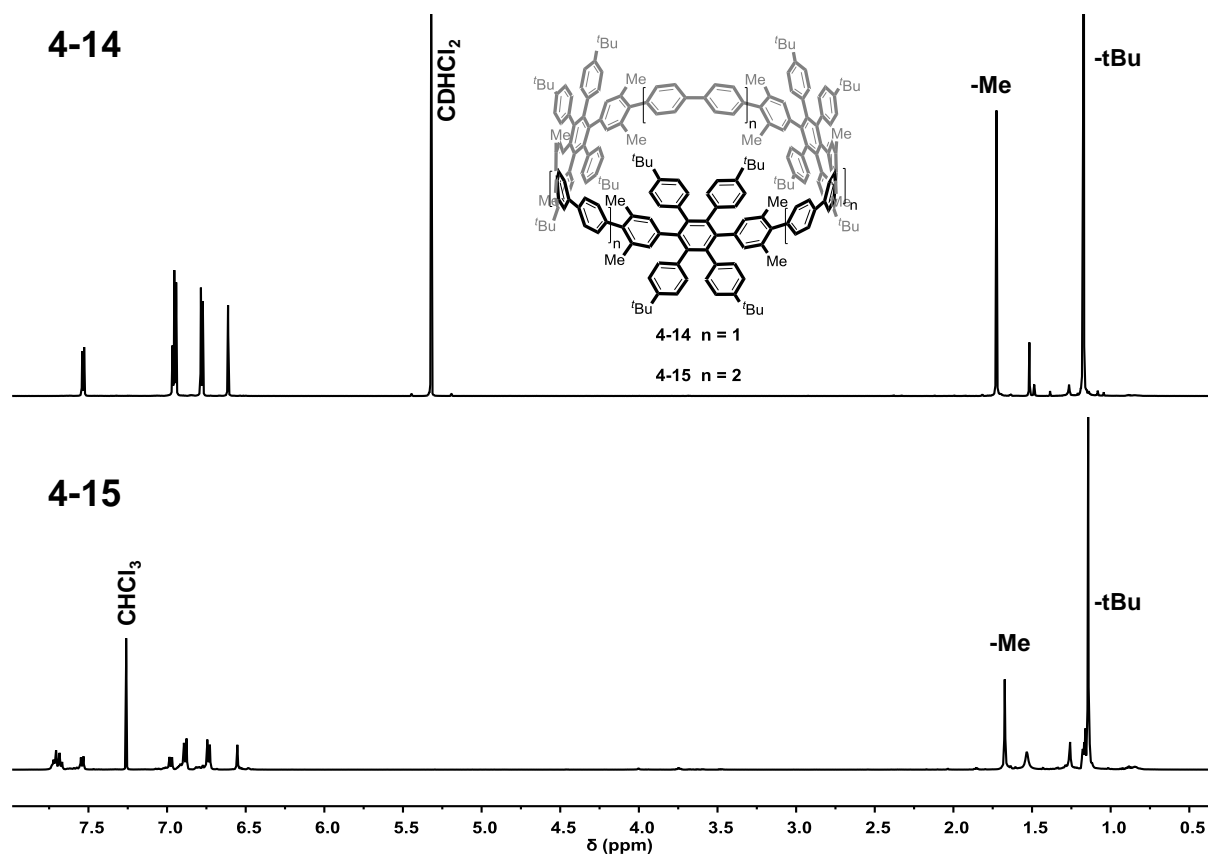


Figure 4-5: $^1\text{H-NMR}$ spectra of top) **4-14** (700 MHz) in CD_2Cl_2 at 298 K and bottom) of **4-15** (500 MHz) in CDCl_3 at 298 K.

In the aromatic region of the $^1\text{H-NMR}$ spectra of **4-14**, a set of signals with the ratio 1 to 3 to 2 to 1, from lower- to higher magnetic field, was observed (Figure 4-6). The singlet at 6.61 ppm was directly assigned to the phenylene protons of the methyl substituted phenylenes

(marked in green). The other signals were assigned using 2D-proton correlation spectroscopy ($^1\text{H}, ^1\text{H}$ -COSY) and 2D-nuclear magnetic resonance spectroscopy ($^1\text{H}, ^1\text{H}$ -NOESY) (Figure 4-7). The signal at 7.54 ppm originates from the phenylene protons marked in magenta, which was confirmed by the $^1\text{H}, ^1\text{H}$ -COSY spectrum. Further, the signal at 6.96 ppm was identified as two doublets, slightly overlapping. The doublet signal, centered at 6.97 ppm, originated from the blue marked phenylene protons in the CPP base, whereas the signal at 6.95 ppm (black) together with the doublet at 6.78 ppm belong to the aryl substituents. With the help of the $^1\text{H}, ^1\text{H}$ -NOESY spectrum, a further differentiation between the signals of the two AB systems was performed. The doublet at 6.95 ppm (black) shows a through space coupling with the *tert*-butyl protons and the doublet at 6.97 ppm (blue) shows cross peaks with the signal of the methyl substituents. Altogether, these findings support the structure of **4-14** as depicted in Figure 4-6.

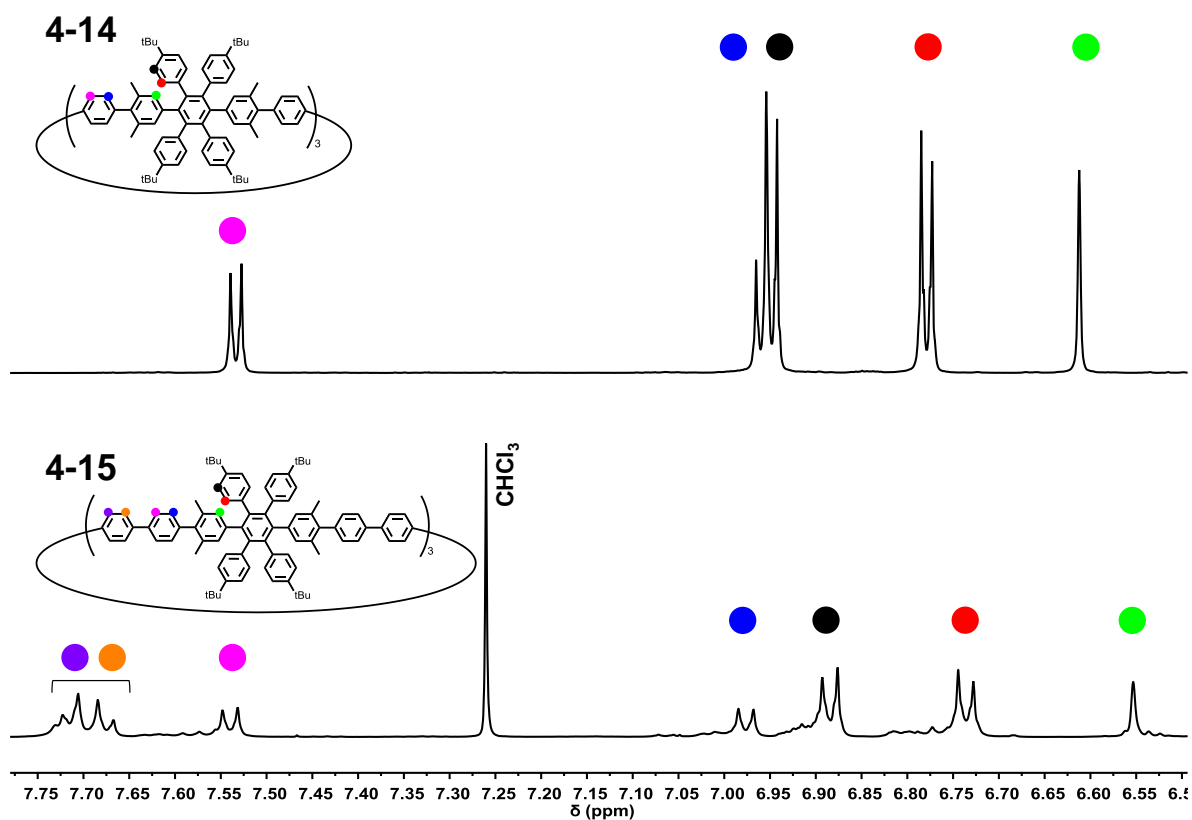


Figure 4-6: Details of the aromatic region of the ^1H -NMR spectra of top) **4-14** (700 MHz) in CD_2Cl_2 at 298 K and bottom) of **4-15** (500 MHz) in CDCl_3 at 298 K.

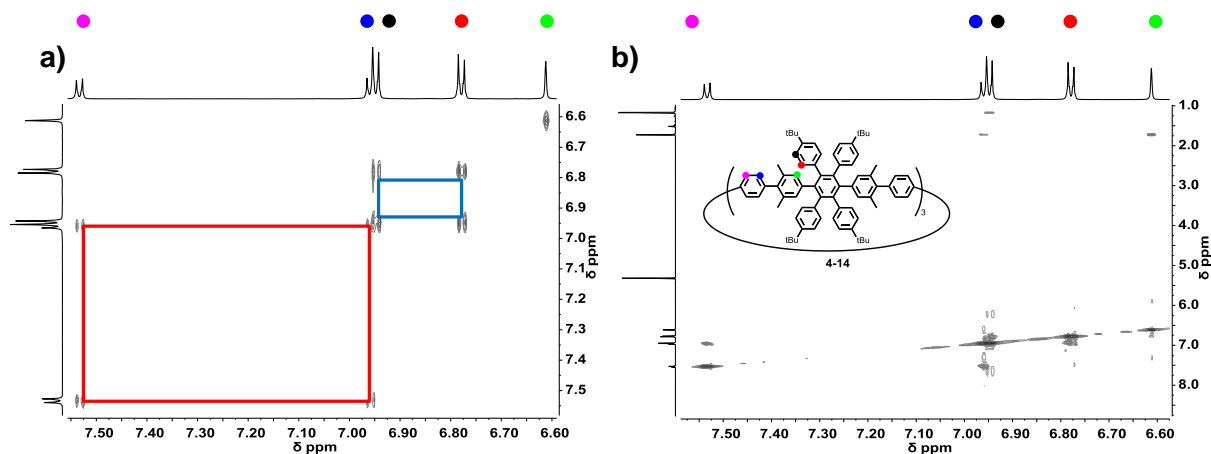


Figure 4-7: 2D-NMR spectra (700 MHz) of **4-14** in CD_2Cl_2 at 298 K; a) $^1\text{H},^1\text{H}$ -COSY NMR spectrum (aromatic region); b) $^1\text{H},^1\text{H}$ -NOESY NMR spectrum.

For **4-15**, the additional phenylene unit results in another AB spin system what was confirmed by the $^1\text{H},^1\text{H}$ -COSY spectrum, showing three correlations for the three AB spin systems (Figure 4-8).

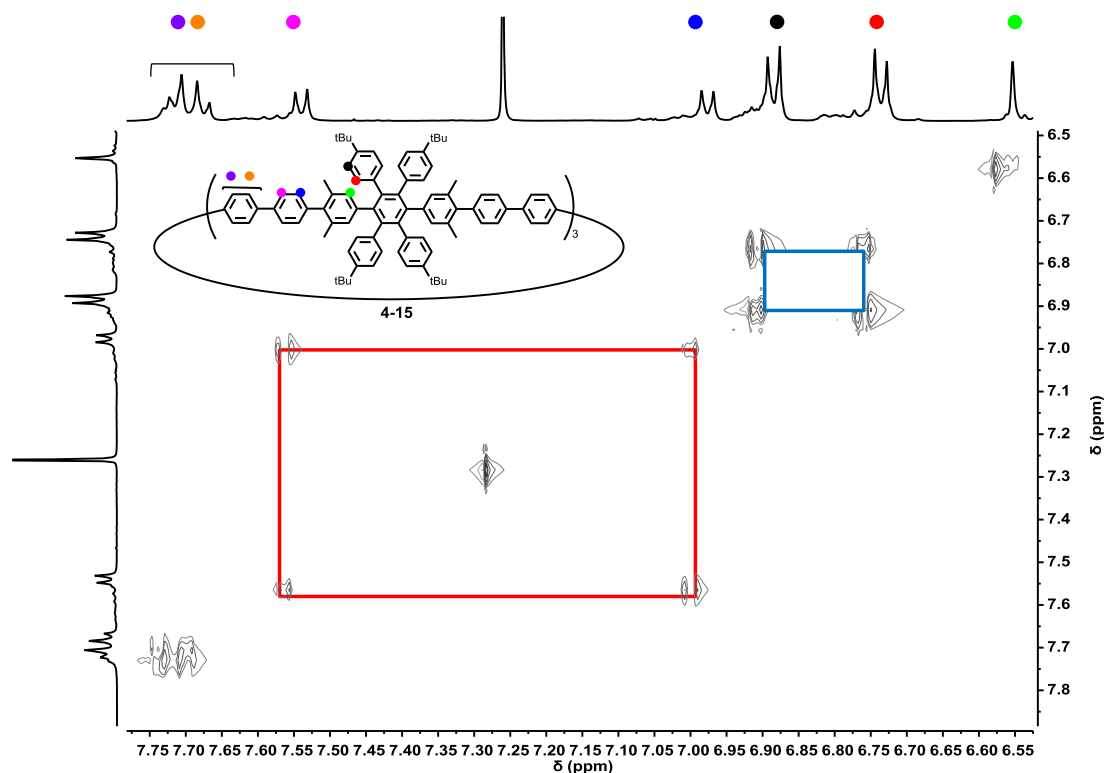


Figure 4-8: 2D- $^1\text{H},^1\text{H}$ -COSY NMR spectrum (500 MHz) of **4-15** in CDCl_3 at 298 K.

The detailed assignment of the protons from the additional phenylene unit could not be accomplished, because the respective through space couplings in the $^1\text{H}, ^1\text{H}$ -NOESY spectrum were not resolved.

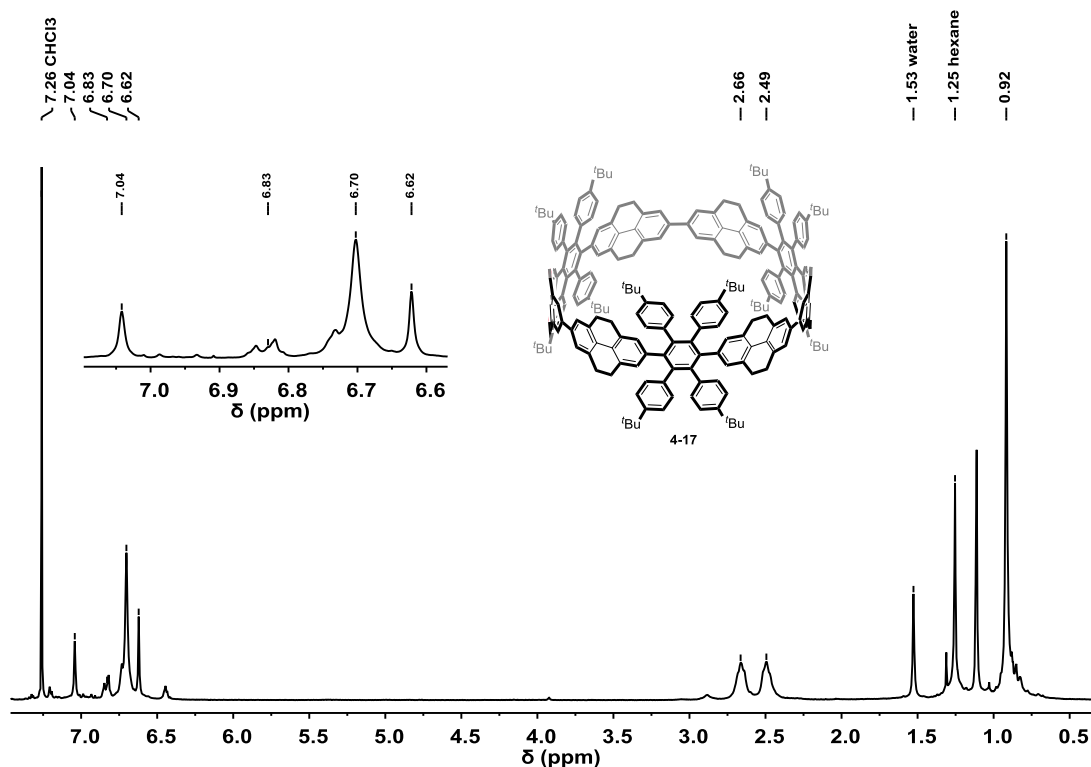


Figure 4-9: ^1H -NMR spectra of **4-17** (300 MHz) in CDCl_3 at 298 K.

The ^1H -NMR signals of **4-17** were rather broad, compared to the spectra of **4-14**, what might be the consequence of the stiffer CPP base due to the ethylene bridges (Figure 4-9). In the aromatic region, four sets of signals with a ratio of 1 to 1 to 3 to 1 were observed. The broad signal at 6.83 ppm and 6.7 ppm originate from the protons of the aryl substituents, whereas the two singlets at 7.04 ppm and 6.62 ppm could be assigned to the protons of the tetrahydropyrene moieties. At high magnetic field, two broad triplets at 2.66 ppm and 2.49 ppm, resulting from the ethylene bridges, were found. A sharp singlet from the *tert*-butyl protons appeared at 0.92 ppm. For the detailed assignment of the different signals 2D NMR techniques were applied (Figure 4-10).

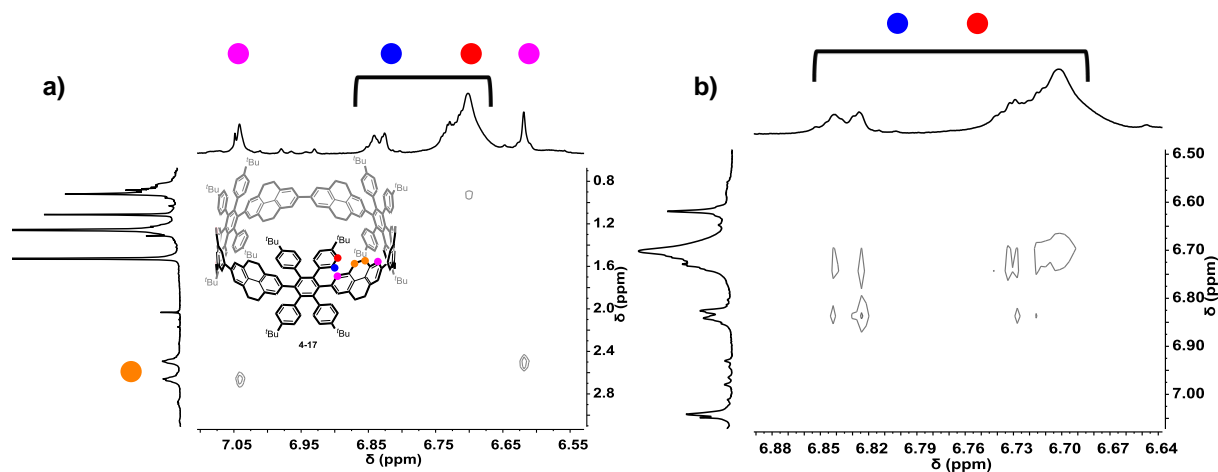


Figure 4-10: 2D-NMR spectra (500 MHz) of **4-17** in CDCl_3 at 298 K; a) $^1\text{H}, ^1\text{H}$ -NOESY NMR spectrum (aromatic region); b) $^1\text{H}, ^1\text{H}$ -COSY NMR spectrum.

The $^1\text{H}, ^1\text{H}$ -NOESY spectrum clarified that the singlets at 7.02 ppm and 6.62 ppm stem from the tetrahydropyrene units (marked in magenta), since cross peaks were observed with the ethylene bridges (Figure 4-10a). The through space coupling with the neighboring aryl substituents (blue) was not resolved. Therefore a further assignment was not possible. However, the through space coupling of the multiplet at 6.7 ppm with the protons of the *tert*-butyl group was detected, but the broad ^1H -NMR signals hampered a further differentiation. With the help of the $^1\text{H}, ^1\text{H}$ -COSY spectrum the correlation of the broadened doublets at 7.04 ppm and 6.62 ppm could be resolved (Figure 4-10). The results were all in accordance with the depicted structure of **4-17**.

Finally, the absorption and emission spectra of **4-14** to **4-17** were recorded to analyze their electronic properties and the results are summarized in Table 3-1. The distortion between the phenylene rings in the alkyl substituted phenylene-extended [3]CHPBs **4-14** and **4-15** was enhanced compared to the non-substituted [3]CHPBs and the CPPs, discussed in (chapter 3.2.2), what was reflected in their UV-Vis spectra (Figure 4-18). For the [3]CHPBs **4-14** and **4-15**, absorption maxima at 280 nm and ~300 nm were found, representing a hypsochromic shift of about 30-40 nm compared to the non-alkylated [3]CHPBs of the same sizes (chapter 3.2.2). Furthermore, the molar absorption coefficients of the alkyl substituted [3]CHPBs **4-14** to **4-17** (Table 3-1) were found to be significantly smaller than for the previously discussed

non-alkylated [3]CHPBs. This was especially pronounced for **4-14**, having the highest strain and distortion.

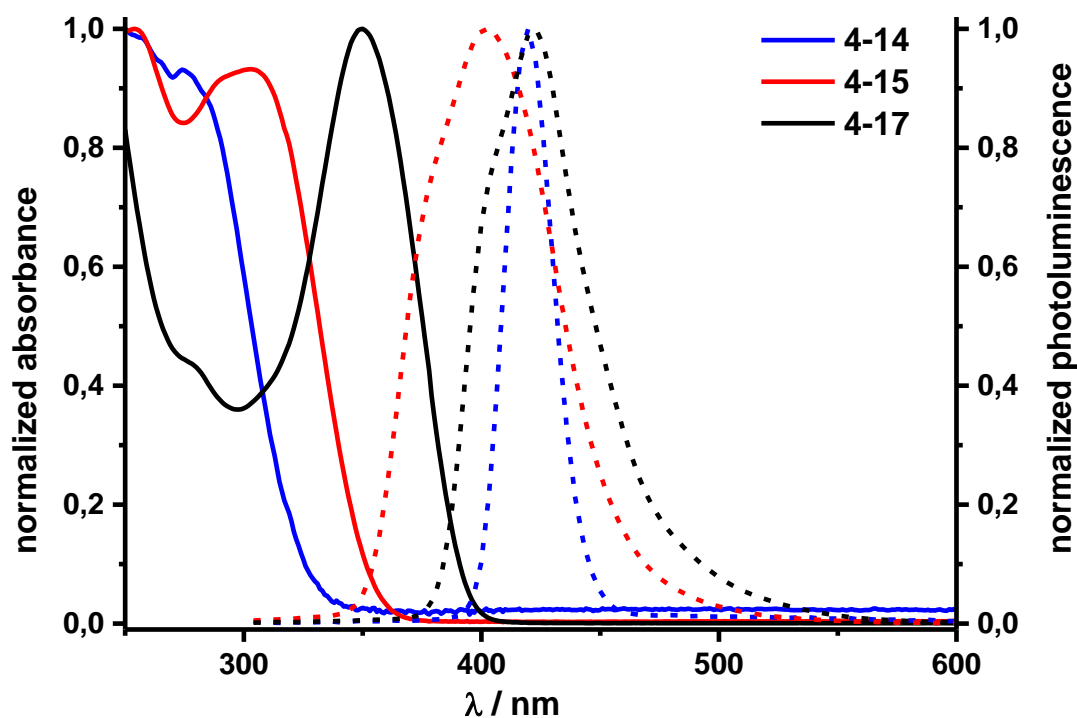


Figure 4-11: Electronic absorption (solid line) and emission (dashed line) spectra of compounds **4-14**, **4-15** and **4-17** ($c = 10^{-6}$ M in DCM).

The absorption maximum of **4-17** at 350 nm reveals the higher conjugation in the CPP backbone due to the ethylene bridges.^[147] Also the molar absorption coefficient of **4-17** was around five times higher than that of **4-14**. The emission maxima of **4-14**, **4-15** and **4-17** were found at 420 nm, 403 nm and 420 nm, respectively.

Table 4-1: The summary of the electronic absorption and emission data for **4-14**, **4-15** and **4-17** ($c = 10^{-6}$ M in DCM).

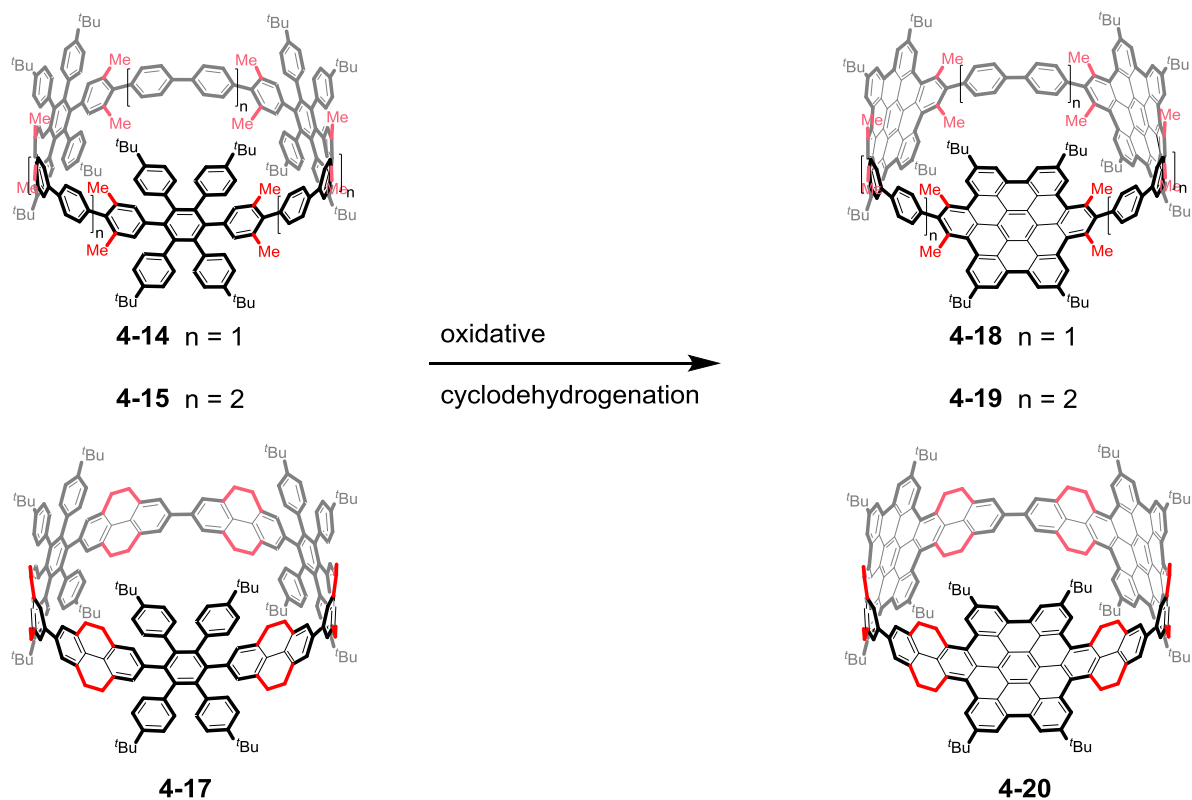
compound	λ_{abs} [nm]	λ_{em} [nm]	$\epsilon_{\lambda, \text{max}}$ [$\text{mol}^{-1}\text{m}^2$]
4-14	280	420	2690
4-15	303	403	16129
4-17	350	420	14000

The largest *Stokes* shift was observed for **4-14** (140) nm, indicating once more the existence of a highly distorted CPP base in the ground state and the release of this distortion in the excited state. ^[65,66,161]

4.2.3. Cyclodehydrogenation towards Alkyl Substituted [3]CHBCs

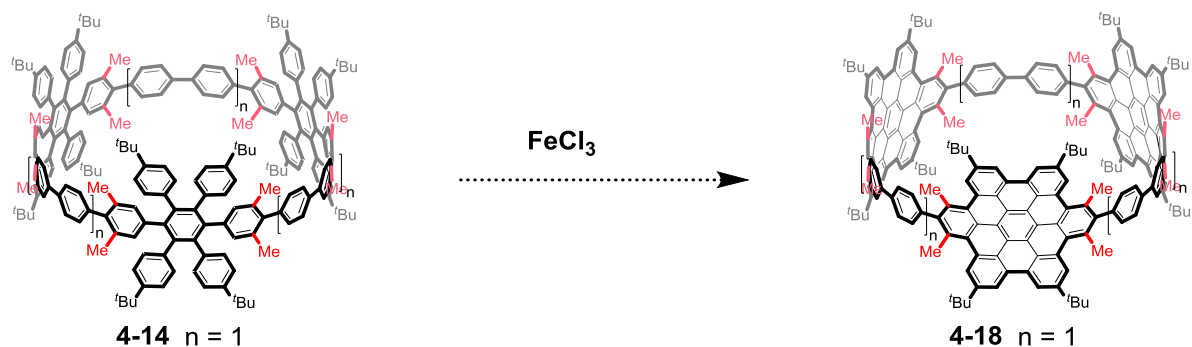
The findings of 3.2.3 clearly showed that 1,2-phenyl shifts in the CPP base occurred as strain releasing side reactions. The ring size extension from a 15- to a 21- and 27-membered CPP base resulted in a reduced tendency towards side reactions. However, the molecular size of the [3]CHPB with a 27-membered CPP base goes along with synthetic and analytical challenges. Therefore, the concept of blocking the critical rearrangement positions was introduced as a second approach to selectively obtain phenylene-extended [3]CHBCs. The synthesis of the alkylated [3]CHPBs **4-14**, **4-15** and **4-17** was described in chapter 4.2.1. In this chapter, the focus is on their oxidative cyclodehydrogenation towards the respective phenylene-extended [3]CHBCs **4-18**, **4-19** and **4-20** (Scheme 4-4).

The study covers the cyclodehydrogenation of [3]CHPBs with a 15- or 21-membered CPP base. Furthermore two different substitution patterns, methyl groups or ethylene bridges, were investigated as blocking substituents.



Scheme 4-4: Schematic illustration of the oxidative cyclodehydrogenation of **4-14**, **4-15** and **4-17** towards **4-18**, **4-19** and **4-20**.

Initially, the cyclodehydrogenation of **4-14** towards **4-18** will be discussed (Scheme 4-5). The cyclodehydrogenation conditions were the same as already described in chapter 3.2.3, using iron chloride as the oxidant in dichloromethane and nitromethane at room temperature.



Scheme 4-5: Cyclodehydrogenation reaction of **4-14** towards **4-18**. Conditions: FeCl_3 , DCM, MeNO_2 , 7 h, RT.

Instead of the expected product **4-18**, products with an additional loss of hydrogens were obtained. The separation of the product mixture by HPLC yielded two main fractions with an additional loss of two (**4-18'a**) and four (**4-18'b**) hydrogen atoms, which were confirmed by MALDI-TOF MS (Figure 4-12).

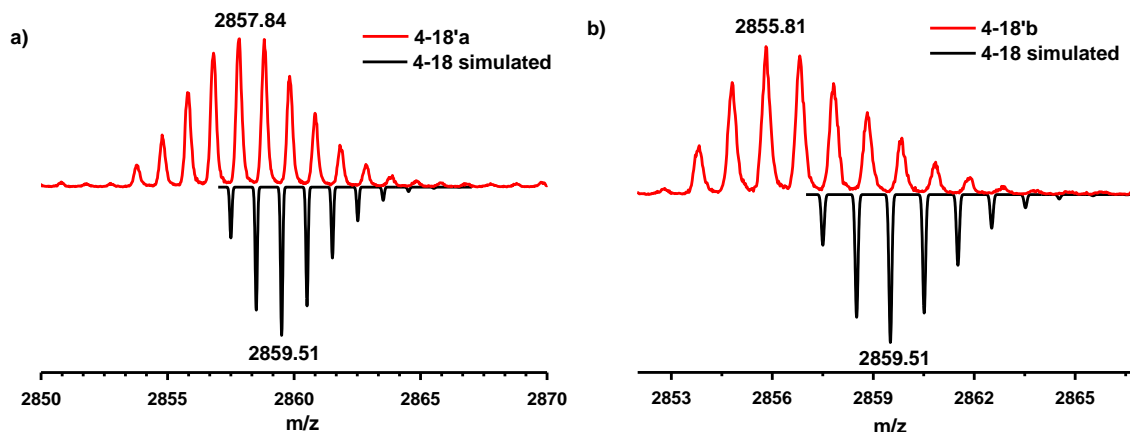
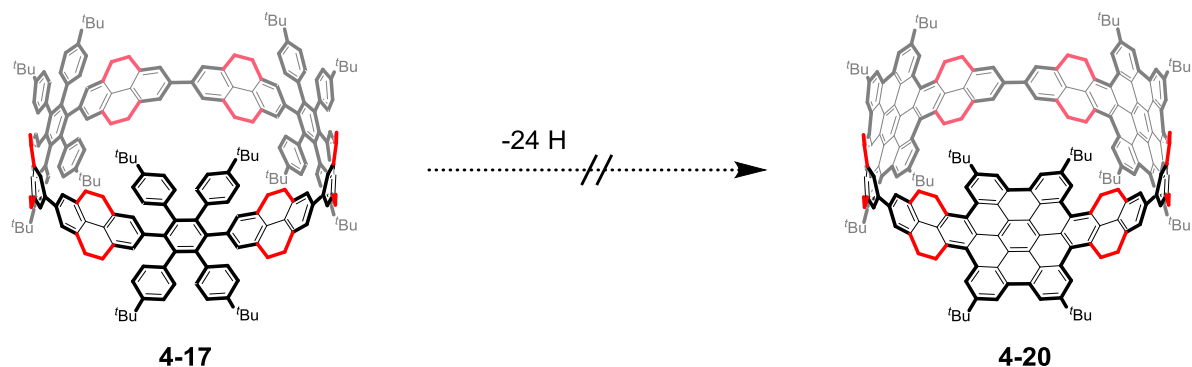


Figure 4-12: MALDI-TOF mass spectra (red) of a) **4-18'a**; b) **4-18'b** and the simulated isotopic pattern of **4-18** (black) (Matrix: DCTB).

The nature of the side reactions could not be elucidated, due to the very small amount left after the HPLC separation procedure. However, the additional loss equaled the formation of one- or two additional bonds. This implies that rearrangements like in chapter 3.2.3 occurred and methyl blocking groups were not sufficient to overcome the strain induced side reactions during the cyclodehydrogenation in a 15-membered [3]CHPB. Based on these findings, the phenylene-extended [3]CHPBs **4-15** and **4-17** were designed, having an increased ring size or ethylene bridged biphenyl units. In the case of **4-17**, it was investigated if side reactions could be prevented by blocking all possible rearrangement positions. With the incorporation of the 4,5,9,10-tetrahydropyrene unit in the 15-membered [3]CHPB, all the critical positions were blocked, causing also the stiffening of the CPP backbone.



Scheme 4-6: Cyclodehydrogenation reaction of **4-17** towards **4-20**. Conditions: FeCl₃, DCM, MeNO₂, 7 h, RT.

The mass spectrometric analysis revealed that still not the clean [3]CHBC was obtained. Instead, the incomplete cyclodehydrogenated product, with approximately 12 closed bonds was detected (Figure 4-13). This result confirmed the assumption that the rearrangements can be blocked by alkyl substitutions and furthermore, that the 15-membered CPP base is still too strained to allow a smooth dehydrogenation.

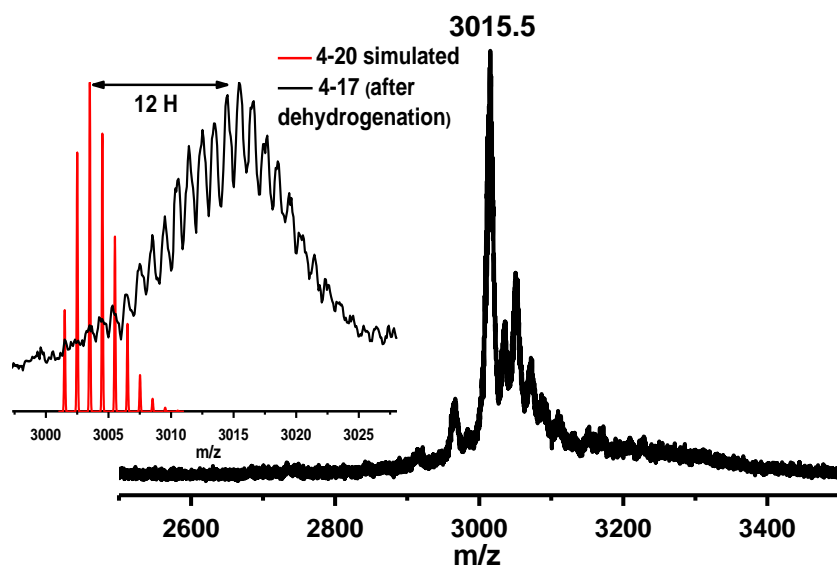


Figure 4-13: MALDI-TOF mass spectra of **4-17** after cyclodehydrogenation (black) and the simulated isotopic pattern of **4-20** (red) (Matrix: DCTB).

Finally, the 21-membered [3]CHPB **4-15** was subjected to cyclodehydrogenation under the same conditions (Figure 4-14).

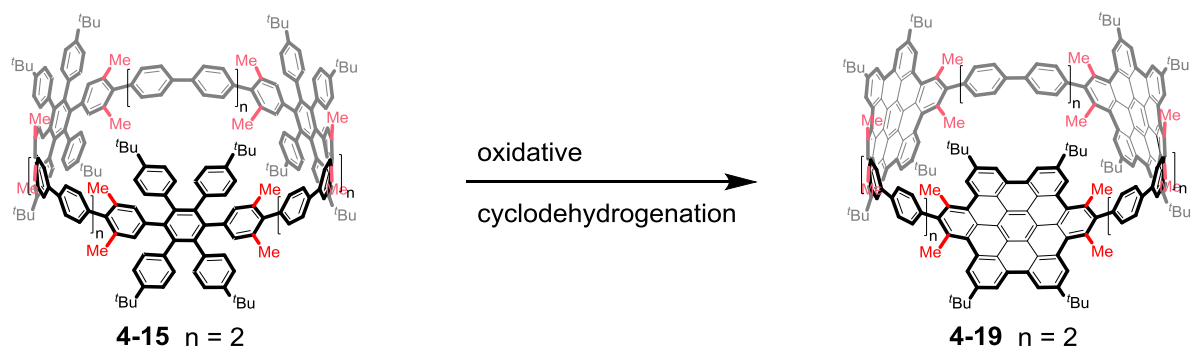


Figure 4-14: Cyclodehydrogenation reaction of **4-15** towards **4-19**. Conditions: FeCl_3 , DCM, MeNO_2 , 7 h, RT.

This time, the phenylene-extended [3]CHBC **4-19** was selectively obtained and confirmed by HR-MALDI-TOF MS (Figure 4-15) as well as NMR spectroscopy (Figure 4-16).

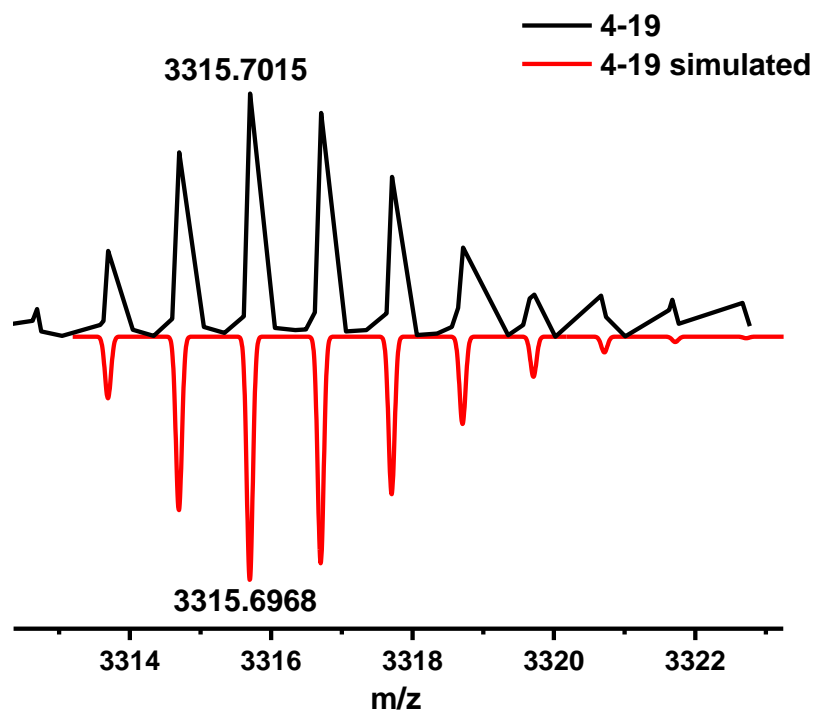


Figure 4-15: HR-MALDI-TOF mass spectrum of **4-19** and the simulated isotopic pattern.

The molecular ion of **4-19** was found at $m/z = 3313.6929$ (calcd. $m/z = 3313.6897$) and the isotopic pattern is in good agreement with the simulation. The final proof of the successful synthesis was accomplished by NMR spectroscopy (Figure 4-16).

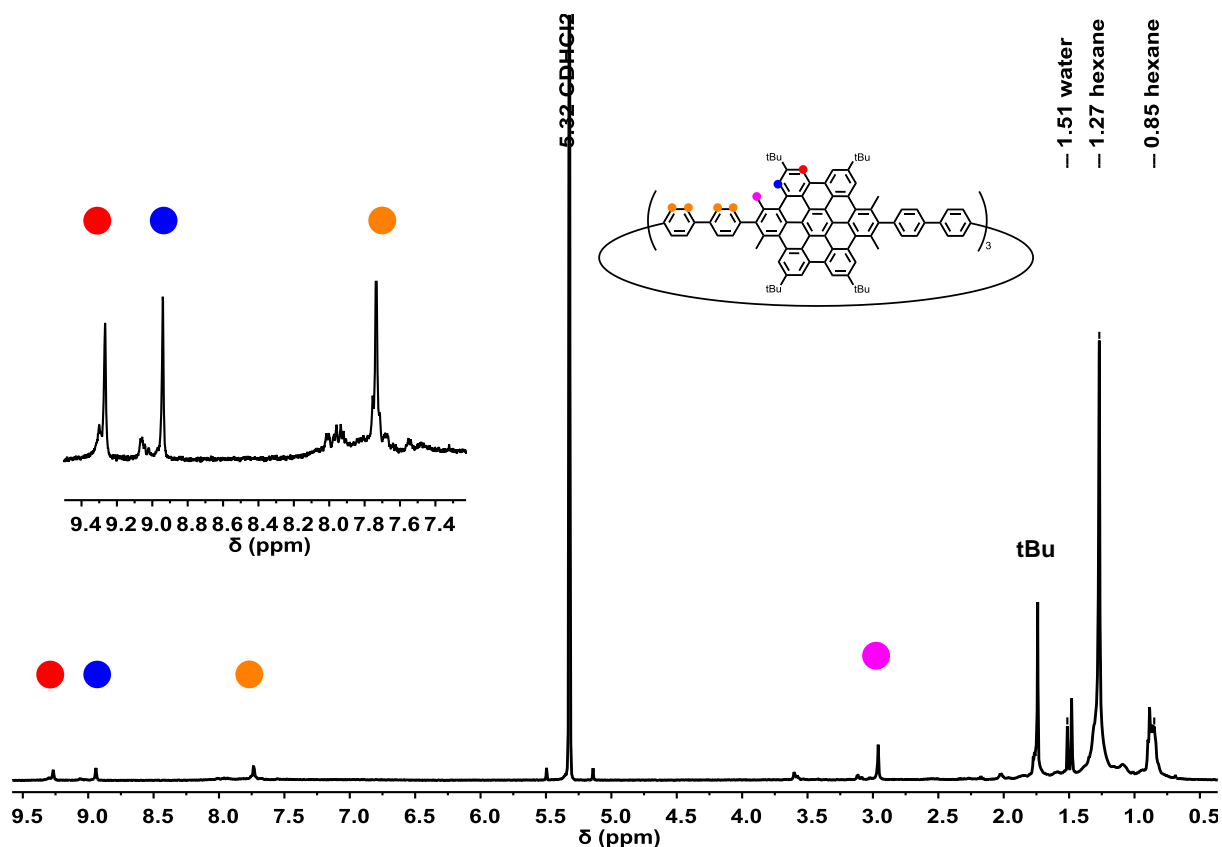


Figure 4-16: $^1\text{H-NMR}$ spectra of **4-19** (500 MHz) in CD_2Cl_2 at 298 K.

A set of two singlets (at 9.27 ppm and 8.94 ppm) and one multiplet (7.73 ppm) in the aromatic region and two singlets (at 2.96 ppm and 1.74 ppm) in the aliphatic region with a ratio of 1 to 1 to 4 to 3 to 9 was found in the $^1\text{H-NMR}$ spectrum of **4-19**, which is consistent with expectations. The phenylene protons, marked in orange, were expected to show four doublets representing the two AB spin systems. Instead, these signals were overlapped and shown as multiplet at 7.73 ppm. For a further structure elucidation, a 2D- $^1\text{H-}^1\text{H-NOESY}$ spectrum (Figure 4-17a) and a 2D- $^1\text{H-}^1\text{H-COSY}$ spectrum (Figure 4-17b) were recorded.

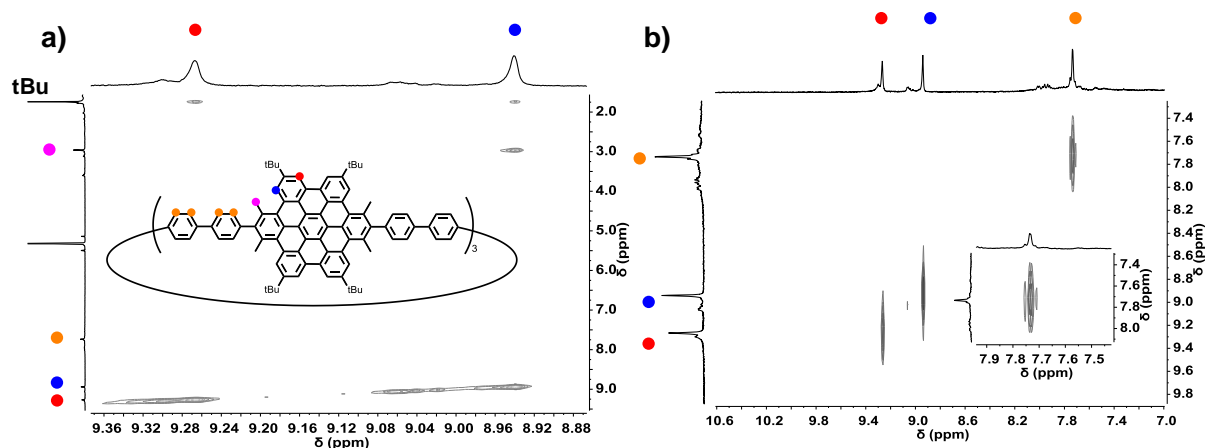


Figure 4-17: 2D-NMR spectra (500 MHz) of **4-19** in CD_2Cl_2 at 298 K; a) $^1\text{H},^1\text{H}$ -NOESY NMR spectrum (aromatic region); b) $^1\text{H},^1\text{H}$ -COSY NMR spectrum (aromatic region).

With the help of the 2D- $^1\text{H}-^1\text{H}$ -NOESY spectrum, the two singlets from the HBC units could be distinguished. The singlet at 9.27 ppm stemmed from the protons marked in red, because cross peaks with the signal of the *tert*-butyl protons were detected. Therefore, the singlet at 8.94 ppm could be assigned to the protons marked in blue and the characteristic cross peaks with the signals of the *tert*-butyl and methyl protons were observed in the NOESY spectrum. The through-space coupling of the methyl groups with the neighboring phenylene protons (marked in orange) could not be resolved, unfortunately. In the 2D- $^1\text{H}-^1\text{H}$ -COSY spectrum (Figure 4-17b) no cross peaks were observed for the singlets and the multiplet in the aromatic region, indicating their separation. The insight of the multiplet at 7.73 ppm indicated that the overlapped signals have a correlation with each other. These findings are consistent with the depicted structure of **4-19** and verify the successful cyclodehydrogenation. For the first time, a phenylene-extended [3]CHBC was selectively obtained by combining the two approaches: increasing the ring size (21-membered CPP base) and the substitutional blocking at the critical positions.

Further, the electronic absorption and emission spectra of **4-19** were recorded (Figure 4-18). In the electronic absorption spectrum of **4-19** weak α - and p -band absorptions at 421 nm and 400 nm were observed, respectively, and a strong β -band at 367 nm. These are distinctive patterns observed in substituted HBCs.^[156,157] For comparison, the absorption spectrum of

4-15 is also depicted in Figure 4-18. The red-shift of the absorption maximum of about 60 nm proved the successful extension of the conjugated π -system after cyclodehydrogenation.

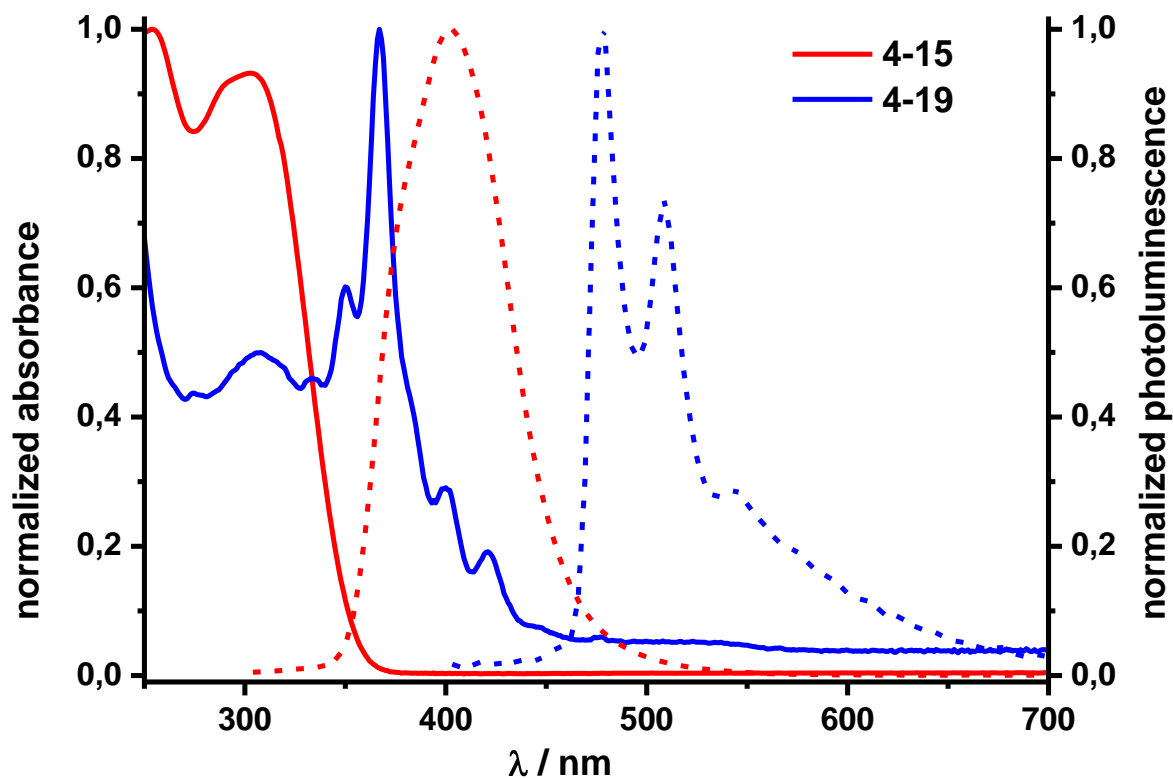


Figure 4-18: Electronic absorption (solid line) and emission (dashed line) spectra of compounds **4-15** and **4-19** ($c = 10^{-6}$ M in DCM).

The emission maxima were found at 479 and 508 nm with a small shoulder at 545 nm what was also in good agreement with the emission data found for HBCs. The complete data set is summarized in Table 4-2.

Table 4-2: The summary of the electronic absorption and emission data for **4-15** and **4-19** ($c = 10^{-6}$ M in DCM).

compound	λ_{abs} [nm]	λ_{em} [nm]	$\epsilon_{\lambda_{\text{max}}}$ [$\text{mol}^{-1}\text{m}^2$]
4-15	303	403	16129
4-19	350, 367, 400, 421	479, 508, 545	n.d.

Additionally, density functional theory (DFT) calculations were performed at the B3LYP/6-31G* level of theory. The calculation necessitated simplification of **4-19**, wherefore alkyl substituents were removed to calculate **4-19'**. It was found that the HOMO-1/HOMO-2 as well as the LUMO+1/LUMO+2 were degenerated. The energy diagram and the optimized structures are depicted in Figure 4-19.

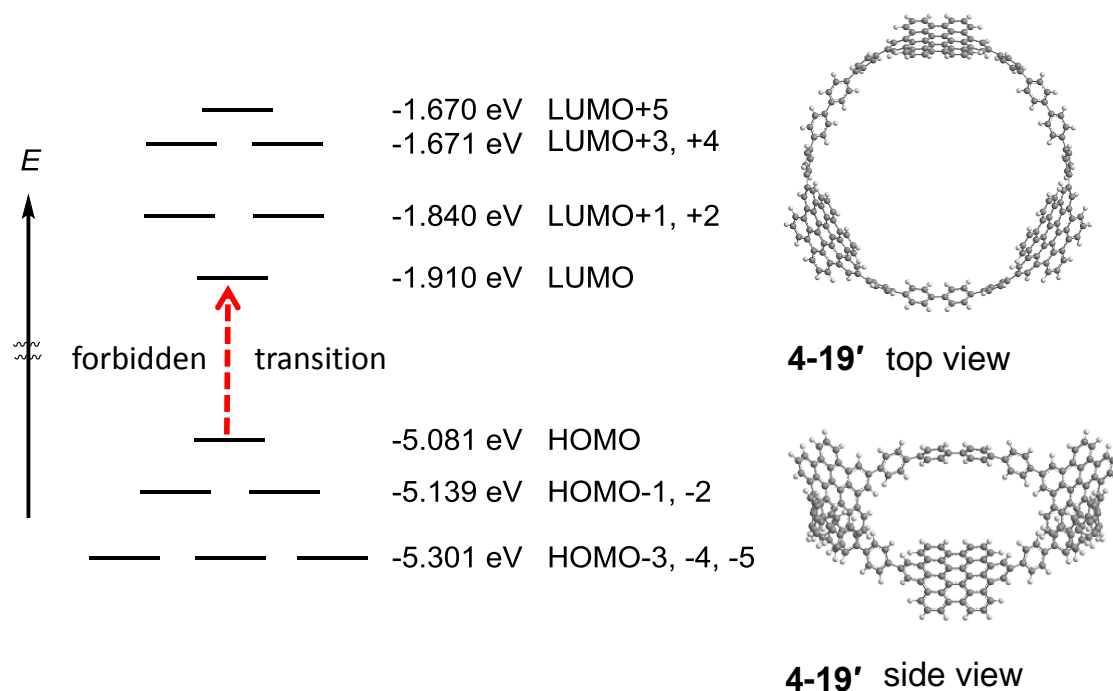


Figure 4-19: Energy diagram and the illustration of the optimized structures of **4-19'** (without alkyl substituents), calculated at the B3LYP/6-31G* level of theory.

With time dependent DFT calculations the different excitations for **4-19'** could be determined. For the HOMO→LUMO transition, an oscillator strength $f = 0.00$ was found, verifying that this transition is symmetry forbidden. The main absorption was calculated to be at ~ 398 nm with an oscillator strength of $f = 1.17$. A multitude of transitions from the HOMO level to higher excited states and transitions from lower energy levels to the LUMO were found to contribute to this absorption. A second strong absorption at 435 nm with $f = 1.08$ was determined, besides minor absorptions at 399 nm and 442 nm. Taking solvent effects in consideration, the calculated absorption values are in good agreement with the observed absorption spectrum showing a strong absorption at 367 nm and minor ones at 400 nm and 421 nm.

4.3. Summary

In conclusion, the phenylene-extended and alkyl substituted [3]CHBC **4-19** was selectively obtained for the first time by cyclodehydrogenation of the [3]CHPB **4-15**. These findings verify that the post-construction method can be applied to form CNT segments from strained cyclic polyphenylene precursors using the *Scholl* reaction.

The synthesis of alkyl substituted phenylene-extended [3]CHPBs of different sizes was described as a second approach to overcome strain releasing side reactions during the oxidative cyclodehydrogenation. The kinked key intermediates **4-6** and **4-8** were obtained by the two-fold incorporation of 5-bromo-2-chloro-1,3-dimethylbenzene into the tetraarylbenzoquinone **3-1**, the alkylation and a further aryl elongation by *Suzuki* cross coupling. In a one-pot macrocyclization of these kinked precursors under *Yamamoto* conditions, cyclic trimers were primarily obtained, which were subsequently aromatized to give the [3]CHPBs **4-14** and **4-15** with circumferences of 15- and 21-phenylene rings in the CPP base. Additionally, a 15-membered [3]CHPBs, containing 4,5,9,10-tetrahydropyrene units was designed to block all critical rearrangement positions. Therefore 2,7-dibromo-4,5,9,10-tetrahydropyrene was incorporated in the first step and the resulting precursor was cyclized under the same conditions to yield **4-17**. The alkyl substituted [3]CHPBs were analyzed by mass spectrometry and NMR spectroscopy. Furthermore, the electronic absorption and emission spectra of **4-14** and **4-15** revealed that the additional methyl substituents caused a higher distortion of the CPP base, whereas the ethylene bridges in **4-17** facilitate a better conjugation in the CPP base, resulting in a red-shift of the absorption maximum.

With the substitutionally blocked [3]CHPBs **4-14** to **4-17** in hand, the cyclodehydrogenation with iron chloride was investigated. It turned out that a circumference of 15 phenylenes was still too strained to undergo a smooth cyclodehydrogenation. In the case of **4-18**, side reactions were observed. The nature and mechanism of these side reactions were not further investigated, but it was supposed that also rearrangements took place, since the higher degree of dehydrogenation implied this. No side reactions were observed for the dehydrogenation of the ethylene bridged [3]CHPB **4-17**, but the dehydrogenation stopped after forming approximately two-thirds of the bonds. The larger [3]CHPB **4-15**, with a 21-membered CPP base, was

selectively transformed into the respective [3]CHBC **4-19** under the same conditions. High resolution mass spectrometry and NMR spectroscopy verified the successful formation of HBC units within a strained macrocycle. Also the electronic absorption and emission spectra of **4-19** showed the distinctive patterns of substituted HBCs, which were also supported by DFT calculations. These findings clearly showed that the post-construction method is a valuable tool for the efficient bottom-up synthesis of defined CNT segments from polyphenylene macrocycles possessing sufficient size and structure to quantitatively form conjugated graphenic sidewalls.

5. Phenanthroline-Indole N₄-Macrocycles

5.1. Introduction

Non-precious metal catalysts (NPMCs), as an alternative to the expensive platinum based cathode catalysts in fuel cells, are needed for an efficient and low-cost energy conversion. In this work, new N₄-macrocyclic ligand systems were designed in order to create highly active NPMCs, comprising cobalt metal centers as active sites.

The concept of combining the very good chelating properties of a porphyrin analogue N₄-cavity and the advantages of a planar, multinuclear complex was the basis for this work. In previous research the novel phenanthroline-indole macrocyclic (PIM) ligand, 5,6-bis(alkoxy)-2,9-((2,2'-phenylmethylene)-bis(3-methyl-1H-indol-7-yl))-1,10-phenanthroline, was developed. This ligand, consisting of 1,10-phenanthroline and indole moieties, showed excellent chelation properties. Having two pyrrolic and two pyridinic nitrogens, neutral metal complexes were formed with M^{II}-metals, like Zn^{II} or Co^{II}. Furthermore, the cobalt complexes showed enhanced activity towards ORR as they were supported on carbon black (Vulcan XC72R). However, mainly the 2-electron pathway was provided and a contribution to the 4-electron reduction was observed after heat-treatment at 700 °C.

Based on these findings, a further development of the PIM catalyst system was the aim of this work. The requirements for a good NPMC catalyst are a high electrocatalytic activity, a high durability and the preference for the direct 4-electron reduction of oxygen to water. The increase of the activity and durability requires a π -extension of the PIM system with a concurrent conjugation of the metal centers. This leads to the assumption, that having two metal centers close to each other, a favorable interaction of those will enhance the activity towards the oxygen reduction, even without heat-treatment (Figure 5-1).

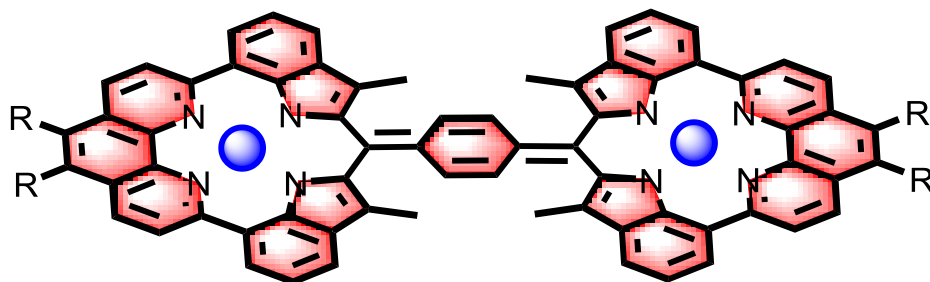


Figure 5-1: Schematic illustration of the dimeric PIM metal complex; blue sphere = metal center.

On account of this, the synthesis of a multinuclear cobalt complex will be presented in the following work by applying different dicarbalddehydes for the macrocyclization of the PIM system (Figure 5-2).

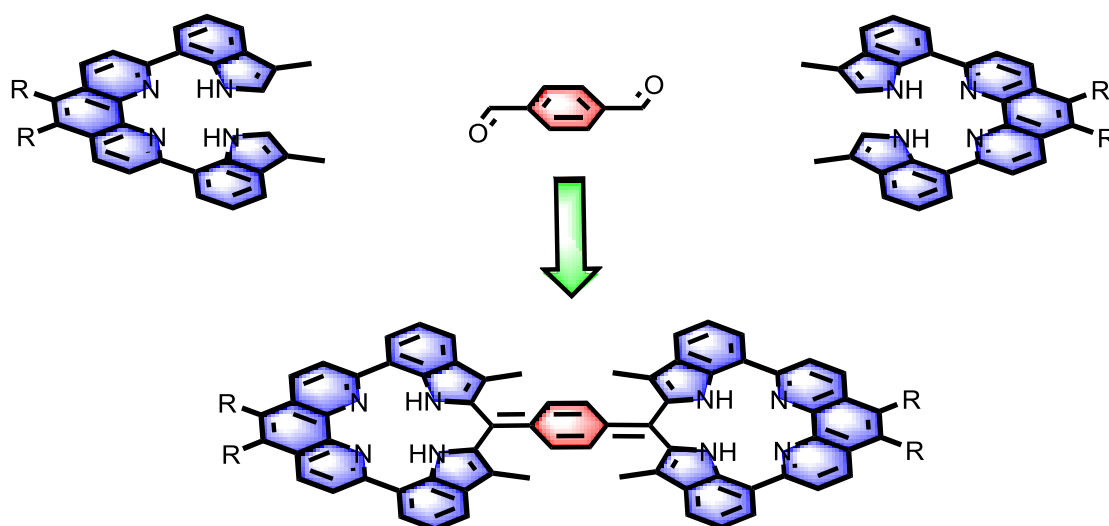


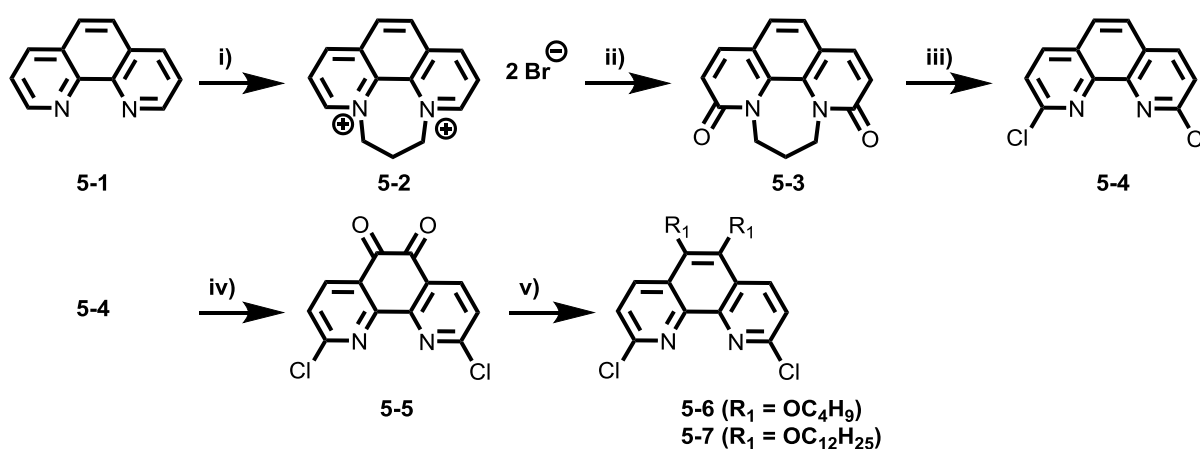
Figure 5-2: Design concept for the dimeric PIM ligand.

In addition, the original synthesis protocol for the mononuclear PIM complexes by *Qi Su* will be specified again.^[162] For all mono- and binuclear PIM ligands, the optical properties and the metal complexation will be described. Furthermore, the electrocatalytic properties of these catalysts in alkaline and acidic conditions are presented.

5.2. Results and Discussion

5.2.1. Synthesis and Characterization

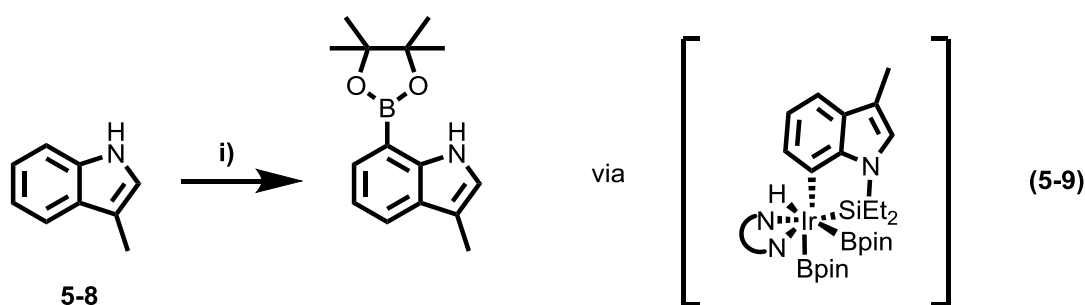
The phenanthroline-indole macrocycles (PIM) **5-13** to **5-18** were synthesized by the Friedel-Crafts condensation of the precursors **5-10** to **5-12** with the respective aldehydes (Scheme 5-4). The synthesis of the functionalized phenanthroline and indole building blocks is depicted in Scheme 5-1 and Scheme 5-2. Starting from 1,10-phenanthroline, 2,9-dichloro-5,6-bis(dodecyloxy)-1,10-phenanthroline was synthesized in five steps (Scheme 5-1) with an overall yield of 13 %. Initially, the 2- and 9-positions were functionalized according to literature,^[163] by protecting the nitrogens with 1,3-dibromopropane, an oxidation with $[K_3Fe(CN)_6]$ and the chlorination with $POCl_3$ and PCl_5 to yield **5-4**. The introduction of solubilizing alkoxy groups was achieved by the oxidation and the subsequent reductive alkylation in the 5- and 6-positions of 1,10-phenanthroline yielding **5-6** and **5-7**.



Scheme 5-1: Synthetic route towards 2,9-dichloro-5,9-dialkoxy-1,10-phenanthroline **5-6**. Conditions: i) 1,3-dibromopropane, 120 °C, 18 h, 78 %; ii) $[K_3Fe(CN)_6]$, NaOH, H_2O , -5 °C to RT, 16 h, 34 %; iii) $POCl_3$, PCl_5 , 110 °C, 16 h, 70 %; iv) H_2SO_4 , HNO_3 , KBr, 80 °C, 3 h; v) alkylbromide, $Na_2S_2O_4$, $(nBu)_4NBr_2$, H_2O , THF, KOH, 40 °C, 48 h, 70 %.

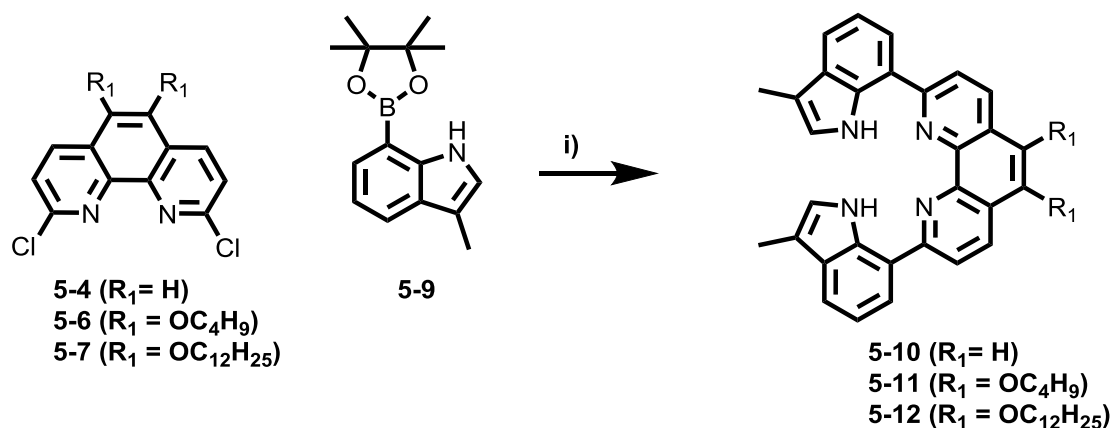
As the second building block, commercially available 3-methylindole was borylated in the 7-position in a one-pot procedure (Scheme 5-2) in 80 % yield.^[164] This procedure, developed in the group of *J.F. Hartwig* et al.^[164], has significant advantages compared to the formation of 7-bromo-3-methylindole *via* the *Bartoli* indole synthesis and the subsequent catalytic boryla-

tion.^[165] The reaction can be conducted as a one-pot reaction, in which initially 1-diethylsilyl-3-methylindole was formed, facilitated by a ruthenium catalyst, followed by an iridium catalyzed, hydrosilyl directed borylation at the 7-position of indole (Scheme 5-2). The high selectivity for the 7-position results from the preference for a five membered ring in the transition state (Scheme 5-2) in contrast to a four membered ring for the functionalization at the 2-position.



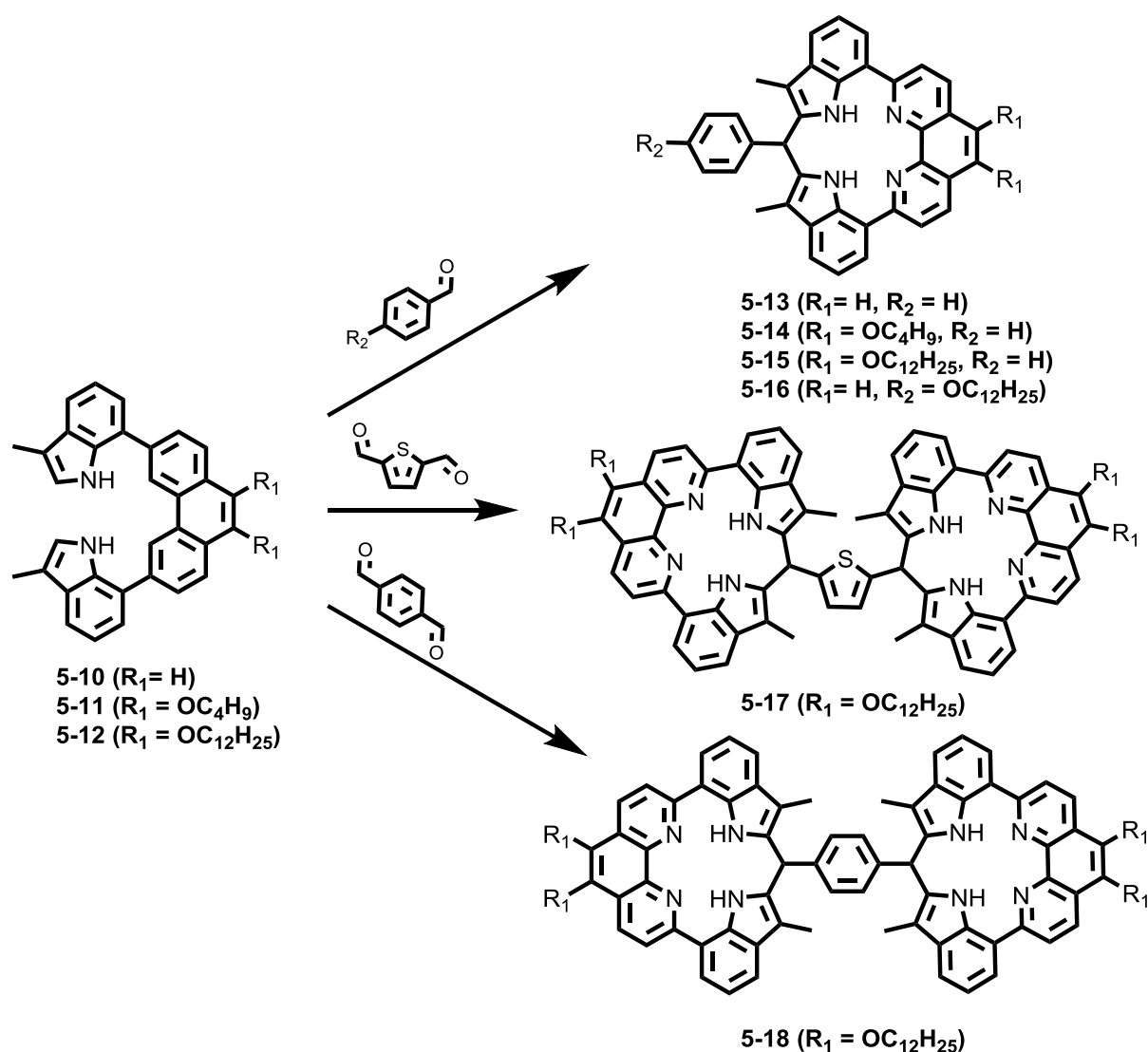
Scheme 5-2: Synthetic route to 3-methyl-7-(4,4,5,5-tetramethyl-1,3,2-dioxaborolan-2-yl)-1H-indole **5-9**. Conditions: i) first: Dichloro(*p*-cymene)ruthenium(II) dimer (1 mol%), Et₂SiH₂, toluene, 80 °C, 16 h; second: Ir₂(cod)₂Cl₂ (0.25 mol%), B₂pin₂, dtbpy, HBpin, THF, 80 °C, 16 h, 80 %.

In a twofold *Suzuki-Miyaura* cross-coupling reaction between **5-4** and **5-9** (Scheme 5-3) the phenanthroline-indole macrocyclic precursor **5-10** was formed. The cross-coupling of aryl chlorides usually affords harsher conditions or high quantities of catalyst.



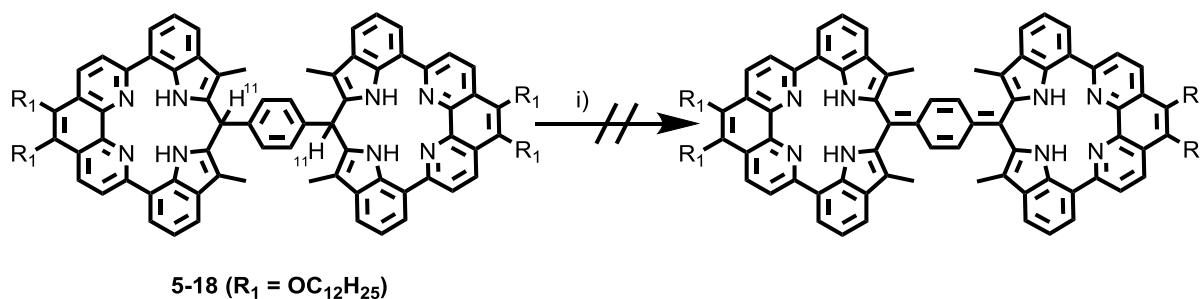
Scheme 5-3: Synthetic route to 5,6-bis(dodecyloxy)-2,9-bis(3-methyl-1H-indol-7-yl)-1,10-phenanthroline **5-12**. Conditions: i) K₃PO₄, S-Phos, Pd(dba)₂ (10 mol%), toluene, H₂O, 105 °C, 16 h, 70 %.

Therefore, the catalyst system developed by *Buchwald* et. al. was used for this coupling, yielding **5-10** in 70 % yield.^[146] All PIM macrocycles were synthesized by a *Lewis* acid catalyzed condensation of the key intermediates **5-10** to **5-12** and different arylaldehydes (Scheme 5-4). The ring closure selectively occurred at the 2-position of the indole units because of the high acidity of the C-2 hydrogen. With this procedure mono- and bicyclic N₄-ligands could have been formed by the same reaction.



Scheme 5-4: Synthetic route to **5-13** to **5-18**. Conditions: CH_2Cl_2 , $BF_3 \cdot OEt_2$, microwave heating: 5 h/110 °C/300 W, 10 min./20 °C/200 W, 5 h/110 °C/300 W, 10 min./20 °C/200 W, 5 h/110 °C/300 W, 5-50 %.

A relatively high temperature of 110 °C, the strong *Lewis* acid BF_3 and microwave irradiation were necessary for the successful condensation of the aldehydes with the precursor **5-10** to **5-12**. Unfortunately these harsh conditions also led to a partial decomposition of the starting materials and therefore a maximum yield of 50 % was obtained for **5-13**. Additionally **5-17** and **5-18** were treated with 2,3-dichloro-5,6-dicyano-1,4-benzoquinone (DDQ), *p*-chloroanil or MnO_2 in order to gain conjugation by the oxidation of C-H_{11} (Scheme 5-5). Even at elevated temperatures no oxidation was observed. In order to lower the energy barrier for the quinoidization, the phenylene bridge in compound **5-17** was replaced by a thienylene bridge. However, the quinoidization was not successful.



Scheme 5-5: Schematic illustration of the oxidation of **5-18** to the all aromatic system; Conditions i) DDQ, MnO_2 or *p*-chloroanil.

The structures of the PIM N_4 -ligands were analyzed by HR-ESI or MALDI-TOF mass spectrometry and NMR spectroscopy. The “dimeric” macrocycle **5-18** has a C_{2v} symmetry and therefore clear signals were obtained, which facilitated the full structure determination (Figure 5-3, Figure 5-4).

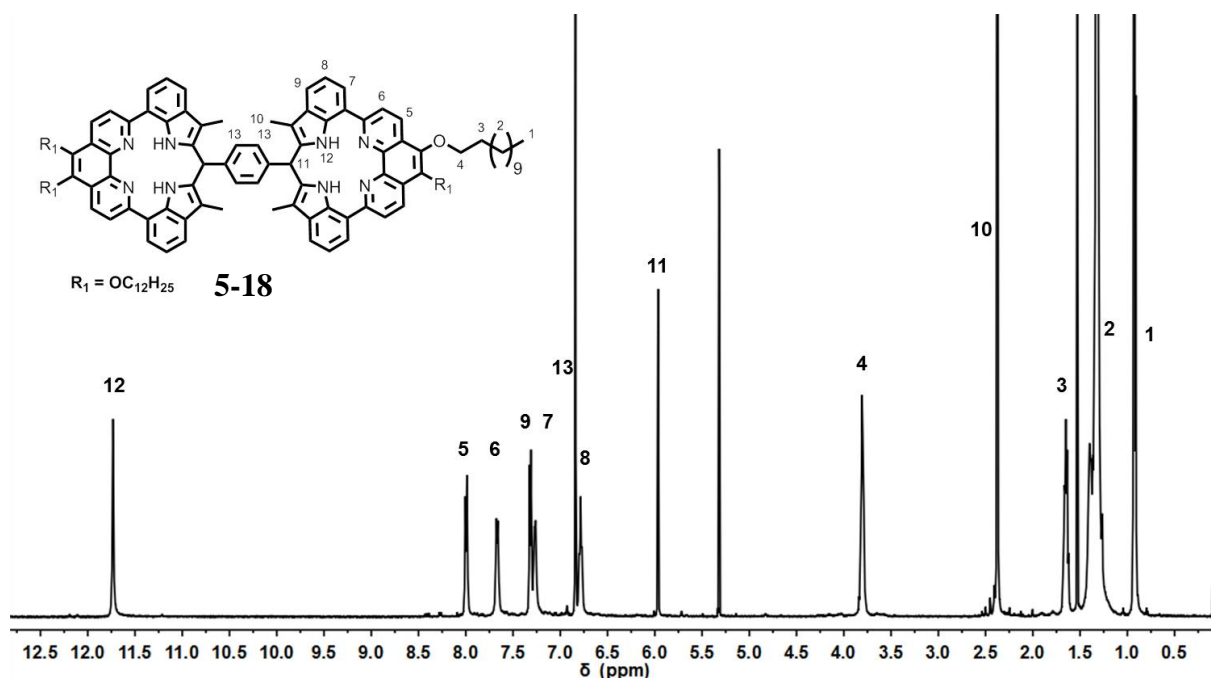


Figure 5-3: ^1H -NMR spectrum of **5-18** in CD_2Cl_2 , 298 K, 500 MHz; chemical shifts are referenced to dichloromethane proton at 5.32 ppm.

The signals for the protons of the phenanthroline and indole units resonated in the same aromatic region as for the macrocycle precursor **5-12** with the NH signal at 11.7 ppm. The disappearance of the signal for the protons at the 2-position of the indole units at 6.6 ppm and the new proton signal at 6.0 ppm (H-11, Figure 5-3) were a proof of the successful macrocyclization. Additionally a 2D- ^1H , ^1H – NOESY NMR spectrum was recorded to distinguish the different proton signals from the phenanthroline and indole units. In a NOESY spectrum nuclei that are close to each other (within 4 Å) show resonances which are connected by cross peaks. Hence, cross peaks were expected for H-6, H-7 and H-10, H-11 (Figure 5-4a & b). These cross peaks were observed in the ^1H , ^1H – NOESY NMR spectrum and therefore the protons could have been assigned to the phenanthroline and indole units, respectively. A further assignment was possible by the recorded ^1H , ^1H – COSY NMR spectrum (Figure 5-4c). The resonances of nuclei that are bonded to each other (up to ^3J) show cross peaks in a ^1H , ^1H – COSY NMR spectrum. For **5-18** cross peaks were observed for H-5, H-6 and H-7, H-8 and H-9. The structure of **5-18** was completely resolved with the information of the ^1H , ^1H – COSY

and ^1H , ^1H – NOESY NMR spectra, being in good agreement with the depicted structure of **5-18** (Figure 5-4d).

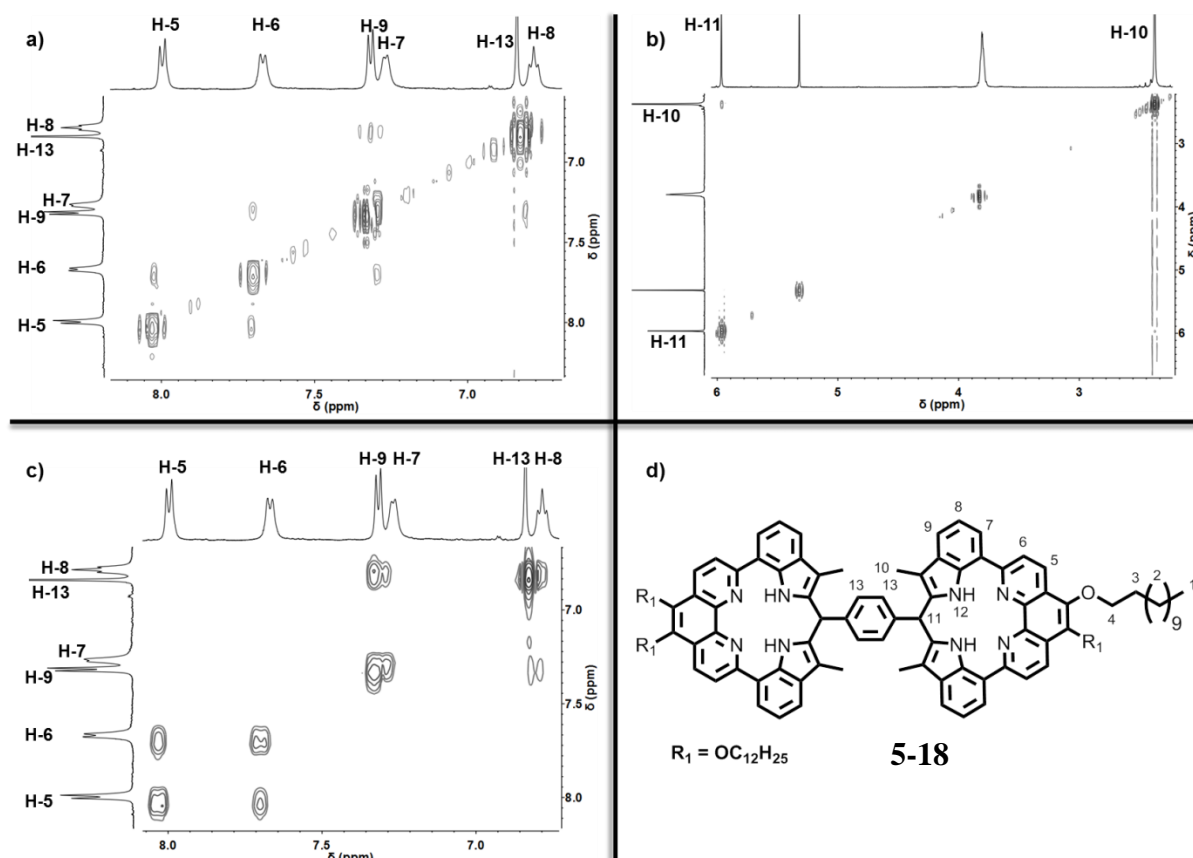


Figure 5-4: a), b): ^1H , ^1H – NOESY NMR spectrum of **5-18** in CD_2Cl_2 , 298 K, 500 MHz; c): ^1H , ^1H – COSY NMR spectrum of **5-18** in CD_2Cl_2 , 298 K, 500 MHz d) structure of **5-18**; chemical shifts are referenced to dichloromethane proton at 5.32 ppm.

The absorption and emission spectra of the PIM N₄-ligands are depicted in Figure 5-5, they all were recorded in CH_2Cl_2 at 298 K ($c = 10^{-5}$ M). The absorption spectra of the PIM compounds exhibited three absorption maxima at ~ 270 nm, 330 nm and 380 nm with a little shoulder at 395 nm. The global maximum at 270 nm originated from the absorption of the 3-methylindole and the 1,10-phenanthroline units ($\lambda_{\text{max}} = 281$ nm and 286 nm) and was only slightly hypsochromically shifted. A fine structure with local maxima at 330 nm, 380 nm and 395 nm was observed for all PIM macrocycles. These absorption maxima can be assigned to

intramolecular charge-transfer interactions between the donor and the acceptor units, indole and phenanthroline, respectively.

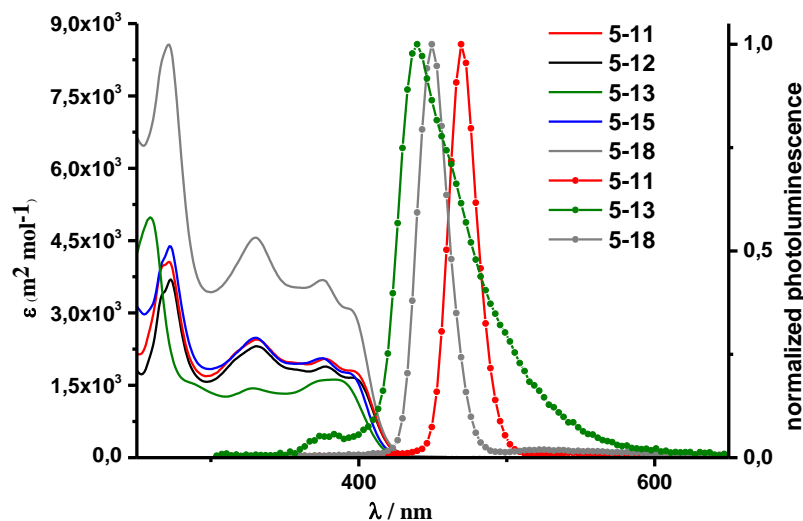


Figure 5-5: Electronic absorption (solid line) and emission spectra (dotted line) of compounds **5-11**, **5-12**, **5-13**, **5-15** and **5-18** ($c = 1 \cdot 10^{-5}$ to $5 \cdot 10^{-5}$ M in DCM).

The intensity of the dimeric PIM macrocycle **5-18** was doubled compared to the one of **5-12**, verifying that there was no extra conjugation between the two N₄-cavities. Only a weak blue emission between 440 nm and 470 nm was observed for these compounds. The absorption and emission data for all compounds are summarized in Table 5-1.

Table 5-1: The summary of the electronic absorption and emission data for the free ligands **5-11** to **5-18** in DCM ($c = 1 \cdot 10^{-5}$ to $5 \cdot 10^{-5}$ M).

compound	λ_{abs} [nm]	λ_{em} [nm]
3-Methylindole	281	n.d.
5-7	286	n.d.
5-11	272, 332, 377, 396	469
5-12	273, 332, 377, 397	n.d.
5-13	260, 330, 380	439
5-15	272, 330, 377, 394	n.d.
5-18	272, 331, 376, 394	449

5.2.2. Crystal Structure

The structure of the macrocyclic precursor **5-11** was further analyzed by X-ray crystallography (Figure 5-6). The crystals were obtained by slow evaporation from dichloromethane. The C₂/c symmetry and the non-planarity were revealed by the crystal structure of **5-11**. The indole units were twisted “up” and “down” from the phenanthroline plane with an average angle of 21.5°. The distances between the pyrrolic nitrogens (N(1) and N(4)) and the pyridinic nitrogens (N(2) and N(3)) were 3.96 Å, comparable with the distances in the porphyrin N₄-cavity. The cavity was nearly quadratic with an edge length of about 2.78 Å, varying only between N(1) and N(4) (3.39 Å) because of the twisted indole units.

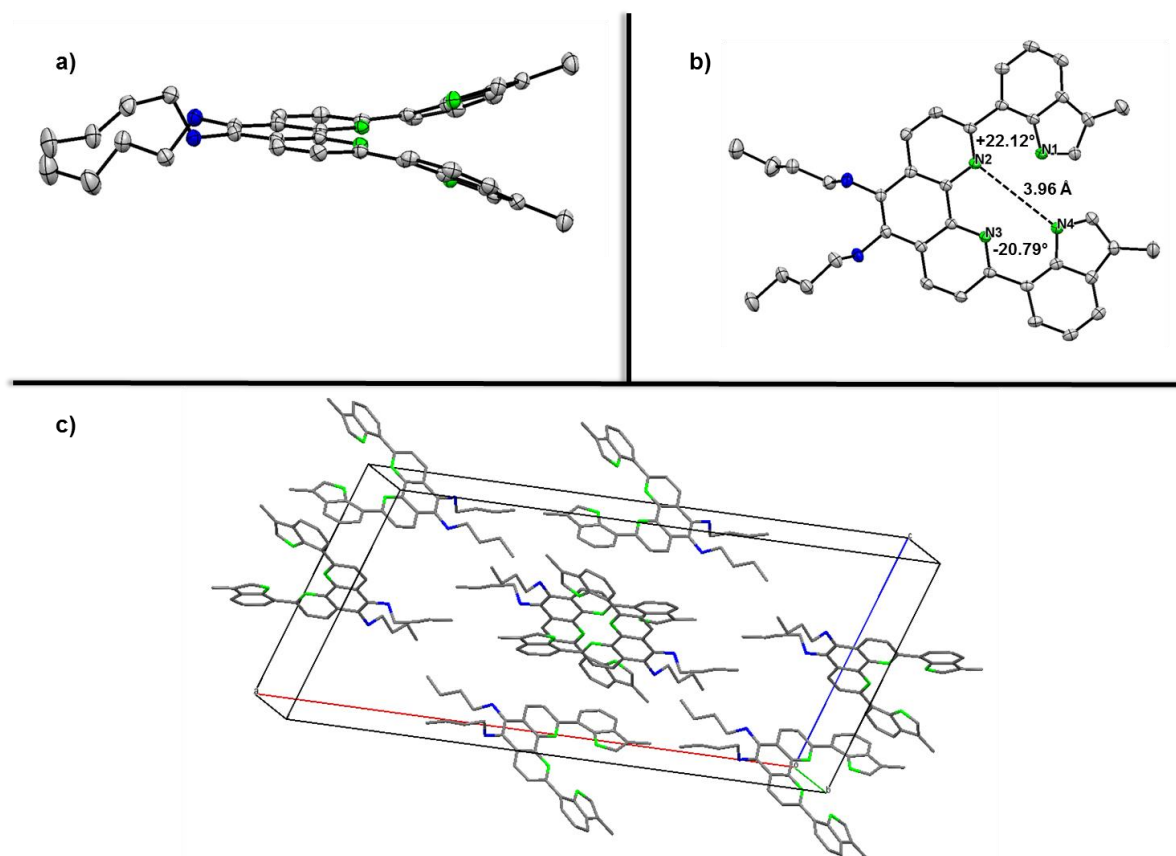


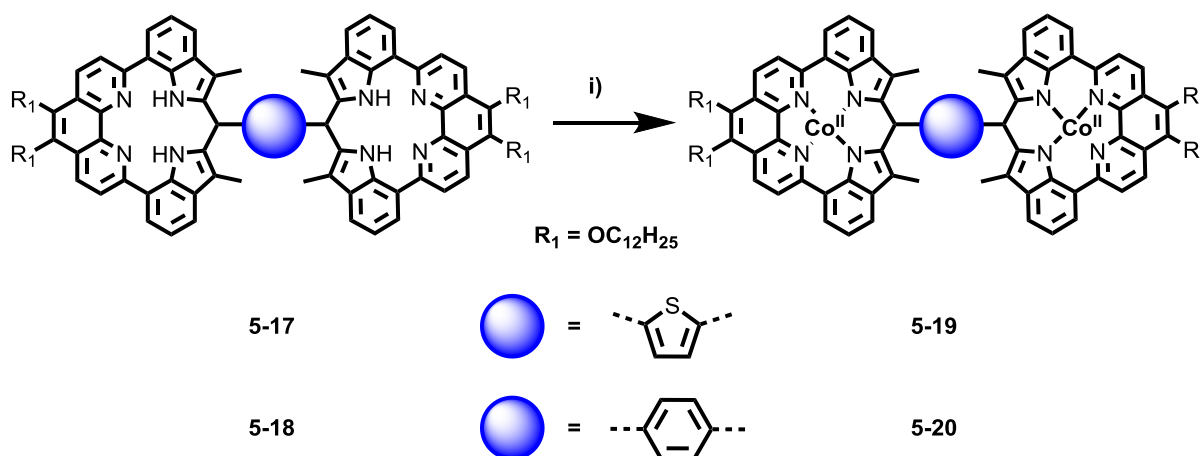
Figure 5-6: Crystal structure of **5-11** with a): side view and b): top view. The side view is showing the twist of the indole units. CH₂Cl₂ solvate molecules are omitted for clarity; the ellipsoids correspond to 50 % probability; dihedral angles are shown in the molecules; c): unit cell; the hydrogen atoms are omitted for clarity.

5.2.3. Metal Complexation

The tetrapyrrole macrocycles, like porphyrin and phthalocyanine, are able to bind a broad variety of metal ions.^[166] The electrocatalytic performance of iron- and cobalt-ion centers were enhanced compared to all other transition metal-ions.^[96] The crystal structure (chapter 5.2.2) revealed that the N₄-cavity of the PIM macrocycle is large enough to bind 3d transition-metal ions with ionic radii between 0.5-0.9 Å.^[167]

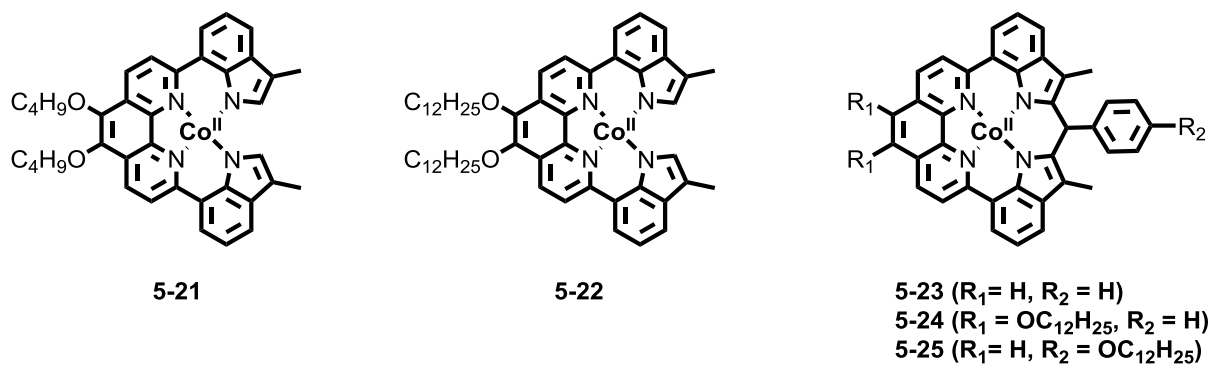
The formation of stable Co^{II}-complexes, based on the ligands **5-13** to **5-16**, was demonstrated in previous work by a former group member, *Qi Su*. In this work the ligand system was extended towards the dimeric macrocyclic ligands **5-17** and **5-18**, having the ability to bind two cobalt-ions. Further, it was investigated if these two metal ion centers affect each other in terms of the catalytic properties.

The cobalt complexes were synthesized by the acetate method^[168], adding stoichiometric amounts of cobalt(II) acetate to a DMF solution of the respective ligand (Scheme 5-6). Subsequently, the mixture was heated to 110 °C under microwave irradiation and after completion, the complexes were precipitated in water, collected by filtration and dried under high vacuum. The cobalt ion insertion was monitored by FT-IR spectroscopy and MALDI-TOF mass spectrometry.



Scheme 5-6: Synthetic route to **5-19** and **5-20**. Conditions: i) DMF, Co(OAc)₂, microwave heating: 2 h/110 °C/300 W, precipitated in water, 50-80 %.

Also the cobalt complexes of the open ligand structures (**5-21**, **5-22**) and the mononuclear macrocycles (**5-23** to **5-25**) were formed according to the described procedure (Scheme 5-7).



Scheme 5-7: Cobalt complexes **5-21** to **5-25**.

A validation of the successful cobalt complexation was obtained by FT-IR spectroscopy, proving the absence of the NH stretching vibrations for the cobalt complex **5-20** in contrast to the free ligand **5-18** (Figure 5-7).

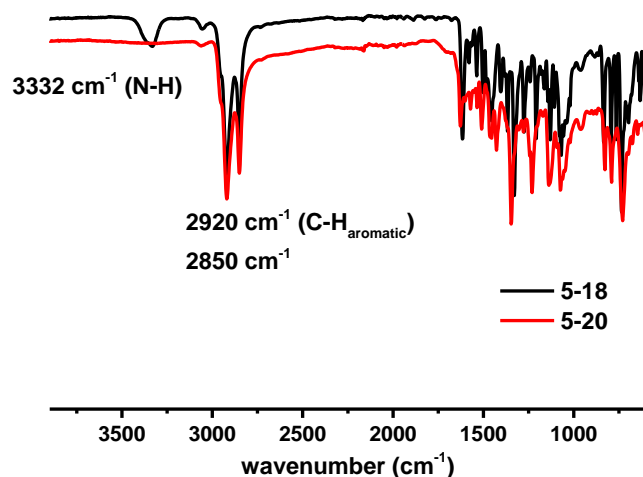


Figure 5-7: FT-IR spectra of dimeric macrocycle **5-18** and its cobalt complex **5-20**.

Further, the complexation was verified by MALDI-TOF mass spectrometry. In Figure 5-8 the experimental and theoretical data are depicted which prove the existence of the binuclear cobalt complexes **5-19** and **5-20**.

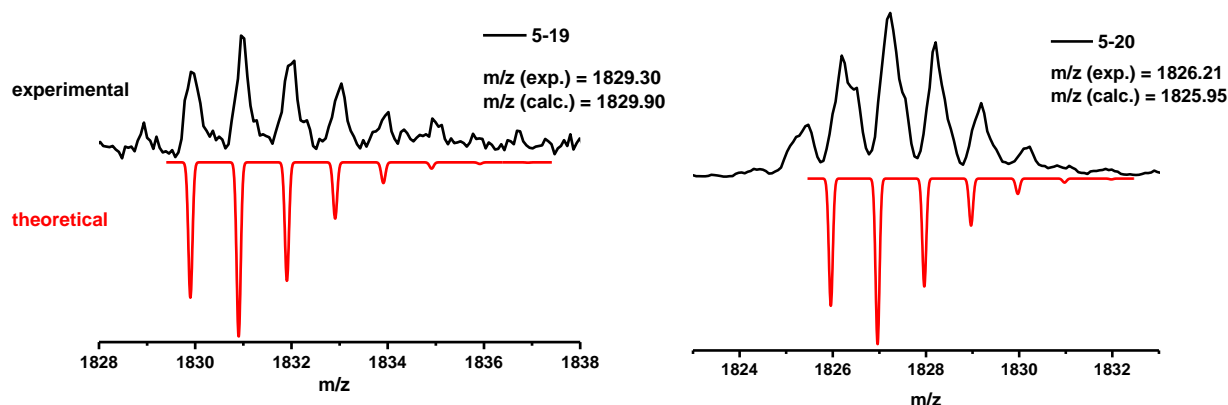


Figure 5-8: MALDI-TOF mass spectra for cobalt complexes a) **5-19** and b) **5-20**; black: experimental data, red: simulated isotopic pattern.

The electronic absorption spectra of the cobalt complexes were measured in dichloromethane ($c = 10^{-5}$ M). Compared to the free ligands, the absorption maxima, originating from the ligand centered absorption, were bathochromically shifted for all cobalt complexes **5-19** to **5-23** to $\lambda = 280$ nm (Figure 5-9).

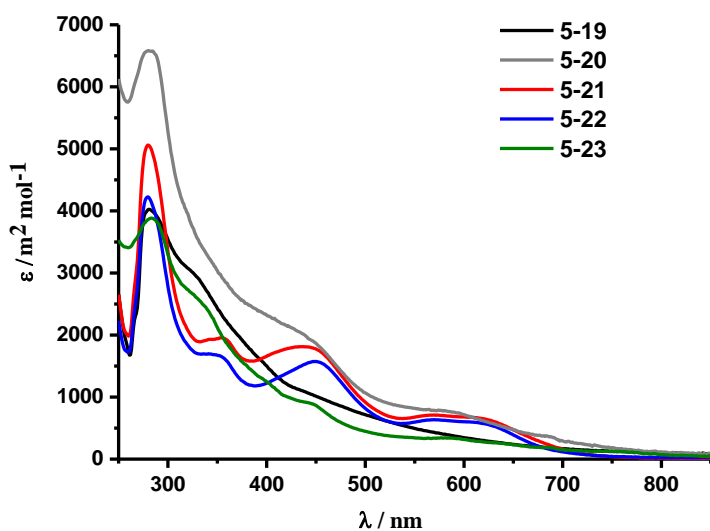


Figure 5-9: Electronic absorption spectra of cobalt complexes **5-19** to **5-23** ($c = 1 \cdot 10^{-5}$ M in DCM).

The spectra of all cobalt complexes were rather broad and structureless in the whole range of the spectrum. This can be explained by the change of symmetry upon metal complexation and the interactions of the cobalt-ion with the macrocyclic ligand.^[169,170] However, in the visible region of the spectrum absorption maxima at ~ 350 nm, ~ 450 nm and a very weak absorption in the region from 550 nm to 700 nm were observed. These red-shifts, in comparison to the free ligands, and the appearing absorption at around 600 nm are due to the metal-to-ligand charge-transfer interaction.^[171,172] The electronic absorption data for the cobalt(II) complexes are summarized in Table 5-2.

Table 5-2: The summary of the electronic absorption data for the compounds **5-19** to **5-23** in DCM ($c = 1 \cdot 10^{-5}$).

compound	λ_{abs} [nm]
5-19	281, 400-500, 550-700
5-20	282, 440, 550-700
5-21	280, 355, 440, 550-700
5-22	280, 350, 450, 550-700
5-23	284, 336, 445, 550-700

5.2.4. RDE measurements

As previously mentioned in chapter 5.1, non-precious metal catalysts (NPMCs) are promising materials for the replacement of the scarce and expensive platinum in fuel cell cathodes. Beginning in the 70s, the research on novel carbon supported metallo N₄-macrocycles and metal free catalysts kept growing till today.^[90,92,100,101,104,105,173–179] The most active metal ion centers in the oxygen reduction reaction (ORR) are iron and cobalt. The electrochemical activity of the Co-PIM and Co-Bis-PIM complexes towards the ORR under alkaline and acidic conditions was tested in cooperation with [REDACTED], using rotating disk electrode (RDE) techniques. For the measurement in an oxygen saturated 0.1 M alkaline KOH or 0.5 M H₂SO₄ solution, the complexes were supported on carbon black (20 wt%, Ketjenblack EC300J). For comparison the performance of a commercially available Pt/C (20 wt%, BASF) and Co-tetra(*p*-methoxyphenyl)porphyrin (Co-TMPP) catalyst was studied. The catalyst ink was transferred on a glassy-carbon RDE, resulting in a catalyst loading of 0.2 mg·cm⁻². In Figure 5-10 the cyclic voltammograms of Pt/C and 5-24/C at a scan rate of 100 mVs⁻¹ are shown. The curves of the argon saturated solutions were quite featureless serving as the benchmark. After saturating the solution with oxygen, distinct cathodic peaks were observed in the range of -0.2 to -0.1 V, indicating the activity towards oxygen reduction. In comparison with the Pt/C catalyst, which is known to be the most active one for the ORR, the Co-PIM/C catalyst 5-24/C showed a similar activity.

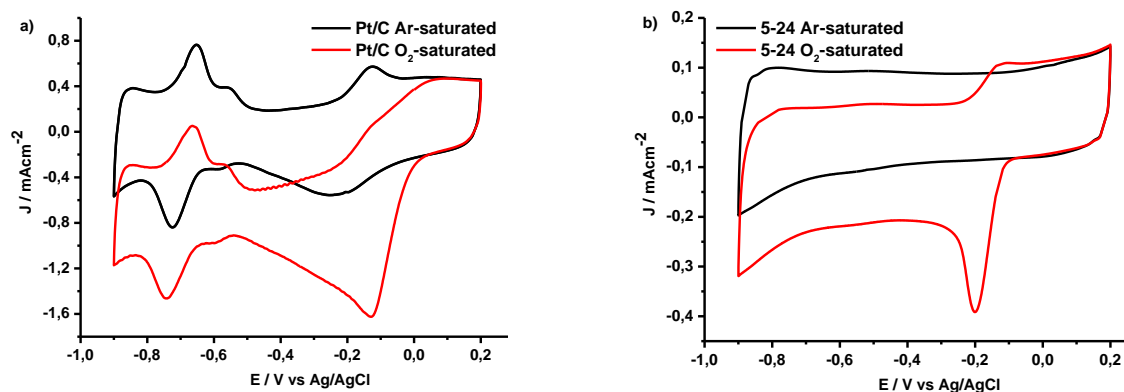


Figure 5-10: Cyclic voltammograms of a) Pt/C and b) 5-24/C on a GC RDE at a scan rate of 100 mVs⁻¹ in Ar-saturated (black) and O₂-saturated (red) solutions of 0.1 M KOH.

Further investigations on the ORR activity were performed using rotating disk voltammetry. The polarization curves at a rotating speed of 1600 rpm under alkaline conditions are depicted in Figure 5-11a,b. The plain PIM ligand **5-11/C** showed only a low activity whereas all cobalt catalysts **5-20/C** to **5-24/C** exhibit a high activity towards the ORR in alkaline conditions. The reduction onset potential (E_{on}) for these complexes was in the range between -0.08 V and -0.13 V and the highest half wave potential ($E_{1/2}$) was observed for **5-21/C** with -0.15 V.

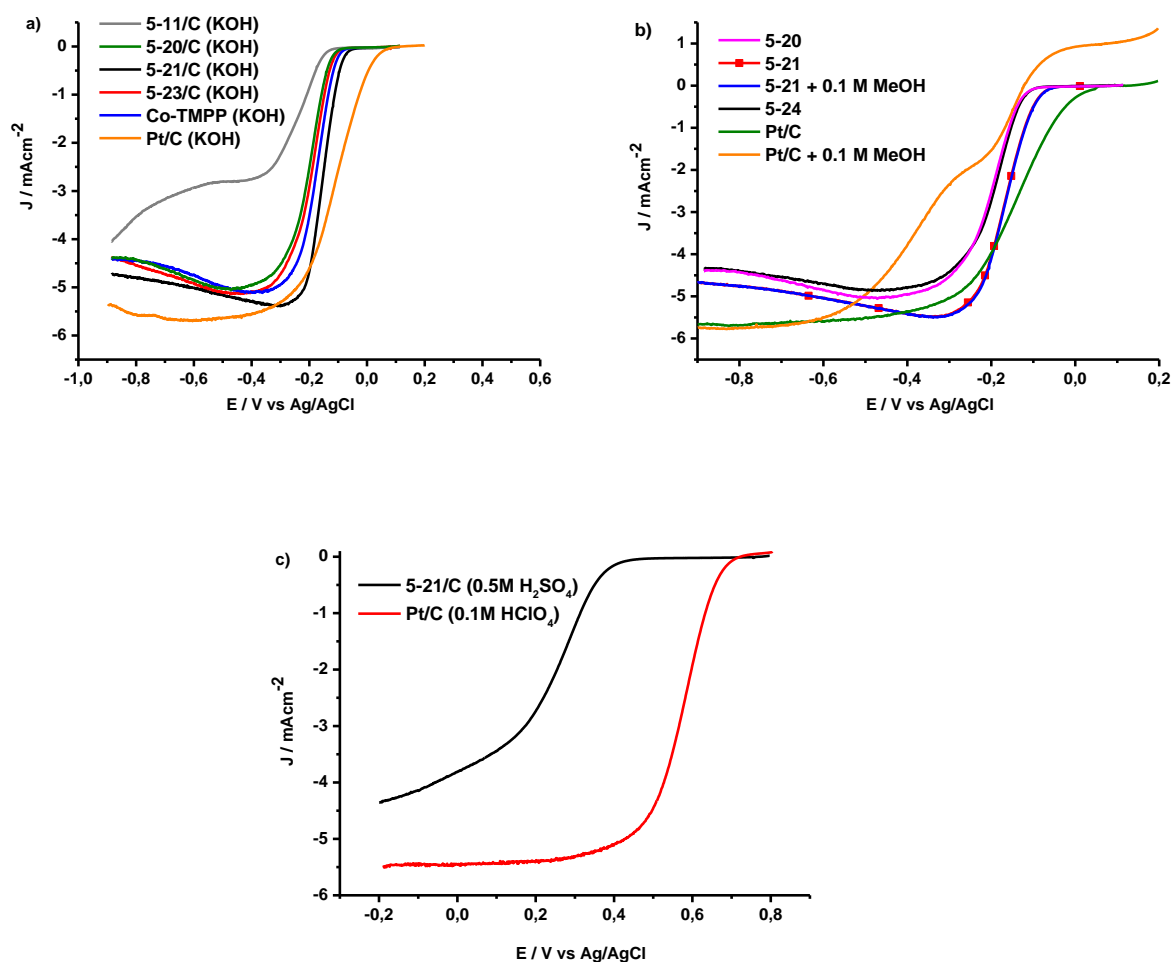


Figure 5-11: a) ORR polarization curves for the different $[\text{Co-N}_4]_n/\text{C}$ catalysts, Co-TMPP and Pt/C in 0.1 M KOH, the electrode rotation rate was 1600 rpm with a scan rate of 10 mVs^{-1} . For all RDE voltammograms the catalyst loading was $0.2 \text{ mg}\cdot\text{cm}^{-2}$, except for Pt/C ($0.1 \text{ mg}\cdot\text{cm}^{-2}$); b) ORR polarization curves in alkaline conditions before and after the addition of MeOH; c) ORR polarization curves for 5-21/C in 0.5 M H_2SO_4 and Pt/C in 0.1 M HClO_4 , rotation and scan rate were similar to a).

In comparison, the onset potential of **Pt/C** and **Co-TMPP** were 0.03 V and -0.11 V with an $E_{1/2}$ of -0.11 V and -0.17 V, respectively. Hence, the electrochemical activity of the Co-PIM catalysts towards ORR in alkaline conditions was better than the **Co-TMPP** system and approximately comparable with the most active catalyst **Pt/C**. Moreover, **5-21/C** tolerated the addition of methanol without any loss of performance. For **Pt/C** the addition of methanol caused a dramatic decrease of the performance what was shown by RDE measurements (Figure 5-11).

Since NPMCs are thought to replace platinum in proton exchange membrane fuel cells (PEMFCs), the activity of the Co-PIM catalysts was also tested in acidic media (0.5 M H_2SO_4 , Figure 5-11c). The catalyst **5-21/C** exhibits activity in acidic conditions with an E_{on} of 0.37 V and an $E_{1/2}$ of 0.29 V. For comparison, **Pt/C** had a higher E_{on} of 0.67 V and a higher $E_{1/2}$ of 0.58 V in 0.1 M $HClO_4$, being much more active towards ORR in acidic conditions. Perchloric acid was used to prevent the formation of adsorbed bisulfates, which would cause a performance loss at higher potentials.^[180] The stability of **5-21/C** in acidic solutions was very poor what will be explained in detail in chapter 5.2.5. Therefore studies on the activity in acidic conditions were not continued. Comparing the different Co-PIM catalysts **5-20/C**, **5-21/C** and **5-24/C** with each other (Figure 5-11b) it is obvious that the cobalt complex of the unclosed N_4 -ligand **5-21/C** showed a superior activity in alkaline solutions. The mononuclear Co-PIM catalyst **5-24/C** and the binuclear catalyst **5-20/C** exhibited similar activities. The results and kinetic parameters for all catalysts are summarized in Table 5-3.

These findings were unexpected as the assumption was an increase of the activity in the order **5-21/C** \approx **5-24/C** < **5-20/C**. Contrary to our expectations an extension to the dimeric cobalt catalysts **5-19/C** and **5-20/C** had no influence on the electrochemical activity. With the ring-closure of the PIM macrocycle ligands, and the formation of a new carbon sp^3 -center, the activity decreased for the mono- and dimeric cobalt PIM catalysts. Due to this sp^3 -center the monomeric and dimeric PIM ligands lack of planarity and conjugation. Therefore the alignment on the carbon black support might be unfavorable what can have influences on the ORR activity.^[92] Moreover, the active site may be blocked and as a result the O_2 -binding ability

may be reduced. However, the activity of **5-20/C** and **5-24/C** was similar to the **Co-TMPP** catalyst and near the activity of **Pt/C**, without any heat treatment of the supported complexes.

Table 5-3: Summarized results and parameters for RDE measurements of the different $[\text{CoN}_4]_n$ complexes, Pt/C and Co-TMPP.

compound	condition	E_{on} [V] ^a	$E_{1/2}$ [V] ^a
5-19	0.1 M KOH	-0.12	-0.19
5-20	0.1 M KOH	-0.13	-0.20
5-21	0.1 M KOH	-0.08	-0.15
5-21	0.5 M H ₂ SO ₄	0.37	0.29
5-22	0.1 M KOH	-0.11	-0.17
5-23	0.1 M KOH	-0.12	-0.19
5-24	0.1 M KOH	-0.13	-0.19
5-25	0.1 M KOH	-0.12	-0.19
Co-TMPP	0.1 M KOH	-0.11	-0.17
Pt/C	0.1 M KOH	0.03	-0.11
Pt/C	0.1 M HClO ₄	0.67	0.58

[a] Determined from RDE voltamograms (Figure 5-11).

In conclusion, the electrochemical catalytic activity of the cobalt complexes **5-20/C** to **5-25/C** towards ORR was demonstrated under alkaline and acidic conditions. In contrast to the expectations, the catalytically most active cobalt complex was the unclosed complex **5-21/C**. The macrocyclic monomeric and dimeric cobalt complexes had similar catalytic activities, comparable with the commercially available **Co-TMPP**. An increase of the cobalt centers had no beneficial influence on the catalytic performance. This unexpected trend can be explained by the non-planarity of the macrocyclic complexes, resulting in an unfavorable alignment on the carbon surface and partially blocked active sites. This implies that planarity is an issue for the future design of NPMCs, influencing the complex-support interactions.^[92] However, the novel

phenanthroline-indole ligands and the resulting cobalt complexes showed a very high catalytic activity without the necessity of any heat pre-treatment. This allows further studies on the relation between the structure of the active site and the performance as fuel cell cathode catalyst. Also the activity and stability of such NPMCs in acidic conditions has to be improved to fulfill the needs in PEMFC applications. As mentioned in chapter 1.4.2 not only the activity, but also the effective 4-electron transfer is a crucial parameter in the performance of a fuel cell cathode catalyst. Rotating ring disk electrode (RRDE) techniques were used to investigate the electron transfer of the Co-PIM catalysts (chapter 5.2.5).

5.2.5. RRDE measurements

In addition to the RDE measurements rotating ring disk measurements were performed to investigate the selectivity and stability of the Co-PIM catalysts. A RRDE electrode with a Pt ring (6.25 mm inner-diameter and 7.92 mm outer-diameter) as counter electrode, a glassy carbon disk working electrode (5.61 mm diameter) and an Ag/AgCl (4M KCl) reference electrode inside a standard three-electrode-electrochemical cell were used for evaluating the ORR selectivity and stability of the Co-PIM catalysts. The catalyst inks were prepared by first dissolving 1.0 mg of $[MN_4]$ -complex in dichloromethane and a subsequent addition of 4.0 mg carbon black (Ketjenblack EC300J) to obtain 20 wt% $[MN_4]$ mixtures. After ultrasonication and drying at RT, the catalyst ink was obtained by blending the dried powder with 50 μ L Nafion solution (0.5 wt%) and 950 μ L ethanol in an ultrasonic bath. 9.9 μ L of catalyst ink was then transferred onto the GC surface, resulting in a catalyst loading of $0.2 \text{ mg}\cdot\text{cm}^{-2}$. A commercially available platinum catalyst (BASF, 20 wt%, supported on carbon black) was used for comparison. The catalyst ink was prepared as described above with a $5 \text{ mg}\cdot\text{ml}^{-1}$ Pt/C suspension, leading to a Pt loading of $20 \text{ }\mu\text{g}\cdot\text{cm}^{-2}$ on the GC-electrode. First, the efficiency of the electron transfer was investigated by RRDE techniques and the results are depicted in Figure 5-12a.

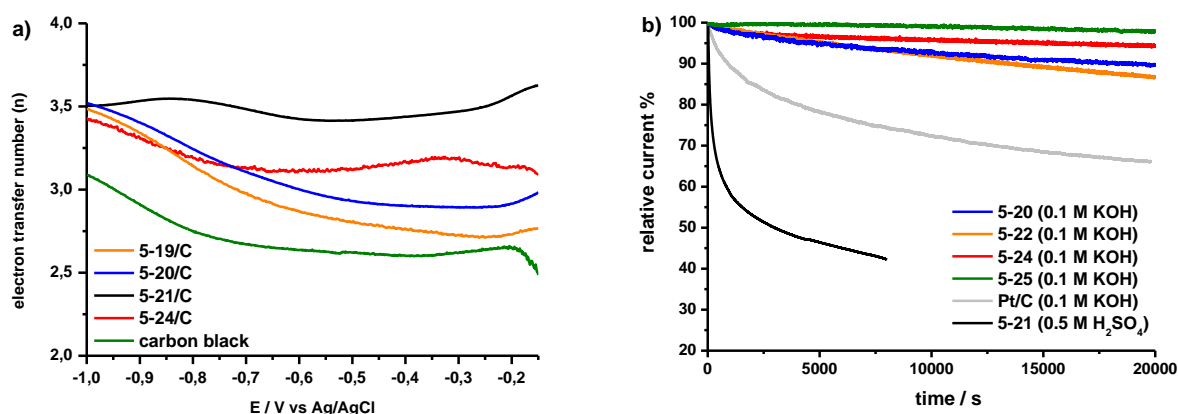


Figure 5-12: a) Electron transfer numbers of **5-19/C** to **5-21/C** and **Pt/C** at different potentials; data derived from RRDE measurements; b) current-time chronoamperometric response of **5-20/C** to **5-25/C** and **Pt/C** modified GC electrode at -0.4 V in O₂-saturated alkaline KOH solution (0.1 M) or acidic H₂SO₄ at a rotation rate of 1600 rpm;

The direct 4-electron reduction of oxygen is the preferred pathway inside a working fuel cell, as mentioned in 1.4. All Co-PIM catalysts contribute to the 4-electron reduction pathway in the range between 35 % (**5-19/C**) and 75 % (**5-21/C**). The same order as seen for the activity can be observed for the selectivity. The unclosed cobalt catalyst **5-21/C** is the most selective catalyst with an electron transfer number of 3.5. The monomeric and dimeric cobalt PIM catalysts had a less efficient electron transfer of ~ 3 electrons, which is a contribution of around 50 % to the 4-electron reduction pathway. Even if the performance of the **Pt/C** catalyst is still superior, the novel Co-PIM catalysts showed very promising results. The detailed values are summarized in Table 5-4. These values for the Co-PIM catalysts were superior compared to other non-pyrolyzed NPMCs reported, like Co^{II}-phthalocyanines (n = 2) and Co^{II}-porphyrines (n = 2.6).^[88,96,181] Only iron-phthalocyanines and multinuclear systems, consisting of metallophthalocyanines and metalloporphyrines are known to provide the direct 4-electron reduction of oxygen to water.^[90] Unexpectedly, the selectivity for the 4-electron pathway for the mononuclear complexes was enhanced compared to previous work. In former studies the cobalt PIM catalysts were supported on Vulcan XC72R with a surface area of 254 m²g⁻¹. In this work Ketjen Black EC300J with a surface area of 800 m²g⁻¹ was used. Additionally the ratio of Nafion[®] to catalyst was ten times lower in this work. This might have hampered the coverage of active sites by the excess Nafion[®], resulting in a higher electrocatalytic activity. How-

ever, good catalyst systems, consisting of active metal complexes and a high surface support, as well as careful preparation are the key requirements for a good catalyst performance.

Table 5-4: Summarized results of the selectivity and durability measurements obtained by the RRDE technique.

compound	%H ₂ O ^a	n ^b	durability ^c
5-19/C	35	2.7	n.d.
5-20/C	45	2.9	90 %
5-21/C	75	3.5	42 % in H ₂ SO ₄
5-22/C	70	3.4	86 %
5-24/C	55	3.1	94 %
5-25/C	n.d.	n.d.	98 %
Co-TMPP ^[96]	30	2.6	n.d.
Pt/C ^[182]	100	4	64 %

[a] efficiency of 4-electron transfer at -0.2V; [b] electron transfer numbers were determined from RRDE measurements at -0.2 V; [c] determined from chronoamperometric measurements at -0.4 V (0.1 M KOH or 0.5 M H₂SO₄, 1600 rpm) in O₂-saturated solution.

Furthermore, the durability of the catalyst is a crucial parameter. Therefore the long-term stability in alkaline and acidic conditions at a constant voltage of -0.4 V over a period of 20000 s was determined. The corresponding results are shown in Figure 5-12b and Table 5-4. A superior long-term stability was observed for all the Co-PIM catalysts in basic media, still having 86 % to 98 % of the initial current after 20000 s. In comparisons, **Pt/C** showed a faster current attenuation, resulting in a remaining current of only 64 % after the same period. Studies by *Mayrhofer et. al.* revealed that silica impurities, resulting from the glass electrochemical cell, can affect the long-term performance of bulk platinum catalysts.^[183,184] If this is also true for nanosized **Pt/C** catalysts remains unclear. However, there was no obvious influence on the performance of the Co-PIM catalyst systems, proving their stability. In acidic media a current loss of about 60 % for **5-21/C** was observed after 8000 s. A similar performance was reported for iron phthalocyanines.^[185] The instability of the iron phthalocyanine was caused by the partial protonation and the subsequent demetallation of the complex. If this was also true for the Co-PIM system could not be investigated within the scope of this work.

Concluding this chapter, the long-term stability and the selectivity for the direct 4-electron reduction of oxygen were determined for the Co-PIM catalysts by RRDE techniques. A very high long-term stability of up to 98 % was found for the catalysts **5-20/C** to **5-25/C**. Further it was demonstrated that the Co-PIM catalysts provided mainly the direct 4-electron reduction of oxygen with an efficiency of up to 75 % for **5-21/C**. In contrast to the first assumption, the extension of the catalytic system towards the dimeric complex **5-20/C** had no positive influence on the electrocatalytic performance. This can be explained by the non-planarity of the dimers, which was already discussed for the catalytic activity in chapter 5.2.4. However, these findings represent a breakthrough in the field of NPMCs, since these materials are non-pyrolyzed and thus the active site was well defined. Studies on the structure-performance relationship and the improvement of the stability in acidic conditions still remain a challenge for future research.

5.3. Summary

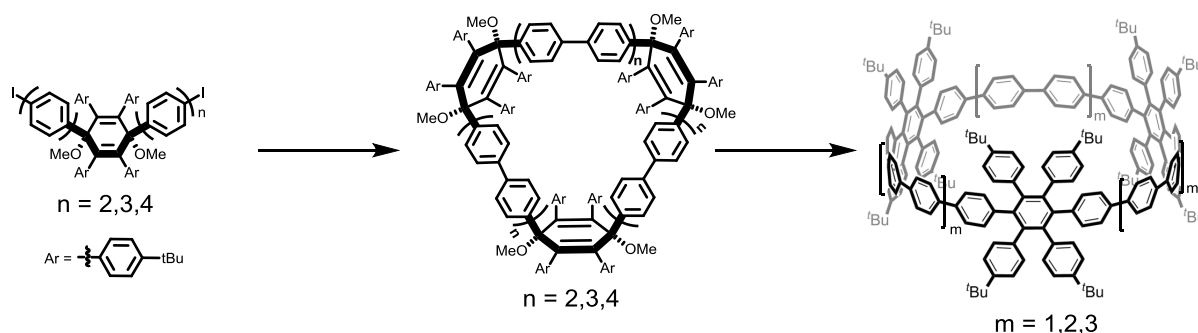
In this chapter, the synthesis of the novel macrocyclic N₄-ligand PIM, consisting of phenanthroline and indole units, was presented. X-ray crystal structure analysis revealed the existence of a well-defined N₄-cavity for **5-11**. Moreover, the “dimeric” ligand structures **5-17** and **5-18** were synthesized, using the same synthetic approach as for the PIM monocycles. Six different PIM mono- and bicycles (**5-13** to **5-18**) were synthesized and their electronic and electrocatalytic properties were studied. They all showed good chelation properties with transition metal-ions and cobalt(II) was chosen to form metal-complexes as catalysts for the electrocatalytic reduction of oxygen to water. The concept of extending the cobalt PIM macrocycles towards binuclear structures was developed to have NPMCs with a higher activity, selectivity and durability, overcoming the drawbacks of previously reported N₄-macrocyclic complexes.^[103,186] The electrocatalytic activity of all Co-PIM catalysts in alkaline solutions was very high, contributing between 50 % and astonishing 75 % (**5-21/C**) to the direct 4-electron reduction pathway, which is outstanding for non-heat-treated N₄-macrocyclic cobalt complexes. In addition, the superior stability in alkaline conditions and an excellent tolerance of methanol crossover were demonstrated. Since, the planarization and full conjugation in PIM mono-

and bicycles was not successful, the stability in acidic conditions could not be improved and no influence on the electrocatalytic performance was observed. However, it turned out that the PIM N₄-cavity can form stable and highly active cobalt(II) complexes, even when the macrocycle is not fully closed (*e.g.* **5-21/C**) or conjugated. In combination with a high surface area carbon black, improved electrocatalytic properties were obtained, representing a promising basis for the development of further NPMCs. Since the state-of-the-art PEMFCs work in acidic conditions, the durability and activity of the PIM complexes need to be optimized. Therefore, the formation of the respective iron complexes and their electrocatalytic investigation might be the way to improve the activity and stability of these complexes and is part of the ongoing research.

6. Conclusion and Outlook

In the first part of this work, the longitudinal extension of cycloparaphenylenes as an approach towards the bottom-up synthesis of ultrashort CNTs was investigated. Therefore the post-construction method was developed, using polyarylated CPP precursors, which can be selectively dehydrogenated towards CNT segments. The study covered the synthesis of *cyclo-para*-hexahenylbenzene ([3]CHPB) derivatives of different ring sizes and different substitution patterns. As a last step the applicability of the *Scholl* reaction in cyclic and strained systems was investigated in order to form *cyclo-para*-hexa-*peri*-hexabenzocoronenes ([3]CHBCs) with graphenic sidewalls.

In chapter 3 the synthesis of the phenylene-extended [3]CHPBs of different sizes was described. The [3]CHPBs are polyarylated CPPs, bearing twelve phenyl substituents at the backbone. These aryl substituents were arranged as three hexaphenylbenzene units within the macrocycle allowing the formation of [3]CHBCs in the last step. To investigate the influence of the ring strain onto the cyclodehydrogenation, three different [3]CHPBs were synthesized, having 15-, 21- and 27-phenylene rings in the CPP base. The [3]CHPBs were synthesized by the trimerization of 3,6-aryl substituted cyclohexadienes, which induce the curvature (Scheme 6-1).



Scheme 6-1: Schematic illustration of the synthesis of [3]CHPBs of different sizes.

As the final step, the oxidative cyclodehydrogenation on these strained macrocycles was investigated (Figure 6-1). Due to the ring strain and the distortion of the benzene rings no clean and selective cyclodehydrogenation was observed for the smallest [3]CHPB **3-12**. A mixture of higher dehydrogenated products was obtained, which was separated and carefully analyzed by ion mobility mass spectrometry in cooperation with *Wen Zhang* and *Hans Joachim Räder*. Different drift times and cross section values indicated that the side reactions went along with structural changes. This side reaction was observed up to three times in the 15-membered [3]CHPB, but only one time in the larger 21-membered [3]CHPB **3-16**. Therefore, NMR techniques could be applied to analyze the nature of this side reaction for the [3]CHPB **3-16**. The analysis supported the assumed mechanism of the 1,2-phenyl shift as side reaction. The reduced tendency towards this strain releasing 1,2-phenyl shift with increasing ring size was verified by the selective synthesis of the 27-membered [3]CHPB **3-17**.

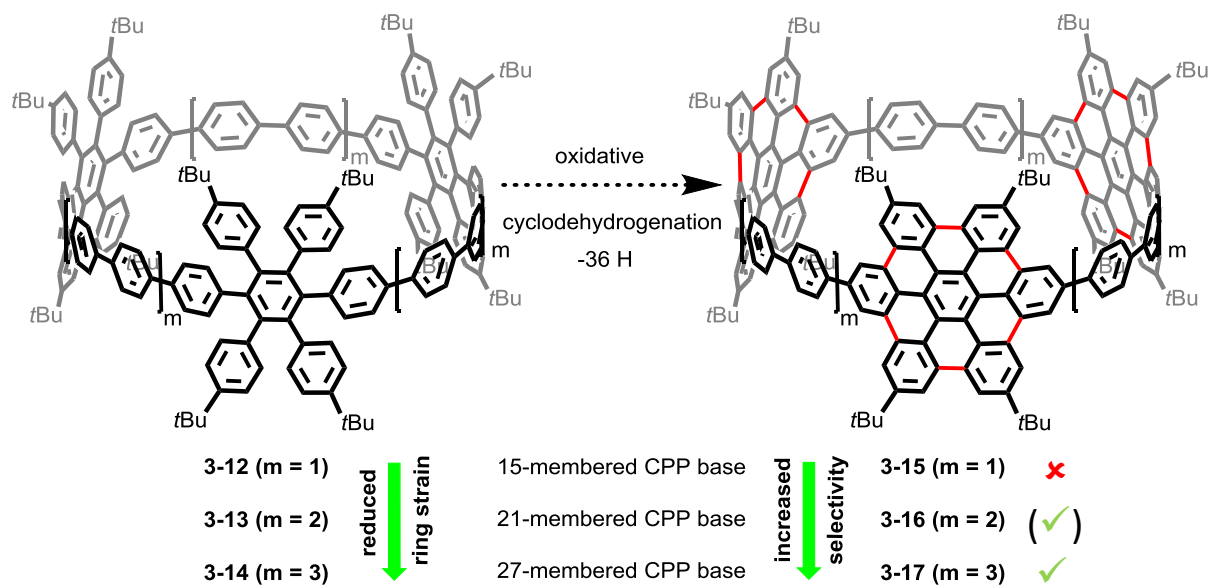


Figure 6-1: Illustration of the cyclodehydrogenation of the [3]CHPBs towards the [3]CHBCs.

Mass spectrometric techniques provided a doubtless proof of the successful synthesis of the giant [3]CHPB **3-17**, even if NMR analysis failed. Altogether, it was demonstrated in chapter 3 that CPPs can be longitudinally extended by incorporating hexaphenylbenzene units, which can be transformed into hexabenzocoronenes by oxidative cyclodehydrogenation. Further-

more, to the best of our knowledge, it was the first time that the *Scholl* reaction was successfully applied in cyclic and strained systems.

However, the increasing ring size goes along with synthetic challenges and the adaption of this strategy for polyphenylene cylinders to create ultrashort CNTs *via* the post-construction method would be difficult for a 27-membered CPP base. Therefore, the concept of substitutional blocking was investigated in the second chapter.

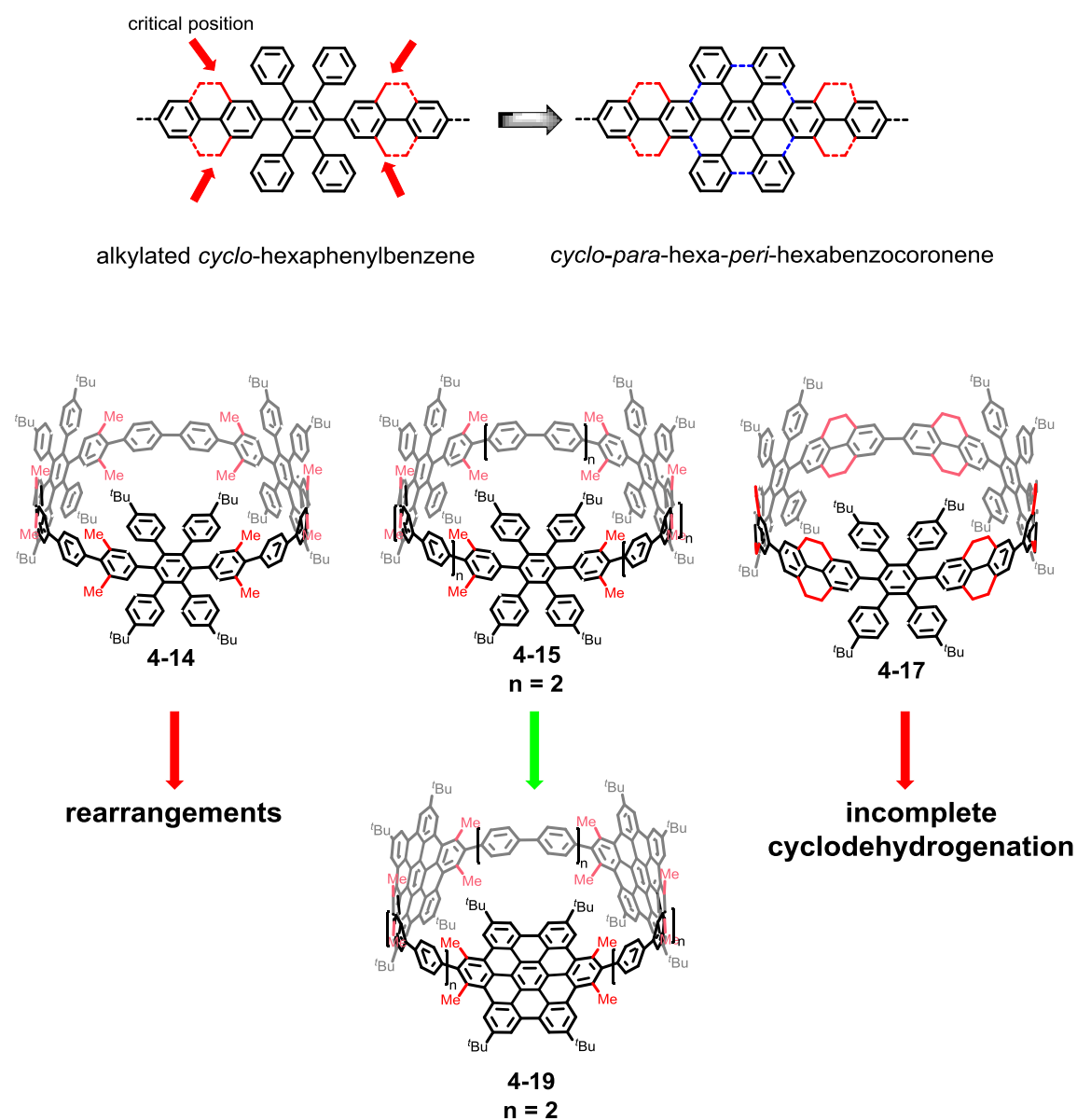


Figure 6-2: top) Illustration of the substitutional blocking concept; bottom) alkyated [3]CHPBs **4-14** to **4-17**.

The critical rearrangement positions were blocked by methyl groups or ethylene bridges to facilitate a smooth cyclodehydrogenation for the [3]CHPBs, possessing a circumference of 15- or 21-phenylene rings. With the modification of the kinked precursor molecules, the substitution pattern was easily changed and the [3]CHPBs **4-14** to **4-17** were obtained *via* the route discussed in chapter 4.2 (Figure 6-2). Nonetheless, the cyclodehydrogenation of the 15-membered [3]CHPBs **4-14** and **4-17**, bearing methyl or ethylene bridges, did not yield the desired [3]CHBCs. Instead side reactions occurred in the case of **4-14** and an incomplete cyclodehydrogenation was observed for **4-17** (Figure 6-2). The side reactions were not further investigated, but the same mechanism as for the non-blocked [3]CHPBs was assumed. These results implied that the 15-membered CPP base was still too strained to undergo a smooth dehydrogenation. The increase towards a 21-phenylene rings containing CPP base in the case of **4-15** successfully yielded the respective [3]CHBC **4-19**, which was analyzed by HR-MALDI-TOF and NMR techniques. These findings were a final proof that the concept of the post-construction method is a feasible way to get access to ultrashort CNTs by the internal dehydrogenation of the respective polyphenylene cylinders. Furthermore, it was proven that the formation of graphenic sidewalls could be accomplished by oxidative cyclodehydrogenation in cyclic and strained systems.

The high ring strain and the additional strain induced during the cyclodehydrogenation remain the major challenges for future synthetic routes towards ultrashort CNTs. Therefore, different ways should be considered for future work. First, a further arylation of the CPP backbone, forming polyphenylene cylinders possessing the right connectivity of benzene rings and sufficient size for a direct dehydrogenation towards ultrashort CNTs. In these terms, also the arrangement of already dehydrogenated segments using platinum complexes should be considered. Second, the functionalization of CPPs and their subsequent dimerization, followed by a final internal fusion by oxidative dehydrogenation could also be a promising synthetic route (Figure 6-3). The cyclic structures are already predetermined what would reduce the additional strain on the CPP backbone during the dehydrogenation.

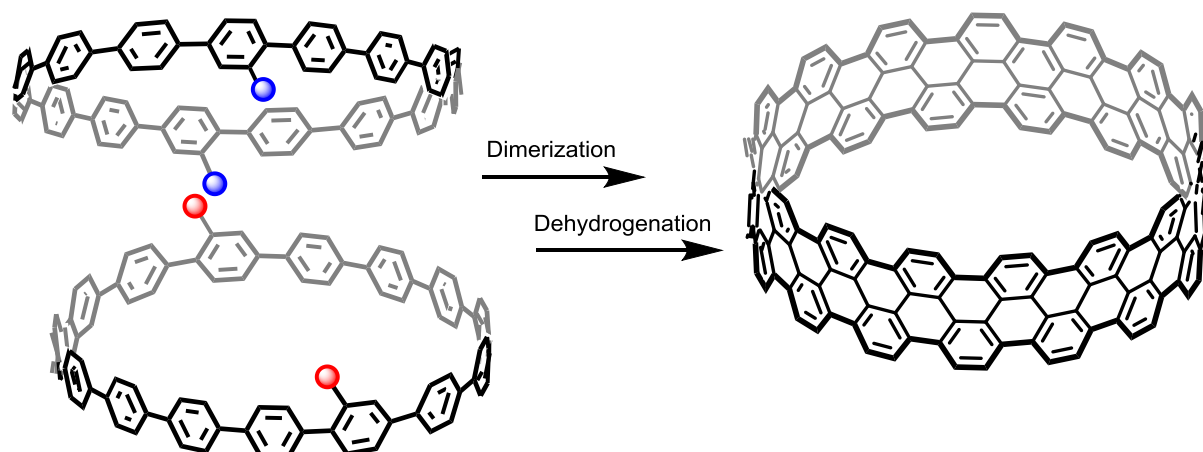


Figure 6-3: Schematic illustration of the fusion of CPPs towards CNT segments; red and blue spheres equal functional groups.

However, the precise bottom-up synthesis of CNT segments remains challenging, but it is worthwhile developing new strategies to reach this goal. Not only because these structures are so beautiful, but to get deep insights into the structure-property relationship of CNTs.

Also the development of new catalysts relies on the understanding of the structure-property relationship in order to design highly active catalysts. For the cathodic oxygen reduction, good working catalysts can be obtained by the pyrolysis of carbon and nitrogen containing precursors in the presence of transition metals. Also nitrogen-doped graphene performs well in ORR. However, little is known about the active sites in these catalysts. Therefore, the precise synthesis of NPMCs with a defined active site is desirable in order to optimize the design of these materials.

Within the scope of the second part of this work, the novel phenanthroline-indole N_4 -macrocyclic ligand, developed in our group, was modified and furthermore, extended towards a dimeric ligand system. In former work of our group it was demonstrated that upon heat pre-treatment at 700 °C the respective cobalt complexes show a catalytic activity towards ORR, promoting partially the direct 4-electron reduction of oxygen. Based on these results, the PIM cobalt complexes were modified by the introduction of different substituents to reach a better solubility, processability and particularly, to overcome the heat pre-treatment.

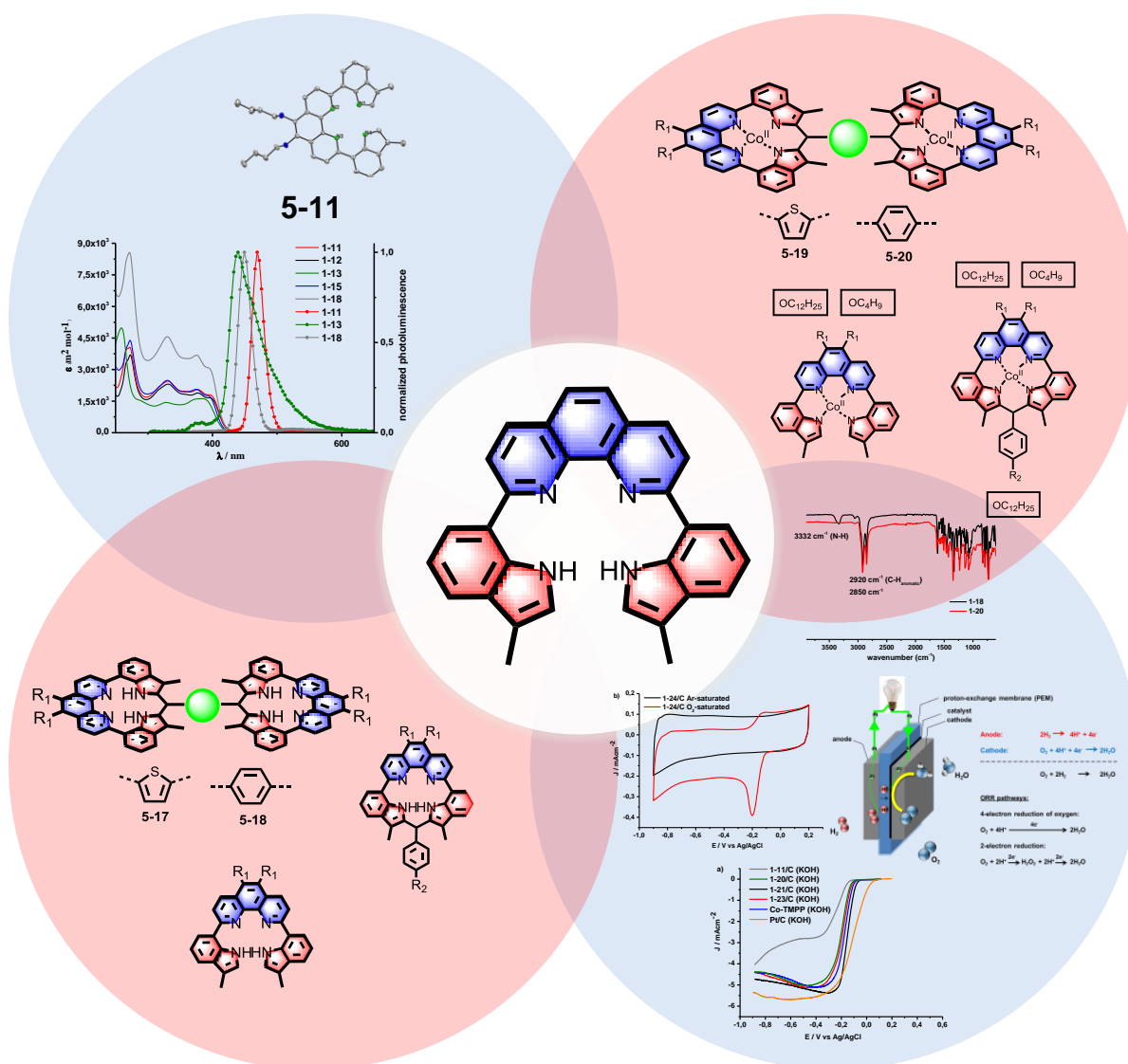


Figure 6-4: Schematic illustration of the different PIM macrocycles, Co-complexes and their properties.

The existing protocols were first optimized, increasing the yield and simplifying the synthesis of the PIM system. The existence of a well-defined N_4 -cavity was demonstrated by the X-ray crystal structure of **5-11**. As an approach to improve the catalytic activity by an accumulation of active sites, the PIM ligand was extended towards the dimeric ligands **5-17** and **5-18**, applying terephthalaldehyde and thiophene-2,5-dicarbaldehyde for the macrocyclization. The energy barrier for a partial planarization of these dimers by oxidation was too high, resulting in two separated metal centers. This work covers the synthesis of all mono- and dimeric PIM structures and their characterization by high resolution mass spectrometry, NMR spectroscopy,

py and X-ray crystal structure analysis. Furthermore, the electronic properties were analyzed by recording the electronic absorption and emission spectra.

For the evaluation of the catalytic activity of these new NPMCs, the resulting cobalt complexes were electrochemically analyzed, using RDE and RRDE techniques. Without any heat pre-treatment, all cobalt complexes contributed to the 4-electron reduction of oxygen in 0.1 M KOH solution, reaching a maximum for **5-21/C** with 75 %. The half-wave potential of **5-21/C** was -0.15 V and the reduction onset was observed at -0.08 V. These values were comparable with the state-of-the-art platinum catalysts. An excellent tolerance of methanol crossover and a superior long-term stability in alkaline solution was demonstrated for all cobalt PIM catalysts. Unexpectedly, the cobalt complex of the non-macrocyclic ligand (**5-21/C**) showed the best performance in ORR. The introduction of the sp^3 carbon center during the macrocyclization might have affected the catalytic performance. Whether poorer contacts to the carbon black support or electronic effects were responsible for this decrease was beyond the scope of this work and is part of ongoing research based on simulations.

Concluding this chapter, stable and highly active cobalt(II) complexes were formed based on the PIM N_4 -cavity. It turned out that even not fully closed (e.g. **5-21/C**) or conjugated macrocyclic complexes (e.g. **5-20/C**) promote the 4-electron reduction of O_2 , using a high surface area carbon black. This represents a promising basis for the development of further NPMCs.

However, the stability and performance in acidic media, the working media for PEMFCs, was rather low. It is supposed that conjugated and planarized binuclear catalysts would show a higher performance and stability in acidic conditions. Therefore, a different dimerization strategy needs to be applied to create stable dimeric complexes as NPMCs in acidic fuel cell applications. Based on the PIM system, the synthetic route depicted in Figure 6-5 might be a feasible way.

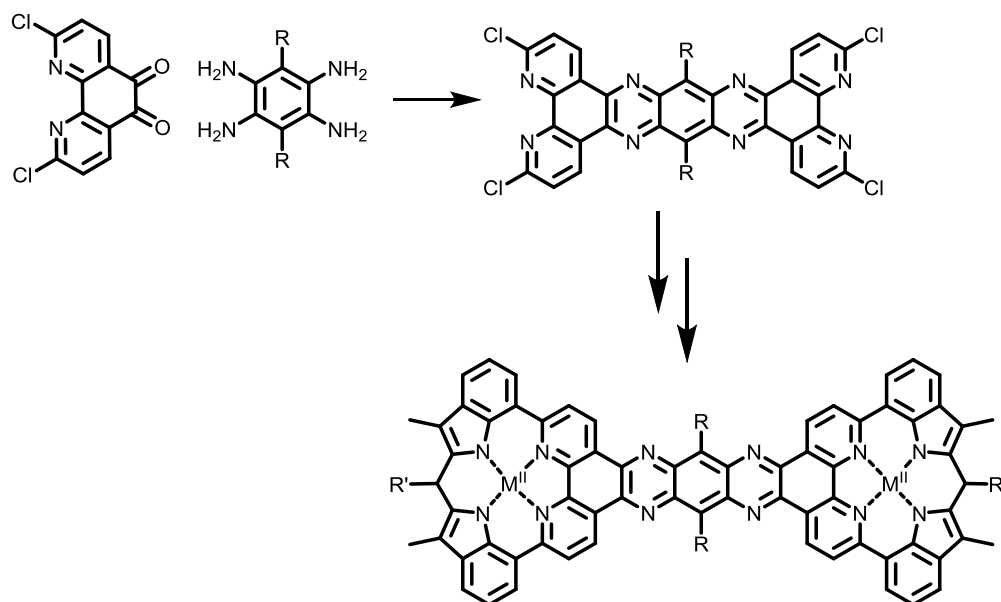


Figure 6-5: Synthetic pathway towards a dimeric and planarized bis-metal complex for ORR.

Different to the binuclear complexes described in chapter 5, the dimerization would connect the phenanthroline moieties in the PIM system instead of the indole moieties. The two metal centers might be not close enough to allow a bridge-*cis* binding of oxygen, but the second metal center can positively affect the ORR performance by electronic effects. Also the incorporation of two different metal-ions is conceivable.

Throughout all chapters it was demonstrated that bottom-up approaches are needed to get insights into the structure-property relationship. The synthesis of CNT segments from polyarylated CPPs is a step towards structurally defined CNTs and the investigation of new NPMCs is needed to understand the influences on the catalytic performance in fuel cells. The findings of this fundamental research can one day contribute to the development of improved materials and applications.

7. Experimental Part

7.1. General Methods

Chemicals and Solvents

The commercially available chemicals and solvents were obtained from the companies Acros Organics, Alpha-Aesar, Apollo-Scientific, Fluka, Merck, Sigma-Aldrich, Strem Chemicals and TCI Europe and they were used as received without further purification.

Inert Atmosphere

Standard Schlenk techniques were used for oxygen- or moisture-sensitive reactions, using argon (grade 4.8, Westfalen AG) as inert gas. A stream of argon was purged through the reaction mixture to degas the reaction.

Chromatography

Preparative column chromatography was performed on silica gel from Macherey-Nagel with a grain size of 0.063–0.200 mm (silica gel) or 0.040–0.063 mm (flash silica gel). Analytical thin layer chromatography (TLC) plates “Alugram Sil G/UV₂₅₄” from Macherey-Nagel with a 0.2 mm silica gel coating and a fluorescence indicator were used. Compounds were detected by fluorescence quenching at 254 nm or self-fluorescence at 366 nm. Pure solvents (p.a. or technical grade) were used as eluents. Preparative thin layer chromatography was performed with PLC silica gel 60, F₂₅₄, 2 mm sheets on glass from Merck.

Microwave-assisted Synthesis

Microwave-assisted reactions were performed in a microwave oven (CEM GmbH, Kamp-Lintfort, Germany, model: Discover). The microwave was equipped with a pressure and temperature sensor and the reaction vessels could hold a pressure of up to 12 bars.

Size-Exclusion Chromatography

Preparative size-exclusion chromatography (SEC) was performed on SEC facility from Shimadzu, pump series LC20AD, a SPD20A UV-detector ($\lambda = 320$ nm) with JAIGEL 2.5H columns and chloroform as eluting solvent at 298 K.

High-Performance Liquid Chromatography

Preparative high-performance liquid chromatography (HPLC) was performed on a HPLC facility from Shimadzu, pump series LC20AD, with a photo detector series SPD20A (wavelength of 320 nm) using a column from Nacalai Tesque (Cosmosil 5PBB, ID: 10 x 250 mm).

7.2. Analytical Methods

NMR Spectroscopy

^1H NMR and ^{13}C NMR measurements were executed in different deuterated solvents and at different temperatures on Bruker AVANCE 300 or Bruker AVANCE III 500 or AVANCE III 700 spectrometers with a 5 mm QXI probe endowed with a z-gradient. The experiments were conducted between 298 K and 393 K, regulated by a standard ^1H methanol (low temperature) and glycol (high temperature) NMR sample. As an internal standard the deuterated solvent was used: for CHDCl_2 $\delta(^1\text{H}) = 5.32$ ppm, CD_2Cl_2 $\delta(^{13}\text{C}) = 54.00$ ppm; for CHCl_3 $\delta(^1\text{H}) = 7.24$ ppm, CDCl_3 $\delta(^{13}\text{C}) = 77.23$ ppm; for $\text{THF-d}_7\text{H}$ $\delta(^1\text{H}) = 3.58$ ppm, THF-d_8 $\delta(^{13}\text{C}) = 67.57$ ppm; for C_2DHCl_4 $\delta(^1\text{H}) = 5.91$ ppm, $\text{C}_2\text{D}_2\text{Cl}_4$ $\delta(^{13}\text{C}) = 74.20$ ppm.

Melting Points

Melting points were determined on a Büchi hot stage apparatus (B-545) and are uncorrected.

Mass Spectrometry

Field desorption (FD) mass spectra were obtained, using a VG Instruments ZAB 2 SE-FPD. MALDI-TOF mass spectra were recorded on a Bruker Reflex II-TOF spectrometer using trans-2-[3-(4-tert-butylphenyl)-2-methyl-2-propenyldiene]-malononitrile (DCTB; Aldrich,

>99 %) as matrix. High resolution (HR) MALDI-TOF mass spectrometry measurements were performed on a Solarix ESI/MALDI-ICR (9.4T) system (Bruker Daltonics, Germany), with a SmartBeam laser II. The system was internally calibrated in positive mode using sodium trifluoroacetate (Fluka, >99 %) or sodium perfluoroheptanoate (Fluka, >99 %) on quadratic calibration mode. A total of 10-400 shots were accumulated for each mass spectrum. The results were calculated using Data Analysis software (Bruker Daltonics, Germany). HR-ESI mass spectra were measured on a QToF Ultima 3 Fa. Micromass/Waters. Ion mobility measurements and tandem mass spectrometry were performed on a SYNAPT G2 Si instrument (Waters Corp., Manchester, UK) with matrix-assisted laser desorption/ionization (MALDI) source.

Elemental Analysis

Elemental analysis was performed on a Foss Heraeus-Vario EL as service measurement at the Institute for Organic Chemistry, Johannes-Gutenberg University Mainz. The samples were dried under high vacuum to remove humidity and solvent residues. However, some samples show a higher variance than 0.40 %, which is a known phenomenon for the analysis of aromatic hydrocarbons due to the entrapment of solvent molecules and atmospheric gases.^[187]

Single Crystal X-Ray Analysis

Single crystal X-ray analysis was done by [REDACTED], using a Nonius-KCCD diffractometer. The structures were solved by direct methods and refined by full-matrix least-squares techniques.

UV-Vis Spectroscopy

Solution UV-Vis absorption spectra were recorded at 298 K on a Perkin-Elmer Lambda 900 spectrophotometer.

Emission Spectroscopy

Solution emission spectra were recorded at 298 K on a J&M TIDAS spectrofluorometer, using Quartz cuvettes from Hellma with 1 cm thickness.

Infrared Spectroscopy

FT-IR measurements were performed on a Nicolet 730 FT-IR spectrometer with an ATR crystal.

Analytical High-Performance Liquid Chromatography

High-performance liquid chromatography (HPLC) was performed on a HPLC facility from Agilent, pump series 1100, with a photo detector series 1200 (wavelength of 380 nm) using a column from Macherey-Nagel (MN HD18 125/4 mm; 5 μm grain-size).

Electrochemical Measurements

All electrochemical measurements were carried out in a conventional three-electrode cell, using a Wave Driver 20 bipotentiostat (Pine Instrument Company, USA) controlled at room temperature. An Ag/AgCl (4 M KCl) and a platinum wire were used as reference and counter electrodes, respectively. All potentials in this study refer to that of the Ag/AgCl electrode. A RRDE electrode with a Pt ring (6.25 mm inner-diameter and 7.92 mm outer-diameter) and a glassy carbon disk (5.61 mm diameter) served as the substrate for the working electrode for evaluating the ORR activity and selectivity of various catalysts. Prior to use, the glassy carbon electrode was polished using aqueous alumina suspensions on felt polishing pads.

For preparing the catalyst ink, 1.0 mg of $[\text{MN}_4]$ -complex was first dissolved in DCM to get a clear solution, and then 4.0 mg carbon black (Ketjenblack EC300J) was added to obtain a 20 wt% $[\text{MN}_4]$ mixture. This mixture was first ultrasonicated for 30 min and stirred overnight to dry at room temperature. Finally, the catalyst ink was obtained by blending the dried powder with a 50 μL Nafion solution (0.5 wt%) and 950 μL ethanol in an ultrasonic bath. 9.9 μL of the catalyst ink was then pipetted onto the GC surface, leading to a catalyst loading of 0.2 $\text{mg}\cdot\text{cm}^{-2}$. For comparison, a commercially available catalyst of 20 wt% Pt supported on carbon black (BASF) was used and 5 $\text{mg}\cdot\text{mL}^{-1}$ Pt/C suspension was also prepared with the same procedure as mentioned above. 4.95 μL of the catalyst ink was then pipetted onto the GC surface, leading to a Pt loading of 20 $\mu\text{g}\cdot\text{cm}^{-2}$.

The four-electron selectivity of catalysts was evaluated based on the H_2O_2 yield, calculated from the following equation:

$$H_2O_2(\%) = 200 \times \frac{I_R / N}{(I_R / N) + I_D}$$

The electron transfer number can be calculated from the following equation:

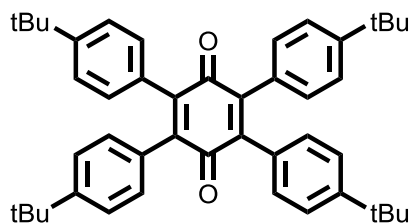
$$n = 4 \times \frac{I_D}{(I_R / N) + I_D}$$

Here, I_D and I_R are the disk and ring currents, respectively, and $N = 0.37$ is the ring collection efficiency.

7.3. Synthesis

7.3.1. *Cyclo-hexa-peri-hexabenzocoronenes*

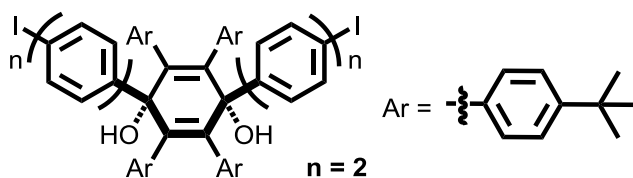
2,3,5,6-Tetrakis(4-*tert*-butylphenyl)cyclohexa-2,5-diene-1,4-dione (**3-1**)



3-1

2,3,5,6-Tetrakis(4-*tert*-butylphenyl)cyclohexa-2,5-diene-1,4-dione (**3-1**) was synthesized according to literature.^[145]

1,4-Bis(4'-iodobiphenyl)-1,4-dihydroxy-2,3,5,6-tetrakis(4''-*tert*-butylphenyl)cyclohexa-2,5-dienes (**3-2** – *cis*-isomer)



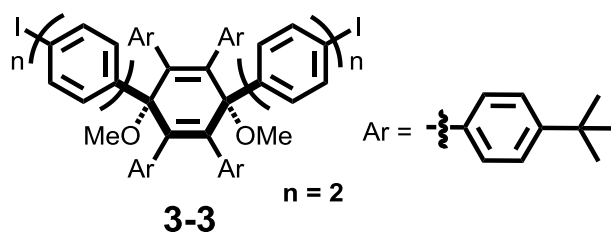
3-2 (syn)

4,4'-Diiodobiphenyl (3.82 g; 9.42 mmol) was dissolved in 200 ml anhydrous THF. The solution was cooled to -78 °C. A *n*-BuLi solution (1.6M, 6.48 ml, 10.3 mmol) was added dropwise. The reaction mixture was stirred at -78 °C for one hour. A THF solution of **3-1** (1.0 g, 1.57 mmol) was added by a syringe. The mixture was slowly warmed to RT and was stirred under an argon atmosphere overnight. Then water was added to quench the reaction. After aqueous work up with CH_2Cl_2 the solvent was evaporated ($T < 40$ °C; due to the decomposition of products at high temperature and under acidic conditions). The resulting raw product

was purified by flash column chromatography on silica (*n*-hexane/CH₂Cl₂ = 1/2 to pure CH₂Cl₂) to afford **3-2** (0.75 g, 0.63 mmol, 40 %) as a colorless solid.

Mp: >60 °C (decomposition); ¹H NMR (300 MHz, THF-d₈) δ 7.76 (d, J = 8.4 Hz, 4H), 7.63 (d, J = 8.4 Hz, 4H), 7.52 (d, J = 8.4 Hz, 4H), 7.44 (d, J = 8.4 Hz, 4H), 6.80 (d, J = 8.4 Hz, 8H), 6.72 (d, J = 8.4 Hz, 8H), 4.50 (s, 2H), 1.06 (s, 36H) ppm; ¹³C NMR (75 MHz, THF-d₈) δ 148.65, 144.84, 142.38, 141.40, 138.83, 138.70, 137.09, 132.76, 129.61, 126.15, 123.69, 93.39, 75.92, 34.84, 31.71 ppm; HR-MS (MALDI) *m/z* calcd for C₇₀H₇₀I₂O₂ [M⁺]: 1196.3460, found 1196.3457.

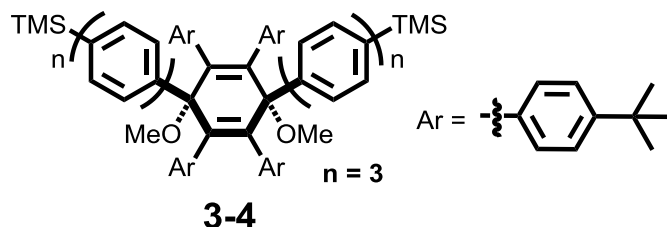
1,4-Bis(4'-iodobiphenyl)-1,4-dimethoxy-2,3,5,6-tetrakis(4''-*tert*-butylphenyl)cyclohexa-2,5-dienes (3-3)



Sodium hydride (60 % in mineral oil) (140.32 mg, 3.51 mmol) was suspended in anhydrous THF (50 ml). The suspension was cooled to -78 °C. 50 ml of a THF solution of **3-2** (0.7 g, 0.58 mmol) was added to the suspension by a syringe. The mixture was stirred at -78 °C for one hour. Iodomethane (0.66 g, 0.29 ml, 4.68 mmol) was added and the mixture was stirred under an argon atmosphere at RT overnight. After aqueous work up with CH₂Cl₂, the organic layers were dried over MgSO₄. Purification by flash column chromatography (*n*-hexane/CH₂Cl₂ = 2/1) afforded **3-3** (0.67 g, 0.55 mmol, 94 %) as a colorless powder.

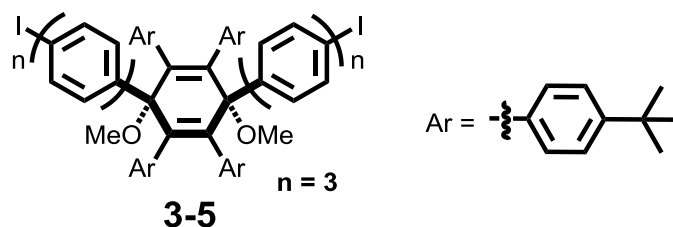
Mp: 225-230 °C; ^1H NMR (300 MHz, CD_2Cl_2) δ 7.78 (d, $J = 8.4$ Hz, 4H), 7.72-7.41 (b, 8H), 7.4 (d, $J = 8.4$ Hz, 4H), 6.85 (d, $J = 8.5$ Hz, 8H), 6.65 (d, $J = 8.5$ Hz, 8H), 3.92 (s, 6H), 1.09 (s, 36H) ppm; ^{13}C NMR (75 MHz, CD_2Cl_2) δ 149.58, 143.38, 143.28, 140.71, 138.68, 138.45, 136.47, 131.55, 129.32, 129.16, 126.22, 124.03, 93.36, 82.02, 52.97, 34.61, 31.44 ppm; HR-MS (ESI) m/z calcd for $\text{C}_{72}\text{H}_{74}\text{I}_2\text{O}_2$ [$\text{M}+\text{Na}^+$]: 1247.3676, found 1247.3680; Anal. Calcd. for $\text{C}_{72}\text{H}_{74}\text{I}_2\text{O}_2$: C 70.58 %, H 6.09 %. Found: C 70.88 %, H 5.79 %.

1,4-Bis(4'-trimethylsilylterphenyl)-1,4-dimethoxy-2,3,5,6-tetrakis(4''-tert-butylphenyl)cyclohexa-2,5-dienes (3-4)



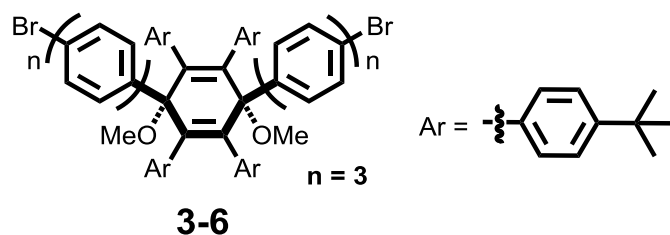
Compound **3-3** (0.6 g, 0.49 mmol), tetrakis(triphenylphosphine)palladium(0) (0.057 g, 0.05 mmol), 4-trimethylsilylphenylboronic acid pinacol ester (0.406 g, 1.47 mmol) and *Aliquat* 336 (1 drop) were mixed inside a flame dried Schlenk flask. A degassed mixture of toluene (15 ml) and a Cs_2CO_3 -solution (3 M, 5 ml) were added to the reaction mixture. After 16 h of heating, the mixture was cooled to ambient temperature. The organic layer was separated, washed with brine and dried over anhydrous MgSO_4 . Purification by column chromatography (n -hexane/ $\text{CH}_2\text{Cl}_2 = 2/1$) afforded **3-4** (0.4 g, 0.32 mmol, 64 %) as a colorless powder.

Mp: 340-345 °C; ^1H NMR (300 MHz, CD_2Cl_2) δ 7.52-7.83 (m, 24H), 6.87 (d, $J = 8.4$ Hz, 8H), 6.68 (d, $J = 8.4$ Hz, 8H), 3.94 (s, 6H), 1.1 (s, 36H), 0.31 (s, 18H) ppm; ^{13}C NMR (75 MHz, CD_2Cl_2) δ 149.51, 143.28, 142.94, 141.38, 140.42, 140.09, 139.23, 136.54, 134.47, 131.57, 127.92, 127.75, 126.7, 126.3, 124.01, 82.03, 53.0, 34.6, 31.42, 0.08 ppm; HR-MS (MALDI) m/z calcd for $\text{C}_{90}\text{H}_{100}\text{O}_2\text{Si}_2$ [M]: 1268.7256, found 1268.7261; Anal. Calcd. for $\text{C}_{90}\text{H}_{100}\text{O}_2\text{Si}_2$: C 85.12%, H 7.94 %. Found: C 85.23 %, H 9.14 %.

1,4-Bis(4'-iodoterphenyl)-1,4-dimethoxy-2,3,5,6-tetrakis(4''-tert-butylphenyl)cyclohexa-2,5-dienes (3-5)

Compound **3-4** (0.4 g, 0.315 mmol) and silver tetrafluoroborate (0.49 g, 2.52 mmol) were dissolved in anhydrous THF (15 ml). The mixture was cooled to 0 °C and iodine monochloride (1 M solution in DCM) (2.52 ml, 2.52 mmol) was added drop by drop. The reaction was quenched with sodium thiosulfate (aq., sat.) after 40 minutes. The mixture was extracted with CH₂Cl₂. The organic layers were washed with brine and dried over MgSO₄. Purification by column chromatography (*n*-hexane/CH₂Cl₂ = 2/1) afforded **3-5** (0.346 g, 0.251 mmol, 80 %) as a colorless powder.

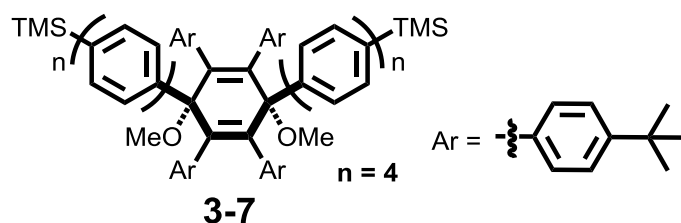
Mp: 227-235 °C; ¹H NMR (300 MHz, CD₂Cl₂) δ 7.41-7.83 (m, 20H), 7.42 (d, J = 8.3 Hz, 4H), 6.87 (d, J = 8.3 Hz, 8H), 6.68 (d, J = 8.3 Hz, 8H), 3.94 (s, 6H), 1.1 (s, 36H) ppm; ¹³C NMR (75 MHz, CD₂Cl₂) δ 149.52, 143.27, 143.08, 140.67, 140.46, 138.49, 136.51, 131.55, 129.33, 129.11, 127.86, 127.71, 126.3, 124.01, 116.48, 100.57, 93.46, 82.01, 53.0, 34.59, 31.41 ppm; HR-MS (MALDI) *m/z* calcd for C₈₄H₈₂I₂O₂ [M⁺]: 1376.4399, found 1376.4398. Anal. Calcd. for C₈₄H₈₂I₂O₂: C 73.25 %, H 6.00 %. Found: C 73.45 %, H 6.23 %.

1,4-Bis(4'-bromoterphenyl)-1,4-dimethoxy-2,3,5,6-tetrakis(4''-tert-butylphenyl)cyclohexa-2,5-dienes (3-6)

Compound **3-4** (0.5 g, 0.394 mmol), silver tetrafluoroborate (268 mg, 1.38 mmol) and sodium acetate (129 mg, 1.57 mmol) were dissolved in anhydrous THF (15 ml). The mixture was cooled to 0 °C and bromine (0.07 ml, 1.38 mmol) was added drop by drop. The reaction was quenched with a sodium sulfite solution (aq., sat.) after 20 min. The mixture was extracted with CH₂Cl₂. The organic layers were washed with brine and dried over MgSO₄. The solid was washed with methanol to afford **3-6** (465 mg, 0.362 mmol, 90 %) as a colorless powder.

Mp: 313-320 °C; ¹H NMR (700 MHz, CD₂Cl₂) δ 7.74 (d, J = 8.7 Hz, 4H), 7.68 (d, J = 8.7 Hz, 4H), 7.58 (m, 16H), 6.87 (d, J = 8.3 Hz, 8H), 6.69 (d, J = 8.3 Hz, 8H), 3.95 (s, 6H), 1.11 (s, 36H) ppm; ¹³C-NMR (176 MHz, CD₂Cl₂): δ 149.52, 143.26, 143.07, 140.40, 140.11, 139.22, 139.06, 136.51, 132.45, 131.55, 129.11, 127.85, 127.77, 126.30, 124.01, 122.03, 82.01, 71.09, 52.96, 34.59, 31.41 ppm; HR-MS (MALDI) *m/z* calcd. for C₈₄H₈₂Br₂O₂ [M⁺] 1280.4676, found 1280.4680.

1,4-Bis(4'-trimethylsilylquaterphenyl)-1,4-dimethoxy-2,3,5,6-tetrakis(4''-tert-butylphenyl)cyclohexa-2,5-dienes (3-7)

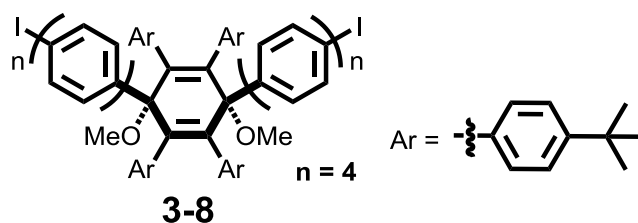


Compound **3-6** (0.5 g, 0.39 mmol), palladium(II) acetate (52.7 mg, 0.234 mmol), 2-dicyclohexylphosphino-2',6'-dimethoxybiphenyl (192 mg, 0.468 mmol), 4-trimethylsilylbenzeneboronic acid pinacol ester (0.646 g, 2.34 mmol) and potassium phosphate (165 mg, 0.78 mmol) were mixed inside a flame dried Schlenk flask. A degassed mixture of toluene (10 ml) and water (1 ml) were added to the reaction mixture. After stirring at 90 °C overnight, the mixture was cooled to ambient temperature. The organic layer was separated, washed with brine and dried over anhydrous MgSO₄. Purification by flash column chromatography on

silica (*n*-hexanes/CH₂Cl₂ = 2/1) afforded **3-7** (322 mg, 0.226 mmol, 58 %) as a colorless solid.

Mp: 343-350 °C; ¹H NMR (300 MHz, CD₂Cl₂) δ 7.79-7.75 (m, 16H), 7.73-7.57 (m, 16H), 6.88 (d, J = 8.5 Hz, 8H), 6.71 (d, J = 8.5 Hz, 8H), 3.95 (s, 6H), 1.11 (s, 36H), 0.31 (s, 18H) ppm; ¹³C-NMR (75 MHz, CD₂Cl₂): δ 149.51, 143.28, 142.97, 141.36, 140.58, 140.11, 140.07, 139.91, 139.20, 136.54, 134.48, 131.57, 129.11, 128.00, 127.81, 126.73, 126.29, 124.02, 82.03, 52.97, 34.60, 31.43, -0.88 ppm; HR-MS (MALDI) *m/z* calcd. for C₁₀₂H₁₀₈O₂Si₂ [M⁺] 1420.7882, found 1420.7886.

1,4-Bis(4'-iodoquaterphenyl)-1,4-dimethoxy-2,3,5,6-tetrakis(4''-tert-butylphenyl)cyclohexa-2,5-dienes (3-8)

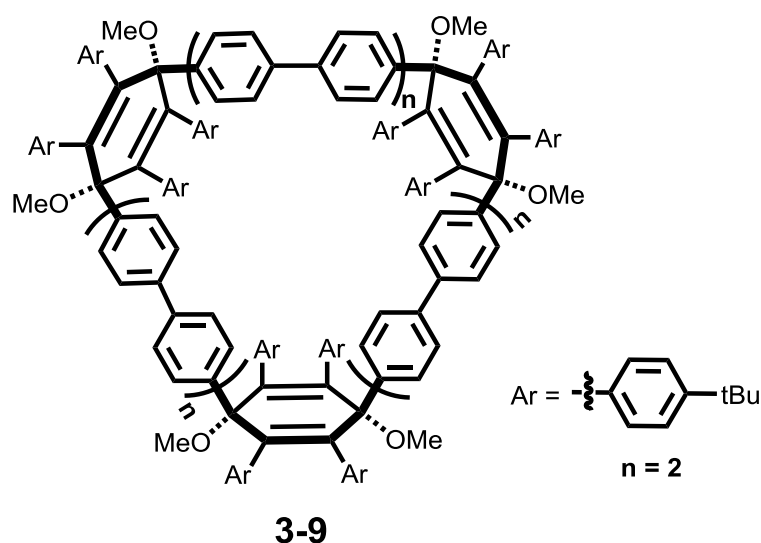


Compound **3-7** (250 mg, 0.176 mmol) and silver tetrafluoroborate (274 mg, 1.41 mmol) were dissolved in anhydrous THF (15 ml) and anhydrous methanol (2 ml). The mixture was cooled to 0 °C and iodine monochloride (1 M solution in DCM) (1.41 ml, 1.41 mmol) was added drop by drop. The reaction was quenched with sodium thiosulfate solution (aq., sat.) after 40 min. The mixture was extracted with CH₂Cl₂. The organic layers were washed with brine and dried over magnesium sulfate. Purification by flash column chromatography on silica (*n*-hexane/CH₂Cl₂ = 2/1) afforded **3-8** (190 mg, 0.124 mmol, 70 %) as a colorless solid.

Mp: 347-355 °C; ¹H NMR (500 MHz, 373 K, CD₂Cl₂) δ 7.75 (d, J = 8.4 Hz, 4H), 7.67 (m, 16H), 7.60 (d, J = 8.4 Hz, 4H), 7.50 (d, J = 8.4 Hz, 4H), 7.34 (d, J = 8.4 Hz, 4H), 6.78 (d, J = 8.5 Hz, 8H), 6.66 (d, J = 8.5 Hz, 8H), 3.89 (s, 6H), 1.07 (s, 36H) ppm; ¹³C-NMR (126 MHz, 373 K, CD₂Cl₂): δ 148.57, 142.65, 142.58, 140.11, 139.96, 139.87, 139.07, 138.73, 138.16, 137.82, 135.77, 131.03, 128.59, 127.23, 127.09, 127.03, 125.27, 122.99, 120.21, 92.75, 81.61,

52.08, 33.81, 30.95 ppm; HR-MS (MALDI) m/z calcd. for $C_{96}H_{90}I_2O_2$ $[M^+]$ 1528.5025, found 1528.5019; Anal. Calcd. for $C_{96}H_{90}I_2O_2$: C 75.38 %, H 5.93 %. Found: C 74.75 %, H 6.37 %.

Synthesis of *Cyclo*-1,4-bis(biphenyl)-1,4-dimethoxy-2,3,5,6-tetrakis(4''-*tert*-butylphenyl)cyclohexa-2,5-diene-trimer (3-9)

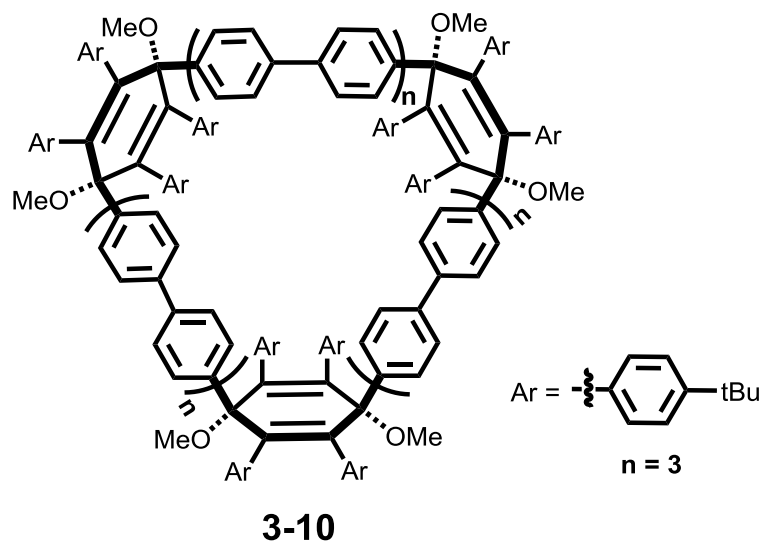


Bis(cyclooctadiene)nickel(0) (0.202 g, 0.74 mmol), 2,2'-bipyridine (0.114 g, 0.74 mmol) and 1,5-cyclooctadiene (0.08 g, 0.74 mmol) were dissolved in toluene (10 ml) and DMF (5 ml). The catalyst mixture was activated at 80 °C for one hour in the absence of light. Compound **3-3** (0.300 g, 0.24 mmol) was dissolved in anhydrous THF (20 ml) and was added to the catalyst solution by syringe. The reaction mixture was stirred at 80 °C under an argon atmosphere overnight. After cooling to RT the reaction was quenched with 2 M hydrochloric acid and the mixture was extracted with CH_2Cl_2 . The organic layers were washed with brine and dried over $MgSO_4$. Purification by flash column chromatography on silica (n -hexane/ CH_2Cl_2 = 2/1) afforded **3-9** (0.11 g, 0.038 mmol, 40 %) as a colorless powder.

Mp: >300 °C; 1H NMR (300 MHz, CD_2Cl_2) δ 7.83-7.51 (br, 48H), 6.91 (d, J = 8.5 Hz, 24H), 6.74 (d, J = 8.5 Hz, 24H), 3.95 (s, 18H), 1.13 (s, 108H) ppm; ^{13}C NMR (75 MHz, CD_2Cl_2) δ 149.57, 143.28, 142.95, 139.97, 139.78, 139.07, 136.52, 131.61, 129.19, 127.81, 127.73,

126.18, 124.05, 82.23, 52.91, 34.61, 31.48 ppm; HR-MS (MALDI) m/z calcd for $C_{216}H_{222}O_6$ $[M+K^+]$: 2950.6698, found 2950.6619.

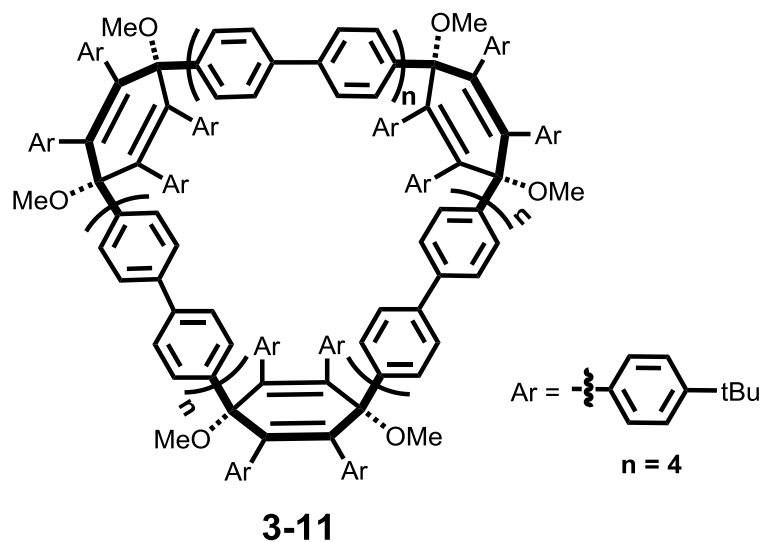
Synthesis of *Cyclo-1,4-bis(terphenyl)-1,4-dimethoxy-2,3,5,6-tetrakis(4''-tert-butylphenyl)cyclohexa-2,5-diene-trimer (3-10)*



The same procedure as for the synthesis of **3-9** was applied, affording **3-10** with 30 % yield.

Mp: >300 °C; 1H NMR (300 MHz, CD_2Cl_2) δ 7.82 (d, $J = 5.2$ Hz, 48H), 7.74-7.51 (br, 24H), 6.90 (d, $J = 8.5$ Hz, 24H), 6.73 (d, $J = 8.5$ Hz, 24H), 3.95 (s, 18H), 1.13 (s, 108H) ppm; ^{13}C NMR (75 MHz, CD_2Cl_2) δ 149.56, 143.29, 142.97, 140.07, 140.03, 139.86, 139.17, 136.54, 131.83, 131.61, 129.15, 127.87, 127.81, 127.78, 126.25, 124.05, 100.58, 82.17, 52.94, 34.62, 31.44 ppm; HR-MS (MALDI) m/z calcd for $C_{252}H_{246}O_6$ $[M^+]$: 3367.8939, found 3367.8900.

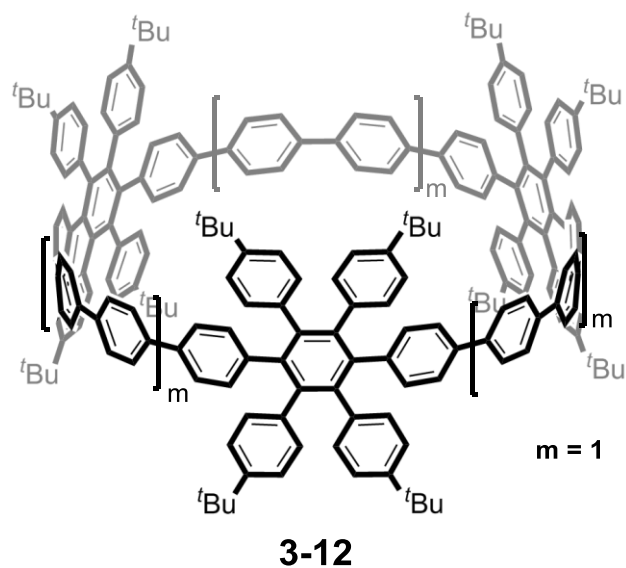
Synthesis of *Cyclo*-1,4-bis(quarterphenyl)-1,4-dimethoxy-2,3,5,6-tetrakis(4''-*tert*-butylphenyl)cyclohexa-2,5-diene-trimer (3-11)



The same procedure as for the synthesis of **3-9** was applied, affording **3-11**. The mixture of cycles was directly aromatized and the purification was done in the next step. Due to the poor solubility, a standard purification of this compound failed. The purification was performed in the next step after aromatization. The successful cyclization was monitored by HR-MS.

HR-MS (MALDI) m/z calcd. for $C_{288}H_{270}O_6$ [M^+] 3824.0817, found 3824.0876.

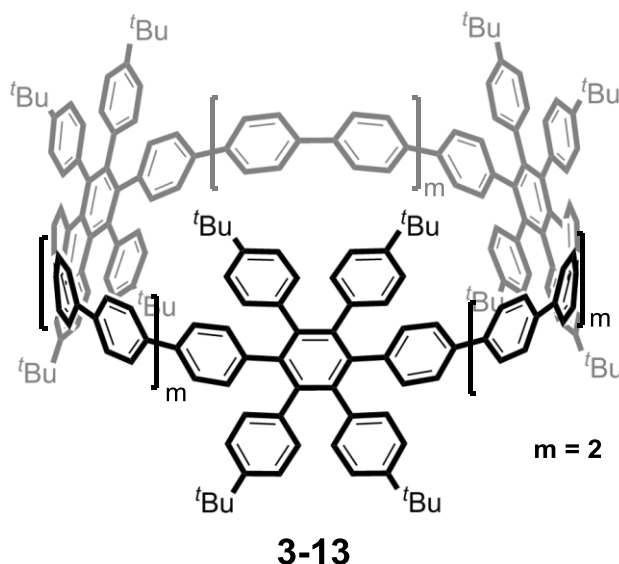
Phenylene Extended [3]CHPB (3-12)



Compound **3-9** (0.158 g, 0.054 mmol) was dissolved in anhydrous THF (10 ml). The solution was cooled to $-78\text{ }^{\circ}\text{C}$ and a 1 M solution of sodium naphthalenide in THF (6.5 ml, 6.5 mmol) was added dropwise. The mixture was quenched with iodine and sodium thiosulfate after one hour of stirring. The reaction mixture was extracted with CH_2Cl_2 , washed with brine and dried over MgSO_4 . Purification by flash column chromatography on silica (*n*-hexane/ $\text{CH}_2\text{Cl}_2 = 2/1$) and gel permeation chromatography (eluent: chloroform) afforded **3-12** (0.053 g, 0.019 mmol, 36 %) as a colorless solid.

Mp: $>300\text{ }^{\circ}\text{C}$; ^1H NMR (300 MHz, CD_2Cl_2) δ 7.53 (d, $J = 8.5\text{ Hz}$, 12H), 7.33 (d, $J = 8.5\text{ Hz}$, 12H), 7.05 (d, $J = 8.4\text{ Hz}$, 12H), 6.95 (d, $J = 8.4\text{ Hz}$, 12H), 6.82 (d, $J = 8.5\text{ Hz}$, 24H), 6.74 (d, $J = 8.5\text{ Hz}$, 24H), 1.04 (s, 108H) ppm; ^{13}C NMR (75 MHz, CD_2Cl_2) δ 148.54, 140.98, 140.76, 140.54, 140.36, 139.08, 138.40, 138.27, 132.87, 131.30, 128.06, 127.52, 125.86, 123.74, 34.51, 31.51 ppm; HR-MS (MALDI) m/z calcd for $\text{C}_{210}\text{H}_{204} [\text{M}^+]$: 2725.5932, found 2725.5958.

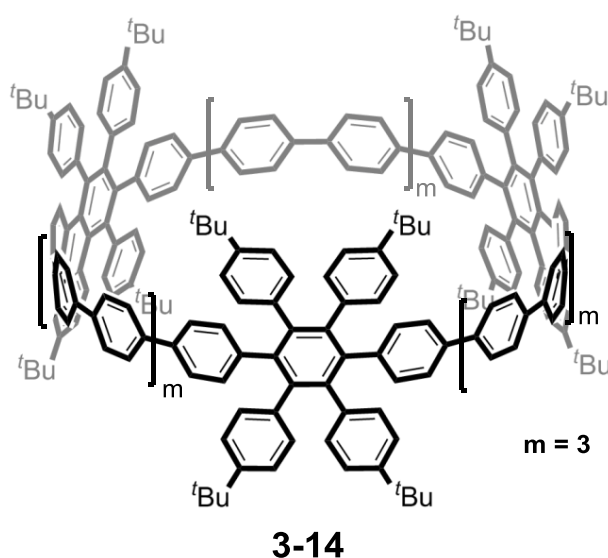
Phenylene Extended [3]CHPB (**3-13**)



The same procedure as for the synthesis of **3-12** was applied, affording **3-13** with 30 % yield.

Mp: >300 °C; ^1H NMR (300 MHz, CD_2Cl_2) δ 7.71 (dd, $J_1 = J_2 = 8.5$ Hz, 24H), 7.62 (d, $J = 8.5$ Hz, 12H), 7.45 (d, $J = 8.5$ Hz, 12H), 7.12 (d, $J = 8.5$ Hz, 12H), 6.95 (d, $J = 8.5$ Hz, 12H), 6.84 (d, $J = 8.5$ Hz, 24H), 6.75 (d, $J = 8.5$ Hz, 24H), 1.01 (s, 108H) ppm; ^{13}C NMR (176 MHz, CD_2Cl_2) δ 148.52, 140.95, 140.74, 140.51, 140.33, 139.07, 138.37, 138.25, 136.85, 132.85, 131.72, 131.28, 128.05, 127.51, 125.97, 125.84, 124.18, 123.73, 34.49, 31.48 ppm; HR-MS (MALDI) m/z calcd for $\text{C}_{246}\text{H}_{228} [\text{M}^+]$: 3181.7836, found 3181.7762.

Phenylene Extended [3]CHPB (3-14)



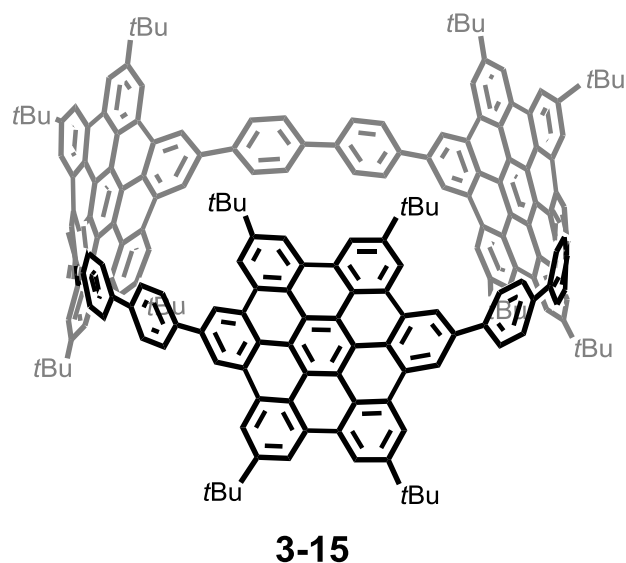
The same procedure as for the synthesis of **3-12** was applied, affording **3-14** with 8 % yield.

Mp: >300 °C; ^1H NMR (500 MHz, 373 K, $\text{C}_2\text{D}_2\text{Cl}_4$) δ 7.68-7.62 (m, 48H), 7.54 (d, $J = 8.5$ Hz, 12H), 7.38 (d, $J = 8.5$ Hz, 12H), 7.04 (d, $J = 8.5$ Hz, 12H), 6.91 (d, $J = 8.5$ Hz, 12H), 6.78 (d, $J = 8.2$ Hz, 24H), 6.70 (d, $J = 8.2$ Hz, 24H), 1.05 (s, 108H) ppm; ^{13}C NMR (176 MHz, CD_2Cl_2): δ 148.58, 141.13, 141.05, 140.96, 140.08, 138.47, 138.37, 132.72, 132.62, 131.61, 131.46, 127.87, 127.63, 125.71, 123.87, 100.57, 71.38, 34.54, 31.40 ppm; HR-MS (MALDI) m/z calcd. for $\text{C}_{282}\text{H}_{252} [\text{M}+\text{H}^+]$ 3638.9792, found 3638.9789;

General procedure for the cyclodehydrogenation towards the phenylene extended [3]CHBCs (3-15 to 3-17)

The phenylene extended [3]CHPBs **3-12** or **3-13** or **3-14** (0.01 g, 0.0034 mmol) were dissolved in anhydrous and unstabilized CH_2Cl_2 (10 ml). A mixture of FeCl_3 (0.073 g, 0.452 mmol) in nitromethane (2 ml) was slowly added at RT. The mixture was stirred at RT for seven hours, purging the solution with a continuous stream of argon. After quenching with methanol or hydrazine, the mixture was extracted with CH_2Cl_2 . The organic layers were separated, washed with brine and dried over MgSO_4 . The raw product was purified by flash column chromatography on silica (CH_2Cl_2). The product was further purified and separated by HPLC (toluene/methanol = 3/1 to 9/1). The cyclodehydrogenated products were analyzed by HR-MS spectrometry, UV-Vis-, fluorescence- and NMR spectroscopy.

[3]CHBC (3-15'a to 3-15'd)



The four major HPLC fractions **3-15'a to 3-15'd** were separated, having an extra loss of zero to six additional hydrogen atoms.

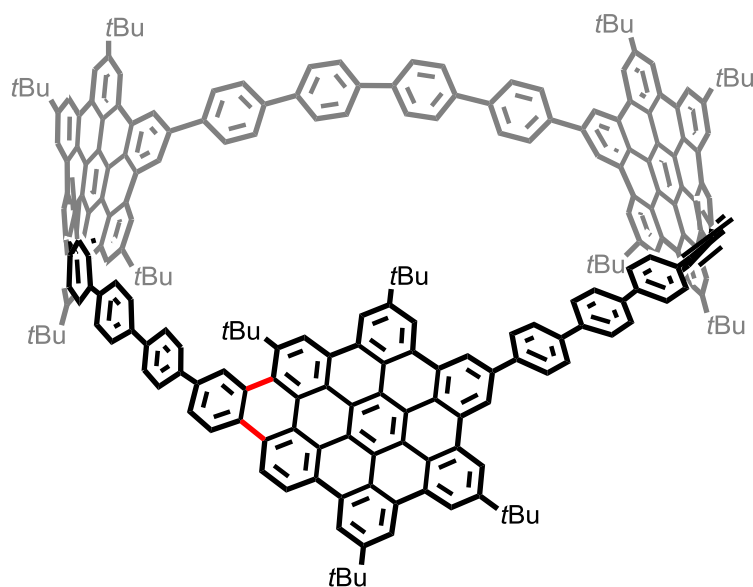
3-15'a: MS (MALDI) m/z calcd for $C_{210}H_{168}$ [M^+]: 2689.31, found 2689.45;

3-15'b: MS (MALDI) m/z calcd for $C_{210}H_{166}$ [M^+]: 2687.30, found 2687.47;

3-15'c: MS (MALDI) m/z calcd for $C_{210}H_{164}$ [M^+]: 2685.28, found 2685.35;

3-15'd: HR-MS (MALDI) m/z calcd for $C_{210}H_{162}$ [M^+]: 2683.2671, found 2683.2604;

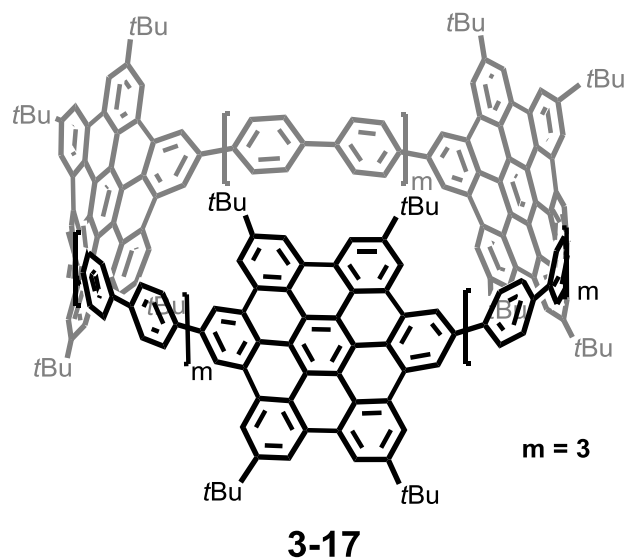
[3]CHBC (3-16')



3-16'

The purification by HPLC afforded **3-16'** (1 mg, 4.2×10^{-7} mol, 12 %).

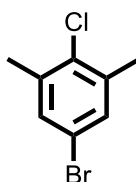
1H NMR (700 MHz, $CS_2/THF-d_8/CD_2Cl_2 = 2/1/1$) δ 9.81-9.78 (m, 3H), 9.62 (br, 1H), 9.55 (br, 1H), 9.50-9.39 (br, 9H), 9.33-9.03 (br, 24H), 8.17-8.09 (br, 8H), 8.01 (br, 4H), 7.83-7.77 (m, 8H), 7.70-7.53 (m, 16H), 7.48-7.38 (m, 8H), 2.02-1.82 (m, $tBu-H$, 108H) ppm; ^{13}C NMR (from 2D $^1H, ^{13}C$ -HSQC experiment, $CS_2/THF-d_8/CD_2Cl_2 = 2/1/1$) δ 138.4, 134.2, 133.1, 132.8, 132.1, 131.2, 131.0, 130.6, 129.8, 129.0, 128.7, 128.1, 127.1, 127.0, 124.7, 123.3, 122.4, 122.3, 121.8, 120.5, 120.3, 119.9, 119.5, 35.2, 32.2 ppm; HR-MS (MALDI) m/z calcd for $C_{246}H_{190}$ [M^+]: 3143.4862, found 3143.4757.

[3]CHBC (3-17)

$^1\text{H NMR}$ (700 MHz, CS_2) δ 9.87 (br, ~24H), 9.95 (br, ~72H), 2.56 (br, ~108H) ppm; HR-MS (MALDI) m/z calcd for $\text{C}_{282}\text{H}_{216}$ [M^+]: 3601.6897, found 3601.6853.

7.3.2. Blocked *Cyclo-hexa-peri-hexabenzocorones*

5-Bromo-2-chloro-1,3-dimethylbenzene (4-2)

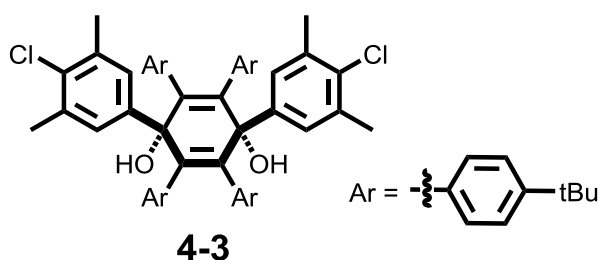


4-2

4-Bromo-2,6-dimethylaniline (5.0 g, 25.0 mmol) was dispersed in water and cooled to 0 °C. Hydrochloric acid (conc., 10 ml) was slowly added and the mixture was stirred at 0 °C for 15 min. Then an aqueous solution of sodium nitrite (3.0 g, 75.0 mmol) was added. The resulting mixture was stirred for one hour at 0 °C, before the addition of copper(I) chloride (9.9 g, 100.0 mmol). The resulting mixture was slowly warmed to 70 °C and stirred for two hours before cooling to RT. The reaction mixture was stirred at RT overnight. The raw product was extracted with CH₂Cl₂ and the organic layers were dried with MgSO₄. Purification by flash column chromatography on silica (*n*-hexane) afforded **4-2** (4.02 g; 18.3 mmol; 73 %) as a colorless liquid.

¹H NMR (300 MHz, CD₂Cl₂): δ 7.23 (s, 2H), 2.34 (s, 6H); ¹³C NMR (75 MHz, CD₂Cl₂): δ 138.83, 134.21, 131.56, 119.85, 20.87 ppm; MS (FD) *m/z* calcd. for C₈H₈BrCl [M⁺] 217.9, found 217.9.

1,4-Bis(4'-chloro-3',5'-dimethylphenyl)-1,4-dihydroxy-2,3,5,6-tetrakis(4''-tert-butylphenyl)cyclohexa-2,5-dienes (4-3, *cis*-isomer)

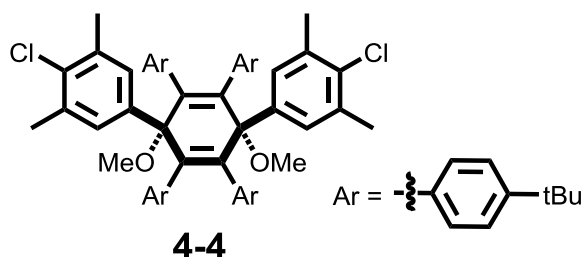


4-3

Compound **4-2** (2,5 g, 11.4 mmol) was dissolved in 20 ml anhydrous THF. The solution was cooled to $-78\text{ }^{\circ}\text{C}$. A 1.6M *n*-BuLi solution in THF (7.2 ml, 9.6 mmol) was added dropwise. The reaction mixture was stirred at $-78\text{ }^{\circ}\text{C}$ for 30 min. A THF solution of compound **3-1** (1.0 g, 1.57 mmol) was added by a syringe. The mixture was slowly warmed to ambient temperature and was stirred under an argon atmosphere overnight. Then water was added to quench the reaction. After aqueous work up with CH_2Cl_2 , the solvent was evaporated ($T < 40\text{ }^{\circ}\text{C}$ due to the decomposition at high temperatures). Purification by flash column chromatography on silica (*n*-hexane/ $\text{CH}_2\text{Cl}_2 = 1/1$ to pure CH_2Cl_2) afforded the title compound (0.87 g, 60 %) as a colorless powder.

Mp: $175\text{-}180\text{ }^{\circ}\text{C}$; ^1H NMR (300 MHz, CD_2Cl_2) δ 7.06 (s, 4H), 6.94 (d, 8H, $J = 8.4\text{ Hz}$), 6.71 (d, 8H, $J = 8.4\text{ Hz}$), 2.5 (s, 2H), 2.28 (s, 12H), 1.12 (s, 36H); ^{13}C NMR (75 MHz, CD_2Cl_2): δ 149.65, 141.20, 140.85, 135.62, 135.09, 133.77, 131.90, 128.44, 124.08, 75.46, 34.66, 31.41, 21.22 ppm; HR-MS (MALDI) m/z calcd. for $\text{C}_{62}\text{H}_{70}\text{Cl}_2\text{O}_2$ [M^+] 916.4747, found 916.4746.

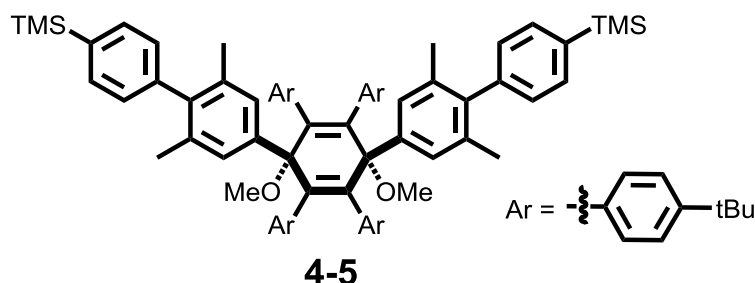
1,4-Bis(4'-chloro-3',5'-dimethylphenyl)-1,4-dimethoxy-2,3,5,6-tetrakis(4''-tert-butylphenyl)cyclohexa-2,5-dienes (4-4)



Sodium hydride (60 % in mineral oil) (79.5 mg, 2.0 mmol) was suspended in anhydrous THF (30 ml). The suspension was cooled to $-78\text{ }^{\circ}\text{C}$. Then 20 ml of a THF solution of **4-3** (0.4 g, 0.33 mmol) were added to the suspension by a syringe. The mixture was stirred at $-78\text{ }^{\circ}\text{C}$ for one hour. Iodomethane (0.38 g, 2.65 mmol) was added and the mixture was warmed to RT and stirred under an argon atmosphere overnight. After aqueous work up with CH_2Cl_2 the organic layers were dried with MgSO_4 . Purification by flash column chromatography on silica (*n*-hexane/ $\text{CH}_2\text{Cl}_2 = 2/1$) afforded **4-4** (0.259 g, 0.21 mmol, 63 %) as a colorless powder.

Mp: 204-210 °C; ^1H NMR (300 MHz, CD_2Cl_2) δ 7.21 (bs, 4H), 6.89 (d, 8 H, $J = 8.5$ Hz), 6.65 (d, 8H, $J = 8.5$ Hz), 3.84 (s, 6H), 2.27 (bs, 12H), 1.12 (s, 36H); ^{13}C NMR (75 MHz, CD_2Cl_2): δ 149.63, 142.94, 141.24, 136.35, 135.53, 133.51, 131.56, 128.87, 124.06, 81.68, 52.81, 34.64, 31.42, 21.23 ppm; HR-MS (MALDI) m/z calcd. for $\text{C}_{64}\text{H}_{74}\text{Cl}_2\text{O}_2$ [M^+] 944.5060, found 944.5052; Anal. Calcd. for $\text{C}_{64}\text{H}_{74}\text{Cl}_2\text{O}_2$: C 81.24 %, H 7.88 %. Found: C 82.06 %, H 8.84 %.

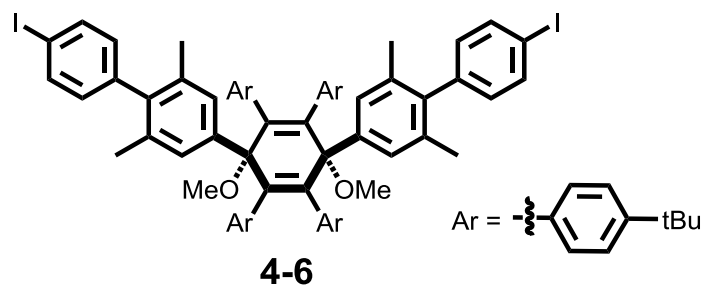
1,4-Bis(4''-trimethylsilyl-2',6'-dimethylbiphenyl)-1,4-dimethoxy-2,3,5,6-tetrakis(4''-tert-butylphenyl)cyclohexa-2,5-dienes (4-5)



Compound **4-4** (0.5 g, 0.53 mmol), palladium(II) acetate (23.7 mg, 0.106 mmol), 2-dicyclohexylphosphino-2',6'-dimethoxybiphenyl (S-Phos) (86.8 mg, 0.211 mmol), 4-trimethylsilylbenzeneboronic acid pinacol ester (0.876 g, 3.17 mmol) and potassium phosphate (224.3 mg, 1.06 mmol) were mixed inside a flame dried Schlenk flask. A degassed mixture of toluene (10 ml) and water (1 ml) were added. After sixteen hours of stirring at 90 °C, the mixture was cooled to ambient temperature. The organic layer was separated, washed with brine, and dried with anhydrous MgSO_4 . Purification by flash column chromatography on silica (n -hexane/ $\text{CH}_2\text{Cl}_2 = 2/1$) afforded **4-5** (0.4 g, 0.34 mmol, 65 %) as a colorless powder.

Mp: 197-205 °C; ^1H NMR (300 MHz, CD_2Cl_2) δ 7.58 (d, 4H, $J = 8.5$ Hz), 7.52-7.18 (b, 4H), 7.13 (d, 4H, $J = 8.5$ Hz), 6.92 (d, 8H, $J = 8.5$ Hz), 6.71 (d, 8H, $J = 8.5$ Hz), 3.92 (s, 6H), 1.92 (s, 12H), 1.14 (s, 36H), 0.3 (s, 18H); ^{13}C NMR (75 MHz, CD_2Cl_2): δ 149.34, 143.09, 142.16, 141.82, 141.03, 138.82, 136.91, 135.28, 133.84, 131.63, 129.21, 127.66, 123.91, 81.97, 52.91, 34.63, 31.47, 21.42, 0.79 ppm; HR-MS (MALDI) m/z calcd. for $\text{C}_{82}\text{H}_{100}\text{O}_2\text{Si}_2$ [M^+] 1172.7256, found 1172.7254; Anal. Calcd. for $\text{C}_{82}\text{H}_{100}\text{O}_2\text{Si}_2$: C 83.90 %, H 8.59 %. Found: C 84.97 %, H 8.89 %.

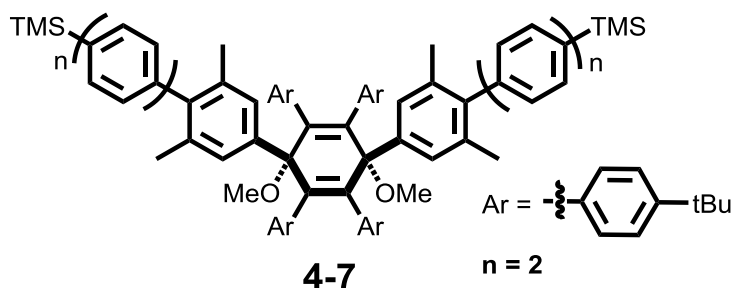
1,4-Bis(4''-iodo-2',6'-dimethylbiphenyl)-1,4-dimethoxy-2,3,5,6-tetrakis(4''-tert-butylphenyl)cyclohexa-2,5-dienes (4-6)



Compound **4-5** (2.0 g, 1.7 mmol) and silver tetrafluoroborate (1.33 g, 6.82 mmol) were dissolved in anhydrous THF (50 ml) and methanol (10 ml). The mixture was cooled to 0 °C and iodine monochloride (1 M solution in CH_2Cl_2) (6.82 ml, 6.82 mmol) was added drop by drop. The reaction was quenched with sodium thiosulfate (aq., sat.) after 40 min. The mixture was extracted with CH_2Cl_2 . The organic layers were washed with brine and dried with MgSO_4 . Purification by flash column chromatography on silica (n -hexane/ $\text{CH}_2\text{Cl}_2 = 2/1$) afforded **4-6** (1.51 g, 1.18 mmol, 70 %) as a colorless powder.

Mp: 287 °C; ^1H NMR (300 MHz, CD_2Cl_2) δ 7.76 (d, 4H, $J = 8.4$ Hz), 7.53-6.98 (b, 4H), 6.91 (d, 4H, $J = 8.4$ Hz), 6.90 (d, 8H, $J = 8.4$ Hz), 6.68 (d, 8H, $J = 8.4$ Hz), 3.91 (s, 6H), 1.92 (s, 12H), 1.13 (s, 36H); ^{13}C NMR (75 MHz, CD_2Cl_2): δ 149.39, 143.06, 142.27, 141.30, 139.81, 138.04, 136.80, 135.18, 132.08, 131.58, 127.76, 123.92, 92.54, 81.91, 52.90, 34.62, 31.44, 21.35 ppm; HR-MS (MALDI) m/z calcd. for $\text{C}_{76}\text{H}_{82}\text{I}_2\text{O}_2$ [M^+] 1280.4399, found 1280.4396; Anal. Calcd. for $\text{C}_{76}\text{H}_{82}\text{I}_2\text{O}_2$: C 71.24 %, H 6.45 %. Found: C 71.93 %, H 7.47 %.

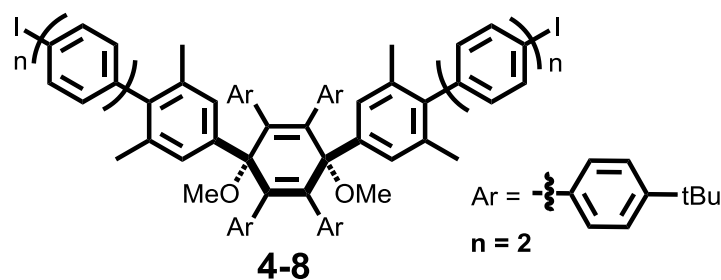
1,4-Bis(4''-trimethylsilyl-2,6-dimethylterphenyl)-1,4-dimethoxy-2,3,5,6-tetrakis(4''-tert-butylphenyl)cyclohexa-2,5-dienes (4-7)



Compound **4-6** (0.475 g, 0.37 mmol), tetrakis(triphenylphosphine)palladium(0) (90.2 mg, 0.08 mmol) 4-trimethyl-silylbenzeneboronic acid pinacol ester (0.647 g, 2.34 mmol) and silver carbonate (0.646 g, 2.34 mmol) were mixed inside a flame dried Schlenk flask. Anhydrous THF was added and the mixture was heated to 70 °C overnight. After cooling to ambient temperature, the mixture was extracted with CH₂Cl₂, the organic layers were washed with brine and dried with anhydrous MgSO₄. Purification by flash column chromatography on silica (*n*-hexane/CH₂Cl₂ = 2/1) afforded **4-7** (0.36 g, 0.27 mmol, 69 %) as a colorless powder.

Mp: 246 °C; ¹H NMR (300 MHz, CD₂Cl₂) δ 7.69-7.60 (m, 12H), 7.49-7.32 (b, 4H), 7.25-7.21 (m, 4H), 6.94 (d, 8H, J = 8.4 Hz), 6.73 (d, 8H, J = 8.4 Hz), 3.94 (s, 6H), 1.99 (s, 12H), 1.15 (s, 36H), 0.31 (s, 18H); ¹³C NMR (75 MHz, CD₂Cl₂): δ 149.35, 143.09, 141.94, 140.90, 140.65, 139.81, 139.69, 136.90, 135.42, 134.43, 131.63, 131.09, 130.43, 128.48, 127.43, 126.75, 123.93, 81.97, 52.92, 34.63, 31.46, 21.48, -0.87 ppm; HR-MS (MALDI) *m/z* calcd. for C₉₄H₁₀₈O₂Si₂ [M⁺] 1324.7882, found 1324.7878.

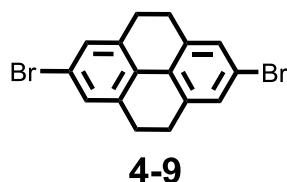
1,4-Bis(4''-iodo-2,6-dimethylterphenyl)-1,4-dimethoxy-2,3,5,6-tetrakis(4''-tert-butylphenyl)cyclohexa-2,5-dienes (4-8)



Compound **4-7** (360 mg, 0.271 mmol) and silver tetrafluoroborate (159 mg, 0.81 mmol) were dissolved in anhydrous THF (15 ml) and methanol (5 ml). The mixture was cooled to 0 °C, and iodine monochloride (1 M solution in CH₂Cl₂) (0.81 ml, 0.81 mmol) was added drop by drop. The reaction was quenched with sodium thiosulfate (aq., sat.) after 40 min. The mixture was extracted with CH₂Cl₂. The organic layers were washed with brine and dried with MgSO₄. Purification by flash column chromatography on silica (*n*-hexane/CH₂Cl₂ = 2/1) afforded **4-8** (330 mg, 0.23 mmol, 85 %) as a colorless powder.

Mp: 300-305 °C; ¹H NMR (300 MHz, CD₂Cl₂) δ 7.8 (d, 4H, J = 8.5 Hz), 7.64 (d, 4H, J = 8.5 Hz), 7.43 (d, 4H, J = 8.5 Hz), 7.34 (b, 4H), 7.23 (d, 4H, J = 8.5 Hz), 6.93 (d, 8H, J = 8.5 Hz), 6.71 (d, 8H, J = 8.5 Hz), 3.93 (s, 6H), 1.97 (s, 12H), 1.14 (s, 36H); ¹³C NMR (75 MHz, CD₂Cl₂): δ 149.37, 143.09, 142.04, 141.33, 141.00, 140.48, 138.57, 138.44, 136.87, 135.35, 131.62, 130.57, 129.39, 127.73, 127.24, 123.93, 93.30, 81.95, 52.91, 34.63, 31.46, 21.45 ppm; HR-MS (MALDI) *m/z* calcd. for C₈₈H₉₀I₂O₂ [M⁺] 1432.5025, found 1432.5029; Anal. calcd. for C₈₈H₉₀I₂O₂: C 73.73 %, H 6.33 %, found: C 74.12 %, H 6.37 %.

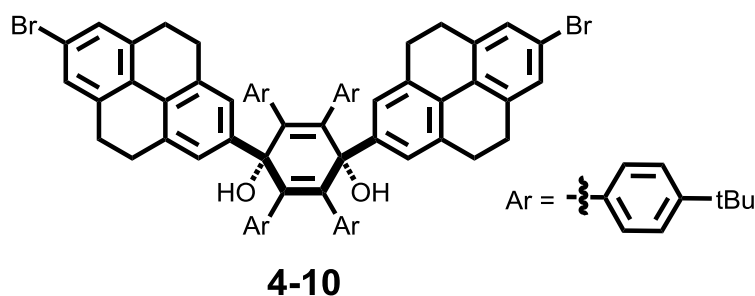
2,7-Dibromo-4,5,9,10-tetrahydropyrene (4-9)



4,5,9,10-Tetrahydropyrene (8.25 g, 40.0 mmol) was dissolved in acidic acid (250 ml). Then a mixture of bromine (12.78 g, 80.0 mmol) and NaOH (3.2 g, 80.0 mmol) in 250 ml water was added. The reaction mixture was stirred at RT overnight. The precipitate was filtered off and the aqueous layer was extracted with CH₂Cl₂, washed with sodium thiosulfate and dried with MgSO₄. The solvents were evaporated and the combined raw product was recrystallized from toluene to yield **4-9** (2.94 g, 8.1 mmol, 20 %) as colorless crystals.

^1H NMR (300 MHz, CD_2Cl_2): δ 7.23 (s, 4H), 2.84 (s, 8H) ppm; ^{13}C NMR (75 MHz, CD_2Cl_2) δ 137.94, 129.37, 126.55, 121.21, 28.39 ppm; MS (FD) m/z calcd. for $\text{C}_{16}\text{H}_{12}\text{Br}_2$ [M^+] 361.9, found 361.6.

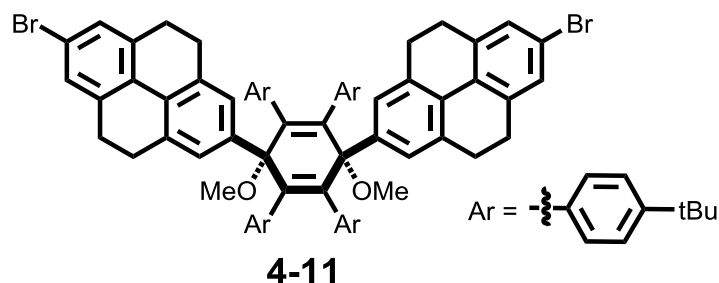
1,4-Bis(2'-bromo-4',5',9',10'-tetrahydropyrenediyl)-1,4-dihydroxy-2,3,5,6-tetrakis(4''-tert-butylphenyl)cyclohexa-2,5-dienes (4-10, *cis*-isomer)



Compound **4-9** (686 mg, 1.8 mmol, 6.0 eq.) was dissolved in 30 ml anhydrous THF. The solution was cooled to -78 °C. A 1.6 M *n*-BuLi solution in THF (1.18 ml, 1.88 mmol) was added dropwise. The reaction mixture was stirred at -78 °C for two hours. A THF solution of **3-1** (200 mg, 0.314 mmol) was added by a syringe. The mixture was slowly warmed to ambient temperature and was stirred for five hours. Then water was added to quench the reaction. After aqueous work up with CH_2Cl_2 the solvent was evaporated ($T < 40$ °C due to the decomposition at high temperatures). Precipitation in MeOH afforded the title compound (133 mg, 35 %) as a colorless powder.

Mp: 171-180 °C; ^1H NMR (300 MHz, THF-d_8) δ 7.24 (s, 4H), 7.22 (s, 4H), 6.81 (dd, 16H, $J = 8.4$ Hz), 4.4 (s, 2H), 2.83 (bt, 8H), 2.74 (bt, 8H), 1.08 (s, 36H); ^{13}C NMR (75 MHz, THF-d_8): δ 148.64, 144.61, 142.03, 138.50, 137.27, 134.54, 132.87, 130.99, 129.64, 129.01, 127.08, 123.65, 120.94, 76.01, 34.87, 31.72, 29.39, 29.17 ppm; HR-MS (ESI) m/z calcd. for $\text{C}_{78}\text{H}_{78}\text{Br}_2\text{O}_2$ [$\text{M}+\text{Na}^+$] 1227.4266, found 1227.4243.

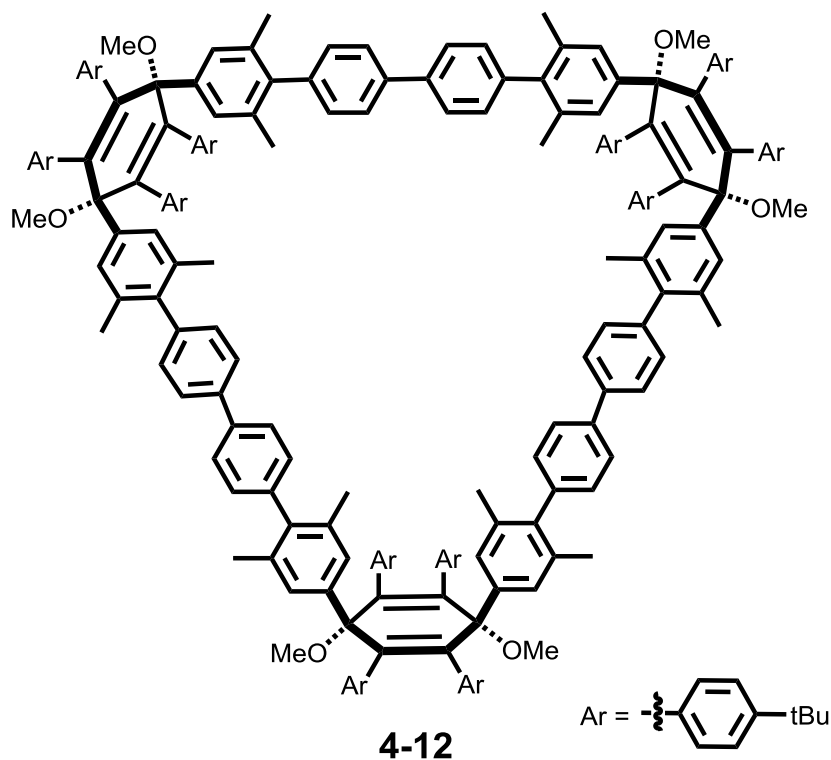
1,4-Bis(2'-bromo-4',5',9',10'-tetrahydropyrenediyl)-1,4-dimethoxy-2,3,5,6-tetrakis(4''-tert-butylphenyl)cyclohexa-2,5-dienes (4-11)



Sodium hydride (60 % in mineral oil) (140.32 mg, 3.51 mmol) was suspended in anhydrous THF (50 ml). The suspension was cooled to $-78\text{ }^{\circ}\text{C}$. 50 ml of a THF solution of **4-10** (0.7 g, 0.58 mmol) was added to the suspension by a syringe. The mixture was stirred at $-78\text{ }^{\circ}\text{C}$ for one hour. Iodomethane (0.66 g, 0.29 ml, 4.68 mmol) was added and the mixture was warmed to RT. The mixture was stirred at RT overnight. After aqueous work up with CH_2Cl_2 , the organic layers were dried over MgSO_4 . Purification by flash column chromatography on silica (*n*-hexane/ CH_2Cl_2 = 2/1) afforded **4-11** (0.67 g, 0.55 mmol, 94 %) as a colorless powder.

Mp: $303\text{-}310\text{ }^{\circ}\text{C}$; ^1H NMR (300 MHz, CD_2Cl_2): δ 7.4-6.97 (br, 8H), 7.24 (s, 4H), 6.90 (d, 8H, $J = 8.6\text{ Hz}$), 6.74 (d, 8H, $J = 8.6\text{ Hz}$), 3.88 (s, 6H), 2.82 (bs, 16H), 1.12 (s, 36H) ppm; ^{13}C NMR (75 MHz, CD_2Cl_2) δ 149.50, 142.93, 142.68, 138.12, 136.66, 136.60, 131.65, 130.32, 129.24, 128.90, 126.43, 124.01, 120.65, 82.21, 52.83, 34.62, 31.43, 28.84, 28.74 ppm; HR-MS (ESI) m/z calcd. for $\text{C}_{80}\text{H}_{82}\text{Br}_2\text{O}_2$ [$\text{M}+\text{Na}^+$] 1255.4579, found 1255.4574.

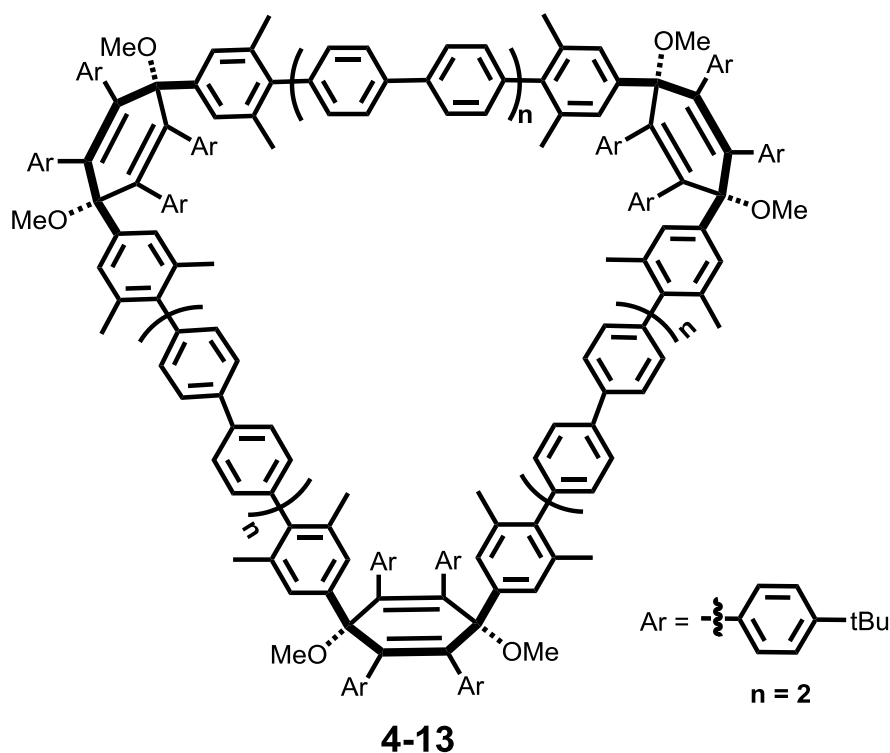
Synthesis of *Cyclo*-1,4-bis(2',6'-dimethylbiphenyl)-1,4-dimethoxy-2,3,5,6-tetrakis(4''-*tert*-butyl phenyl)cyclohexa-2,5-diene-trimer (4-12)



Bis(cyclooctadiene)nickel(0) (0.376 g, 1.37 mmol), 2,2'-bipyridine (0.213 g, 1.37 mmol) and cyclooctadiene (0.170 ml, 1.37 mmol) were dissolved in toluene (15 ml) and DMF (10 ml). The catalyst mixture was activated at 80 °C for one hour in the absence of light. Compound **4-6** (0.500 g, 0.39 mmol) was dissolved in THF (20 ml) and added to the catalyst solution by syringe. The reaction mixture was stirred under an argon atmosphere at 80 °C overnight. After cooling to ambient temperature the reaction was quenched with 2 M hydrochloric acid and the mixture was extracted with CH₂Cl₂. The organic layers were washed with brine and dried over MgSO₄. Purification by flash column chromatography on silica (*n*-hexane/CH₂Cl₂ = 2/1 to 1/1) afforded **4-12** (0.091 g, 0.03 mmol, 23 %) as a colorless powder.

Mp: 240-245 °C; ^1H NMR (700 MHz, CD_2Cl_2) δ 7.78-7.70 (m, 12H), 7.24 (d, 12H, $J = 8.4$ Hz), 7.70-6.60 (b, 12H), 6.94 (d, 24H, $J = 8.4$ Hz), 6.73 (d, 24H, $J = 8.4$ Hz), 3.94 (s, 18H), 1.99 (bs, 36H), 1.15 (s, 108H); ^{13}C NMR (176 MHz, CD_2Cl_2): δ 149.37, 143.10, 141.92, 140.84, 140.73, 139.10, 136.91, 135.39, 131.63, 130.47, 127.48, 127.05, 123.94, 82.02, 52.90, 34.64, 31.47, 21.46 ppm; HR-MS (MALDI) m/z calcd. for $\text{C}_{228}\text{H}_{246}\text{O}_6$ [M^+] 3079.8939, found 3079.8948.

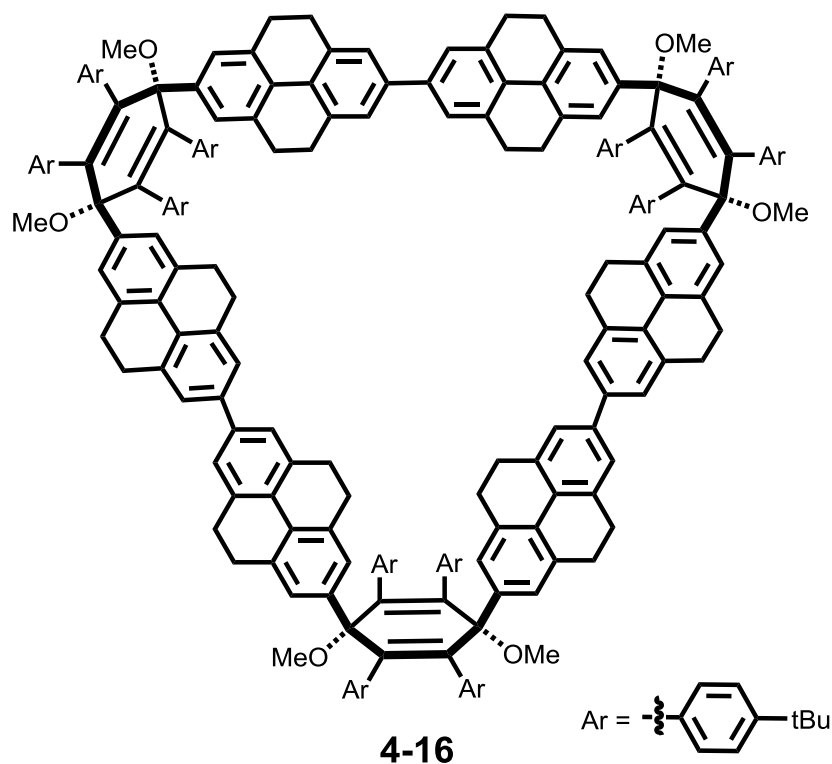
Synthesis of *Cyclo*-1,4-bis(2',6'-dimethylterphenyl)-1,4-dimethoxy-2,3,5,6-tetrakis(4''-*tert*-butyl phenyl)cyclohexa-2,5-diene-trimer (4-13)



The same procedure as for the synthesis of **4-12** was applied, affording **4-13** with 19 % yield.

Mp: 260-265 °C; ^1H NMR (300 MHz, CD_2Cl_2) δ 7.79 (bs, 28H, aromatic proton), 7.75 (d, 12H, $J = 8.0$ Hz), 7.67-7.32 (br, 8H, aromatic proton), 7.27(d, 12H, $J = 8.0$ Hz), 6.95 (d, 24H, $J = 8.5$ Hz), 6.75 (d, 24H, $J = 8.5$ Hz), 3.94 (s, 18H), 2.02 (bs, 36H), 1.16 (s, 108H) ppm; ^{13}C NMR (75 MHz, CD_2Cl_2): δ 153.23, 149.39, 143.12, 141.98, 141.00, 140.67, 140.40, 139.86, 139.13, 136.92, 135.42, 134.00, 131.66, 130.53, 127.88, 127.81, 127.32, 123.96, 82.05, 34.66, 31.48, 21.55 ppm; HR-MS (MALDI) m/z calcd. for $\text{C}_{264}\text{H}_{270}\text{O}_6$ [M^+] 3536.0817, found 3536.0857.

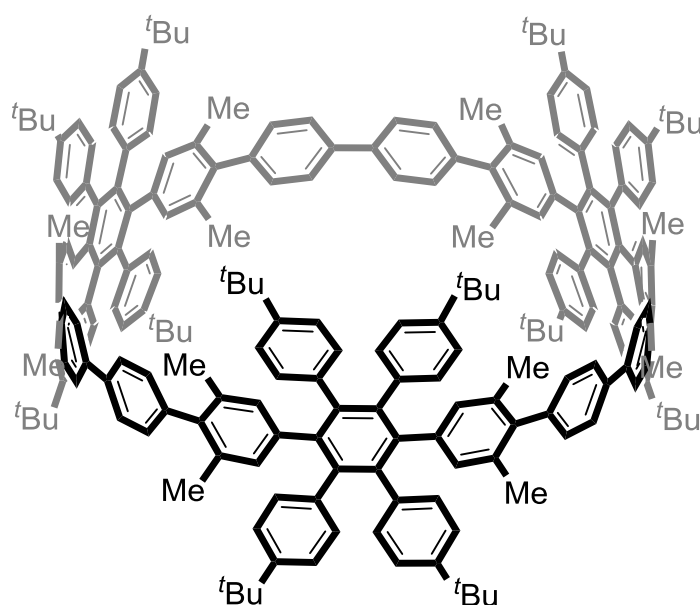
Synthesis of *Cyclo*-1,4-bis(4',5',9',10'-tetrahydropyrenediyl)-1,4-dimethoxy-2,3,5,6-tetrakis(4''-tert-butylphenyl)cyclohexa-2,5-diene-trimer (4-16)



The same procedure as for the synthesis of **4-12** was applied, affording **4-16** with 23 % yield.

Mp: 345-350 °C; ^1H NMR (300 MHz, CD_2Cl_2) δ 7.74-7.08 (m, 24H), 6.92 (d, $J = 8.7$ Hz, 24H), 6.79 (d, $J = 8.7$ Hz, 24H), 3.38 (s, 18H), 3.09-2.61 (br, 48H), 1.13 (s, 108H) ppm; ^{13}C NMR could not be recorded due to decomposition at elevated temperature; HR-MS (MALDI) m/z calcd. for $\text{C}_{240}\text{H}_{246}\text{O}_6$ [M^+] 3223.8939, found 3223.8898.

Methyl Substituted and Phenylene Extended [3]CHPB (4-14)

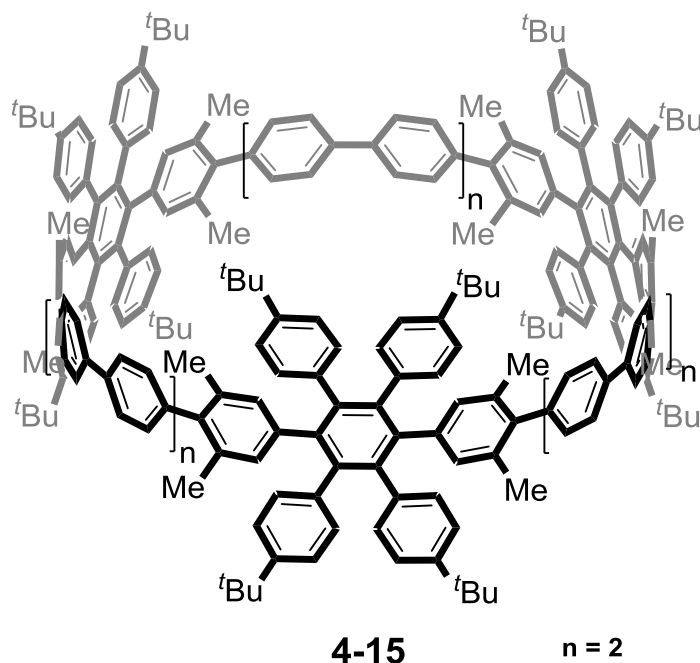


4-14

Compound **4-12** (150 mg, 0.049 mmol) was dissolved in anhydrous tetrahydrofuran (15 ml). The solution was cooled to -78 °C and a 1 M solution of sodium naphthalenide in THF (5.8 ml, 5.8 mmol) was added dropwise. The mixture was quenched with iodine and sodium thio-sulfate after one hour. The reaction mixture was extracted with CH_2Cl_2 , washed with brine and dried over MgSO_4 . Purification by flash column chromatography on silica (n -hexane/ $\text{CH}_2\text{Cl}_2 = 1/1$) and gel permeation chromatography (eluent: CHCl_3) afforded **4-14** (33 mg, 0.014 mmol, 23 %) as a colorless solid.

Mp: >350 °C; ^1H NMR (700 MHz, CD_2Cl_2): δ 7.54 (d, 12H, $J = 8.0$ Hz), 6.97 (d, 12H, $J = 8.0$ Hz), 6.95 (d, 24H, $J = 8.5$ Hz), 6.78 (d, 24H, $J = 8.5$ Hz), 6.61 (s, 12H), 1.73 (s, 36H), 1.17 (s, 108H); ^{13}C NMR (176 MHz, CD_2Cl_2): δ 148.38, 140.83, 140.76, 140.72, 140.41, 139.71, 139.30, 138.51, 134.92, 131.90, 131.43, 131.11, 127.15, 123.68, 34.64, 31.57, 20.82 ppm; HR-MS (MALDI) m/z calcd. for $\text{C}_{222}\text{H}_{228} [\text{M}^+]$ 2893.7836, found 2893.7817.

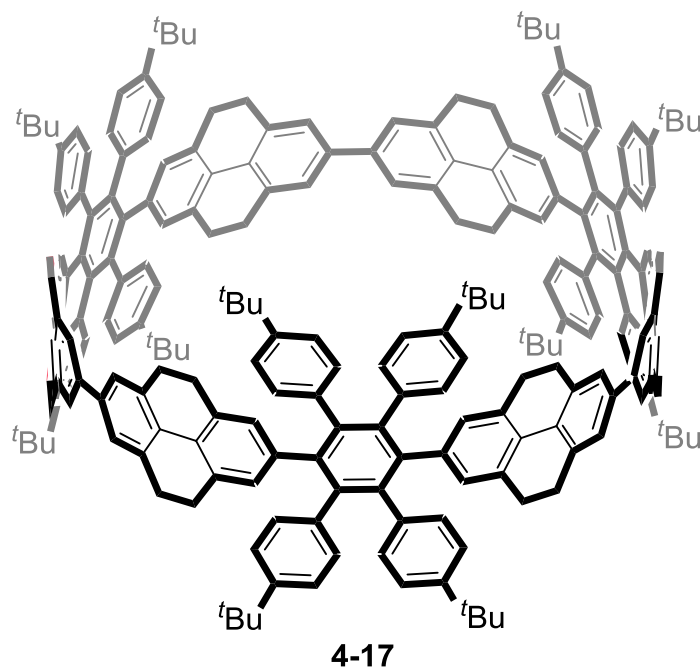
Methyl Substituted and Phenylene Extended [3]CHPB (4-15)



The same procedure as for the synthesis of **4-14** was applied, yielding **4-15** (17.5 mg, 0.005 mmol, 17 %).

Mp: >350 °C; ^1H NMR (300 MHz, CDCl_3): δ 7.73-7.66 (m, 24H), 7.54 (d, 12H, $J = 8.3$ Hz), 6.98 (d, 12H, $J = 8.3$ Hz), 6.88 (d, 24H, $J = 8.3$ Hz), 6.73 (d, 24H, $J = 8.3$ Hz), 6.55 (s, 12H), 1.67 (s, 36H), 1.14 (s, 108H); ^{13}C NMR (126 MHz, CDCl_3): δ 147.53, 140.82, 140.46, 140.22, 140.05, 139.32, 138.73, 138.33, 138.27, 133.95, 131.40, 131.15, 130.36, 127.79, 127.46, 126.81, 123.17, 100.15, 34.30, 31.43, 20.53 ppm; HR-MS (MALDI) m/z calcd. for $\text{C}_{258}\text{H}_{252}$ [M^+] 3349.9714, found 3349.9655.

Ethylene Bridged and Phenylene Extended [3]CHPB (4-17)



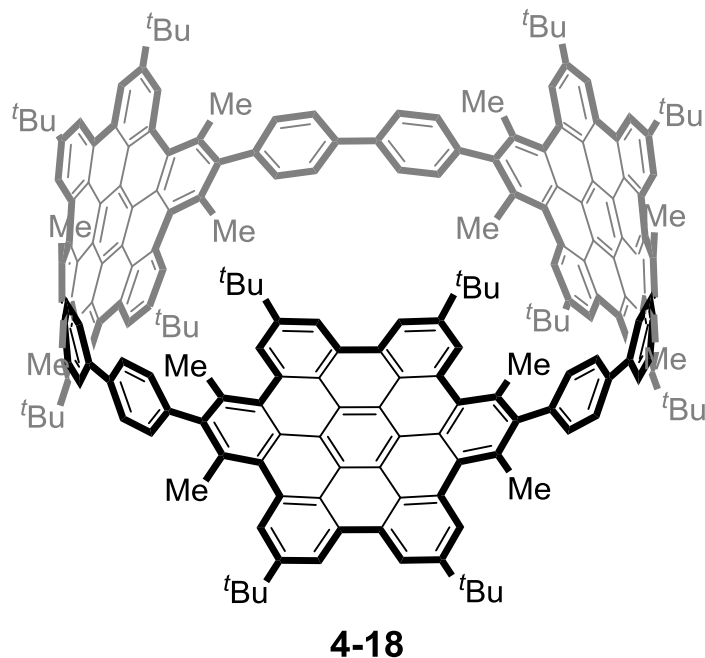
To an ice cooled titanium tetrachloride (0.85 g, 4.5 mmol) solution in THF (5 ml) LiAlH_4 (2 M in THF) (9 ml, 18.0 mmol) was slowly added. The mixture was warmed to 80 °C and stirred for one hour. **4-16** (53 mg, 0.015 mmol) in THF (15 ml) was added by a syringe. The reaction mixture was stirred at 80 °C for two days. After cooling the reaction to 0 °C, it was quenched with water and hydrochloric acid (Attention: very reactive). The mixture was extracted with CH_2Cl_2 and filtered off over Celite. The solvents were evaporated and the raw

product was precipitated in methanol. Purification by preparative GPC yielded **4-17** (12.0 mg, 0.004 mmol, 26 %) as a colorless powder.

Mp: >350 °C; ¹H NMR (300 MHz, CD₂Cl₂): δ 7.04 (s, 12H), 6.83 (m, 12H), 6.7 (m, 36H), 6.62 (s, 12H), 2.66 (t, 24H), 2.49 (t, 24H), 0.92 (s, 108H); ¹³C NMR (75 MHz, CD₂Cl₂): δ 148.20, 141.30, 141.08, 140.99, 138.46, 135.59, 134.03, 131.84, 131.18, 130.56, 129.37, 125.05, 123.77, 123.53, 54.00, 34.43, 31.47, 30.27 ppm; HR-MS (MALDI) *m/z* calcd. for C₂₃₄H₂₂₈ [M⁺] 3037.7836, found 3037.7798.

General Procedure for the Cyclodehydrogenation towards Substitutionally blocked and Phenylene Extended [3]CHBCs (4-18 to 4-20)

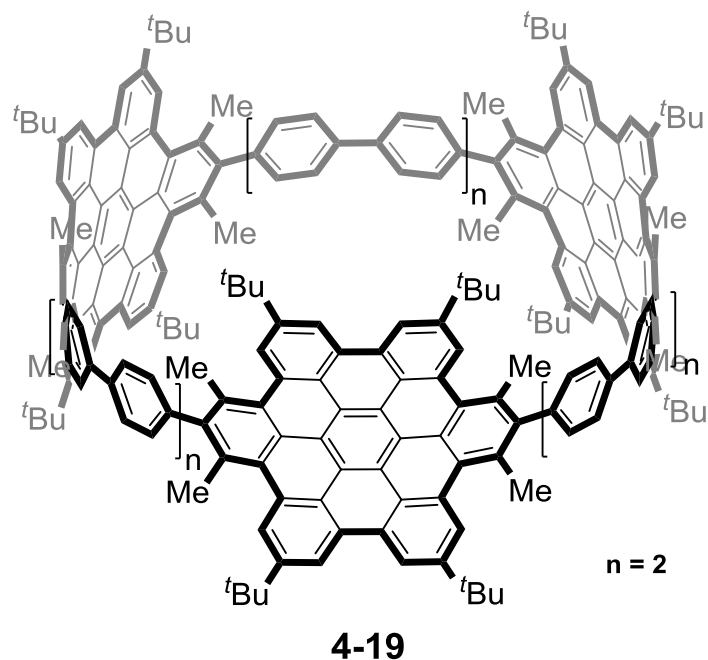
The phenylene-extended [3]CHPB macrocycles **4-14** or **4-15** or **4-17** (0.01 g, 0.0034 mmol) were dissolved in anhydrous and unstabilized CH₂Cl₂ (10 ml). A mixture of FeCl₃ (0.073 g, 0.452 mmol) in nitromethane (2 ml) was slowly added at RT. The mixture was stirred at RT for seven hours, purging the solution with a continuous stream of argon. After quenching with methanol or hydrazine, the mixture was extracted with CH₂Cl₂. The organic layers were separated, washed with brine and dried over MgSO₄. The raw product was purified by flash column chromatography on silica (CH₂Cl₂). The product was further purified and separated by HPLC (toluene/methanol = 3/1 to 9/1). The cyclodehydrogenated products were analyzed by HR-MS spectrometry, UV-Vis-, fluorescence- and NMR spectroscopy.

[3]CHBC (4-18)

Side reactions were observed during the cyclodehydrogenation, since compounds with a higher degree of dehydrogenation were obtained. Two fractions, **4-18'a** and **4-18'b**, were separated by preparative HPLC, having an additional loss of two and four hydrogen atoms. The fractions were analyzed by MALDI-TOF MS.

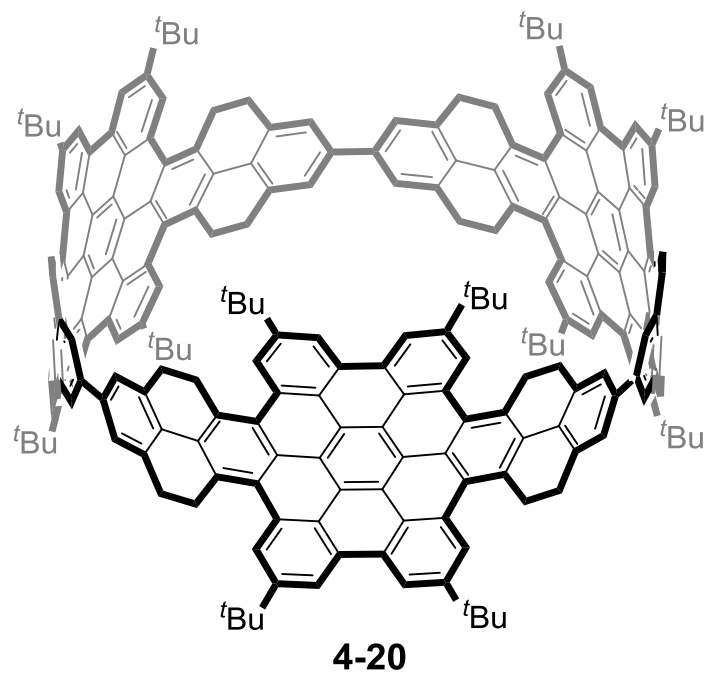
4-18'a: MS (MALDI) m/z calcd for $C_{222}H_{190}$ [M^+]: 2855.4686, found 2855.7174.

4-18'b: MS (MALDI) m/z calcd for $C_{222}H_{188}$ [M^+]: 2853.4711, found 2853.7009.

[3]CHBC (4-19)

A short column chromatography on silica afforded **7b** (2 mg, 6×10^{-7} mol).

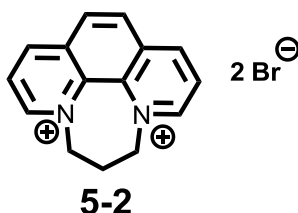
^1H NMR (700 MHz, CD_2Cl_2) δ 9.27 (s, 12H), 8.94 (s, 12H), 7.73 (m, 48H), 2.96 (s, 36H), 1.74 (s, 108H); ^{13}C NMR (from 2D $^1\text{H},^{13}\text{C}$ -HSQC and 2D $^1\text{H},^{13}\text{C}$ -HMBC experiment, CD_2Cl_2) δ 147.51, 131.08, 129.35, 128.47, 128.21, 128.14, 127.98, 126.68, 118.04, 35.59, 32.22, 23.46 ppm; HR-MS (MALDI) m/z calcd for $\text{C}_{258}\text{H}_{216}$ [M^+]: 3313.6897, found 3313.6929.

[3]CHBC (4-20)

The reaction was incomplete, because the cyclodehydrogenation stopped after a loss of approximately 24 hydrogen atoms. A further analysis was not possible.

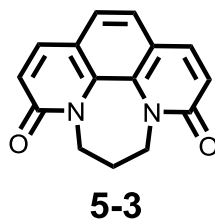
7.3.3. Phenanthroline-Indole N₄-Macrocycles

6,7-Dihydro-5H-[1,4]diazepino[1,2,3,4-lmn]-[1,10]phenanthroline-4,8-diiumdibromide (5-2)



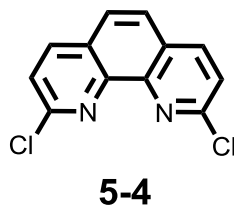
6,7-Dihydro-5H-[1,4]diazepino[1,2,3,4-lmn]-[1,10]phenanthroline-4,8-diiumdibromide was synthesized according to literature.^[163]

6,7-Dihydro-3H-[1,4]diazepino[1,2,3,4-lmn]-[1,10]phenanthroline-3,9(5H)-dione (5-3)

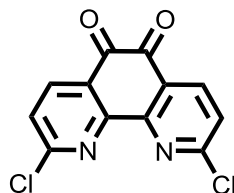


6,7-Dihydro-3H-[1,4]diazepino[1,2,3,4-lmn]-[1,10]phenanthroline-3,9(5H)-dione was synthesized according to literature.^[163]

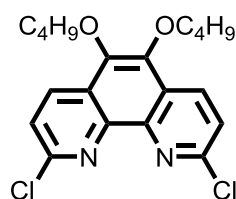
2,9-Dichloro-1,10-phenanthroline (5-4)



2,9-Dichloro-1,10-phenanthroline was synthesized according to literature.^[163]

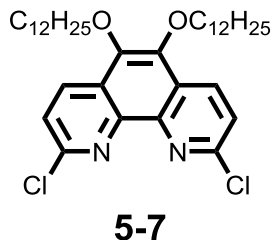
2,9-Dichloro-1,10-phenanthroline-5,6-dione (5-5)**5-5**

2,9-Dichloro-1,10-phenanthroline-5,6-dione was synthesized according to literature.^[163]

5,6-Dibutoxy-2,9-dichloro-1,10-phenanthroline (5-6)**5-6**

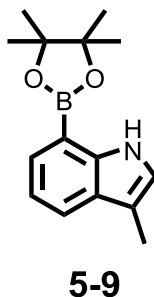
To a mixed solution of H₂O (20 ml) and THF (20 ml) **5-5** (2.5 g, 8.96 mmol), tetrabutylammonium bromide (1.45 g, 4.48 mmol) and Na₂S₂O₄ (9.36 g, 53.75 mmol) were added. Then 1-bromobutane (4.91 g, 35.83 mmol) was given to the mixture. A solution of KOH (6.0 g, 108.3 mmol) in 40 ml H₂O was subsequently appended. The reaction mixture turned black immediately and was stirred for 2 days at 40 °C. After dilution with H₂O the crude compound was extracted with CH₂Cl₂ (3 x 50 ml). The organic phase was washed with brine, dried with MgSO₄ and the solvents were evaporated under reduced pressure. The crude product was purified by flash column chromatography on silica (*n*-hexane/CH₂Cl₂ = 3/7 to 1/9) to yield **5-6** (1.8 g, 4.6 mmol, 51 %) as light yellow crystals.

Mp: 190.6 °C; ¹H NMR (300 MHz, CD₂Cl₂) δ 8.53 (d, J = 8.7 Hz, 2H), 7.64 (d, J = 8.7 Hz, 2H), 4.24 (t, J = 6.4 Hz, 4H), 1.86 (qi, J = 6.4 Hz, 4H), 1.57 (sx, J = 7.1 Hz, 4H), 1.01 (t, J = 7.3 Hz, 6H) ppm; ¹³C NMR (75 MHz, CD₂Cl₂): δ 150.81, 143.20, 143.07, 134.27, 126.43, 124.93, 74.48, 32.93, 19.95, 14.27 ppm; MS (FD) *m/z* calcd for C₂₀H₂₂Cl₂N₂O₂ [M⁺]: 392.11, found 391.63; HR-MS (ESI) calcd for C₂₀H₂₂Cl₂N₂O₂ [M+H⁺] 393.1137, found 393.1125.

2,9-Dichloro-5,6-bis(dodecyloxy)-1,10-phenanthroline (5-7)

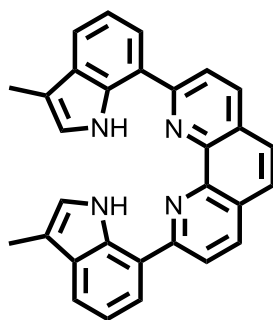
To a mixed solution of H₂O (40 ml) and THF (40 ml), **5-5** (2.0 g, 7.17 mmol), tetrabutylammonium bromide (1.50 g, 4.66 mmol) and Na₂S₂O₄ (7.54 g, 43.32 mmol) were added. Then dodecyl bromide (6.0 g, 24.04 mmol) was given to the mixture. A solution of KOH (6.0 g, 108.3 mmol) in 40 ml H₂O was subsequently appended. The reaction mixture turned black immediately and was stirred for 2 days at 40 °C. After dilution with H₂O, the crude compound was extracted with CH₂Cl₂ (3 x 50 ml). The organic phase was washed with brine, dried with MgSO₄ and the solvents were evaporated under reduced pressure. The crude product was purified by flash column chromatography on silica (*n*-hexane/ethyl acetate = 9/1) to yield **5-7** (3.0 g, 4.9 mmol, 62 %) as light yellow crystals.

Mp: 90.5 °C; ¹H NMR (250 MHz, CD₂Cl₂) δ 8.53 (d, J = 8.7 Hz, 2H), 7.63 (d, J = 8.7 Hz, 2H), 4.22 (t, J = 6.7 Hz, 4H), 1.87 (qi, J = 6.8 Hz, 4H), 1.54 (m, 4H), 1.27 (bs, 32H), 0.88 (t, J₁ = J₂ = 6.8 Hz, 6H) ppm; ¹³C NMR (75 MHz, CD₂Cl₂): δ 150.78, 143.16, 143.06, 134.24, 126.38, 124.89, 74.76, 32.53, 30.89, 30.28, 30.25, 30.23, 30.21, 30.07, 29.96, 29.84, 29.71, 26.73, 23.29, 14.48 ppm; MS (FD) *m/z* calcd for C₃₆H₅₄Cl₂N₂O₂ [M⁺]: 617.7, found 618.6; HR-MS (ESI) calcd for C₃₆H₅₄Cl₂N₂O₂ [M+H⁺] 617.3641, found 616.3631.

3-Methyl-7-(4,4,5,5-tetramethyl-1,3,2-dioxaborolan-2-yl)-1H-indole (5-9)

3-methyl-7-(4,4,5,5-tetramethyl-1,3,2-dioxaborolan-2-yl)-1H-indole was synthesized according to literature.^[188]

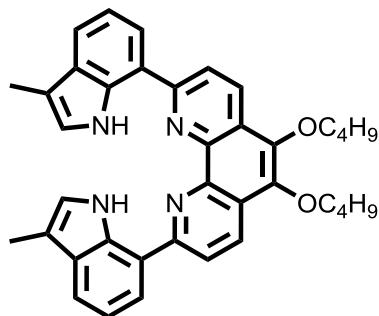
2,9-Bis(3-methyl-1H-indol-7-yl)-1,10-phenanthroline (5-10)



5-10

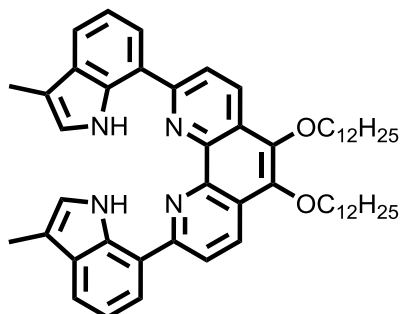
Compound **5-4** (0.5 g, 2.01 mmol), **5-9** (1.55 g, 6.02 mmol), bis(dibenzylideneacetone) palladium(0) (0.115 g, 0.20 mmol), 2-dicyclohexylphosphino-2',6'-dimethoxybiphenyl (0.165 g, 0.401 mmol) and potassium phosphate (2.56 g, 12.04 mmol) were dissolved in a degassed mixture of toluene (20 ml) and water (0.5 ml). The mixture was heated to 90 °C for 48 h. After cooling to RT the organic layer was separated and was washed with brine and subsequently dried with MgSO₄. Purification by flash column chromatography on silica (*n*-hexane/CH₂Cl₂ = 7/3) afforded **5-10** (0.48 g, 1.08 mmol, 54 %) as light yellow crystals.

Mp: 257.8 °C; ¹H NMR (250 MHz, CD₂Cl₂) δ 11.72 (s, 2H), 8.39 (dd, J₁ = 8.6 Hz, J₂ = 8.4 Hz, 4H), 7.96 (d, J = 7.4 Hz, 2H), 7.87 (s, 2H), 7.77 (d, J = 7.4 Hz, 2H), 7.3 (t, J = 7.4 Hz, 2H), 6.60 (s, 2H), 2.40 (s, 6H) ppm; ¹³C NMR (75 MHz, CD₂Cl₂) δ 137.33, 130.49, 127.83, 126.40, 124.20, 122.25, 121.58, 121.05, 120.86, 119.50, 119.28, 119.19, 111.42, 111.25, 54.00, 9.94 ppm; MS (FD) calcd for C₃₀H₂₂N₄ [M⁺] 438.2, found 438.1; HR-MS (ESI) calcd for C₃₀H₂₂N₄ [M+H⁺] 439.1923, found 439.1919.

5,6-Dibutoxy-2,9-bis(3-methyl-1H-indol-7-yl)-1,10-phenanthroline (5-11)**5-11**

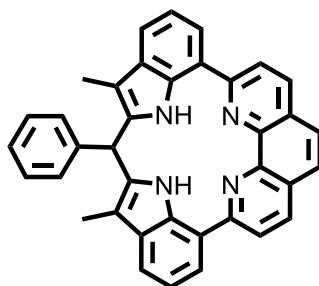
Compound **5-6** (1.5 g, 3.81 mmol), **5-9** (4.9 g, 19.07 mmol), potassium phosphate (1.62 g, 7.63 mmol), 2-dicyclohexylphosphino-2',6'-dimethoxybiphenyl (1.25 g, 3.05 mmol) and palladium acetate (0.34 g, 1.53 mmol) were placed into a flame dried flask. A degassed mixture of toluene (15 ml) and water (2 ml) was added. The reaction mixture was heated under an argon atmosphere to 90 °C overnight. After cooling to RT, the organic layer was separated, washed with brine and dried over MgSO₄. Purification by flash column chromatography on silica (*n*-hexane/CH₂Cl₂ = 1/1) afforded **5-11** (1.27 g, 2.18 mmol, 57 %) as a light yellow solid.

¹H NMR (700 MHz, CD₂Cl₂) δ 11.66 (s, 2H, N-H), 8.69 (d, J = 8.5 Hz, 2H), 8.34 (d, J = 8.5 Hz, 2H), 7.94 (d, J = 7.5 Hz, 2H), 7.76 (d, J = 7.5 Hz, 2H), 7.29 (t, J = 7.6 Hz, 2H), 6.59 (s, 2H), 4.32 (t, J = 6.5 Hz, 4H), 2.39 (s, 6H), 1.94 (qi, J = 6.5 Hz, 4H), 1.65 (sx, J = 7.4 Hz, 4H), 1.06 (t, J = 7.3 Hz, 6H) ppm; ¹³C NMR (176 MHz, CD₂Cl₂): δ 157.10, 143.85, 142.92, 135.42, 131.81, 130.42, 125.29, 124.16, 122.22, 121.36, 120.90, 120.64, 119.26, 111.19, 74.37, 33.08, 20.05, 14.36, 9.94 ppm; HR-MS (ESI) calcd for C₃₈H₃₈N₄O₂ [M+Na⁺] 605.2892, found 605.2880.

5,6-Bis(dodecyloxy)-2,9-bis(3-methyl-1H-indol-7-yl)-1,10-phenanthroline (5-12)**5-12**

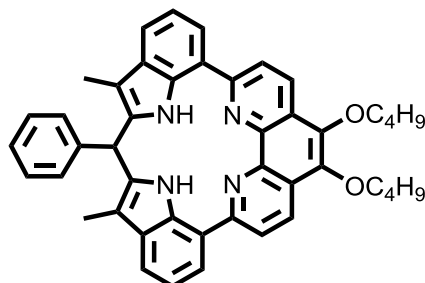
Compound **5-7** (0.8 g, 1.3 mmol), **5-9** (1.0 g, 3.9 mmol), tris(dibenzylideneacetone)dipalladium(0) (0.12 g, 0.13 mmol), 2-dicyclohexylphosphino-2',6'-dimethoxybiphenyl (0.11 g, 0.26) and potassium carbonate (1.65 g, 7.78 mmol) were dissolved in a degassed mixture of toluene (20 ml) and water (0.5 ml). The mixture was heated under an argon atmosphere to 90 °C and was stirred overnight. After cooling to RT the organic layer was separated and was washed with water. Purification by flash column chromatography on silica (*n*-hexane/CH₂Cl₂ = 7/3) afforded **5-12** (0.58 g, 0.72 mmol, 55 %) as light yellow crystals.

Mp: 102 °C; ¹H NMR (300 MHz, THF-d₈) δ 11.8 (s, 2H), 8.71(d, J = 8.8 Hz, 2H), 8.41 (d, J = 8.8 Hz, 2H), 7.94 (d, J = 7.3 Hz, 2H), 7.7 (d, J = 7.7 Hz, 2H), 7.22 (t, J = 7.5 Hz, 2H), 6.61 (s, 2H), 4.33 (t, J = 6.7 Hz, 4H), 2.37 (s, 6H), 1.97 (qi, J = 6.8 Hz, 4H), 1.64 (m, 4H), 1.36 (s, 36H), 1.01 (t, J = 6.7 Hz, 6H) ppm; ¹³C NMR (75 MHz, THF-d₈) δ 157.99, 144.53, 143.42, 136.20, 132.11, 131.12, 125.54, 124.66, 122.95, 121.59, 121.38, 121.22, 119.49, 111.08, 74.93, 33.07, 32.90, 31.54, 30.86, 30.73, 30.52, 30.40, 29.98, 27.41, 23.75, 14.61, 9.97 ppm; HR-MS (ESI) calcd for C₅₄H₇₀N₄O₂ [M+Na⁺] 829.5396, found 829.5411.

2,9-((2,2'-Phenylmethylene)-bis(3-methyl-1H-indol-7-yl))-1,10-phenanthroline (5-13)**5-13**

Compound **5-10** (50 mg, 0.11 mmol) and benzaldehyde (12.1 mg, 0.11 mmol) were mixed inside a 35 ml microwave tube and were dissolved in 10 ml anhydrous CH_2Cl_2 . Argon was bubbled through the reaction mixture for 30 min. Boron trifluoride etherate (324 mg, 1.14 mmol) was added prior to microwave heating: 5 h/110 °C/300 W, 10 min./20 °C /200 W, 5 h/110 °C/300 W, 10 min./20 °C /200 W, 5 h/110 °C/300 W. The reaction mixture was purified by flash column chromatography on silica (CH_2Cl_2) yielding **5-13** (29.8 mg, 0.057 mmol; 50 %) as a light yellow solid.

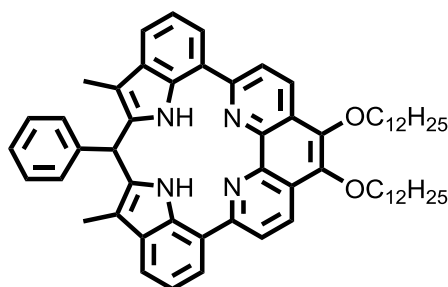
Mp: >360 °C; $^1\text{H-NMR}$ (300 MHz, CD_2Cl_2) δ 11.96 (s, 2H), 8.41 (dd, 4H), 7.90 (d, $J = 7.0$ Hz, 2H), 7.88 (s, 2H), 7.78 (d, $J = 7.8$ Hz, 2H), 7.31 (t, $J = 7.6$ Hz, 2H), 7.07 7.03 (m, 3H), 6.94 6.90 (m, 2H), 6.17 (s, 1H), 2.59 (s, 6H) ppm; $^{13}\text{C NMR}$ (75 MHz, CD_2Cl_2) δ 158.30, 145.72, 137.75, 135.76, 134.86, 133.15, 130.42, 128.95, 128.29, 127.70, 126.92, 126.52, 121.46, 121.39, 121.33, 120.91, 119.79, 109.80, 38.69, 9.24 ppm; HR-MS (ESI) calcd for $\text{C}_{37}\text{H}_{26}\text{N}_4$ $[\text{M}+\text{H}^+]$ 527.2230, found 527.2228.

5,6-Dibutoxy-2,9-(2,2'-phenylmethylene)-bis(3-methyl-1H-indol-7-yl)-1,10-phenanthroline (5-14)**5-14**

Compound **5-11** (0.1 g, 0.23 mmol) and benzaldehyde (0.0242 g, 0.23 mmol) were mixed inside a 35 ml microwave tube with 15 ml anhydrous CH_2Cl_2 . Argon was bubbled through the reaction-mixture for 30 minutes. Boron trifluoride etherate (0.324 g, 2.28 mmol) was added prior to microwave heating: 5 h/110 °C/300 W, 10 min./20 °C /200 W, 5 h/110 °C/300 W, 10 min./20 °C /200 W, 5 h/110 °C/300 W. The reaction mixture was purified by flash column chromatography on silica (*n*-hexane/ CH_2Cl_2 = 1/1) yielding **5-14** (0.008 g, 0.012 mmol; 14 %) as a light yellow solid.

Mp: 232.2 °C; ^1H NMR (300 MHz, CD_2Cl_2) δ 11.89 (s, 2H), 8.72 (d, J = 8.7 Hz, 2H), 8.37 (d, J = 8.9 Hz, 2H), 7.88 (d, J = 7.2 Hz, 2H), 7.76 (d, J = 7.7 Hz, 2H), 7.30 (t, J = 7.6 Hz, 2H), 7.05-6.98 (m, 3H), 6.91 (d, J = 8.1 Hz, 2H), 6.16 (s, 1H), 4.30 (t, J = 6.5 Hz, 4H), 2.59 (s, 6H), 1.92 (qi, J = 6.8 Hz, 4H), 1.63 (sx, J = 7.4 Hz, 4H), 1.04 (t, J = 7.3 Hz, 6H) ppm; ^{13}C NMR (75 MHz, CD_2Cl_2) δ 156.85, 143.46, 142.75, 142.53, 135.50, 131.85, 130.18, 129.18, 128.74, 127.50, 126.71, 125.49, 121.30, 120.97, 120.92, 120.57, 119.60, 109.55, 74.12, 32.85, 19.85, 14.17, 9.05 ppm; HR-MS (ESI) calcd for $\text{C}_{45}\text{H}_{42}\text{N}_4\text{O}_2$ [$\text{M}+\text{Na}^+$] 693.3205, found 693.3197.

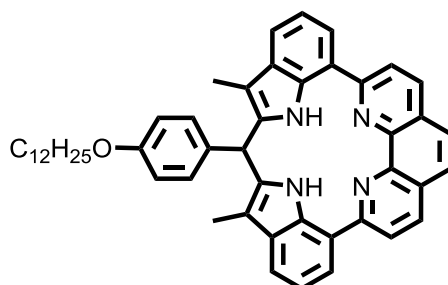
5,6-Bis(dodecyloxy)-2,9-(2,2'-phenylmethylene)-bis(3-methyl-1H-indol-7-yl)-1,10-phenanthroline (5-15)



5-15

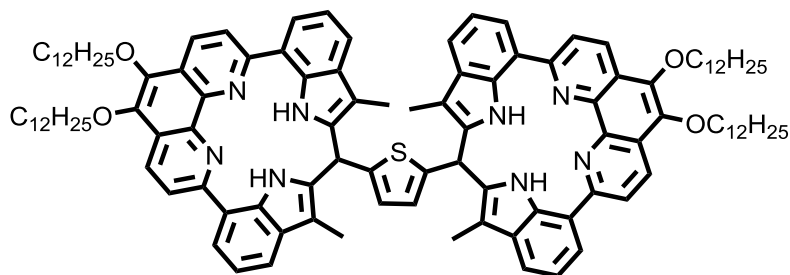
Compound **5-12** (100 mg, 0.12 mmol) and benzaldehyde (16 mg, 0.14 mmol) were mixed inside a 35 ml microwave tube with 10 ml anhydrous CH₂Cl₂. Argon was bubbled through the reaction-mixture for 10 min. Boron trifluoride etherate (170 mg, 1.23 mmol) was added prior to microwave heating: 5 h/110 °C/300 W, 10 min./20 °C /200 W, 5 h/110 °C/300 W, 10 min./20 °C /200 W, 5 h/110 °C/300 W. The reaction mixture was purified by flash column chromatography on silica (*n*-hexane/CH₂Cl₂ = 1/1) yielding **5-15** (38 mg, 0.042 mmol; 34 %) as a light yellow solid.

Mp: 138 °C; ¹H NMR (300 MHz, CD₂Cl₂) δ 11.91 (s, 2H), 8.67 (d, J = 8.7 Hz, 2H), 8.33 (d, J = 8.7 Hz, 2H), 7.87 (d, J = 7.5 Hz, 2H), 7.75 (d, J = 7.5 Hz, 2H), 7.29 (t, J = 7.6 Hz, 2H), 7.10-7.00 (m, 3H), 6.93-6.90 (m, 2H), 6.16 (s, 1H), 4.25 (t, J = 6.5 Hz, 4H), 2.59 (s, 6H), 1.90 (qi, J = 6.7 Hz, 4H), 1.57 (m, 4H), 1.29 (s, 32H), 0.89 (t, J = 6.7 Hz, 6H) ppm; ¹³C NMR (75 MHz, CD₂Cl₂) δ 157.06, 143.67, 142.93, 142.75, 135.69, 134.82, 132.08, 130.38, 128.93, 127.69, 126.90, 125.70, 121.49, 121.17, 121.11, 120.77, 119.79, 109.74, 74.64, 38.69, 32.53, 30.97, 30.31, 30.26, 30.13, 29.97, 26.81, 23.29, 14.47, 9.24 ppm; HR-MS (ESI) calcd for C₆₁H₇₄N₄O₂ [M+H⁺] 895.5890, found 895.5917.

2,9-((2,2'(4-Dodecyloxyphenyl)methylene)-bis(3-methyl-1H-indol-7-yl))-1,10-phenanthroline (5-16)**5-16**

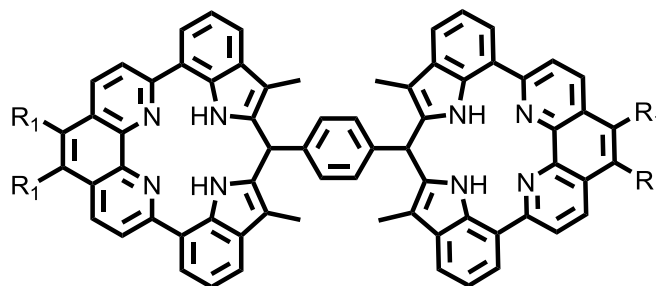
Compound **5-10** (100 mg, 0.23 mmol) and 4-dodecyloxybenzaldehyde (73 mg, 0.25 mmol) were mixed inside a 35 ml microwave tube and dissolved in 15 ml anhydrous CH_2Cl_2 . Argon was bubbled through the reaction mixture for 30 min. Boron trifluoride etherate (289 mg, 2.28 mmol) was added prior to microwave heating: 5 h/110 °C/300 W, 10 min./20 °C /200 W, 5 h/110 °C/300 W, 10 min./20 °C /200 W, 5 h/110 °C/300 W. The reaction mixture was purified by flash column chromatography on silica (*n*-hexane/ CH_2Cl_2 = 1/1) yielding **5-16** (26.6 mg, 0.077 mmol; 17 %) as a light yellow solid.

^1H NMR (300 MHz, CD_2Cl_2) δ 11.92 (s, 2H), 8.29 (s, 4H), 7.83 (d, J = 7.5 Hz, 2H), 7.75 (d, J = 7.5 Hz, 2H), 7.72 (s, 2H), 7.27 (t, J = 7.6 Hz, 2H), 6.8 (d, J = 8.3 Hz, 2H), 6.58 (d, J = 8.7 Hz, 2H), 6.10 (s, 1H), 3.71 (t, J = 6.7 Hz, 2H), 2.58 (s, 6H), 1.56 (qi, J = 6.7 Hz, 2H), 1.17 (m, 18H), 0.85 (t, J = 6.7 Hz, 3H) ppm; ^{13}C NMR (75 MHz, CD_2Cl_2) δ 158.32, 158.22, 145.62, 137.65, 135.72, 135.22, 134.74, 130.43, 128.66, 128.22, 126.44, 121.41, 121.32, 121.24, 120.81, 119.73, 114.84, 109.55, 68.49, 37.90, 32.45, 30.27, 30.14, 30.08, 30.05, 29.86, 29.84, 29.67, 26.43, 23.23, 14.42, 9.22 ppm; HR-MS (ESI) calcd for $\text{C}_{49}\text{H}_{50}\text{N}_4\text{O}$ $[\text{M}+\text{H}^+]$ 711.4057, found 711.4073.

Thienylene-bridged PIM Dimer (5-17)**5-17**

Compound **5-12** (0.1 g, 0.23 mmol) and thiophene-2,5-dicarbaldehyde (0.0168 g, 0.12 mmol) were mixed inside a 35 ml microwave tube with 15 ml anhydrous CH_2Cl_2 . Argon was bubbled through the reaction mixture for 30 min. Boron trifluoride etherate (0.324 g, 2.28 mmol) was added prior to microwave heating: 5 h/110 °C/300 W, 10 min./20 °C /200 W, 5 h/110 °C/300 W, 10 min./20 °C /200 W, 5 h/110 °C/300 W. The reaction mixture was purified by flash column chromatography on silica (*n*-hexane/ CH_2Cl_2 = 1/1) yielding **5-17** (0.008 g, 0.012 mmol; 14 %) as a light yellow solid.

^1H NMR (500 MHz, CD_2Cl_2) δ 11.76 (s, 4H), 8.57 (d, J = 8.7 Hz, 4H), 8.20 (d, J = 8.9 Hz, 4H), 7.73 (d, J = 7.2 Hz, 4H), 7.59 (d, J = 7.8 Hz, 4H), 7.16 (t, J = 7.5 Hz, 4H), 6.03 (s, 2H), 5.91 (s, 2H), 4.19 (t, J = 6.9 Hz, 8H), 2.37 (s, 12H), 1.88 (qi, J = 6.9 Hz, 8H), 1.41 (m, 8H), 1.30 (s, 64H), 0.89 (t, J = 6.9 Hz, 12H) ppm; ^{13}C NMR (126 MHz, CD_2Cl_2) δ 156.88, 147.12, 143.53, 142.66, 135.43, 134.16, 131.92, 130.07, 125.56, 124.47, 121.42, 121.20, 121.18, 120.66, 119.66, 109.12, 74.55, 35.22, 32.54, 30.97, 30.33, 30.29, 30.27, 30.15, 29.99, 26.82, 23.30, 14.48, 9.02 ppm; HR-MS (MALDI) m/z calcd. for $\text{C}_{114}\text{H}_{140}\text{N}_8\text{O}_4\text{S}$ [$\text{M}-\text{H}^+$] 1716.0635, found 1716.0646.

Phenylene-bridged PIM Dimer (5-18)**5-18**

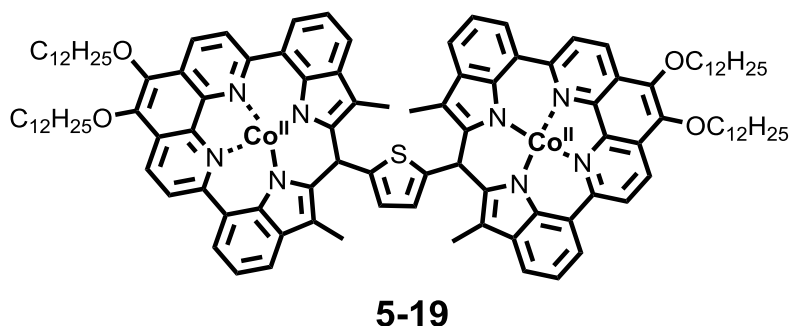
Compound **5-12** (100 mg, 0.12 mmol) and terephthalaldehyde (8.3 mg, 0.062 mmol) were mixed inside a 35 ml microwave tube and were dissolved in 15 ml anhydrous CH_2Cl_2 . Argon was bubbled through the reaction mixture for 30 minutes. Boron trifluoride etherate (42 mg, 0.62 mmol) was added prior to microwave heating: 5 h/110 °C/300 W, 10 min./20 °C /200 W, 5 h/110 °C/300 W, 10 min./20 °C /200 W, 5 h/110 °C/300 W. The reaction mixture was purified by flash column chromatography on silica (hexane/dichloromethane = 1/1) yielding **5-18** (22 mg, 0.013 mmol; 21 %) as a light yellow solid.

Mp: 335.4 °C; ^1H NMR (500 MHz, CD_2Cl_2) δ 11.74 (s, 4H), 8.03 (d, $J = 8.8$ Hz, 4H), 7.7 (d, $J = 8.8$ Hz, 4H), 7.33 (d, $J = 7.7$ Hz, 4H), 7.30 (d, $J = 7.7$ Hz, 4H), 6.83 (s, 4H), 6.81 (t, $J = 7.7$ Hz, 4H), 5.96 (s, 2H), 3.83 (t, $J = 6.4$ Hz, 8H), 2.38 (s, 12H), 1.67 (qi, $J = 6.4$ Hz, 8H), 1.41 (m, 8H), 1.32 (s, 64H), 0.92 (t, $J = 6.4$ Hz, 12H) ppm; ^{13}C NMR (75 MHz, CD_2Cl_2) δ 156.27, 152.68, 146.89, 143.05, 142.16, 141.96, 135.20, 134.49, 131.14, 129.91, 127.79, 124.94, 120.72, 120.52, 120.05, 119.24, 108.92, 74.11, 32.59, 30.97, 30.37, 30.30, 30.22, 30.05, 26.84, 23.34, 14.51, 9.11 ppm; HR-MS (ESI) calcd for $\text{C}_{116}\text{H}_{142}\text{N}_8\text{O}_4$ $[\text{M}+\text{H}^+]$ 1712.1227, found 1712.1216.

Formation of Cobalt Complexes – General Procedure

Mono- and dimeric PIM macrocycles **5-11**, **5-12** and **5-13** to **5-18** (1.0 eq.) and cobalt(II) acetate (1.5 eq. (3.0 eq. for PIM Dimer)) were dissolved in anhydrous *N,N*-dimethylformamide (3 ml) inside a 10 ml microwave vial. The mixture was placed into a microwave and heated to 180 °C (300 W) for two hours. After cooling to RT the reaction mixture was poured into water (100 ml). The black precipitate was filtered off and dried under high vacuum.

Binuclear Cobalt Complex (**5-19**)

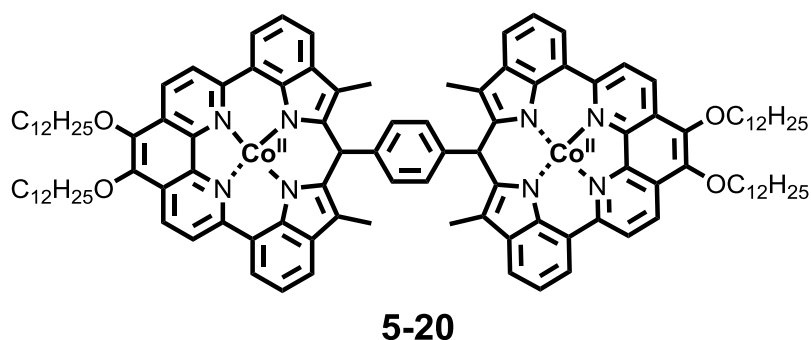


Cobalt complex **5-19** (5 mg, 0.017 mmol, 47 %) was obtained as a black solid.

MS (MALDI) m/z calcd for $C_{114}H_{136}Co_2N_8O_4S_4$ [M^+]: 1830.91, found 1830.98;

IR(ATR): 2927, 2856, 1462, 1350, 1254, 1021, 931, 793, 757, 583, 521 cm^{-1} .

Binuclear Cobalt Complex (**5-20**)

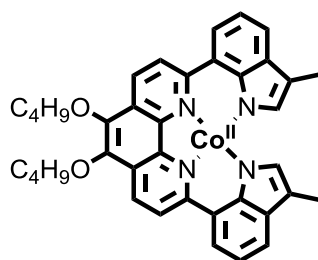


Cobalt complex **5-20** (31 mg, 0.017 mmol, 58 %) was obtained as a black solid.

MS (MALDI) m/z calcd for $C_{116}H_{138}Co_2N_8O_4$ [M^+]: 1825.95, found 1826.21.

IR (ATR): 2920, 2850, 1627, 1602, 1571, 1552, 1535, 1510, 1463, 1455, 1428, 1346, 1305, 1278, 1243, 1231, 1170, 1138, 1093, 1073, 1062, 1049, 1020, 961, 910, 892, 874, 858, 828, 791, 729, 698, 675, 646, 631, 621 cm^{-1} .

Cobalt Complex (5-21)



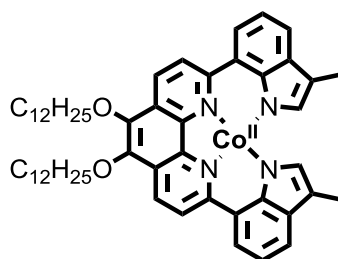
5-21

Cobalt complex **5-21** (82 mg, 0.128 mmol, 75 %) was obtained as a black solid.

MS (FD) m/z calcd for $C_{38}H_{36}CoN_4O_2$ [M^+]: 639.2, found 639.3;

IR(ATR): 2955, 2927, 2869, 1623, 1565, 1503, 1473, 1455, 1422, 1377, 1340, 1323, 1282, 1239, 1222, 1194, 1140, 1117, 1100, 1090, 1059, 1019, 988, 964, 948, 892, 821, 792, 730, 716, 649, 598, 582, 555, 544, 522 cm^{-1} .

Cobalt Complex (5-22)

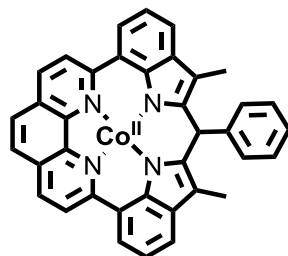


5-22

Cobalt complex **5-22** (31 mg, 0.036 mmol, 58 %) was obtained as a black solid.

MS (FD) m/z calcd for $C_{54}H_{68}CoN_4O_2$ [M^+]: 863.5, found 864.0

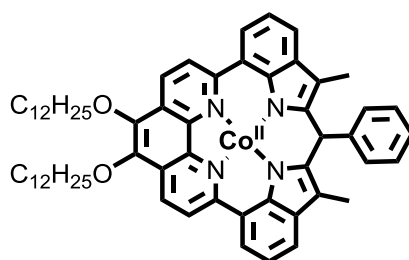
IR(ATR): 2918, 2853, 1625, 1592, 1566, 1524, 1505, 1465, 1426, 1342, 1238, 1226, 1125, 1105, 1091, 1055, 985, 965, 948, 895, 824, 793, 743, 718, 653, 600, 580, 541, 527 cm^{-1} .

Cobalt Complex (5-23)**5-23**

Cobalt complex **5-23** (15 mg, 0.026 mmol, 68 %) was obtained as a black solid.

MS (FD) m/z calcd for $C_{37}H_{24}CoN_4 [M^+]$: 583.1, found 583.1;

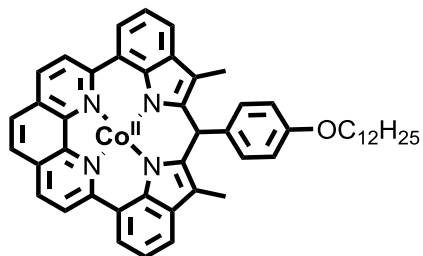
IR(ATR): 2956, 2924, 2854, 1730, 1581, 1301, 1278, 1257, 911, 759, 614 cm^{-1} .

Cobalt Complex (5-24)**5-24**

Cobalt complex **5-24** (25 mg, 0.026 mmol, 77 %) was obtained as a black solid.

MS (MALDI) m/z calcd for $C_{61}H_{72}CoN_4O_2 [M^+]$: 951.5, found 952.2.

IR (ATR): 2921, 2851, 1614, 1587, 1570, 1551, 1517, 1493, 1464, 1430, 1418, 1342, 1311, 1296, 1251, 1223, 1203, 1172, 1141, 1070, 1051, 958, 924, 912, 832, 796, 739, 722, 698, 645, 632, 621 cm^{-1} .

Cobalt Complex 5-25**5-25**

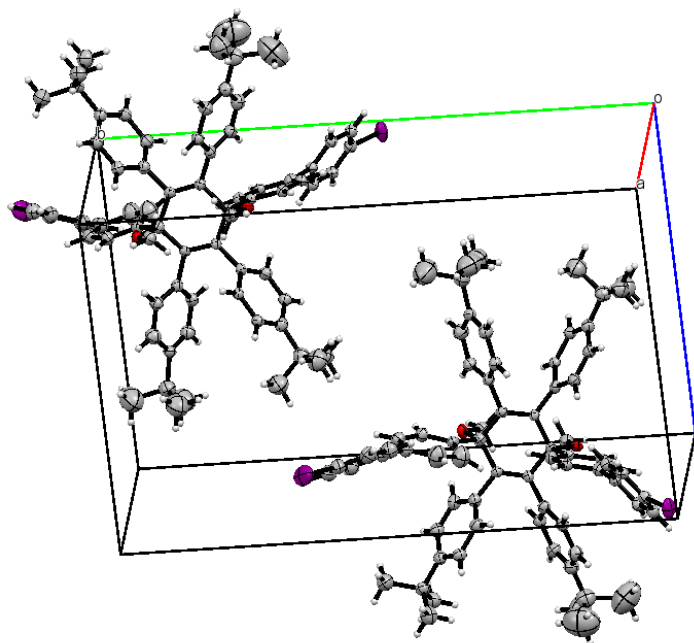
Cobalt complex **5-25** (8.1 mg, 0.011 mmol, 78 %) was obtained as a black solid.

MS (FD) m/z calcd for $C_{49}H_{48}CoN_4O$ [M^+]: 767.3, found 767.5.

IR (ATR): 2923, 2852, 1592, 1568, 1505, 1466, 1416, 1367, 1338, 1295, 1264, 1243, 1215, 1176, 1142, 1068, 1050, 845, 781, 729, 564, 546, 532, 522 cm^{-1} .

7.4. Crystal Data

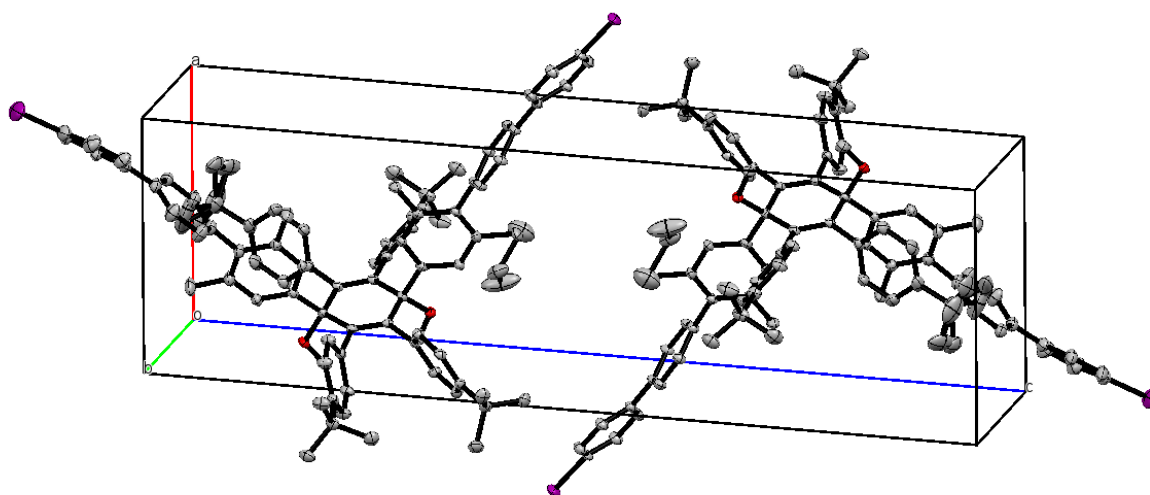
1,4-Bis(4'-iodobiphenyl)-1,4-dimethoxy-2,3,5,6-tetrakis(4''-*tert*-butylphenyl)cyclohexa-2,5-dienes (3-3)



$C_{72}H_{74}I_2O_2$, $M = 1225.17$ g/mol, monoclinic, space group $P2_1$, $a = 9.5794(7)$ Å, $b = 23.4392(9)$ Å, $c = 15.8229(9)$ Å, $\beta = 97.535(5)^\circ$, $V = 3522.09$ Å³, $R = 0.0406$.

Cambridge Crystallographic Data Centre identifier: CCDC-1046763

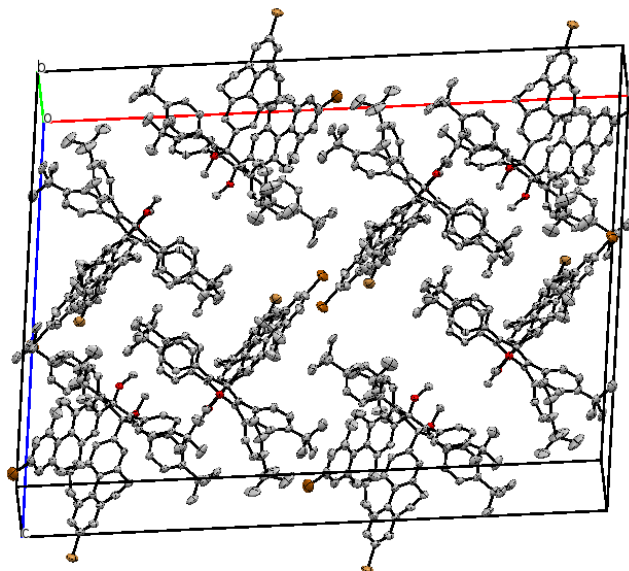
1,4-Bis(4''-iodo-2,6-dimethylterphenyl)-1,4-dimethoxy-2,3,5,6-tetrakis(4''-tert-butylphenyl)cyclohexa-2,5-dienes (4-8)



$C_{88}H_{90}I_2O_2$, $M = 1433.47$ g/mol, triclinic, space group P-1, $a = 11.3065(3)$ Å, $b = 12.8409(3)$ Å, $c = 31.2985(8)$ Å, $\alpha = 88.7245(9)^\circ$, $\beta = 97.535(5)^\circ$, $\gamma = 65.5059(9)^\circ$, $V = 4134.11$ Å³, $R = 0.0786$.

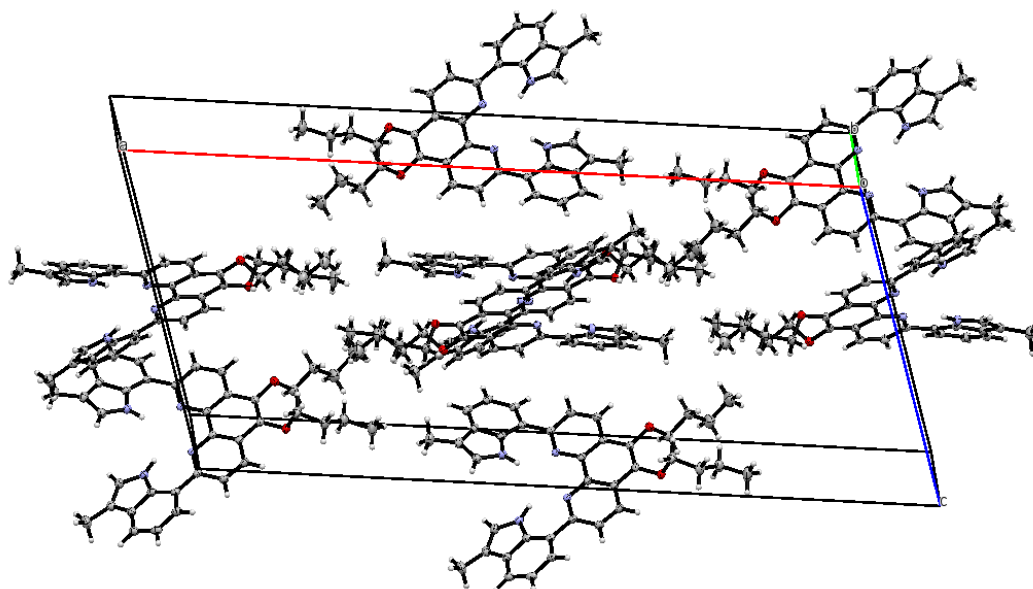
Cambridge Crystallographic Data Centre identifier: CCDC-1046762

1,4-Bis(2'-bromo-4',5',9',10'-tetrahydropyrene)-1,4-dimethoxy-2,3,5,6-tetrakis(4''-tert-butylphenyl)cyclohexa-2,5-dienes (4-11)



$C_{80}H_{82}Br_2O_2$, $M = 1235.32$ g/mol, monoclinic, space group $C2/c$, $a = 40.4282(14)$ Å, $b = 11.7707(3)$ Å, $c = 29.9626(10)$ Å, $\beta = 94.940(3)^\circ$, $V = 14205.3$ Å³.

Cambridge Crystallographic Data Centre identifier: CCDC-1046764

5,6-Dibutoxy-2,9-bis(3-methyl-1H-indol-7-yl)-1,10-phenanthroline (5-11)

$C_{38}H_{38}N_4O_2$, $M = 582.74$ g/mol, monoclinic, space group $C2/c$, $a = 37.1467(7)$ Å, $b = 10.3222(2)$ Å, $c = 17.0086(4)$ Å, $\beta = 107.3595(9)^\circ$, $V = 6224.65$ Å³, $R = 0.0553$.

Cambridge Crystallographic Data Centre identifier: CCDC-1046623

8. Bibliography

- [1] H. P. Boehm, A. Clauss, G. O. Fischer, U. Hofmann, *Zeitschrift für Anorg. und Allg. Chemie* **1962**, *316*, 119–127.
- [2] H.-P. Boehm, R. Setton, E. Stumpp, *Pure Appl. Chem.* **1994**, *66*, 1893–1901.
- [3] K. S. Novoselov, a K. Geim, S. V Morozov, D. Jiang, Y. Zhang, S. V Dubonos, I. V Grigorieva, a a Firsov, *Science* **2004**, *306*, 666–669.
- [4] D. Jariwala, V. K. Sangwan, L. J. Lauhon, T. J. Marks, M. C. Hersam, *Chem. Soc. Rev.* **2013**, *42*, 2824–2860.
- [5] M. A. Petrukhina, L. T. Scott, *Fragments of Fullerenes and Carbon Nanotubes*, John Wiley & Sons, Inc., Hoboken, NJ, USA, **2011**.
- [6] S. Bae, H. Kim, Y. Lee, X. Xu, J.-S. Park, Y. Zheng, J. Balakrishnan, T. Lei, H. R. Kim, Y. Il Song, et al., *Nat. Nanotechnol.* **2010**, *5*, 574–578.
- [7] X. Wang, L. Zhi, K. Müllen, *Nano Lett.* **2008**, *8*, 323–327.
- [8] J. N. Coleman, *Adv. Funct. Mater.* **2009**, *19*, 3680–3695.
- [9] Y. Hernandez, V. Nicolosi, M. Lotya, F. M. Blighe, Z. Sun, S. De, I. T. McGovern, B. Holland, M. Byrne, Y. K. Gun'Ko, et al., *Nat. Nanotechnol.* **2008**, *3*, 563–568.
- [10] L. Chen, Y. Hernandez, X. Feng, K. Müllen, *Angew. Chemie - Int. Ed.* **2012**, *51*, 7640–7654.
- [11] W. S. Hummers, R. E. Offeman, *J. Am. Chem. Soc.* **1958**, *80*, 1339–1339.
- [12] X. Li, Y. Zhu, W. Cai, M. Borysiak, B. Han, D. Chen, R. D. Piner, L. Colombo, R. S. Ruoff, *Nano Lett.* **2009**, *9*, 4359–4363.
- [13] Y. Liang, J. Frisch, L. Zhi, H. Norouzi-Arasi, X. Feng, J. P. Rabe, N. Koch, K. Müllen, *Nanotechnology* **2009**, *20*, 434007.
- [14] a. Vázquez de Parga, F. Calleja, B. Borca, M. Passeggi, J. Hinarejos, F. Guinea, R. Miranda, *Phys. Rev. Lett.* **2008**, *100*, 056807.

- [15] J. Coraux, A. T. N'Diaye, C. Busse, T. Michely, *Nano Lett.* **2008**, *8*, 565–570.
- [16] H. Ueta, M. Saida, C. Nakai, Y. Yamada, M. Sasaki, S. Yamamoto, *Surf. Sci.* **2004**, *560*, 183–190.
- [17] S. Marchini, S. Günther, J. Winterlin, *Phys. Rev. B* **2007**, *76*, 075429.
- [18] E. Clar, *The Aromatic Sextet*, John Wiley & Sons, **1972**.
- [19] E. Clar, *Polycyclic Hydrocarbons*, Academic Press, New York, **1964**.
- [20] M. Zander, *Handbook of Polycyclic Aromatic Hydrocarbons*, E. Dekker, New York, **1983**.
- [21] R. Scholl, C. Seer, *Justus Liebig's Ann. der Chemie* **1912**, *394*, 111–177.
- [22] M. D. Watson, A. Fechtenkötter, K. Müllen, *Chem. Rev.* **2001**, *101*, 1267–1300.
- [23] I. Gutman, S. Cyvin, *Introduction to the Theory of Benzenoid Hydrocarbons*, Springer-Verlag, Berlin, **1989**.
- [24] H. Franck, J. Stadelhofer, *Industrielle Aromatenchemie: Rohstoffe, Verfahren, Produkte*, Springer-Verlag, Berlin, **1987**.
- [25] X. Feng, W. Pisula, T. Kudernac, D. Wu, L. Zhi, S. De Feyter, K. Müllen, *J. Am. Chem. Soc.* **2009**, *131*, 4439–4448.
- [26] P. Rempala, J. Kroulík, B. T. King, *J. Org. Chem.* **2006**, *71*, 5067–5081.
- [27] L. Britnell, R. V Gorbachev, R. Jalil, B. D. Belle, F. Schedin, A. Mishchenko, T. Georgiou, M. I. Katsnelson, L. Eaves, S. V Morozov, et al., *Science* **2012**, *335*, 947–950.
- [28] H. Yang, J. Heo, S. Park, H. J. Song, D. H. Seo, K. Byun, P. Kim, I. Yoo, H. Chung, K. Kim, *Science* **2012**, *336*, 1140–1143.
- [29] L. Xie, H. Wang, C. Jin, X. Wang, L. Jiao, K. Suenaga, H. Dai, *J. Am. Chem. Soc.* **2011**, *133*, 10394–10397.
- [30] R. Denk, M. Hohage, P. Zeppenfeld, J. Cai, C. a Pignedoli, H. Söde, R. Fasel, X. Feng, K. Müllen, S. Wang, et al., *Nat. Commun.* **2014**, *5*, 4253.
- [31] J. Cai, P. Ruffieux, R. Jaafar, M. Bieri, T. Braun, S. Blankenburg, M. Muoth, A. P. Seitsonen, M. Saleh, X. Feng, et al., *Nature* **2010**, *466*, 470–473.

- [32] A. Narita, X. Feng, Y. Hernandez, S. a Jensen, M. Bonn, G. Fytas, O. Ivasenko, S. De Feyter, K. Müllen, *Nat. Chem.* **2014**, *6*, 126–132.
- [33] M. F. L. De Volder, S. H. Tawfick, R. H. Baughman, a J. Hart, *Science* **2013**, *339*, 535–539.
- [34] S. Iijima, *Nature* **1991**, *354*, 56–58.
- [35] L. V. Radushkevich, V. M. Lukyanovich, *Sov. J. Phys. Chem.* **1952**, *26*, 88–95.
- [36] H. G. Tennent, *Carbon Fibrils, Method for Producing Same and Compositions Containing Same*, **1987**, US 4663230.
- [37] J. Abrahamson, P. G. Wiles, B. L. Rhoades, *Carbon N. Y.* **1999**, *37*, 1873–1874.
- [38] M. Endo, M. S. Dresselhaus, *Carbon Fibres and Carbon Nanotubes*, Nagano, **2002**.
- [39] A. Oberlin, M. Endo, T. Koyama, *J. Cryst. Growth* **1976**, *32*, 335–349.
- [40] X. Lu, Z. Chen, *Chem. Rev.* **2005**, *105*, 3643–3696.
- [41] D. S. Bethune, C. H. Klang, M. S. de Vries, G. Gorman, R. Savoy, J. Vazquez, R. Beyers, *Nature* **1993**, *363*, 605–607.
- [42] T. Guo, T. Guo, P. Nikolaev, P. Nikolaev, a Thess, a Thess, D. T. Colbert, D. T. Colbert, R. E. Smalley, R. E. Smalley, *Chem. Phys. Lett* **1995**, *243*, 49–54.
- [43] O. Smiljanic, B. L. Stansfield, J.-P. Dodelet, A. Serventi, S. Désilets, *Chem. Phys. Lett.* **2002**, *356*, 189–193.
- [44] M. Endo, T. Hayashi, Y.-A. Kim, *Pure Appl. Chem.* **2006**, *78*, 1703–1713.
- [45] H. Zhang, B. Wu, W. Hu, Y. Liu, *Chem. Soc. Rev.* **2011**, *40*, 1324–1336.
- [46] H. Omachi, T. Nakayama, E. Takahashi, Y. Segawa, K. Itami, *Nat. Chem.* **2013**, *5*, 572–576.
- [47] V. C. Parekh, P. C. Guha, *J. Indian Chem. Soc.* **1934**, *11*, 95–100.
- [48] R. Friederich, M. Nieger, F. Vögtle, *Chem. Ber.* **1993**, *126*, 1723–1732.
- [49] S. Kammermeier, P. G. Jones, R. Herges, *Angew. Chemie Int. Ed.* **1996**, *35*, 2669–2671.

- [50] R. Jasti, J. Bhattacharjee, J. B. Neaton, C. R. Bertozzi, *J. Am. Chem. Soc.* **2008**, *130*, 17646–17647.
- [51] H. Takaba, H. Omachi, Y. Yamamoto, J. Bouffard, K. Itami, *Angew. Chemie Int. Ed.* **2009**, *48*, 6112–6116.
- [52] S. Yamago, Y. Watanabe, T. Iwamoto, *Angew. Chem. Int. Ed. Engl.* **2010**, *49*, 757–759.
- [53] F. Zhang, G. Götz, H. D. F. Winkler, C. A. Schalley, P. Bäuerle, *Angew. Chemie* **2009**, *121*, 6758–6762.
- [54] C. Huang, Y. Huang, N. G. Akhmedov, B. V Popp, J. L. Petersen, K. K. Wang, *Org. Lett.* **2014**, 10–13.
- [55] P. J. Evans, E. R. Darzi, R. Jasti, *Nat. Chem.* **2014**, *6*, 404–408.
- [56] E. Kayahara, V. K. Patel, S. Yamago, *J. Am. Chem. Soc.* **2014**, *136*, 2284–2287.
- [57] T. Matsuno, S. Kamata, S. Hitosugi, H. Isobe, *Chem. Sci.* **2013**, *4*, 3179–3183.
- [58] H. Omachi, Y. Segawa, K. Itami, *Org. Lett.* **2011**, *13*, 2480–2483.
- [59] S. Hitosugi, W. Nakanishi, T. Yamasaki, H. Isobe, *Nat. Commun.* **2011**, *2*, 492–496.
- [60] S. Hitosugi, T. Yamasaki, H. Isobe, *J. Am. Chem. Soc.* **2012**, *134*, 12442–12445.
- [61] K. Matsui, Y. Segawa, K. Itami, *Org. Lett.* **2012**, *14*, 1888–1891.
- [62] H. Ito, Y. Mitamura, Y. Segawa, K. Itami, *Angew. Chemie Int. Ed.* **2014**, *54*, 159–163.
- [63] M. R. Golder, B. M. Wong, R. Jasti, *Chem. Sci.* **2013**, *4*, 4285.
- [64] M. Peña Alvarez, P. Mayorga Burrezo, M. Kertesz, T. Iwamoto, S. Yamago, J. Xia, R. Jasti, J. T. López Navarrete, M. Taravillo, V. G. Baonza, et al., *Angew. Chemie Int. Ed.* **2014**, *53*, 7033–7037.
- [65] M. Fujitsuka, D. W. Cho, T. Iwamoto, S. Yamago, T. Majima, *Phys. Chem. Chem. Phys.* **2012**, *14*, 14585–14588.
- [66] L. Adamska, I. Nayyar, H. Chen, A. K. Swan, N. Oldani, S. Fernandez-Alberti, M. R. Golder, R. Jasti, S. K. Doorn, S. Tretiak, *Nano Lett.* **2014**, *14*, 6539–6546.
- [67] H. Isobe, S. Hitosugi, T. Yamasaki, R. Iizuka, *Chem. Sci.* **2013**, *4*, 1293.

- [68] Y. Nakanishi, H. Omachi, S. Matsuura, Y. Miyata, R. Kitaura, Y. Segawa, K. Itami, H. Shinohara, *Angew. Chemie Int. Ed.* **2014**, *53*, 3102–3106.
- [69] T. Iwamoto, Y. Watanabe, T. Sadahiro, T. Haino, S. Yamago, *Angew. Chemie Int. Ed.* **2011**, *50*, 8342–8344.
- [70] J. Xia, J. W. Bacon, R. Jasti, *Chem. Sci.* **2012**, *3*, 3018.
- [71] S. Hitosugi, R. Iizuka, T. Yamasaki, R. Zhang, Y. Murata, H. Isobe, *Org. Lett.* **2013**, *15*, 3199–3201.
- [72] E. H. Fort, L. T. Scott, *Angew. Chemie - Int. Ed.* **2010**, *49*, 6626–6628.
- [73] J. Xia, M. R. Golder, M. E. Foster, B. M. Wong, R. Jasti, *J. Am. Chem. Soc.* **2012**, *134*, 19709–19715.
- [74] Y. Ishii, S. Matsuura, Y. Segawa, K. Itami, *Org. Lett.* **2014**, *16*, 2174–2176.
- [75] T. Iwamoto, E. Kayahara, N. Yasuda, T. Suzuki, S. Yamago, *Angew. Chemie Int. Ed.* **2014**, *53*, 6430–6434.
- [76] T. Nishiuchi, X. Feng, V. Enkelmann, M. Wagner, K. Müllen, *Chemistry* **2012**, *18*, 16621–16625.
- [77] B. C. Steele, A. Heinzl, *Nature* **2001**, *414*, 345–352.
- [78] M. Z. Jacobson, W. G. Colella, D. M. Golden, *Science* **2005**, *308*, 1901–1905.
- [79] K. J. Euler, *Chemie unserer Zeit* **1967**, *1*, 85–93.
- [80] N. Fouquet, in *Polym. Electrolyte Fuel Cells* (Ed.: A. Franco), Pan Stanford Publishing, Singapore, **2013**, pp. 1–28.
- [81] D. Brett, D. J. Brett, in *Funct. Mater. Sustain. Energy Appl.*, **2012**, p. 249.
- [82] G. Arzamendi, P. M. Die, L. M. Gandi, *Renewable Hydrogen Technologies*, Elsevier, **2013**.
- [83] C. Acar, I. Dincer, *Int. J. Hydrogen Energy* **2014**, *39*, 1–12.
- [84] J. Andrews, B. Shabani, *Procedia Eng.* **2012**, *49*, 15–25.
- [85] R. Bashyam, P. Zelenay, *Nature* **2006**, *443*, 63–66.

- [86] H. a. Gasteiger, S. S. Kocha, B. Sompalli, F. T. Wagner, *Appl. Catal. B Environ.* **2005**, *56*, 9–35.
- [87] I. E. L. Stephens, A. S. Bondarenko, U. Grønbjerg, J. Rossmeisl, I. Chorkendorff, *Energy Environ. Sci.* **2012**, *5*, 6744.
- [88] Z. Chen, D. Higgins, A. Yu, L. Zhang, J. Zhang, *Energy Environ. Sci.* **2011**, *4*, 3167–3192.
- [89] A. Bouwkamp-Wijnoltz, W. Visscher, *Electrochim. Acta* **1999**, *45*, 379–386.
- [90] J. H. Zagal, F. Bedioui, J.-P. Dodelet, *N4-Macrocyclic Metal Complexes*, Springer, **2006**.
- [91] R. Jasinski, *Nature* **1964**, *201*, 1212–1213.
- [92] H. Jahnke, M. Schönborn, G. Zimmermann, *Top. Curr. Chem.* **1976**, *61*, 133–181.
- [93] D. C. Higgins, Z. Chen, *Can. J. Chem. Eng.* **2013**, *91*, 1881–1895.
- [94] R. Liu, C. von Malotki, L. Arnold, N. Koshino, H. Higashimura, M. Baumgarten, K. Müllen, *J. Am. Chem. Soc.* **2011**, *133*, 10372–10375.
- [95] J. Zagal, P. Bindra, E. Yeager, *J. Electrochem. Soc.* **1980**, 1506–1517.
- [96] P. Vasudevan, N. Mann, S. Tyagi, *Transit. Met. Chem.* **1990**, *90*, 81–90.
- [97] C. Shi, F. C. Anson, *Inorg. Chem.* **1996**, *35*, 7928–7931.
- [98] C. K. Chang, I. Abdalmuhdi, *J. Org. Chem.* **1983**, *48*, 5388–5390.
- [99] J. P. Collman, J. E. Hutchison, M. A. Lopez, A. Tabard, R. Guilard, W. K. Seok, J. A. Ibers, M. L’Her, *J. Am. Chem. Soc.* **1992**, *114*, 9869–9877.
- [100] J. P. Collman, P. S. Wagenknecht, J. E. Hutchison, *Angew. Chemie Int. Ed.* **1994**, *33*, 1537–1554.
- [101] J. P. Collman, P. Denisevich, Y. Konai, M. Marrocco, C. Koval, F. C. Anson, *J. Am. Chem. Soc.* **1980**, *102*, 6027–6036.
- [102] R. R. Durand, C. S. Bencosme, J. P. Collman, F. C. Anson, *J. Am. Chem. Soc.* **1983**, *105*, 2710–2718.

- [103] A. van der Putten, A. Elzing, W. Visscher, E. Barendrecht, *J. Chem. Soc. Chem. Commun.* **1986**, 477–479.
- [104] Y. Zheng, Y. Jiao, L. Ge, M. Jaroniec, S. Z. Qiao, *Angew. Chemie Int. Ed.* **2013**, *52*, 3110–3116.
- [105] Y. J. Sa, C. Park, H. Y. Jeong, S.-H. Park, Z. Lee, K. T. Kim, G.-G. Park, S. H. Joo, *Angew. Chemie* **2014**, *126*, 4186–4190.
- [106] J. Liang, X. Du, C. Gibson, X. W. Du, S. Z. Qiao, *Adv. Mater.* **2013**, *25*, 6226–6231.
- [107] K. Wiesener, D. Ohms, V. Neumann, R. Franke, *Mater. Chem. Phys.* **1989**, *22*, 457–475.
- [108] A. N. Frumkin, L. N. Nekrasov, *Dokl. Akad. Nauk SSSR* **1959**, *126*, 115.
- [109] E. Negishi, *Angew. Chemie Int. Ed.* **2011**, *50*, 6738–64.
- [110] A. Suzuki, *Angew. Chemie Int. Ed.* **2011**, *50*, 6722–37.
- [111] M. Yu, *Science (80-.)*. **2000**, *287*, 637–640.
- [112] Y. C. Tseng, P. Xuan, A. Javey, R. Malloy, Q. Wang, J. Bokor, H. Dai, *Nano Lett.* **2004**, *4*, 123–127.
- [113] I. Singh, A. K. Rehni, P. Kumar, M. Kumar, H. Y. Aboul-Enein, *Fullerenes, Nanotub. Carbon Nanostructures* **2009**, *17*, 361–377.
- [114] K. T. Rim, M. Sijaj, S. Xiao, M. Myers, V. D. Carpentier, L. Liu, C. Su, M. L. Steigerwald, M. S. Hybertsen, P. H. McBreen, et al., *Angew. Chemie - Int. Ed.* **2007**, *46*, 7891–7895.
- [115] X. Yu, J. Zhang, W. Choi, J.-Y. Choi, J. M. Kim, L. Gan, Z. Liu, *Nano Lett.* **2010**, *10*, 3343–3349.
- [116] J. R. Sanchez-Valencia, T. Dienel, O. Gröning, I. Shorubalko, A. Mueller, M. Jansen, K. Amsharov, P. Ruffieux, R. Fasel, *Nature* **2014**, *512*, 61–64.
- [117] L. T. Scott, E. a Jackson, Q. Zhang, B. D. Steinberg, M. Bancu, B. Li, *J. Am. Chem. Soc.* **2012**, *134*, 107–10.
- [118] A. Yagi, G. Venkataramana, Y. Segawa, K. Itami, *Chem. Commun.* **2014**, *50*, 957–959.

- [119] F. Sibbel, K. Matsui, Y. Segawa, A. Studer, K. Itami, *Chem. Commun.* **2014**, *50*, 954–956.
- [120] A.-F. Tran-Van, E. Huxol, J. M. Basler, M. Neuburger, J.-J. Adjizian, C. P. Ewels, H. a Wegner, *Org. Lett.* **2014**, *16*, 1594–1597.
- [121] A. Yagi, Y. Segawa, K. Itami, *J. Am. Chem. Soc.* **2012**, *134*, 2962–2965.
- [122] J. Xia, R. Jasti, *Angew. Chemie* **2012**, *124*, 2524–2526.
- [123] S. Hitosugi, W. Nakanishi, H. Isobe, *Chem. Asian J.* **2012**, *7*, 1550–1552.
- [124] T. J. Sisto, X. Tian, R. Jasti, *J. Org. Chem.* **2012**, *77*, 5857–5860.
- [125] T. Iwamoto, Y. Watanabe, Y. Sakamoto, T. Suzuki, S. Yamago, *J. Am. Chem. Soc.* **2011**, *133*, 8354–8361.
- [126] Y. Segawa, P. Šenel, S. Matsuura, H. Omachi, K. Itami, *Chem. Lett.* **2011**, *40*, 423–425.
- [127] H. Omachi, S. Matsuura, Y. Segawa, K. Itami, *Angew. Chemie (International ed.)* **2010**, *49*, 10202–10205.
- [128] X. Feng, V. Marcon, W. Pisula, M. R. Hansen, J. Kirkpatrick, F. Grozema, D. Andrienko, K. Kremer, K. Müllen, *Nat. Mater.* **2009**, *8*, 421–426.
- [129] V. S. Iyer, K. Yoshimura, V. Enkelmann, R. Epsch, J. P. Rabe, K. Müllen, *Angew. Chemie Int. Ed.* **1998**, *37*, 2696–2699.
- [130] M. Müller, V. S. Iyer, C. Kübel, V. Enkelmann, K. Müllen, *Angew. Chemie Int. Ed.* **1997**, *36*, 1607–1610.
- [131] D. Wasserfallen, M. Kastler, W. Pisula, W. A. Hofer, Y. Fogel, Z. Wang, K. Müllen, *J. Am. Chem. Soc.* **2006**, *128*, 1334–1339.
- [132] S. M. Draper, D. J. Gregg, R. Madathil, *J. Am. Chem. Soc.* **2002**, *124*, 3486–3487.
- [133] R. Berger, A. Giannakopoulos, P. Ravat, M. Wagner, D. Beljonne, X. Feng, K. Müllen, *Angew. Chemie Int. Ed.* **2014**, *53*, 10520–10524.
- [134] Y. Fogel, L. Zhi, A. Rouhanipour, D. Andrienko, H. J. Räder, K. Müllen, *Macromolecules* **2009**, *42*, 6878–6884.

- [135] M. G. Schwab, A. Narita, Y. Hernandez, T. Balandina, K. S. Mali, S. De Feyter, X. Feng, K. Müllen, *J. Am. Chem. Soc.* **2012**, *134*, 18169–18172.
- [136] L. Dössel, L. Gherghel, X. Feng, K. Müllen, *Angew. Chemie Int. Ed.* **2011**, *50*, 2540–2543.
- [137] Y. Avlasevich, C. Kohl, K. Müllen, *J. Mater. Chem.* **2006**, *16*, 1053.
- [138] K. Kawasumi, Q. Zhang, Y. Segawa, L. T. Scott, K. Itami, *Nat. Chem.* **2013**, *5*, 739–744.
- [139] Y. Sakamoto, T. Suzuki, *J. Am. Chem. Soc.* **2013**, *135*, 14074–14077.
- [140] Y.-T. Wu, J. S. Siegel, *Chem. Rev.* **2006**, *106*, 4843–4867.
- [141] V. M. Tsefrikas, L. T. Scott, **2006**, 4868–4884.
- [142] S. Yamago, Y. Watanabe, T. Iwamoto, *Angew. Chemie Int. Ed.* **2010**, *49*, 757–759.
- [143] Q. Su, Graphene Based Electrode Materials for Solar Cell and Electrochemical Oxygen Reduction, Johannes Gutenberg-Universität Mainz, **2012**.
- [144] N. Fukui, H. Yorimitsu, J. M. Lim, D. Kim, A. Osuka, *Angew. Chem. Int. Ed. Engl.* **2014**, *53*, 1–5.
- [145] I. Ullah, R. A. Khera, M. Hussain, A. Villinger, P. Langer, *Tetrahedron Lett.* **2009**, *50*, 4651–4653.
- [146] S. D. Walker, T. E. Barder, J. R. Martinelli, S. L. Buchwald, *Angew. Chemie Int. Ed.* **2004**, *43*, 1871–1876.
- [147] D. Sundholm, S. Taubert, F. Pichierri, *Phys. Chem. Chem. Phys.* **2010**, *12*, 2751–2757.
- [148] T. Nishihara, Y. Segawa, K. Itami, Y. Kanemitsu, *J. Phys. Chem. Lett.* **2012**, *3*, 3125–3128.
- [149] L. Zhai, R. Shukla, R. Rathore, *Org. Lett.* **2009**, *11*, 3474–3477.
- [150] D. J. Jones, B. Purushothaman, S. Ji, A. B. Holmes, W. W. H. Wong, *Chem. Commun.* **2012**, *48*, 8066–8068.
- [151] A. Konishi, Y. Hirao, K. Matsumoto, H. Kurata, T. Kubo, *Chem. Lett.* **2013**, *42*, 592–594.

- [152] A. Konishi, Y. Hirao, K. Matsumoto, H. Kurata, R. Kishi, Y. Shigeta, M. Nakano, K. Tokunaga, K. Kamada, T. Kubo, *J. Am. Chem. Soc.* **2013**, *135*, 1430–1437.
- [153] A. M. Yol, C. Wesdemiotis, *React. Funct. Polym.* **2014**, *80*, 95–108.
- [154] X. Li, Y. Chan, M. Casiano-Maldonado, J. Yu, G. A. Carri, G. R. Newkome, C. Wesdemiotis, *Anal. Chem.* **2011**, *83*, 6667–6674.
- [155] K. Yoshimura, L. Przybilla, S. Ito, D. Brand, M. Wehmeir, H. J. Räder, K. Müllen, *Macromol. Chem. Phys.* **2001**, *202*, 215–222.
- [156] Z. Wang, M. D. Watson, J. Wu, K. Müllen, *Chem. Commun.* **2004**, 336–337.
- [157] M. Kastler, W. Pisula, D. Wasserfallen, T. Pakula, K. Müllen, *J. Am. Chem. Soc.* **2005**, *127*, 4286–4296.
- [158] Z. Zhou, T. Yamamoto, *J. Organomet. Chem.* **1991**, *414*, 119–127.
- [159] T. T. Tsou, J. K. Kochi, *J. Am. Chem. Soc.* **1979**, *101*, 7547–7560.
- [160] Y. Segawa, S. Miyamoto, H. Omachi, S. Matsuura, P. Šenel, T. Sasamori, N. Tokitoh, K. Itami, *Angew. Chemie Int. Ed.* **2011**, *50*, 3244–3248.
- [161] F. E. Golling, M. Quernheim, M. Wagner, T. Nishiuchi, K. Müllen, *Angew. Chemie Int. Ed.* **2014**, *53*, 1525–1528.
- [162] M. Quernheim, H. Liang, Q. Su, M. Baumgarten, N. Koshino, H. Higashimura, K. Müllen, *Chem. - A Eur. J.* **2014**, *20*, 14178–14183.
- [163] J. Frey, T. Kraus, V. Heitz, J.-P. Sauvage, *Chemistry (Easton)*. **2007**, *13*, 7584–7594.
- [164] D. W. Robbins, T. a Boebel, J. F. Hartwig, *J. Am. Chem. Soc.* **2010**, *132*, 4068–4069.
- [165] G. Bartoli, G. Palmieri, M. Bosco, R. Dalpozzo, *Tetrahedron Lett.* **1989**, *30*, 2129–2132.
- [166] L. Cuesta, J. L. Sessler, *Chem. Soc. Rev.* **2009**, *38*, 2716–2729.
- [167] R. D. Shannon, *Acta Crystallogr. Sect. A* **1976**, *32*, 751–767.
- [168] K. Wang, C.-T. Poon, W.-K. Wong, W.-Y. Wong, C. Y. Choi, D. W. J. Kwong, H. Zhang, Z.-Y. Li, *Eur. J. Inorg. Chem.* **2009**, *2009*, 922–928.
- [169] X. Huang, K. Nakanishi, N. Berova, *Chirality* **2000**, *12*, 237–255.

- [170] M. Lan, H. Zhao, H. Yuan, C. Jiang, S. Zuo, Y. Jiang, *Dye. Pigment.* **2007**, *74*, 357–362.
- [171] M. S. Mudadu, A. N. Singh, R. P. Thummel, *J. Org. Chem.* **2008**, *73*, 6513–6520.
- [172] K. Suslick, R. Watson, *New. J. Chem* **1992**, 633–642.
- [173] C. Chang, H. Liu, I. Abdalmuhdi, *J. Am. Chem. Soc.* **1984**, *106*, 2725–2726.
- [174] C. J. Chang, Z.-H. Loh, C. Shi, F. C. Anson, D. G. Nocera, *J. Am. Chem. Soc.* **2004**, *126*, 10013–10020.
- [175] J. B. Love, *Chem. Commun.* **2009**, 3154–3165.
- [176] L. Zhang, J. Niu, M. Li, Z. Xia, *J. Phys. Chem. C* **2014**, *118*, 3545–3553.
- [177] K. a. Kurak, A. B. Anderson, *J. Phys. Chem. C* **2009**, *113*, 6730–6734.
- [178] Y. Jiao, Y. Zheng, M. Jaroniec, S. Z. Qiao, *J. Am. Chem. Soc.* **2014**, *136*, 4394–4403.
- [179] J. Duan, S. Chen, S. Dai, S. Z. Qiao, *Adv. Funct. Mater.* **2014**, *24*, 2072–2078.
- [180] G. Wu, K. L. More, C. M. Johnston, P. Zelenay, *Science* **2011**, *332*, 443–447.
- [181] R. Othman, A. L. Dicks, Z. Zhu, *Int. J. Hydrogen Energy* **2012**, *37*, 357–372.
- [182] E. Yeager, *Electrochim. Acta* **1984**, *29*, 1527–1537.
- [183] K. J. J. Mayrhofer, G. K. H. Wiberg, M. Arenz, *J. Electrochem. Soc.* **2008**, *155*, P1.
- [184] K. J. J. Mayrhofer, a. S. Crampton, G. K. H. Wiberg, M. Arenz, *J. Electrochem. Soc.* **2008**, *155*, P78.
- [185] S. Baranton, C. Coutanceau, C. Roux, F. Hahn, J.-M. Léger, *J. Electroanal. Chem.* **2005**, *577*, 223–234.
- [186] J. Zagal, *Coord. Chem. Rev.* **1992**, *119*, 89–136.
- [187] M. G. Schwab, From Large Polycyclic Aromatic Hydrocarbons to Extended Aromate-Rich Networks, Johannes Gutenberg-Universität Mainz, **2011**.
- [188] D. W. Robbins, T. a Boebel, J. F. Hartwig, *J. Am. Chem. Soc.* **2010**, *132*, 4068–4069.

9. Acknowledgement

First of all, I would like to thank my PhD advisor, [REDACTED], for his continuous scientific and personal support. The fruitful discussions in numerous meetings were essential for the success of this work. I never met a scientist before, who was so enthusiastic and passionate about science and research.

I would like to thank [REDACTED] for the scientific support.

Furthermore, I like to thank [REDACTED], who created the basis for the success of this work. Moreover, he supervised my research and helped me in every situation with his profound knowledge in cycloparaphenylene chemistry.

I would like to thank my wife [REDACTED], who always supported me. Without her, it would have been impossible to be successful. The same is true for my whole family. Thank you!

I like to thank my cooperation partners, [REDACTED] and [REDACTED], for the great mass spectrometric measurements. I was surprised to learn that a mass spectrometer can do more than just measuring masses.

I would like to thank [REDACTED], who supported my work with the electrochemical measurements.

Further, I thank all collaborators from the Max Planck Institute for Polymer Research, namely:

- [REDACTED] for his fantastic NMR measurements
- [REDACTED] for the numerous crystal structures resolved

And I thank all members from the [REDACTED] group for the magnificent collegueship, in particular:

- [REDACTED], who always helped me during my whole PhD as well as [REDACTED] for the fruitful discussions
- My office mates [REDACTED]
[REDACTED]
[REDACTED]
- My lab mates: [REDACTED]
[REDACTED]
[REDACTED]
- I especially acknowledge my cooking students [REDACTED] and [REDACTED], who provided me with numerous compounds and therefore, supported the success of this work
- I would also like to thank all the group members who organized parties, barbecues and other social events

10. List of Publications

1. Quernheim, M., Nishiuchi, T., Golling, F. E., Müllen, K.: “Synthesis of cyclic para-hexaphenylbenzene - an approach to structurally defined carbon nanotubes”, *Abstracts of Papers of the American Chemical Society - 245th ACS National Meeting & Exposition, New Orleans, 2013*.
2. Golling, F. E., Quernheim, M., Wagner, M., Nishiuchi, T., Müllen, K.: “Concise Synthesis of 3D π -Extended Polyphenylene Cylinders“, *Angewandte Chemie*, **2014**, *126*(6), 1551–1554.
3. Quernheim, M., Liang, H., Su, Q., Baumgarten, M., Koshino, N., Higashimura, H., Müllen, K.: “Cobalt Phenanthroline-Indole Macrocycles as Highly Active Electrocatalysts for Oxygen Reduction”, *Chemistry - A European Journal*, **2014**, *20*(44), 14178–14183.
4. Quernheim, M., Golling, F. E., Zhang, W., Wagner, M., Räder, J., Nishiuchi, T., Müllen, K.: “The Precise Synthesis of Phenylene Extended Cyclic Hexa-*peri*-hexabenzocoronenes from Polyarylated [*n*]Cycloparaphenylenes *via* the Scholl Reaction”, *submitted*.
5. F. E. Golling, M. Quernheim, M. Wagner, K. Müllen: “ π -Extended [12]Cycloparaphenylenes: from a Hexaphenylbenzene Cyclohexamer to its Unexpected C₂-symmetric Congener,” *submitted*.
6. Zhang, W., Quernheim, M., Räder, H. J., Müllen, K.: “Fragmentation Ion Mobility Mass Spectrometry for the Elucidation of Unknown Structures in Strained PAH Macrocycles“, *in preparation*.

11. Curriculum Vitae

Martin Quernheim, née Günther

Graduate Chemist

* 11. October 1984 - Tuttlingen

[Redacted]

Education

[Redacted]

[Redacted]

[Redacted]

[Redacted]

[Redacted]

[Redacted]

Professional Experience

[Redacted]

[Redacted]

[Redacted]

[Redacted]

[Redacted text block]

Language Skills

[Redacted text block]

IT Skills

[Redacted text block]

Interests

[Redacted text block]